A D S O R P T I O N O F G A S E S

O N Z E O L I T E L

A N D R E L A T E D S T R U C T U R E S

by

Iliana Minkova Galabova

A thesis
submitted for the degree of
Doctor of Philosophy
in the University of London

Chemistry Department,
Imperial College,
London, S.W.7.

May, 1970.

T O B O R I A N A

A C K N O W L E D G E M E N T S

I would like to express my gratitude to Professor R.M. Barrer, F.R.S. - a most admirable teacher and helpful critic, without whose unfailing assistance this work could not have been completed.

I would also like to thank all those friends and colleagues who have in various ways helped with the preparation of this thesis, among them Mr. B.O. Okoli, Dr. Sylvia Harvie and Mrs. Mercia MacDermott. My thanks also go to Mrs. M. Michael, who typed the text.

I owe much to Dr. H. Villiger and Dr. I.S. Kerr for many useful discussions on problems of crystallography and to Miss R. Osborn for preparing numerous X-ray patterns.

My thanks are also due to my compatriots Professor S. Christov, Dr. P. Voutov, Dr. S. Raicheva and S. Ikonopisov for their support and encouragement.

I wish to acknowledge with thanks the award of a grant from W.R. Grace and Co., which enabled me to undertake this work.

Last, but by no means least, I want to say a special word of thanks to my mother, who has encouraged me from my first steps throughout my academic life.

INDEX

page

ABSTRACT

Zeolite L is a novel synthetic zeolite for which promising adsorption properties have previously been reported. The sorption behaviour of Zeolite L and of the structurally related zeolites erionite and offretite were studied in the present work, using rare gases as sorbates. Ion-exchanged forms prepared for the adsorption experiments were Li-, Na-, K-, Cs-, Ba- and La-enriched forms of L; Na- and K-enriched forms of erionite; and decationated forms from all three zeolites. The degrees of ion-exchange were found to be restricted within specific limits for a given zeolite. Unit cell parameters of the ion-exchanged forms of L were determined and a dependence on cation composition found. Reversible changes in the structure at high temperature were found for all ion-exchanged forms of Zeolite L (except LiL and HL) and for decationated offretite. Irreversible alterations were observed for the exchanged forms of erionite. For the Ba-form of zeolite L an X-ray structure analysis showed a migration of the Ba cation at high temperatures.

For all sorbents the saturation capacities for Ar(77.3°K), isosteric heats of Kr, micropore volumes (via Ar adsorption), equilibrium constants for Kr and thermodynamic properties of the sorbent/sorbate systems were determined.

Further studies were made on selected systems as follows:

a) Krypton isotherms on KL, BaL and LaL were used to evaluate the coefficients, A, of the isotherm equation $K = \frac{C_s}{p} \exp(2A_1 C_s + \frac{3}{2}A_2 C_s^2 + \frac{4}{3}A_3 C_s^3 + \ldots)$ and the thermodynamic properties in the standard state;

b) from argon and xenon adsorption on NaL, KL and BaL, isosteric heats, entropies and other thermodynamic properties were determined;

c) krypton adsorption on decationated forms of the three zeolites was used to calculate and compare entropies of the sorbed gas.

Syntheses of zeolite L and related structures yielded pure, well crystalline samples of L; new phases Na, K-BB and Li, K-VV; and poorly crystalline offretite. Reproducible co-crystallisation of zeolite L, erionite and offretite was found and attributed to building units common to the three zeolites. Epitaxy of L and offretite and intergrowth of erionite and offretite were often observed.

INTRODUCTION

1. Zeolites, Zeolite L and related structures

Among the alumosilicates(1) zeolites present an individual group, because of their typical open framework structures, enclosing channels and cavities. These interstices comprise the free volumes of a structure, and are filled with cations and water molecules, both loosely bonded and capable of replacement(2).

The cations maintain the neutrality of the framework structure(1). Since they possess a considerable freedom of movement, they undergo ion-exchange. A wide variety of industrial techniques(3) are based on these properties of the zeolites. The scavenging of radionuclides is one of the most interesting achievements in this field(4).

Zeolitic water(1) is easily and reversibly removed by heating and evacuation. The resulting dehydrated crystal is, in many cases, highly stable. Its emptied channels and cavities, which now provide a free pore system, have diameters of molecular dimensions. The diameters are "quite precise and controlled as accurately as the positions of the lattice atoms surrounding them".(5) The pores are tailored all to one or a few sets of dimensions(6). These facts form the main basis for the extensive application of zeolites in industry as molecular sieves(3) selective sorbents(5), desiccants(7) and catalysts(8).

The structure of a given zeolite is its most specific and individual characteristic, dominating even its chemical composition. On the basis of their structures, zeolites are classified in seven groups(6) named after typical members: analcite, natrolite, chabazite, philipsite, heulandite, mordenite and faujasite. Yugawaralite(9) does not belong to any one of the above groups.

The chabazite group was one of the first to attract the attention of physical chemists(10). It consists of the zeolites gmelinite, chabazite, erionite and levynite. In addition, two felspathoids - cancrinite and sodalite hydrates - are usually grouped with the chabazite family. Offretite and zeolite L should be included in the above list, in view of their structures, which were recently determined(11,12).

The members of the chabazite group are normally hexagonal or trigonal. They possess a common type of simple chains of 4-membered rings(6) and in most cases they have SBU* in common, such as hexagonal prisms, cancrinite and gmelinite cages.

Within the chabazite group, small subgroups could be formed, consisting of members which have a greater mutual resemblance, than that possessed by the group as a whole. Zeolite L, offretite and erionite form such a subgroup. The structures of the three zeolites reveal their closer relationship.

Information about space groups, unit cell dimensions, chemical composition and free volumes of these three zeolites is presented in Table 1. Each of the considered zeolites has, parallel to its c direction, chains of alternatively following cancrinite cages and hexagonal prisms (Figs. 1a, b and c). For zeolite L and offretite the chains are identical, having in each layer exactly the same orientation of the cancrinite cages (Fig. 2a). The chains in erionite are built in a different way: each cancrinite cage is rotated

---

* SBU - secondary building units.

TABLE 1

The space groups and unit cells with their contents for the three zeolites considered

Offretite	Erionite	Zeolite L
$P\bar{6}m2$	$P6_3/mmc$	$P6/mmm$
$a = 13.31\text{Å}$	$a = 13.26\text{Å}$	$a = 18.4\text{Å}$
$c = 7.59\text{Å}$	$c = 15.12\text{Å}$	$c = 7.5\text{Å}$
$(Ca,Mg,K_2)_{2.5}Al_5$	$(Ca,Mg,Na_2,K_2)_{4.5}$	$K_6Na_3Al_9$
$Si_{13}O_{36}15H_2O$	$Al_9Si_{27}O_{72}27H_2O$	$Si_{27}O_{72}21H_2O$
Bennett and Gard (1967)	Staples and Gard (1959)	Barrer and Villiger (1969)
Sheppard and Gude (1969)		
$V^{*1} = 1160$	$V = 2320$	$V = 2205$
$V_f^{*2} = 400$	$V_f = 800$	$V_f = 610$
$\frac{V_f}{V} = 0.40$	$\frac{V_f}{V} = 0.40$	$\frac{V_f}{V} = 0.28$

*1 V - volume of the unit cell, Å^3.

*2 V_f - free volume of the unit cell, Å^3.

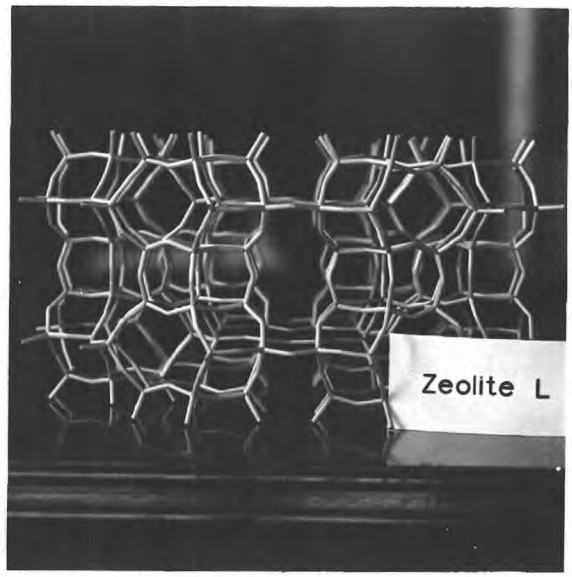

a

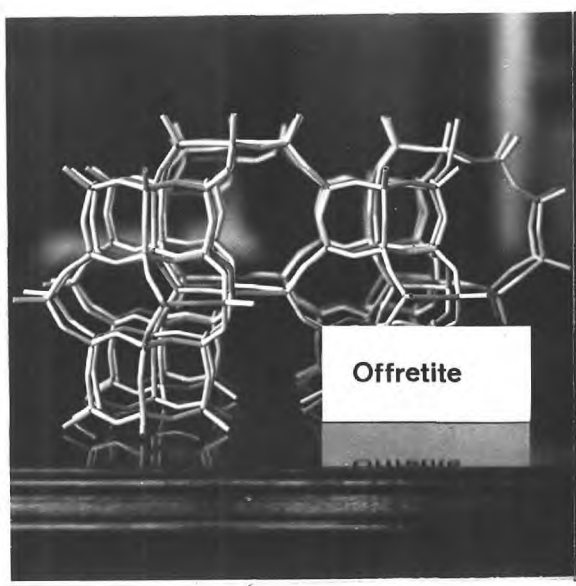

b

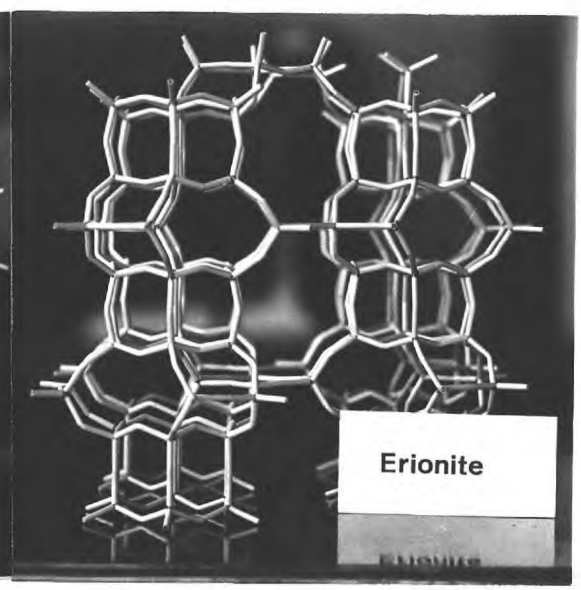

c

Figs. 1a, b and c. The structures viewed down a axis.

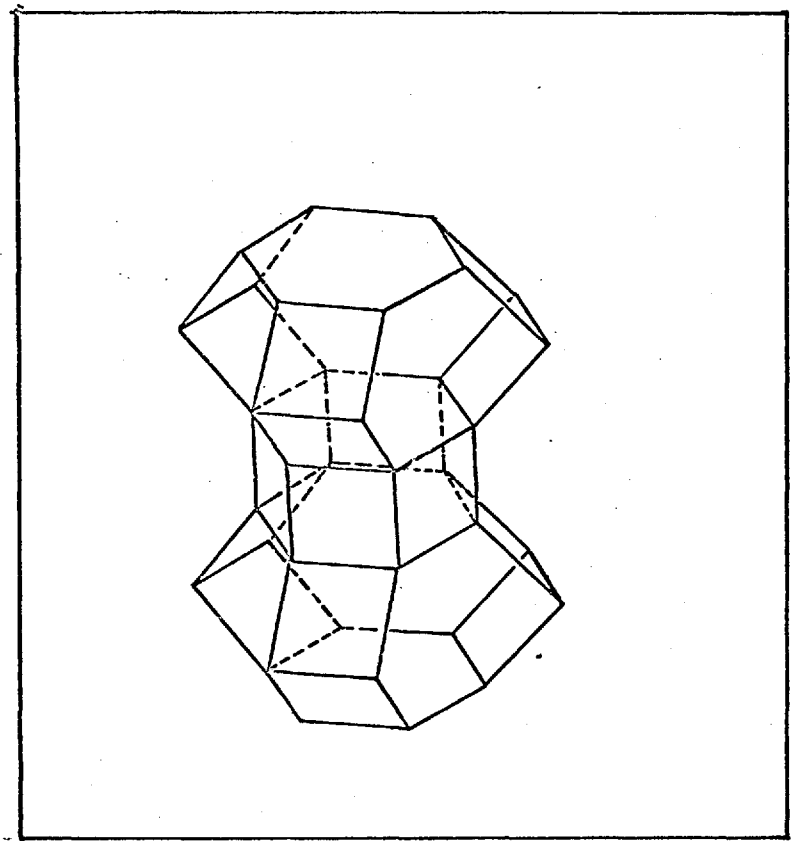

Fig 2a
Chain in
Zeolite L and
Offretite

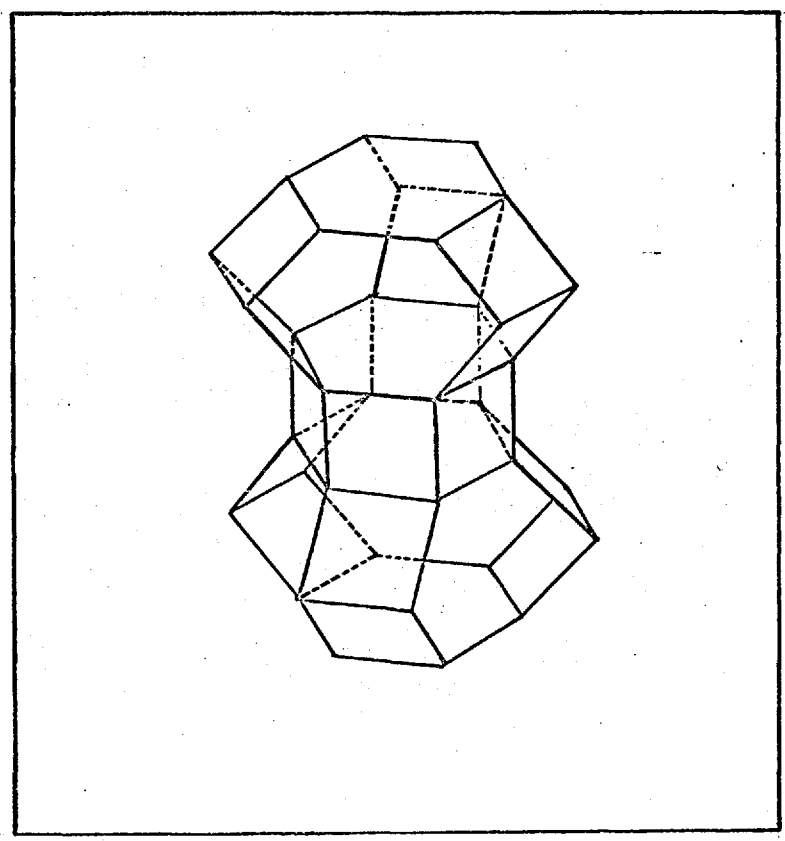

Fig 2b
Chain in
Erionite

on its axis through 60° relative to the previous cage. (Fig. 2b).

In zeolite L the chains are joined together to form planar twelve membered rings, which circumscribe wide channels running in the c direction with "entrances" of 7.1-7.8Å and largest free diameters of 13Å (Figs. 3a and 4a). The joining of the chains in erionite and offretite does not result in planar twelve membered rings. Distorted twelve membered rings are formed with a maximum free diameter of 6.3Å. In offretite these twelve membered rings form cylindrical channels, parallel to the c direction (Fig. 3b and 4b). In erionite they circumscribe only cavities down the c direction (Fig. 1c) with the above diameter and with a length of 15.12Å. The cavities are capped at the top and bottom by six membered rings (Fig. 3c and 4c) and are joined together by eight membered rings with free diameter 3.5Å. Apertures of eight membered rings exist also in offretite. They give access from the main channel to side pockets (Fig. 1b), which consist of gmelinite cages(6).

From the above description and figures it is easy to visualise not only the identical chains (see p. 15) parallel to the c direction in zeolite L and offretite, but also identical layers, perpendicular to c direction, in erionite and offretite (Fig. 4b and 4c). This exact resemblance of particular domains of the structures of zeolite L, offretite and erionite has an important effect on their crystallisation.

From the above a similarity could be deduced also for the type and magnitude of the free volumes of the three zeolites. The channel systems in zeolite L and offretite are fairly similar (Fig. 3a and 3b), while erionite and offretite possess exactly the same total free volumes, but these are distributed in different types of voids (Fig. 1b,c

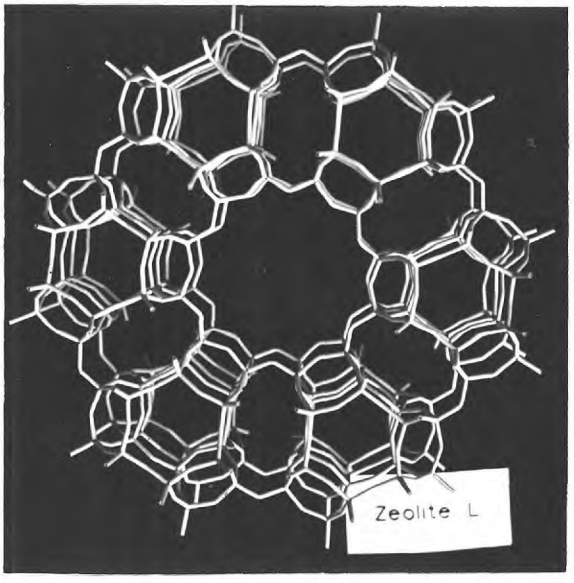

a

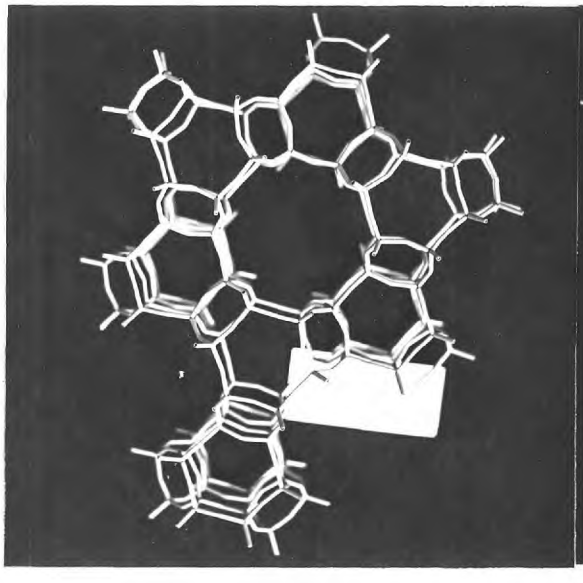

b

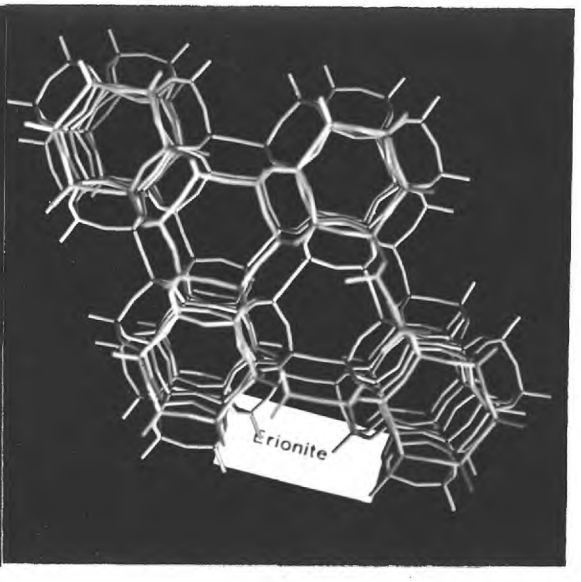

c

Figs. 3a, b and c. The structures viewed down c-axis.

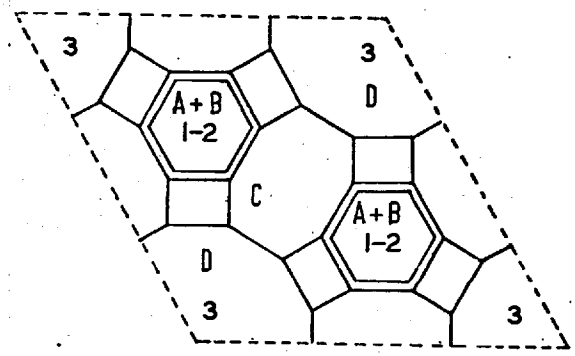

a. Zeolite L.

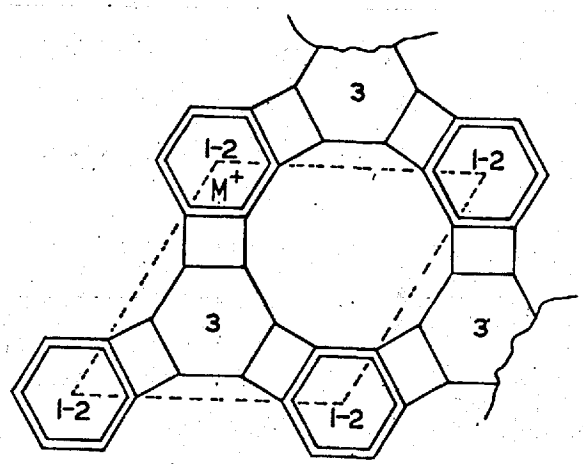

b. Offretite.

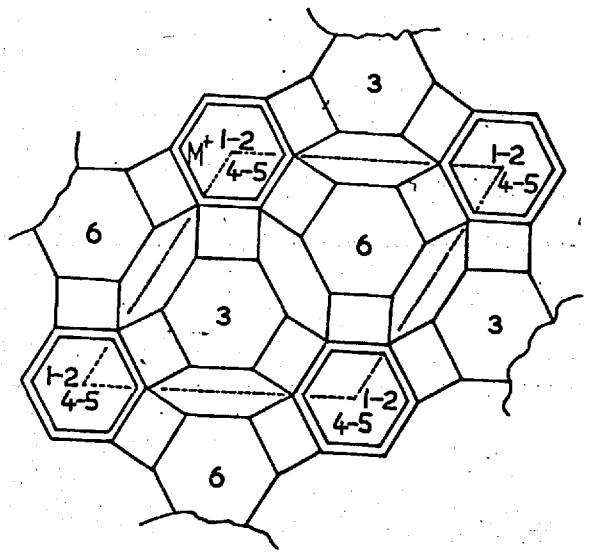

c. Erionite.

Figs. 4a, b and c. c projection. Unit Cells.

and 3b,c). Since it is in the free volumes within the structure that the adsorption takes place in case of zeolites, this resemblance is of great importance. It is directly connected with the adsorption behaviour of zeolite L, offretite and erionite. Thus, adsorption of large molecules should be common for zeolite L and offretite. Adsorption of large molecules will be limited in erionite by the eight membered rings, therefore its behaviour will be drastically different from that of offretite in such cases. Conversely, for small molecules, penetrating the eight membered rings, the adsorption behaviour of erionite and offretite will be closely comparable.

However, the type and magnitude of the free volumes in a structure is a dominating, but not the only factor which controls the adsorption behaviour of a given zeolite. The total chemical composition, the nature and position of cations could greatly alter the properties, exhibited by the same zeolite. This makes it desirable to have all possible information, including the above, when studying adsorption.

The positions of the cations in zeolite L are known(11). The cations are accommodated at four different types of sites named in Fig. 4a and Table 2 as sites A, B, C and D. Site A is located in the middle of the hexagonal prism;

TABLE 2*

Cation	Site	Fractional Occupancy.	x	y	z
Na,K	A	0.7	1/3	2/3	0
K(1)	B	1.0	1/3	2/3	1/2
K(2)	C	0.9	0	1/2	1/2
Na(2)	D	0.6	0	0.303	0

* From the data of Table 1 in (11).

site B - in the middle of the cancrinite cage; site C - midway between the centres of two adjacent cancrinite cavities; and site D - in the main channel, in front of the midway position.

The positions of the cations in erionite and offretite have still not been determined with certainty. The first proposal (13) had assumed that the cations are "situated with random distribution on the principal axes of the cavities". That assumption was later disregarded and one cation position was located in the middle of the cancrinite cages(14) (Fig. 4b and c). In the present research this question is further elaborated on the basis of ion-exchange and adsorption data.

2. Literature survey on Zeolite L, Erionite and Offretite

Synthesis of zeolite L was first announced by Breck and Acara in 1962(15). Formulae were given for the preparation of the zeolite at 100°C from K - and (K,Na)-alumosilicate gels. From the original K- and (K,Na)- forms of zeolite L, those containing Ba, Ca, Ce, Mg, Sr and Zn were prepared for which 20 to 70% of ion-exchange was reported. A considerable adsorption of water, rare gases, benzene, iso-butane, thiophene, cyclohexane, p-xylene and m-xylene was observed, but no detailed adsorption study was attempted.

In 1964 Barrer and Marshall(16) had obtained from Ba containing aluminosilicate gels crystals termed Ba-G which sorbed oxygen, and were subsequently found to resemble zeolite L. However at that time the sample was not further investigated.

In a series of syntheses from K- and (K,Na)-aluminosilicate gels, Zdanov also obtained zeolite L.(17)

Barrer and Lee(18) investigated adsorption of n-paraffin

(C_1-C_7), iso-butane, benzene and cyclohexane on the zeolite and found properties which indicated a fluid character in the sorbed phases but with some physical restriction beyond that observed in the bulk liquids. The sample used was identical with L-IC (see p. 68).

Barrer and Kanellopoulos(19) established that sorption of ammonia and "ammonium chloride" vapour on the K form of zeolite L was reversible and that sorption from the mixture of ammonia and hydrogen chloride, obtained from the dissociated ammonium chloride, was several times higher than from the pure gases. Decationated forms of zeolite L were prepared and their thermal stability and the adsorption of ammonia were investigated.

Natural erionite was first described by Eakle in 1898(20) and natural offretite by Gonnard in 1890(21). Erionite is abundant in nature(22), but a few years ago it was still considered as a very rare mineral(13). Offretite is found in Montbrison (France)(21), in the Palau Islands and in the Caroline Islands(23).

The problem of the identity of the two zeolites is of interest. After comparing the X-ray powder patterns Hey and Fejer(24) stated that offretite and erionite are identical. In 1967 Bennet and Gard(12), on the basis of electron diffraction and X-ray single crystal studies, established that offretite has a structure which is distinct from that of erionite (see p.13).

In agreement with Bennet's and Gard's work, Harada(25) drew attention to the difference between the AABAAC type of stacking of layers for erionite and the ABC stacking for offretite.

Recently, Sheppard and Gude(26) showed that offretite characteristically has indices of refraction that are higher than those for erionite and in addition that offretite has a

negative optical sign, while erionite has a positive one. Those facts can be used as auxiliary means for distinguishing between the two zeolites.

Eberly found(27) that long chain n-paraffins above n-heptane were hardly sorbed by Li, Na, Ca, Sr and K forms of natural erionite and that nitrogen was not sorbed by K-erionite at -196°C. Peterson et al(28), on the other hand, found a considerable uptake even of C_{14}, and sorption of nitrogen at -78°C on a sample rich in K. Both studies reported a maximum degree of ion exchange of 50%. Peterson et al(28) noticed differences in sorption properties among the eight samples investigated.

Barrer and Peterson(29) calculated interaction potentials between n-paraffins and the oxygen atoms of eight membered rings in erionite, chabazite and zeolite 5A. In accord with the calculated values they found for one of the samples investigated that the rates of adsorption of n-paraffins were in the order: 5A > chabazite > erionite. However, a second sample of erionite showed rates of adsorption nearly the same as those in 5A.

Eberly found(30) that adsorption rates of n-paraffins (C_5-C_8) on erionite decreased markedly with the molecular weight at the paraffin, while on 5A these rates remained nearly constant.

According to Ames, natural erionite showed good cation selectivity(31) and a replacement series independent of the hydration state of the entering cations(32).

Adsorption and ion-exchange studies on natural offretite have not been published so far.

In 1960 Breck and Acara patented a synthesis of zeolite T(33) which was believed to be a synthetic erionite. The zeolite is prepared from (K,Na)-containing aluminosilicate

gels. It was found that only molecules with critical dimensions under 5Å can enter the internal cavities.

Shortly after the above patent, a series (34,35,36) of similar syntheses using different starting materials were published. The products were described as identical with erionite and zeolite T.

Bennet and Gard(12) showed that it is not correct to identify zeolite T with erionite, but with a disordered intergrowth of erionite and offretite.

Before this finding of Bennet and Gard, several works were published on ion-exchange(37,38) and adsorption(39,40) properties of synthetic samples considered as erionite. Shirinskaya et al(37) prepared crystals enriched in Ni, Co, Zn, Cd, Ca, Sr, Ba, Mg and Pb and found degrees of ion exchange between 40 and 67%; and also a reversible exchange back into the original (K,Na)- forms, with the exception the phases enriched in Pb, Ba and Sr. The stabilities of the crystal lattices of the latter three forms were investigated(38) by X-ray powder method and water adsorption. No damage of the structures was observed. Zdanov and Novikov(40) prepared decationated forms by acid treatment and found that the water sorption on these products and on the NH_4^+ form depended on the temperature of outgassing.

Sherry carried out an ion-exchange study(41) on zeolite T after Bennet and Gard's publication. He considered the species as almost pure offretite and found 75% maximum ion-exchange and a strong preference towards cations of large size with the exception of K^+ and NH_4^+.

Further relevant details from the above papers will be discussed at appropriate places in Chapter 3.

3. Aim of the present work

The principal aim of the present work is to study the sorption properties of zeolite L, using rare gases as sorbates. A series of ion-exchanged forms was prepared to investigate the dependence of the properties of zeolite L upon the cation composition. Rare gases were chosen for this purpose, because of the simplicity of their molecules. Conclusions drawn from such systems can give basic information about the behaviour of both polar and non-polar sorbates(42).

The thermostabilities of different ion-exchanged forms of zeolite L were also of interest in this research. In connection with this, the alteration of the structures during dehydration was examined and attempts were made to locate cation positions in the hydrated and the dehydrated state for one sample.

The conditions of syntheses of zeolite L were a further object of this work, both from a practical and theoretical point of view. The practical interest arose from the need to prepare a pure and well crystallized phase of zeolite L. The theoretical one was connected with the importance of the SBU in the cases of zeolite co-crystallization.

Zeolite L is a new sorbent with a variety of possible applications(15). Previous work on the zeolite has been far from sufficient and therefore a further investigation is timely.

As zeolites erionite and offretite are closely related to zeolite L, it was of interest to compare the properties of these three zeolites. The information on adsorption properties of erionite and offretite in the literature is quite scanty and there is much contradiction due mainly to misidentification. Thus it was desirable to combine research

on L with at least partial investigation of the two other zeolites. For this purpose a few ion-exchanged forms of erionite and offretite were prepared and investigated. Decationated forms of the three zeolites were also examined, as were molecular sieve properties of erionite towards rare gases. The conditions of syntheses of erionite and offretite were likewise of interest both practically and theoretically.

CHAPTER I

THEORETICAL BACKGROUND AND GENERAL INFORMATION

1. DIFFRACTION METHODS FOR STRUCTURE INVESTIGATIONS

1.1 X-RAY DIFFRACTION

1.1.1 Crystal symmetry and application of the X-ray method

Atoms, ions and molecules in solids usually pack regularly with a long range order. Thus, any crystal may be considered as being built by periodic repetition in three dimensions of a certain atomic arrangement termed a unit cell. A full description of a crystal structure requires a determination of the space group(43), the size and the shape of the unit cell and the position of all atoms in the unit cell. The elaborate and sophisticated way of achieving this by diffraction of X-rays from a single crystal or crystalline powder is based on two main facts: 1) The specific periodicity of a given crystal determines (according to Bragg's law(43)) a unique diffraction pattern. 2) The nature and position of the atoms in the unit cell determine the intensities of the lines (powder methods) or spots (single crystal diffraction) of the pattern.

For the purpose of the present work, certain aspects of the above problem will be dealt with briefly. They are indexing of X-ray powder patterns; calculation of intensities of the diffracted lines; and Fourier synthesis.

1.1.2 Indexing of X-ray powder pattern

Indexing of an X-ray powder pattern consists of the assignment of Miller indices(43) to each line of the pattern. This is done by relating the directly measured angles $\Theta_{hk\ell}$ to the indices ($hk\ell$) through the squared reciprocal lattice vector r^{*2}(43). The latter is often called, in practice, $Q_{hk\ell}$:

$$Q_{hk\ell} = r^{*2} = \frac{1}{d^2_{hk\ell}} = \frac{4\sin^2\theta_{hk\ell}}{\lambda^2} \quad \ldots\ (1.1\text{-}1)$$

$$r^{*2} = h^2a^{*2} + k^2b^{*2} + \ell^2c^{*2} + 2hka^*b^*\cos\gamma^* + 2h\ell a^*c^*\cos\beta^* + 2k\ell b^*c^*\cos\alpha^* \quad \ldots\ (1.1\text{-}2)$$

$(hk\ell)$ Miller indices. Give the coordinates of a point in the reciprocal space.

$d_{hk\ell}$ spacing between planes $(hk\ell)$

$\theta_{hk\ell}$ Bragg angle(43).

λ wavelength of X-ray.

a^*, b^* and c^* lengths of edges of the reciprocal lattice.

α^*, β^* and γ^* interaxial angles of the reciprocal lattice unit cell.

In the case of a hexagonal lattice, the above equation is simplified to

$$Q_{hk\ell} = (h^2 + hk + k^2)a^{*2} + \ell^2c^{*2} = N\,a^{*2} + \ell^2c^* \quad \ldots\ (1.1\text{-}3)$$

N = 1, 3, 4, 7 ... etc. ℓ^2 = 1, 4, 9, 16 ... etc.

Although the quoting of d-values and the relative intensities is alone an accepted method for characterizing a sample (ASTM system), an indexed pattern provides much fuller information. This makes it possible to estimate a change in the magnitude of the lattice parameters or to interpret an alteration in the intensity of certain lines.

1.1.3 Scattering of X-rays by a unit cell; the structure factor and computation of intensities

The efficiency of scattering of X-rays by an atom is known as the atomic scattering factor - f_j, and it is

expressed as

$$f_j = \frac{A_o}{A_c} \qquad \ldots\ (1.1\text{-}4)$$

A_o - full scattering power of the atom.
A_c - scattering power of a single, free electron.

Whereas the scattering from an atom depends on the number and distribution of its electrons, the scattering from a unit cell depends on its total atomic composition and arrangement. The resulting scattering of a unit cell is expressed by a complex quantity F - a structure factor(44)

$$F_{hk\ell} = \sum_{j=1}^{J} f_j e^{2\pi i(hx_j + ky_i + \ell z_j)} \qquad \ldots\ (1.1\text{-}5)$$

J - number of atoms in a unit cell .
f_i - atomic scattering factor.
x_j, y_j and z_j - fractional coordinates of an atom in the unit cell.
$(hk\ell)$ - Miller indices.

The structure factor is often expressed in terms of its real and imaginary components:

$$F_{hk\ell} = A + iB \qquad \ldots\ (1.1\text{-}6)$$
$$A = \sum f_j \cos 2\pi (hx_j + ky_j + \ell z_j) \qquad \ldots\ (1.1\text{-}6a)$$
$$B = \sum f_j \sin 2\pi (hx_j + ky_j + \ell z_j) \qquad \ldots\ (1.1\text{-}6b)$$

The magnitude of the structure factor is called the structure amplitude $|F_{hkl}|$:

$$|F_{hk\ell}| = \sqrt{A^2 + B^2} \qquad \ldots\ (1.1\text{-}7)$$

The intensity of scattering is directly related to $|F_{hk\ell}|^2$. For the powder method the relation is:

$$I^{cal}_{hk\ell} = I_o \sum L_p M_j \left| s F_{hk\ell} \right|^2 \quad \ldots\ (1.1\text{-}8)$$

I_o - intensity of the direct X-ray beam.

M_j - multiplicity factor of reflecting planes, which is given by the number of planes in a crystal which contribute to the same diffraction arc.

L_p - Lorentz polarization factors(44) $L_p = \frac{1+\cos 2\theta}{\sin\theta\cos\theta}$, where θ is the Bragg angle.

s - scale factor; a constant having the same value for reflections recorded on one photograph.

1.1.4 Fourier syntheses

As the atoms are arranged in a periodic fashion in space, the electron density also varies periodically through the crystal. The structure could be deduced, or structural alteration found, from the positions of peaks of the electron density map. The three dimensional electron density function $\varphi_{(xyz)}$ is the Fourier transform of the sum of all the structure factors $F_{hk\ell}$ with their phases.

$$\varphi_{(xyz)} = \frac{1}{V} \sum_h \sum_k \sum_\ell F_{hk\ell} \exp(-2\pi i(hx + ky + \ell z)) \quad \ldots\ (1.1\text{-}9$$

V - volume of the unit cell.
The other quantities are as defined previously.

The summation is to be made over all possible values of $hk\ell$ and requires knowledge of the structure factors and their phase angles(44). The last are not experimentally obtainable(44), so the Fourier syntheses are usually carried out with gradual refinement of the phases on the basis of a number of methods to estimate them or by use of the trial and error methods.

With the calculated values of the Fourier transforms(1.1-9), two types of Fourier maps are computed: maps based on the calculated values of the structure factor, F_c, and maps based on the "observed" values, F_o, of the structure factor. From the differences of the corresponding $\varrho_{(xyz)}$ values in the above maps, difference Fourier maps are produced, which "judge" the fit between the computed structure and the real one. The quality of the fit is usually expressed by the reliability factors:

$$R_{(F)} = \left[\sum \left| (\text{"}F_{obs}\text{"} - |F_{cal}|) \right| \right] / \sum \text{"}F_{obs}\text{"} \quad \ldots (1.1\text{-}10)$$

$$R_{(I)} = \left[\sum \left| (I_{obs} - I_{cal}) \right| \right] / \sum I_{obs} \quad \ldots (1.1\text{-}11)$$

$R_{(F)}$ - reliability factor based on the structure factor.
$R_{(I)}$ - reliability factor based on intensities.

1.2 ELECTRON DIFFRACTION

1.2.1 Specific features of diffraction of electrons by crystals. Application.

The general principles which govern X-ray and electron diffraction*[1] are broadly similar. There are, however, a number of important differences which enable the results from the two methods to complement each other(45,46). A specific characteristic of the electron beam*[2] is its short wavelength which determines most of the practical and theoretical peculiarities of ED. Some of them are considered below.

The electron beams interact far more readily with matter than X-rays, and this makes it necessary to use in practice very small single crystals of 500Å up to 1000Å edge. Thus, the ED is a useful method for studying fine crystalline materials, from which a single crystal large enough for X-ray diffraction cannot be selected. This is often the situation in the case of synthetic zeolites.

The short wavelength has its theoretical importance in explaining the formation of ED patterns from single crystals(45,47) and their resemblance to the X-ray ones from the precession camera(48). It is also the reason for extremely low limits of the Bragg angles in ED. This last result follows from a direct application of Bragg's law:

Example: $\lambda = 0.042\text{Å}$ at V = 80kv.

$$d_{hk\ell} = 0.5\text{Å}$$

$$\sin\theta \simeq \theta_{hk\ell} = \frac{\lambda}{2d} = 3^{\circ}$$

---

*1 Electron diffraction will be abbreviated to ED.

*2 Fast electrons(45) are under consideration. In the text the term "electrons" will refer only to fast ones.

Many formula simplifications(45,47) and experimental techniques(45,46) are based on the small Bragg angles in case of ED.

A few important applications of ED are identification of minority species of crystals in mixtures; elucidation of the unit cell and thus the providing of data for indexing X-ray powder patterns; examination of selected areas from a crystal agglomerate; and correlation of the morphology of a crystal with its unit cell. Some of the above cases will be elaborated in the text.

1.2.2 Electron diffraction from polycrystalline materials. Calibration of the electron microscope.

ED from polycrystalline materials is an analogue of the Debye-Scherrer method, but the short wavelength of the electron beam makes it possible to derive simpler relationships, which are the basis for solving ED patterns from polycrystalline materials and also for calibration of the electron microscope.

From the diagram presented in Fig. 5 it follows that:

$$tg2\theta_{hk\ell} = \frac{R}{L} \qquad \ldots (1.2\text{-}1)$$

R - radius of a reflection ring from (h,k,ℓ) planes.
L - "length" between the sample and the film.

Combining Bragg's law with the above equation and taking into account the limits of Bragg angles (see p. 32) one could obtain the following expression for the interplanar distances ($d_{hk\ell}$)

$$d_{hk\ell} = \frac{\lambda L}{R} \qquad \ldots (1.2\text{-}2)$$

λ - wavelength of the electron beam at a given voltage.

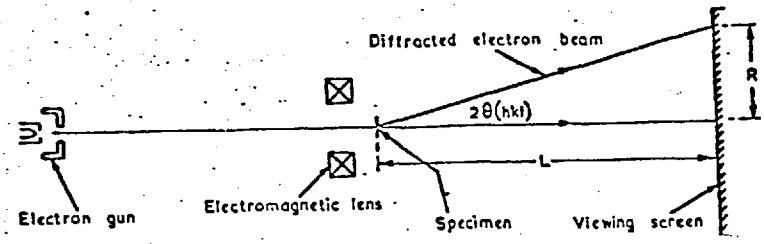

Fig. 5 Basic elements of electron diffraction camera(47).

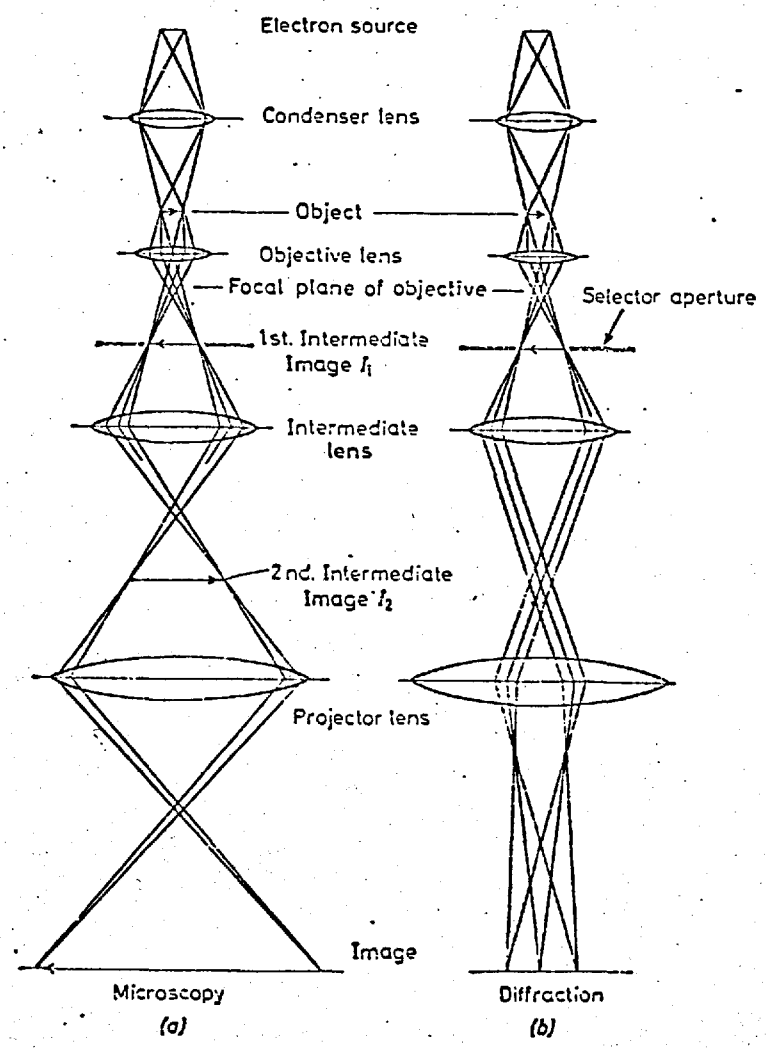

Fig. 6 Ray paths in the electron microscope
(a) under microscopy conditions
(b) diffraction conditions(47).

The "length" L, as described above, is in fact a fictitious length which depends upon the lens magnification. That becomes clear from the optical ray diagrams (Fig. 6), presenting an electron microscope in use for high magnification and for ED.

It is usual to refer to λL as a diffraction constant of the electron microscope at a given voltage. The values of λL must be determined for each standard set of lens setting used. That, in practice, is done mainly by the use of a standard of Au and comprises the calibration of the electron microscope.

1.2.3 Electron diffraction from single crystals. Formation and solving of the patterns.

The theoretical importance of the short wavelength of the electron beam, mentioned above, becomes apparent when one considers the conditions for reflection in reciprocal space(43). The low values of λ cause the radius of the sphere of reflection to be considerably larger (27Å^{-1} at 100kv) compared with the distance between the neighbouring reciprocal lattice points. It is, therefore, adequate for many purposes to consider that the sphere of reflection approximates to a plane(47). Thus, if a plane of the reciprocal lattice is tangential to the reflecting sphere, a cross-grating pattern will be formed and on the photographic film an enlarged projection of a plane of the reciprocal lattice will be observed. (Fig. 7).

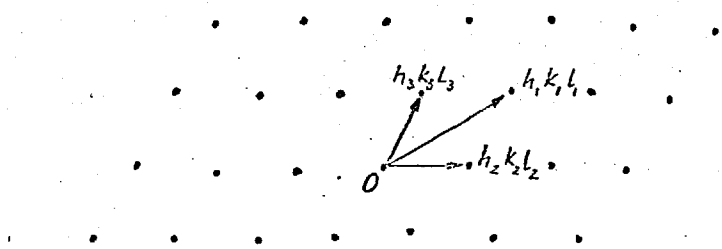

Fig. 7.

In order to derive the formulae used for solving ED patterns, let us consider ED from a single row of atoms. In Fig. 8(49) such a case is presented. The electron beam falls at an angle ξ_o, while the diffracted beam is propagated at an angle ξ. From the above figure it follows that:

$$\varphi = \pi - \xi_o - \xi \qquad \ldots\ (1.2\text{-}3)$$

φ - angle between incident and diffracted beam, equal to double the Bragg angle.

The Laue condition(50) could be applied to the above case:

$$h\lambda = a\cos\xi_o + a\cos\xi \qquad \ldots\ (1.2\text{-}4)$$

λ - wavelength of the electron beam.
h - order of reflection.
a - distance of separation between the atoms.

If the equations (1.2-3) and (1.2-4) are combined and the small value of the Bragg angle is taken into account, it follows that:

$$\varphi = \frac{h\lambda}{a\sin\xi_o} \qquad \ldots\ (1.2\text{-}5)$$

Further consideration of Fig. 8 gives

$$tg\varphi = \frac{S}{L} \qquad \ldots\ (1.2\text{-}6)$$

which helps to transform equation (1.2-5) to one of the final relationships used for solving ED patterns of single crystals.

$$s = \frac{h\lambda L}{a\sin\xi_o} \qquad \ldots\ (1.2\text{-}7)$$

s - separation distance between diffraction bands.
λL - diffraction constant of the electron microscope.

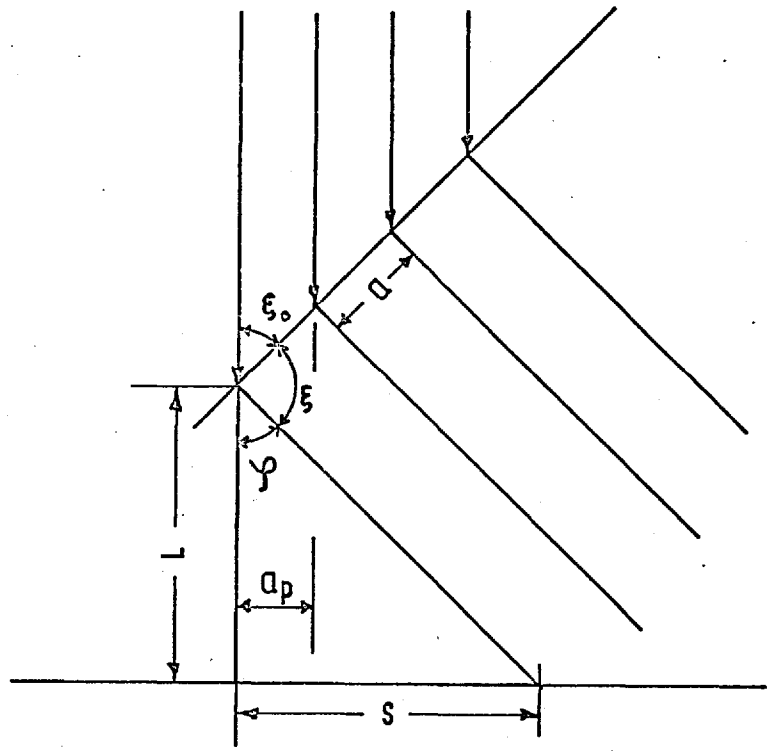

Fig 8

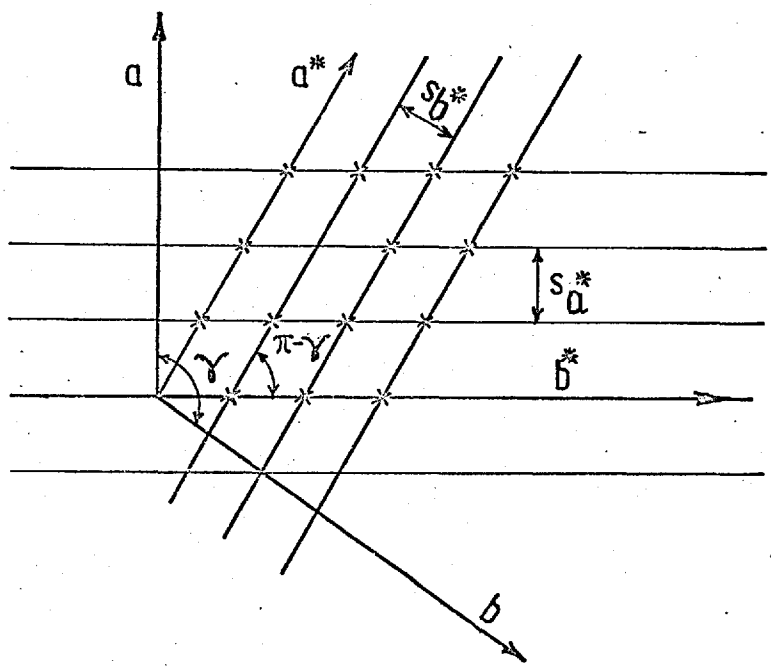

Fig 9

When the electron beam is perpendicular to a row, equation (1.2-7) is simplified to:

$$s = \frac{h\lambda L}{a} \qquad \ldots (1.2\text{-}8)$$

If two rows of atoms are considered, and the beam is perpendicular to both, the separation distances of the two diffraction bands (Fig. 9) will be expressed as follows:

$$s_{a^*} = \frac{\lambda L}{a} \qquad s_{b^*} = \frac{\lambda L}{b} \qquad \ldots (1.2\text{-}9)$$

s_{a^*} - separation of the rows along a* direction.
s_{b^*} - separation of the rows along b* direction.

The relation between the reciprocal lattice constants $\underline{a}^*$ and $\underline{b}^*$ and the real lattice constants $\underline{a}$ and $\underline{b}$ follows from equation (1.2-9) and simple geometrical consideration of Fig. 9

$$s_{a^*} = a^*\sin(\pi-\gamma) = \frac{\lambda L}{a} \text{ resp. } b^*\sin(\pi-\gamma) = \frac{\lambda L}{b} = s_{b^*} \qquad \ldots (1.2\text{-}10)$$

γ - angle between lattice directions $\underline{a}$ and $\underline{b}$.

As the reciprocal lattice constants are measured directly from the ED pattern, equation (1.2-10) makes it possible to estimate the constants of the unit cell.

Depending on the orientation of the crystal towards the electron beam, corresponding relationships have been worked out(49). In the case of arbitrary orientation the reciprocal lattice vector r* (see p. 28) for a given point of the pattern can be measured and compared with the theoretical value.

1.2.4 Stacking faults

These faults arise from disordered stacking of layers in a crystal structure. The presence of such faults can be proved by an examination of the electron- or X-ray diffraction patterns of a single crystal. An elongation of the spots is observed, sometimes leading to streaking, in the direction of the faulting. This behaviour is found because the spot size is determined by the thickness of the crystal normal to the plane responsible for the reflection. This dependence is expressed by the following relation:

$$B = \frac{\lambda L}{t} \qquad \ldots \quad (1.2\text{-}11)$$

B - width of the spot.

t - thickness defined as above.

λL - diffraction constant of the electron microscope.

If we apply the above equation to a faulted crystal, we must not use the external thickness, but the thickness of the unfaulted region. In the case of a heavily faulted crystal, these regions will be thin and the spots correspondingly elongated. In the limiting case the spots will be drawn out into streaks.

If we considered a structure which is built by stacking of layers, the thickness of the unfaulted regions will be determined by the number of consecutive, correctly stacked layers. The lower this number, the thinner the region and the longer the spots. On the other hand, when the layers are all packed correctly on top of each other, an unfaulted crystal of a great thickness is built up and the streaks shorten so that only small spots exist.

Stacking faults are more readily detected by electron- than by X-ray diffraction from a single crystal, because of the smaller single crystals used in the former technique.

2. MODIFICATION AND SYNTHESIS OF ZEOLITES

2.1 MODIFICATION OF ZEOLITES

2.1.1 Modification by ion-exchange and decationation

A simple way of modification of zeolites is by ion-exchange. Cations are always present in the zeolite voids in number electrochemically equivalent to the negative framework charge whereas water and other neutral molecules are only casual visitors(51). The nature, size, density and position of the cations are of importance because they alter respectively the polarity of the structure, the actual free volume within it, the size of the apertures and, to a considerable extent, the stability of the structure. Thus, the cations in a given zeolite influence both its molecular sieving properties and heats of adsorption.

Cations located in or near apertures or windows giving access to intracrystalline cavities will, by obstructing the windows, reduce rates of intracrystalline diffusion of molecules, especially when the windows are of small or moderate size - for example, when they are eight membered rings. Cations which are within the cavities and channels attract polar guest molecules in particular and will share space with them and thus will influence both initial isosteric heats and the adsorption capacity. On the other hand cations in small subsidiary polyhedral cavities, such as hexagonal prisms, cancrinite cages and small side pockets inaccessible to guest molecules will have no direct contact with these molecules and will effect mainly (if not solely) the stability of the structure. Usually only the cations in the first two kinds of position readily undergo ion-exchange at room temperature and moderate concentrations. Thus, their number per unit cell determines the degree of ion-exchange under these conditions.

An exchange of cations of the same valency but different size ($K^+ \rightleftarrows Cs^+$) alters the fraction of the free volume occupied by cations, while the density of cations remains constant. An exchange of cations of different valency, but of comparable size ($2K^+ \rightleftarrows Ba^{2+}$) produces the opposite result. When the difference in valency is greater ($3K^+ \rightleftarrows La^{3+}$), the density of the cations is further altered. All these exchanges will also modify the local electrostatic field in the structure.

The importance of cations has led to various attempts, mainly by X-ray diffraction study, to locate both cation sites and degree of occupation of each kind of site. However, cation positions cannot be regarded as established with the same certainty as those of the framework O, Aℓ and Si(6). Thermal and positional disorder, partial occupancy of sites, twinning and other imperfections, and frequently lack of crystals big enough for single crystal X-ray diffraction, have usually hampered the investigations. Considerable success has been achieved in the case of less porous zeolites like natrolite(52) and gismondite(53), where there is only one kind of fully occupied cation position. For zeolites with more open structures the problem is far more difficult. More than one type of cation site may exist(54,55) and often the sites are only partially occupied. Furthermore, both the number and positions of cation sites depend on temperature and degree of dehydration(6).

Exchange to the hydrogen zeolites (decationation) brings a specific modification of significance in catalysis by zeolites. Treatment by dilute mineral acid is used for decationation of highly siliceous zeolites(56), while for all others, the decationated forms are obtained by heating the NH_4-zeolite:

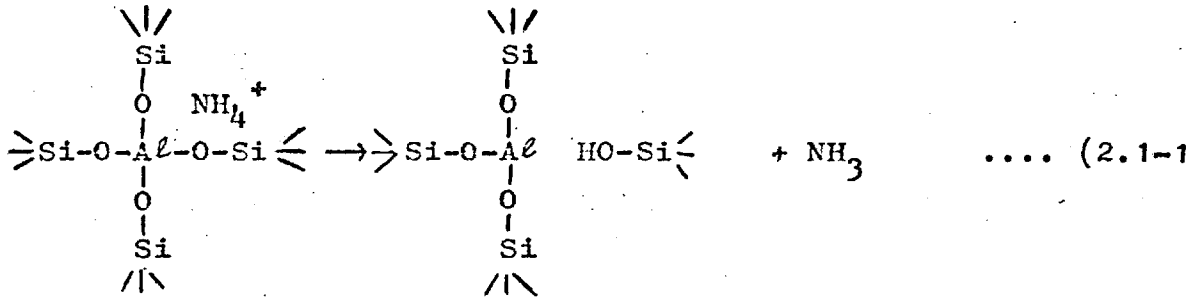

Decationated forms are usually reported as less stable to heating than the parent forms, containing Na^{+}, Ca^{++}, etc. (57,58). Completely opposite observations were recently announced(59), claiming stability of decationised zeolite Y up to 1000°C. An explanation of this effect was offered(60), based on the role of the chemical water and formation of cationic aluminium:

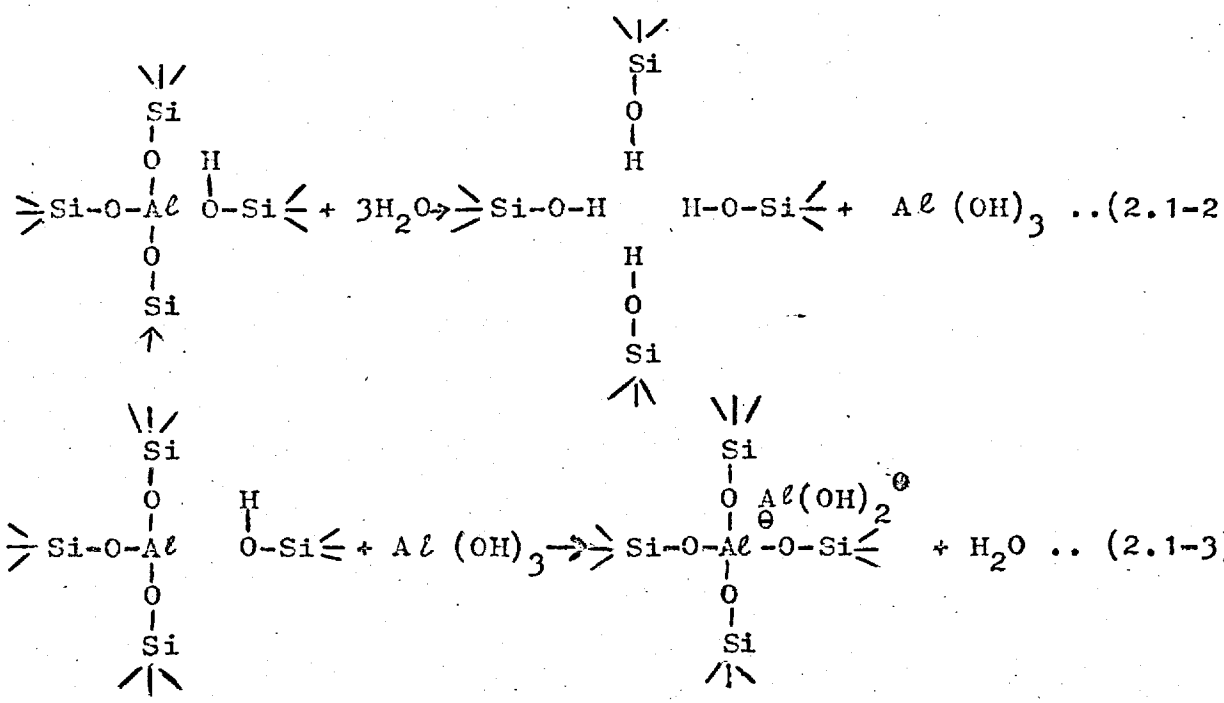

The above mechanism in fact treats a case where decationation is followed by dealumination(61). However, if this mechanism is correct any technique in which a little of the chemical water is kept in the system during the

heating process, might be favourable for obtaining a stable product.

A partial decationation of zeolites can occur when they are treated with water(15,62). It was found(62) that such hydrolysis depends strictly on the Si/Aℓ ratio in the zeolite, regardless of the nature of the zeolite. The higher the ratio, the less the hydrolysis.

Zeolites are fairly stable towards alkali. Nevertheless, treatment by alkali solution can lead to a partial dissolving of the zeolite and in many cases a recrystallisation into another structure has been observed(62). An impressive example of that is the formation of basic sodalite from NaA, after treatment of the latter with 10% NaOH(64). Similar undesirable "modifications" should be always borne in mind while carrying out an ordinary ion-exchange in strongly alkaline solutions.

2.1.2 Zeolite modification by pre-sorbing polar molecules

A quick and reversible modification of certain zeolites has been achieved by presorption, at low temperatures, of small polar molecules like NH_3, H_2O, CH_3NH_2. Such molecules, strongly held and immobile at low temperatures, can reduce the diffusion coefficients of other non-polar sorbates within the crystals(65) progressively and selectively. The effect was found(65) to depend on the time of cooling the sample after presorption, presumably because fast cooling rates result in a different, non-equilibrium distribution of the presorbed molecules.

Similar modifications can occur when a zeolite is partially dehydrated due to the residual water molecules. The wide and often split endothermal peaks in the DTA curves of zeolites(66,67) indicate that one may easily leave residual water.

2.1.3 Thermal stability of zeolites

The chemical reactivity of zeolites towards water at high temperatures makes them liable to damage during the activation(68). Realization of this led to an early appreciation of the importance of raising the temperature slowly during dehydration, in order to prevent sintering. Recent information on the migration of cations during heating and dehydration(6) makes it necessary to consider also the rate of cooling the sample.

Zeolites with high Si/Al ratio are known to be of high thermal stability(66). It has also been pointed out(66,69) that the nature of the cations in the structure is of importance. Poor thermal stability has been reported both for polyvalent heavy cations like Cu, Co, Fe, Ni, etc. (69,70) and for cations with small radius, such as Li(70). A generalisation, however, is hardly possible, as for different structures the cation which improves thermal stability can be different.

The degree of ion-exchange also effects the stability and the optimum degree of ion-exchange is different for different cations(69).

The thermal stability of zeolites can be influenced by the sorbate, such as gaseous hydrogen halides or water. In the case of such sorbates, damage can occur after a single adsorption/desorption cycle (110).

Thermal stability can be influenced by the degree of washing of the zeolite. It has been found(73) that the stability of NaX containing an excess of alkali is poorer than that of NaX washed free from alkali.

The dispersal of synthetically obtained zeolites considerably affects their stability(74). Usually, the higher the dispersal, the poorer the stability.

2.2 SYNTHESES OF ZEOLITES

2.2.1 Factors governing zeolite crystallisation

In nature zeolites are formed under alkaline, hydrothermal conditions(1). For syntheses of zeolites in the laboratory natural processes are usually closely imitated(75). Zeolite crystallisation could lead to any one of a range of products, and kinetic as well as thermodynamic factors determine the final product. Important factors include the composition of the reaction mixture, and the temperature and pressure, but many examples could be given(75,76) to show that the type of product obtained depends also on the state and origin of the raw materials used, on the individual steps in the whole procedure and on the length of time for crystallisation. Some of the above factors may be considered more fully. For a particular synthesis, one usually restricts the ratio of Si and Al , water content, pH and nature of cations. Some authors emphasise the importance of each of these factors in the order in which they are listed above.(75,77) The importance of cation-type is illustrated by the formation of zeolite A from Na-containing mixtures and of zeolite F from corresponding K-containing mixtures(78).

As far as the individual steps of the process are concerned, the most important are the order of introducing the ingredients of the mixture (15), the manner and the time of their mixing (33), the interval between mixing of the components and processing them, i.e. time of ageing (77), time of heating (75), and time of keeping the crystals in contact with the mother liquor(78).

Long-term emperical work has suggested the following important conditions for zeolite syntheses: reactive starting materials, such as co-precipitated gels; a

relatively high pH; low temperature hydrothermal conditions at saturated water vapour pressure; and a high degree of supersaturation of the components in the gel, which leads to nucleation of a very large number of small crystals(78).

2.2.2 Mechanism of zeolite crystallisation

Synthetic zeolites are often not true equilibrium phases because where highly reactive amorphous reactants are used - which is the case with the mixtures for zeolite syntheses - metastable ensembles may easily form and persist. The Ostwald step rule(79) has a wide application here.

The actual 'routes' through which the zeolite nucleation goes are not yet clear. It seems unlikely that the growth of complex alumosilicates crystals proceeds by capture of single SiO_4^{4-} and $A\ell O_4^{5-}$ tetrahedral ions and cations by the developing lattice. Barrer considers(75) that a condensation polymerisation of polygonals or polyhedral ions is a more probable way of zeolite growth: One could think of a variety of simple complex anions of joined Si-Aℓ tetrahedras, such as 4-, 6- or 8-membered rings, cubic units and hexagonal prisms (Fig. 10a). Such units may be recognized in many zeolite structures(6).

If some terminal OH groups are visualised in the above secondary building units (SBU), a further condensation polymerisation could take place and produce larger aggregates like those shown in Fig. 10b. Such chains of 4-membered rings are found in various structures and, in addition, a number of hypothetical structures can be described on the basis of symmetry operations involving them(11).

By joining the above described rings, cubes, prisms, chains, etc., it is possible to produce SBU still larger in size such as cancrinite cages, gmelinite cages and

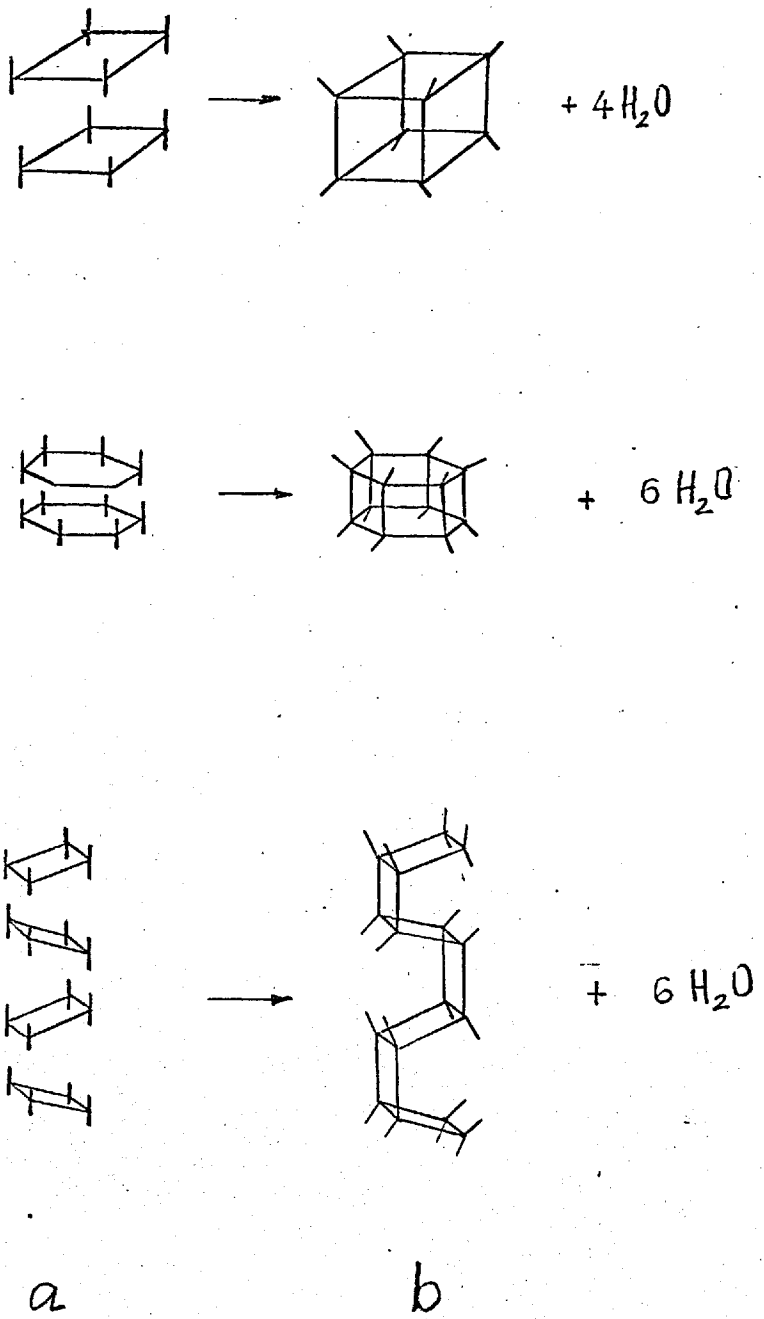

Fig. 10 Condensation polymerisation(75).

cubo-octaedras. Such units also exist in many zeolites(6).

Physical proof of the existence of the polygonal and polyhedral anions in alkaline aqueous media, containing alumina and silica is hard to obtain, but at least there is some evidence(80) that soluble anionic species existing in the liquid phase of the reaction mixtures are responsible for the growth of zeolite crystals.

The systems, from which zeolites crystallise are essentially heterogeneous ones. The problem which phase is of primary importance in zeolite nucleation - the solid or the liquid - has been discussed by several authors. One view(78) holds that the zeolite crystals are formed in the solid phase of gels, and that the components of the liquid phase do not directly affect the crystal formation. In a considerable number of cases, Zdanov et al have shown(77) that, on the contrary, gel crystallisation cannot be attributed to the Si-O-Aℓ network in the gel skeleton. In almost all cases investigated, they have found the silica content in the solid phase of the gel to be greater than that in the zeolite crystals, so that the crystal formation has to proceed not only by rearrangement of the structure of the (Si-O-Aℓ) network of the gel but with changes in its composition. An example of the role of the liquid phase is the case of recrystallisation of zeolite A into zeolite X when its mother liquor is washed out and replaced by 1nNaOH(81). Several similar examples have been also observed(64).

2.2.3 Co-crystallisation of zeolites

The simultaneous or consecutive growth of natural zeolites seems to occur readily since zeolite deposits usually consist not of one but of several zeolite phases. Specimens resulting from hydrothermal syntheses in the laboratory or in industry are also frequently mixtures

and the tendency of synthetic zeolites towards co-crystallisation is a well known problem there. Co-crystallisation is not surprising considering that the zeolite crystallisation process involves competitive nucleation of several metastable phases, as discussed in the previous section. Information given in Table 3 illustrates cases of co-crystallisation.

TABLE 3.

Data from hydrothermal syntheses

Co-crystallising phases	Cation*1	Reference
Analcite, mordenite.	Na	(117),(121),(63)
Analcite, sodolite.	Na	(121)
Analcite, mordenite, ferrierite.	Ca	(119)
Analcite, phillipsite.	K	(83)
Analcite, phillipsite.	Na	(63)
Analcite, mordenite, wairakite.	Ca	(82)
Analcite, cancrinite.	Na	(75)
Epistilbite, harmotome.	Ca	(119)
Epistilbite, heulandite.	Na	(120)
Faujasite, chabazite, phillipsite.	Na,K	(81)
Faujasite, phillipsite, sodalite, Linde Y.	Na	(81)
Faujasite, sodalite.	TMA*2	(119)
Faujasite, phillipsite, erionite.	Na,K	(40)
Sodalite, harmotome.	TMA	(119)
NaX, NaY, sodolite.	Na	(63),(122)
Chabazite, phillipsite, K-I.	K	(122)
Chabazite, phillipsite, zeolite F.	K	(34), (35)
Chabazite, erionite.	K,Na	(77)
Na-chabazite, phillipsite.	Na	(63)
K-chabazite, phillipsite.	K	(83)
Chabazite, zeolite F, zeolite K-I.	K	(77)
Phillipsite, mordenite.	Na	(63)
Phillipsite, chabazite, erionite.	K,Na	(122)
Tomsonite, epistilbite.	Ca	(119)
Zeolite A, sodalite.	Na	(81), (140)

*1 Cation contained in the alumosilicate gel.

*2 Tetramethyl ammonium cation.

3. ADSORPTION

3.1 THERMODYNAMICS OF ADSORPTION

In spite of the long history of the study of adsorption and extensive experimental work in that field, the application of thermodynamics to physical adsorption in a comprehensive way is quite recent. There are several ways in which the adsorption system could be regarded from a thermodynamical point of view. In modern thermodynamics two main approaches have become popular. The first considers the adsorption system as a two component system of sorbate+sorbent in equilibrium with unadsorbed sorbate. This is the method of solution thermodynamics, introduced by Coolidge(84), but developed in detail by Hill(85). The method leads to an evaluation of partial molar thermodynamic properties. The latter have been found(86,87) to be more sensitive to small differences in energy of the adsorbed molecules, than the corresponding molar properties. In the second approach - that of the adsorption thermodynamics(88) - the sorbed molecules are regarded as a one component phase in the field of an inert sorbent phase. This approach leads to an evaluation of the molar thermodynamic properties and operates with the so-called "spreading pressure", φ(88) as an independent characteristic of the sorbate. The evaluation of φ is tedious and may lead to errors in the calculated properties. In general this method is less often applied.

In the present work the approach of solution thermodynamics is employed more frequently, but this of adsorption thermodynamics is also used.

3.1.1 Thermodynamic properties of the sorbent/sorbate system.

Isosteric heat.

The most explicit and widely used thermodynamic characteristic of a given adsorption process is its isosteric heat, q_{st},(89) which is usually evaluated from the Clausius-Clapeyron equation. For a vapour which obeys the laws of perfect gases, this equation is given in the following well known form:

$$\left(\frac{\delta \ln P}{\delta T}\right)_a = \frac{\overset{\infty}{H}_g - \bar{H}_1}{RT^2} = \frac{-\Delta\bar{H}_1}{RT^2} = \frac{q_{st}}{RT^2} \qquad \ldots (3.1\text{-}1)$$

P - equilibrium pressure of adsorption.

T - equilibrium temperature of adsorption.

$\overset{\infty}{H}_g$ - molar entalpy of the sorbate in the gas phase.

$\bar{H}_1$- differential entalpy of the sorbate in the adsorbed phase.

The isosteric heats are obtained by plotting $\ln P$ for a fixed uptake vs $1/T$ for each of a series of experimental isotherms measured at different temperatures. The integral (molar) heat of adsorption, $-\Delta\overset{\infty}{H}_1$, can be estimated by a graphical integration of plots of the differential quantities, $\Delta\bar{H}_1$, $(= -q_{st})$ against the corresponding amounts adsorbed, n:

$$\Delta\overset{\infty}{H}_1 = \frac{1}{n_1}\int_0^{n_1} \Delta\bar{H}_1 dn \qquad \ldots (3.1\text{-}2)$$

If we define an ideal surface as one which is energetically homogeneous (case A) and an ideal sorbate (case B), as one whose molecules do not interact with each other, we can present four typical curves showing the depen-

dence of $-\Delta\bar{H}_1$ (or $-\Delta\overset{\infty}{H}_1$) on the amount adsorbed (89). The curve will be horizontal only when both cases A and B are true.

Entropy of sorption

The differential entropy of sorption(90), $\Delta\bar{S}_1$, can be expressed as:

$$-\Delta\bar{S}_1 = \bar{S}_1 - \overset{\infty}{S}_g = \frac{\Delta\bar{H}_1}{T} \qquad (3.1\text{-}3)$$

$\bar{S}_1$ - differential entropy of the sorbate in the sorbed phase.
$\overset{\infty}{S}_g$ - molar entropy of the sorbate in the gas phase.
T - equilibrium temperature.

The value of $\overset{\infty}{S}_g$ can be computed from the tabulated standard entropies of gases, S_g^o(91). For this purpose the following formula can be used.

$$\overset{\infty}{S}_g = \overset{\infty}{S}_g{}^o + R\ln P^o/P + \int_{T_o}^{T} \frac{c_p dT}{T} \qquad (3.1\text{-}4)$$

P^o, T^o - standard pressure and temperature respectively
P, T - equilibrium pressure and temperature respectively.
c_p - specific heat of the sorbate at pressure p.

If we combine equations (3.1-3) and (3.1-4) we obtain the following expression:

$$\bar{S}_1 = \frac{\Delta\bar{H}_1}{T} + \overset{\infty}{S}_g{}^o + R\ln \frac{P_o}{P} + \int_{T_o}^{T} \frac{c_p dT}{T} \qquad (3.1\text{-}5)$$

which can be used for evaluation of the differential entropy of the sorbed phase, $\bar{S}_1$. From the latter one can calculate the integral (molar) entropy of the sorbed phase, $\overset{\infty}{S}_1$, by the method described for the calculation of $\Delta\overset{\infty}{H}_1$(p 52).

An examination of equation (3.1-3) shows that when $\Delta\bar{H}_1(=-q_{st})$ is, within experimental error, independent of T, the function $(\overset{\infty}{S}_g + \int\frac{c_p dT}{T} - \bar{S}_1)$ called the half standard entropy of sorption - is also, within experimental error, temperature

independent. This fact is used for obtaining by extrapolation the values of $\bar{S}_1$ for temperatures exceeding those of the experiment.

Affinity of sorption.

The change in the chemical potential, $-\Delta\mu$, when a mole of sorbate is transferred isothermally and reversibly from the gas phase of standard pressure P^o into an infinite amount of sorbate-sorbent mixture at equilibrium pressure P is expressed as:

$$-\Delta\mu = RT \ln \frac{P^o}{P} \qquad (3.1\text{-}6)$$

The values of $-\Delta\mu$ are a measure of the affinity of adsorption and can be directly computed from the adsorption isotherms.

A practical important characteristic of a sorbent is its selectivity towards different sorbates. A quantitive measure of this is provided by the affinity of adsorption.

3.1.2 Thermodynamic properties of the sorbent.

When adsorption takes place, the sorbent also undergoes an alteration. It can be shown(92) by using Gibbs-Duhem equation that the change in the chemical potential of the sorbent, $\Delta\mu_2$, is given by the following expression:

$$\Delta\mu_2 = \mu_2 - \mu_2^o = \int_o^P V dP - \frac{RTM}{m} \int_o^P \frac{x}{P} dP \qquad (3.1\text{-}7)$$

μ_2 - the chemical potential of the lattice forming units of the sorbent, when the sorbate is imbibed.

μ_2^o - the chemical potential of these units when free of sorbate.

V - the volume of the lattice forming units.

M - molecular weight of the above volume.

x - weight sorbate in g per g sorbent

m - molecular weight of the sorbate.

P - equilibrium pressure.

The term $\int_0^p VdP$ is usually ignored and $\Delta\mu_2$ can be evaluated by graphical integration of plots of $\frac{x}{p}$ against p.

3.2 PHYSICAL MODELS OF THE SORBED PHASE

In order to give a physical description of the sorbed phase, different theoretical models are usually tested by comparing the measured thermodynamic quantities with those predicted from the models. Two models of the sorbed phase are often examined: those for localised and non-localised sorption.

According to the ideal localised model(93) the molecules, adsorbed on immobile, identical sites vibrate about mean positions on these sites and do not interact with each other. The isotherm equation deduced for this model is the well known Langmuir isotherm:

$$\theta = \frac{bp}{1+bp} \qquad \ldots (3.2\text{-}1)$$

θ - degree of coverage of the surface.
p - pressure of the gas in equilibrium with the sorbed phase.
b - constant.

It has been shown(94) that b is expressed as:

$$b = K_o\, e^{-q/kT} \qquad \ldots (3.2\text{-}2)$$

K_o - term dependent on the thermal entropy of adsorption.
q - heat involved when a molecule is adsorbed.

The quantity b will be constant if the standard free energy of adsorption on each site is constant(95). This is a necessary and sufficient condition for application of the Langmuir's equation. Accordingly, Langmuir's isotherm follows under rather wider conditions than those normally given.

For ideal localised sorption the differential entropy of adsorption, $\bar{S}_1$, can be expressed as the sum of the

differential thermal entropy, $\bar{S}_{th}$, and the configurational entropy, $\bar{S}_c$:

$$\bar{S}_1 = \bar{S}_{th} + \bar{S}_c \qquad (3.2\text{-}3)$$

According to the localised model, the last term, $\bar{S}_c$, is given by:

$$\bar{S}_c = R \ell n \frac{(1-\theta)}{\theta} \qquad (3.2\text{-}4)$$

Hence, equation (3.2-3) allows evaluation of the differential thermal entropy, S_{th}, which must be independent of θ.

Taking into account the interaction between the adsorbed molecules, an equation similar to (3.2-1) but with an extra energy term has been derived(96). Its application seldom has more success than that of Langmuir.

The mobile model assumes that all the molecules have sufficient thermal energy to surmount the potential energy barrier between sites so that they possess translational freedom. If the equation of state is that of Volmer the adsorption isotherm for the mobile model is given as(97):

$$P = K_v \frac{\theta}{1-\theta} \exp \frac{\theta}{1-\theta} \qquad (3.2\text{-}5)$$

The effect of interaction between sorbed molecules has been considered by Hill(98) and the above equation has been altered accordingly, assuming van der Waals equation of state.

Experience has shown that the above two models, and their variations - including the BET equation - are seldom quantitatively valid. The discrepancies are commonly attributed to the heterogeneity of real surfaces(89). In the case of microporous sorbents like activated charcoal or zeolites it seems that there is also another reason

which increases these discrepancies. The reason concerns the actual nature of the sorption phenomena in such sorbents.

3.3 ADSORPTION IN MICROPORES

Pores with radii below 16Å are considered as micropores(99) and adsorption in solids possessing mainly such pores is regarded as different from that in other solids. McBain held such kind of view and in the early 1930's he introduced(100) the term persorption to describe sorption in the fine pores of activated charcoal. Considering zeolites, he talked (ibid, p.171) about the "artificiality of the concept of adsorption upon the so-called interior surface ..." Recently the specific feature of adsorption in micropores has been discussed at length by Dubinin(99).

We can describe the peculiarities of adsorption in micropores in the following way: Owing to the size of the micropores the action of the adsorption forces, set up by the solid body is felt within the whole free volume of these pores. In such a "volume force field", the adsorption is likely to be more a process of volume filling than of surface covering. Indeed, in the limited space of the micropores, the molecules successively adsorbed cannot form adsorption layers and the customary convention of layer by layer coverage and monolayer surface area(89) lose their physical significance. The volume of the micropores turns out to be a more appropriate characteristic of the microporous sorbents than its surface(99). Barrer introduced in 1958 the term "monolayer equivalent area"(101) as one which should replace for the case of zeolites, the classical term of monolayer surface area. The new term can also be applied to other

microporous sorbents.

If in the case of adsorption in micropores, the classical Langmuir or Volmer view of surface coverings is unsatisfactory, the alternative is to turn to a general adsorption theory, which does not specify a model of the sorbed phase, such as Polanyi's potential theory of adsorption(102). According to this theory, the adsorption space in the vicinity of a solid surface is characterised by a series of equipotential surfaces. The adsorption potential, ϵ, of each such surface is different and is given by the following expression

$$\epsilon = RT \ell n \frac{P_o}{P} \qquad (3.3\text{-}1)$$

P_o - saturated vapour pressure of the sorbate.
P - pressure in the gas phase at equilibrium.

The adsorbate is considered to be a liquid-like phase with volume W, where

$$W = \frac{x}{\rho} \qquad (3.3\text{-}2)$$

x - weight of gas adsorbed in grams at the equilibrium pressure P.
ρ - density of the liquid at the equilibrium temperature T.

A plot of ϵ vs W produces a temperature independent characteristic curve(102) for a given sorbent/sorbate system. From this curve it is possible to predict the adsorption at different temperatures.

Polanyi made no attempt to derive an expression for the adsorption isotherm, which was the strongest feature of his theory and at the same time an essential weakness. Dubinin and co-workers applied Polanyi's theory particularly to microporous sorbents and offered(99) an equation for

the adsorption isotherm by introducing the term affinity coefficient, β , and accepting a Gaussian distribution of the adsorption potential in the volume of the sorbent. The affinity coefficient is expressed as a ratio of the temperature independent parachors of a given substance, $\underline{P}$, and a standard one, $\underline{P_o}$,

$$\beta = \frac{P}{P_o} \qquad \ldots\ (3.3\text{-}3)$$

The equation of the adsorption isotherm is as follows:

$$x = W_o \rho \exp \frac{K}{\beta} \quad (2.303RT \log_{10} \frac{P_o}{P})^2 \quad ..(3.3\text{-}4)$$

x - amount adsorbed in prams.
W_o- total volume of all the micropores.
P - eqilibrium pressure of the gas.
P_o- saturation vapour pressure of the gas.
K - constant, characterising the pore size distribution.

From plots of logx against $\log P_o/P$, one can estimate the total volume of the micropores, W_o, which is the desirable characteristic of a microporous sorbent. Further in his method Dubinin suggests equations for isosteric heats and some thermodynamic functions(99).

Although a development of Polanyi's theory, Dubinin's method, is based on some different concepts from those accepted by Polanyi. The latter considers the equipotential surfaces as approximately reproducing the geometric shape of the adsorbent surface and thus he gives a significance to the surface of the sorbent. While applying Polanyi's theory to microporous sorbents, Dubinin rejects the concept of a surface and regards strictly the adsorption in this case as a volume filling phenomenon. (He even entitled his method "theory of volume filling of micropores").

It is hard to judge the correctness of Dubinin's method and its total approach, since at the present moment sufficiently complete information on the adsorption field in micropores can be obtained only from adsorption experiments. This fact, indeed, keeps the method still far from a real theory. However, numerous experiments(99) have supported Dubinin's method and thus it has at least a value of a good approximation for adsorption in microporous sorbents.

3.4 EMPIRICAL ISOTHERM EQUATION

Besides the above discussed classical adsorption models and the Dubinin's phenomenological method, another way of describing the adsorption phenomenon is based on general thermodynamic relationships together with a virial equation of state for the sorbed phase. Such an approach can lead to an empirical isotherm equation and evaluation of the thermodynamic properties of the sorbent/sorbate system. We can start by applying Van't Hoff's isotherm:

$$\Delta G = -RT \ln \left(\frac{a_s}{a_g}\right)_{eq} + RT \ln \frac{a_s^o}{a_g^o} \qquad \ldots (3.4\text{-}1)$$

ΔG - change of the free energy of adsorption.
a_s - activity of the gas, which is adsorbed.
a_g - activity of the gas, in the gas phase.
eq - refers to equilibrium state.
o - refers to arbitrary state.

If the sorbate is in its standard state(103) and the arbitrary state is $a_s^o = a_g^o = 1$, equation (3.4-1) leads to an estimation of the equilibrium constant of adsorption, K, through the change of the standard free energy, ΔG^o:

$$\Delta G = \Delta G^{o} = -RT \ell n \left(\frac{a_s}{a_g}\right)_{eq} = -RT \ell n K \qquad \ldots (3.4\text{-}2)$$

Further we can involve the change of the entropy and entalpy at standard state, ΔS^{o} resp. ΔH^{o}.

$$-\frac{\delta G^{o}}{\delta T} = \Delta S^{o} = R \ell n K + RT \frac{\delta \ell n K}{\delta T} = -\frac{\Delta G^{o}}{T} + \frac{\Delta H^{o}}{T} \qquad \ldots (3.4\text{-}3)$$

The equilibrium constant can be also expressed as:

$$K = \left(\frac{a_s}{a_g}\right)_{eq} = \frac{c_s \gamma}{P} \qquad \ldots (3.4\text{-}4)$$

c_s - concentration of the adsorbed phase as the number moles per litre free volume of zeolite.

P - equilibrium pressure of the sorbate in the gas phase.

γ - activity coefficient of the sorbate.

In section 3.1.2 in this chapter the change in the chemical potential of the sorbent is given as:

$$\Delta \mu_2 = -\frac{MRT}{m} \int_{o}^{p} \frac{x}{P} \, dP \qquad \ldots (3.1\text{-}7)$$

$\Delta \mu_2$ may also be written

$$\Delta \mu_2 = \int_{o}^{-\pi} V dP \qquad \ldots (3.4\text{-}5)$$

$-\pi$ is the tension that would have to be applied to the sorbate free zeolite to reduce its chemical potential to that of the zeolite when sorption has taken place. π is the equivalent of an osmotic pressure.

Combining equations (3.1-7) and (3.4-5) we get:

$$\Delta \mu_2 = \pi V = \frac{MRT}{m} \int_{o}^{p} \frac{x}{P} \, dP \qquad \ldots (3.4\text{-}6)$$

The ratio $\frac{M\,x}{V\,m}$ represents C_s and equation (3.4-6) can be rearranged as:

$$\frac{\pi}{C_s RT} = \frac{1}{C_s} \int_0^P \frac{C_s dP}{P} \qquad \ldots (3.4\text{-}7)$$

For the osmotic ratio $\frac{\pi}{C_s RT}$ we can write an ordinary virial equation:

$$\frac{\pi}{C_s RT} = 1 + A_1 C_s + A_2 C_s^2 + A_3 C_s^3 + \ldots \qquad \ldots (3.4\text{-}8)$$

By combining equations (3.4-7) and (3.4-8) we can derive the following expression for the adsorption isotherm:

$$K = C_s/P \exp\left(2A_1 C_s + \frac{3}{2} A_2 C_s^2 + \frac{4}{3} A_3 C_s^3 \ldots\right) \qquad \ldots (3.4\text{-}9)$$

where $\gamma = \exp\left(2A_1 C_s + \frac{3}{2} A_2 C_s^2 + \frac{4}{3} A_3 C_s^3 \ldots\right)$ ... (3.4-10)

Thus the equilibrium constant K may be obtained from plots of $\ln C_s/P$ vs C_s, as $\ln K$ is the extrapolated value of $\ln C_s/P$ when $C_s \rightarrow 0$. If sufficient data is not available for extrapolation, K may be estimated by solving several simultaneous equations like (3.4-9). In this way the virial coefficients will also be obtained.

In the standard state, the activity of the sorbate, a_s, must be unity. By substituting this in equation (3.4-4) we can estimate graphically the concentration C_s^o in the standard state.

The method described here provides also a sensitive test of the ideal adsorption models. The test is made by a comparison of the empirical activity coefficients with those derived for the given model(93,97).

3.5 FORCES AND ENERGY INVOLVED IN THE PHYSICAL ADSORPTION

3.5.1 Physical adsorption forces.

Since the adsorption results from interatomic or intermolecular interaction, the forces involved are the same as those in any other physical interaction phenomenon. The physical interactions encountered in the case of adsorption of non-polar molecules are dispersion, close-range repulsion and polarization forces.

The dispersion forces(104) originate through the rapidly changing electron density in an atom (visualised by London as "orchestra of instantaneous dipole moments"), which induces a corresponding electrical moment in a near neighbour and thus leads to attraction between the two atoms. The potential energy, E_D, of the two isolated atoms, separated by a distance r is given as:

$$E_D = -\frac{A}{r^6} \qquad \ldots (3.5\text{-}1)$$

A - constant of interaction.

According to Kirkwood and Müller(105) the constant A relates the polarizabilities α_1 and α_2 and magnetic susceptibilities χ_1 and χ_2 of the two atoms with the mass of the electron, e, and the velocity of light, c. The relation is as follows:

$$A = 6mc^2 \frac{\alpha_1 \alpha_2}{\alpha_1/\chi_1 + \alpha_2/\chi_2} \qquad \ldots (3.5\text{-}2)$$

The potential energy of dispersion forces between adsorbed molecules and a plane surface, E_D^a, is given(106) as:

$$E_D^a = \frac{N\pi_A}{6z^3} \qquad \ldots (3.5\text{-}3)$$

z - the perpendicular distance from the adsorbed atom

to the surface of the solid.

N - number of adsorbed atoms per unit volume.

The repulsion forces arise only at short distances when the electron clouds of the two atoms overlap sufficiently. The energy due to repulsion forces between two atoms at distance r is expressed empirically as

$$E_R = \frac{B}{r^{12}} \qquad \ldots (3.5\text{-}4)$$

B - constant; $B = \frac{-Ar_o^6}{2}$, where r_o is the equilibrium separation distance.

The potential energy resulting from dispersion and repulsion interaction of two atoms is then given by Lennard-Jones 6:12 potential:

$$E_D + E_R = -A\left(\frac{1}{r^6} - \frac{r_o^6}{2r^{12}}\right) \qquad \ldots (3.5\text{-}5)$$

Polarization forces arise if an atom or molecule is placed in an external electrostatic field, F. This field induces in the atom or molecule, a dipole moment, μ_{ind}. The potential energy, E_p, of this introduction is:

$$E_p = \int_o^F \mu_{ind}\, dF = -\tfrac{1}{2}\, \alpha F^2 \qquad \ldots (3.5\text{-}6)$$

- the mean polarisability of the atom (molecule).

If we consider a field created by an isolated cation with a charge e, at a distance r from an atom (molecule), the corresponding energy, E_p^{CAT}, will be expressed as:

$$E_p^{CAT} = -\alpha_e^2/2r^4 \qquad \ldots (3.5\text{-}7)$$

In the general case of adsorption of non-polar sorbates, the dispersion forces represent the major contribution to

the total energy of adsorption. The dependence of the dispersion forces on the distance from the surface and the coordination number of the sorbed molecule results in considerably stronger fields within pores, than above a plane surface. De Boer and Custers(107) have shown this by calculating the dispersion energy of molecules at different surface environments.

3.5.2 Interpretation of heats of adsorption in terms of intermolecular forces.

We can consider the isosteric heat at $0^{o}K$, q_{st}^{o}. At such a low temperature only the potential energy need be considered and if zero-point energy is neglected, we can write:

$$q_{st}^{o} = -\phi - n_1 \left(\frac{\delta \phi}{\delta n_1}\right)_{P,T,n_2} \qquad \ldots (3.5\text{-}8)$$

ϕ - interaction energy of the sorbate with the sorbent.
n_1- moles sorbate in the mixture.
n_2- moles sorbent in the mixture.

As was mentioned before, for non-polar sorbates the total potential energy comprises only dispersion (E_D), repulsion (E_R) and polarization (E_p) components, so:

$$\phi = E_D + E_R + E_p \qquad \ldots (3.5\text{-}9)$$

For rare gases the isosteric heat does not vary appreciably with the temperature(68) and formula (3.5-8) holds for other temperatures as well. However, calculation of ϕ is difficult and in many ways uncertain. Information about many physical quantities is needed and often the

numerical values of the constants are not known with accuracy.(108) Attempts have been made to calculate the heats of adsorption of rare gases in zeolite X(68) and mordenite(108) and of ammonia and carbon dioxide in faujasite(109 & 110).

CHAPTER II

MATERIALS, APPARATUS AND METHODS

1 MATERIALS

1.1 SORBATES

The sorbates used were spectroscopically pure Ar and O_2, Kr (99-100% balance Xe) and Xe (99-100% balance Kr). All sorbates were supplied by British Oxygen Company Limited.

1.2 SORBENTS

The sorbents used were:

Name	Supplied from	Supplied as	Label	Note
Synthetic zeolite L	Union Carbide(15)	K,Na form	L	
Synthetic zeolite L	These laboratories M. Damm.	K,Na form	L-IC	Contaminated by gibbsite, ER and OFF.
Synthetic offretite	These laboratories R. Aiello.	K, $(CH_3)_4N^+$ form	OFF	
Natural erionite	Pine Valley,Nevada, U.S.A.	K,Na form	ER	

The following ion-exchanged forms were prepared from the above samples:

Sample	Ion-exchanged forms	Label
L	Hydrogen, lithium, sodium, potassium, caesium, barium and lanthanum.	HL; LiL; NaL; KL; CsL; BaL; LaL.
L-IC	Sodium, potassium and calcium	NaL-IC; KL-IC; CaL-IC.
OFF	Hydrogen.	H-OFF.
ER	Hydrogen, sodium and potassium.	H-ER; Na-ER; K-ER.

These selected ion-exchanged forms gave an opportunity to investigate several effects on the adsorption behaviour:

1. Cation size at constant valency for a given structure, (LiL; NaL; KL and CsL) and for different structures (NaL and KL; Na-ER and K-ER).

2. Cation density in a given structure (KL; BaL; LaL - specially the first two cases, as the sizes of the cations are very similar).

3. Influence of the framework (HL, H-OFF and H-ER).

1.2.1 Preparation of cation-exchanged forms of zeolite L, erionite and offretite.

All the ion-exchanged forms of zeolite L and erionite (except HL and H-ER) were prepared by a direct mixing of a given amount of the original sample with a nearly saturated solution of the corresponding chloride (Table 4). The mixtures were left at room temperature for about 72 hours, shaken from time to time and then filtered, washed and dried. The washing should ideally be continued until the crystals were free of chloride, but because of hydrolysis, excessive washing was avoided, and traces of Cl may have remained in certain of the samples (see Table 4). All the ion-exchanged forms after washing and drying were left for equilibration with water vapour for at least a week, in a desiccator with saturated NH_4Cl.

1.2.2. Preparation of decationated forms (H-forms) of zeolite L, erionite and offretite.

HL and H-ER were prepared from the NH_4-form of the corresponding zeolite, following heating at 350°C for at least 24 hours in a stream of O_2 :

TABLE 4

Ion Exchange form	Salt	Purity	Concentration of the saturated solution	Concentration g/100 g.H_2O	Notes
NaL, NaL-IC, Na-ER	NaCl	AnalaR	36.5 g/100 g. H_2O at 25°C	30	
KL, Kl-IC, K-ER.	KNO_3 KCl	AnalaR	31.6 g/100 g. H_2O at 20 (27.6 g/100 or H_2O at 25°C)	28	
CaL-IC	$CaCl_2.6H_2O$	AnalaR	74.3 g/100 g. H_2O at 25°C	60	Traces of Cl'
BaL	$BaCl_2.2H_2O$	AnalaR	39.9 g/100 g. H_2O at 25	35	
LiL	$LiCl.6H_2O$	AnalaR	78.5 g/100 g. H_2O at 20	70	
CsL	Cs Cl .aq	AnalaR	186 gr/100 g. H_2O at 25°C	100	
LaL	$LaCl_3.3H_2O$	BDH29008	-	50	

$$2O_2 + 2NH_4^{+}\text{zeolite} \rightarrow 2H\text{-zeolite} + 4H_2O + N_2 \quad \ldots (2.1\text{-}1)$$

The NH_4-forms were prepared by the technique described above for the other cation-exchanged forms.

H-OFF was prepared from the original sample containing K - tetramethyl ammonium ions by heating at 500°C in a constant flow of O_2:

$$\left\{K_{1-x}\left[(CH_3)_4N\right]_x\right\}\text{-Zeolite} + 15xO_2 \rightarrow 4\left\{K_{1-x}H_x\right\}\text{-Zeolite} + 4xCO_2 + 22xH_2O \quad \ldots (2.1\text{-}2)$$

2 APPARATUS

An apparatus was built (Fig. 11) consisting of three volumetric systems (A, B and C); two gas reservoirs (D_1 and D_2); Toepler pump (E); two outgassing systems (F_1 and F_2); pressure measuring device (G) and pumping system (H). A gas reservoir and the Toepler pump are shown on Fig. 12 in more detail.

2.1 PUMPING SYSTEM AND VOLUMETRIC SORPTION SYSTEM

The pumping system consists of a single stage mercury diffusion pump, backed by a rotary oil pump. A single volumetric system (Fig. 13) contained a bulb gas burette(1); manometer(2); adsorption bulb(3); communication volume (dead volume, V_D), joining volume V_B and cold volume V_C.

The manometers were constructed from 0.6 cm. diameter Verdia tubing. A calibration mark was fixed on the arm of the gas-line. The calibration of the gas burettes was effected by weighing with mercury(92).

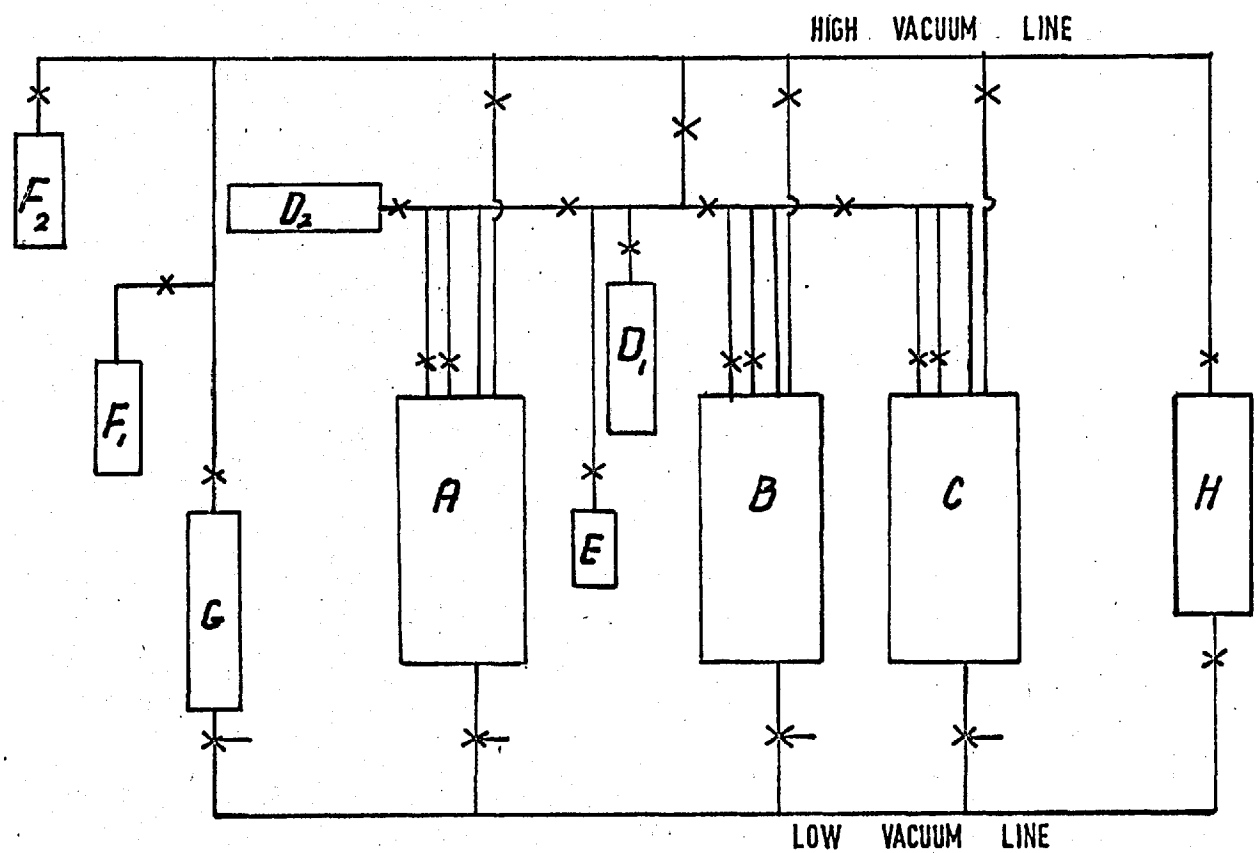

Fig. 11. VACUUM VOLUMETRIC SYSTEM for ADSORPTION

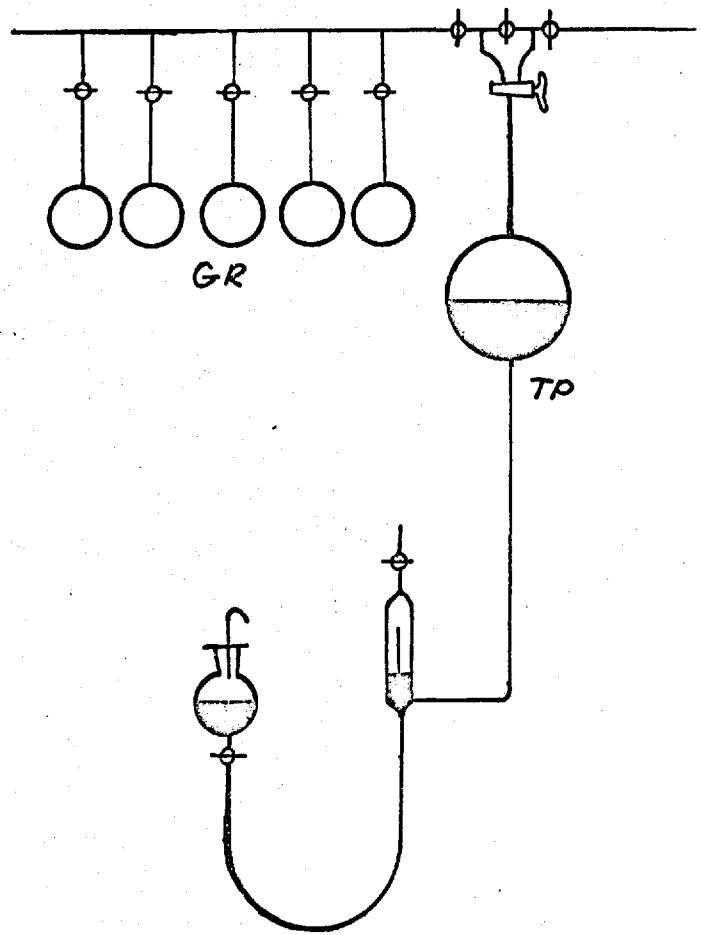

Fig. 12 GAS RESERVOIR and TOEPLER PUMP

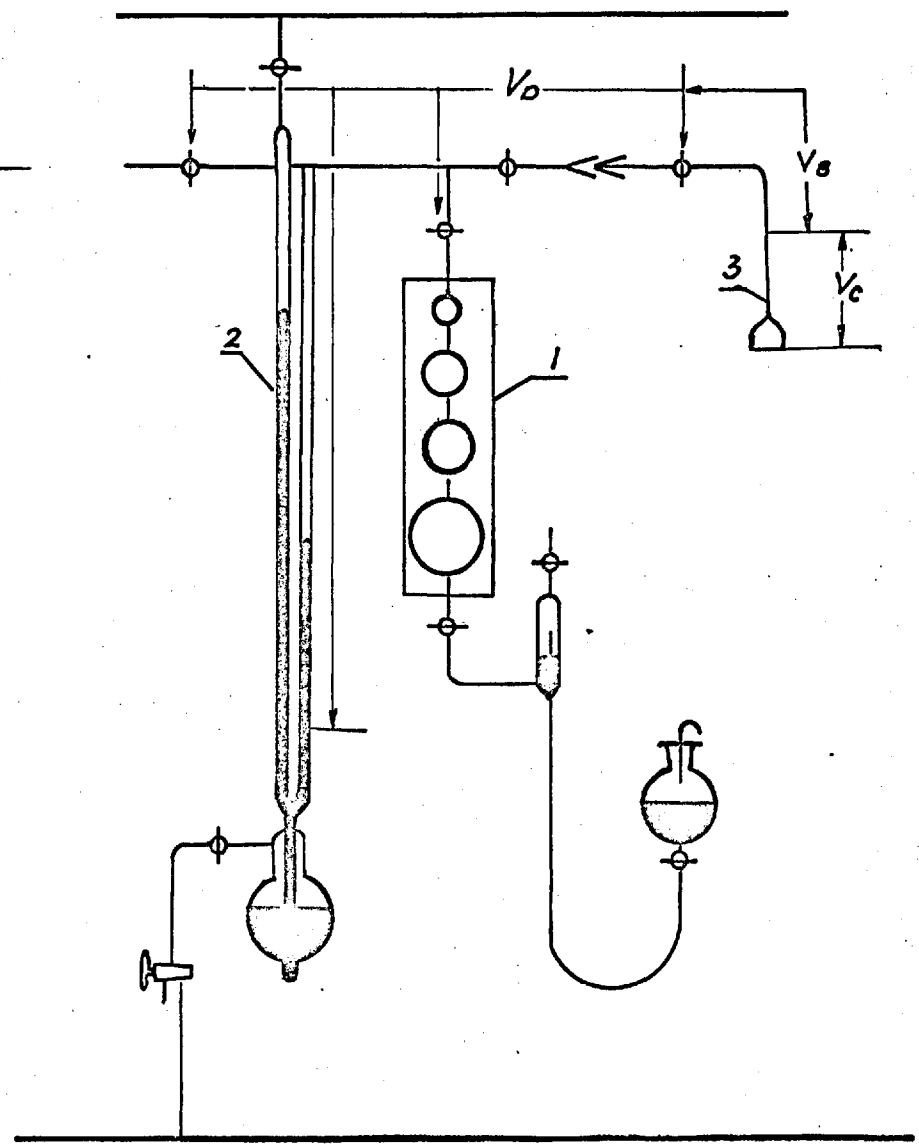

Fig. 13 SINGLE VOLUMETRIC SYSTEM

2.2 THERMOSTATS AND TEMPERATURE CONTROL

Thermostats as described previously(68) were used for obtaining temperatures between -20°C and -150°C. The organic liquids, used for filling the internal Dewar of the thermostat, were as follows:-

TABLE 5

Temperature interval	Liquid
-20°C to -40°C	Methanol
-40°C to -100°C	Petrolcum ether
-100°C to -150°C	Isopentane

The temperature control was realized by a Sunvic controller(68) and the accuracy obtained was ±0.1°C. The temperature was read by a vapour pressure thermometer, chosen as indicated in the table below:

TABLE 6

Temperature interval	Vapour
-18°C to -40°C	n-butane
-40°C to -68°C	Ammonia
-70°C to -108°C	Carbon dioxide.
-105°C to -150°C	Ethylene.

Direct baths of liquid nitrogen and liquid oxygen were also used.

3 METHODS

3.1 PREPARATION OF SAMPLES FOR ADSORPTION. OUTGASSING OF THE SAMPLE

About 0.5g of the sample was placed in a weighed sorption bulb and its weight determined accurately. The bulb was then carefully blown to a bent glass tube with a stopcock and a cone. The volume of the tube was determined beforehand by weighing with mercury.

A standard procedure was followed for the outgassing of most of the samples. The sorbent was outgassed at room temperature to about 10^{-5}mm.Hg and the temperature then raised during evacuation, by not more than 70°C per hour, up to 350°C. Outgassing was continued at 350°C for 24 hours (or longer, for the initial outgassing) and finally the temperature was slowly lowered to room temperature over an interval of at least 3 hours. Outgassing of sorbates between runs, was carried out under milder temperature conditions of 200°C for at least 5 hours. It had formerly been accepted that only the rate at which the temperature of the sample was increased was of importance (because of the danger of sintering by release of excess water) and the rate of cooling has usually been neglected. Possible resiting of cations at high temperature during outgassing(6) makes it desirable to regulate the speed of cooling so as to permit ion-distributions to adjust towards those appropriate for room temperatures.

3.2 MEASUREMENT OF ISOTHERMS

Measurement of the isotherm involved reading the dosage and equilibrium pressures at fixed temperatures. The time allowed for reaching the equilibrium was about

an hour for temperatures lower than -150°C, and not less than 20 mins., for other temperatures.

The amount adsorbed was expressed in cc (at STP) sorbate per gram of dehydrated zeolite; or as the number of molecules of sorbate per unit cell of dehydrated zeolite.

All the pressures were read on a cathetometer with an accuracy of 0.005 cm.

3.3 X-RAY EXAMINATION

The X-ray powder method, with CuK_α radiation was used for the following purposes:

a) identification of species from syntheses;
b) characterisation of the ion-exchanged forms;
c) estimation of the changes in the sample after outgassing;
d) observation of the alteration, which occurs while heating the zeolite
e) estimation of the positions of the cations before outgassing
f) estimation of the positions of the cations after outgassing.

For a, b and c a Guinier camera was used. This technique was found to be not satisfactory for case c, because of low accuracy in estimation of the intensities and an inevitable rehydration of the sample. Attempts to overcome the first difficulty by X-raying a mixture of the sample and a standard ($Pb(NO_3)_2$, quartz or a chosen convenient zeolite) did not give sufficient improvement, but using a diffractometer instead of a Guinier camera gave reliable evidence of the irreversible alteration of a few lines after outgassing. The problem of rehydration was solved by using a Lenne camera(111), which allows a

continuous diffraction pattern to be taken, during heating, in the range from room temperature to 1200°C. A comparison of the patterns on the Lenne camera at room temperature, before heating, and at high temperature, after outgassing, gave the information needed, although a pumping system attached to the Lenne camera would be an improvement.

For case d continuous patterns, taken from room temperature up to 550°C or 700°C on the Lenne camera, were used. For case f powder patterns were obtained, on the same camera, at 550°C after a given time of heating of the zeolite, causing full dehydration.

For the purposes of case e powder patterns were recorded on an XRD-6 diffractometer(112) to give more accurate estimation of the intensities.

3.4 ELECTRON MICROSCOPY AND ELECTRON DIFFRACTION

The electron micrographs and electron diffraction patterns were obtained on electron microscope Philips EM100.

A sample for microscopy was prepared as follows: A few drops of a weak (0.5g./100) solution of Formvar in chloroform were spread on a microscopy slide and allowed to dry, leaving a thin film in about one minute. The film was cut into small, roughly-square pieces (about $3mm^2$ area) The glass with the film was then gently dipped into water, on the surface of which the film-squares floated. By inserting an electron-microscope grid, held in a pair of forceps under each piece of film and lifting it, the film was mounted and left to dry for about 30 minutes. A suspension was made by shaking a few specks of the zeolite with distilled water and the strength adjusted by estimate the cloudiness visually.

A drop of suspension was put on top of the already prepared grid, covered with a film, left for about an hour to dry and then fitted into a specimen holder(45). The sample prepared this way was used for obtaining both electron micrographs and electron diffraction patterns. The electron micrographs were taken by means of the usual technique(45) at 80kv and range of magnification between 2000 to 12000-fold. The negatives were enlarged about 3 to 4-fold in printing.

Electron diffraction patterns were taken at 80kv or 100kv in the following manner: The crystal chosen at a given magnification was singled out by means of adjustable leaves of a shutter, which operates at the intermediate image(47). The magnification was dropped to zero and after that the microscope was focussed until the electron-diffraction pattern was observed. This was then recorded on 35mm film. In printing the photographs an enlargement of about 10 to 12-fold was obtained, so that the distances between the spots could be easily measured in mm. A standard electron diffraction pattern of Au was taken and used as a reference for moreaccurate λL calibration(45).

3.5 THERMOGRAVIMETRIC AND DIFFERENTIAL THERMAL ANALYSIS

A Stanton thermogravimetric balance TR11 was used and the temperature was raised from that of the room up to 1200°C over a period of about 5 hours, using the slow cam.(113). The charts obtained were used for several purposes:

a) to estimate the loss of water at atmospheric pressure up to 500°C, where a plateau was usually observed. The water content so obtained was considered along with that determined by ignition;

b) to compare the TGA curves of different samples;

c) to characterise the behaviour of the zeolite in the whole temperature interval, for comparison with DTA data and X-ray patterns from LENNE.

A classical DTA were carried out on Dupont 900 DTA. A direct heating of the reference material and the sample from room temperature was found to be unsatisfactory and the samples were therefore cooled with liquid nitrogen before starting the run:

3.6 CHEMICAL ANALYSES AND SPECTROSCOPICAL METHODS

Classical silicate analyses(114) were employed for determining the complete composition of the sorbents. The degree of ion-exchange was determined spectrophotometrically(115) after full digestion of the zeolite(115). K^+, Na^+ and Ba^{++} were determined using absorption spectra, and Li^+, Cs^+ and La^{++} using emission spectra.

The degree of decationation was estimated by determination of the cation deficiency of the decationated form compared with the original sample.

CHAPTER III

RESULTS AND DISCUSSION.

1. ZEOLITE CRYSTALLISATION

Syntheses of zeolite L were carried out for practical and theoretical reasons. It was found (p.160) that samples L-IC (p.68) had higher adsorption capacities towards rare gases, compared with sample L (p.68), but lower stability. Comparison by electron microscopy (EM) and X-ray techniques revealed, for L-IC, poorer crystallinity and the presence of contaminants. To prepare pure, well crystallised phases of zeolite L and structures related to L, both hypothetical and naturally occurring, was the practical aim. Repeated and reproducible co-crystallisation of phases with common building units made the phenomenon of zeolite co-crystallisation and the role of the secondary building units of theoretical interest.(11)

1.1 SYNTHESES

Two types of syntheses have been completed. Firstly the reported compositions for syntheses of zeolite L(15) and zeolite T(33) (which was originally considered (p.22) to be erionite) were used. Secondly, variations of these compositions were explored.

Examination of the reported compositions (Table 7) indicates close similarity in the conditions for syntheses of zeolites L and T. The mole ratio of silica to alumina was 20 for all except L_1^*, for which it was 17.7. The alkali-oxide to silica ratio was close to 0.4 for all cases, except T_3, for which the value was 0.5. A common value of 40 for the mole ratio of water to alkali oxide was found

---

* Subscribed symbols for each zeolite refer to different preparation as given in the corresponding patents (15 and 33).

TABLE 7.

Compositions and conditions of synthesis of Zeolites L and T(15,33)

		L_1	L_2	T_1	T_2	T_3
1	KOH(g)	28.7	13.7	41.1	7.16	8.57
2	NaOH(g)	-	7.3	43.2	15.3	15.9
3	$NaALO_2$(g)	-	5.0	30.0	-	5.0
4	$AL(OH)_3$(g)	5.6	-	-	5.0	-
5	"SYTON"(g)	130.0	124.0	145.0	130.0	124.2
6	$H_2O(cm^3)$	17.1	84.5	501.0	86.1	127.3
7	t^oC	100	100.0	100.0	100	120.0
8	τ (hrs)	169	64.0	160.0	8.8	8.0
9	SiO_2(g)	30.35	30.64	219.83	38.35	36.64
10	SiO_2(moles)	0.638	0.610	3.638	0.638	0.610
11	AL_2O_3(moles)	0.036	0.030	0.183	0.032	0.030
12	Na_2O (moles)	0.000	0.121	1.097	0.191	0.231
13	K_2O(moles)	0.253	0.122	0.366	0.064	0.076
14	Na_2O+K_2O(moles)	0.253	0.233	1.463	0.255	0.307
15	H_2O(moles)	6.042	9.551	57.343	0.875	11.937
16	$Na_2O/(K_2O+Na_2O)$	0.000	0.520	0.749	0.750	0.753
17	$(Na_2O+K_2O)/SiO_2$	0.396	0.382	0.392	0.399	0.503
18	SiO_2/AL_2O_3	17.7	20.3	20.00	20.00	20.3
19	$H_2O/(Na_2O+K_2O)$	23.8	41.0	39.20	33.20	38.8

L_1 and L_2 - preparation 1 and 2 respectively from (15).
T_1, T_2 and T_3 - preparation 1, 2 and 3 respectively from (33).

for L_2, T_1 and T_3. The temperature was 100°C for all preparations except that of T_3. The order and manner of mixing the components was the same.— Homogeneous solutions of alkali-aluminate constituents were prepared and added, with continuous stirring, to the "Syeton" sol.

The only significant difference between the compositions for preparation of zeolite L and T was in the mole ratio $Na_2O/(Na_2O + K_2O)$, which was 0.75 for all T formulae, but 0.00 and 0.52 for L_1 and L_2 respectively. The time of crystallisation of T_2 and T_3 was noticeably shorter than for the remainder of the preparations.

In Tables 8 and 9 are summarised the conditions and results of syntheses. Because in 30% of the cases of the first series (Table 8) amorphous material was obtained, in the second series (Table 9) the time for crystallisation was in general extended. In the second series, the composition of the initial solution was altered significantly for two cases - 15" and 16" - and only for these are the full composition given in Table 9. For all cases the time of crystallisation is given.

The purest and best crystalline phase of zeolite L obtained was 1' (Fig. 14). The X-ray powder pattern contained only lines relating to the true structure(11) and the crystals were formed. They were slightly larger than those supplied by Union Carbide (Fig. 15). Preparation L_1 reliably produced a single phase of L for cases 1', 1", 2" and 3". The only other phase found using preparation L_1 was gibbsite (Fig. 16), as seen in cases 3', 5' and 4", or as a mixed phase with L, in case 11'.

Preparation L_2 led to pure phillipsite for cases 8', 7" and 8" (Fig. 17); and to a mixture of zeolites L, erionite and offretite in cases 2', 5", 6", L-IC (Figs 18a,

TABLE 8.

Compositions and conditions of synthesis - Series I

	Order Number of Experiment															
	1'	2'	3'	4'	5'	7'	8'	10'	11'	12'	13'	14'	16'	17'	18'	19'
KOH(g)	28.7	13.7	14.3	6.8	14.3	6.8	7.0	8.4	15.0	8.0	3.5	3.5	4.5	2.0	1.8	7.2
NaOH(g)	-	7.3	-	3.7	1.0	2.0	2.1	2.0	2.0	2.5	1.8	1.8	0.8	3.7	3.8	-
$NaALO_2$(g)	-	5.0	-	2.5	-	2.6	3.0	2.5	-	2.5	1.2	1.2	1.2	1.5	-	-
$AL(OH)_3$(g)	5.6	-	2.8	-	2.8	-	-	-	3.0	-	-	-	-	-	1.25	1.4
"SYTON"(g)	130.0	124.2	65.0	62.1	56.0	62.0	42.2	52.5	65.0	60.0	27.0	27.0	25	31.3	31.3	27.5
$H_2O(cm^3)$	17.1	84.5	6.55	42.2	65.0	42.2	57.0	42.5	10.0	45.0	23.0	23.0	23.0	23.0	22.0	5.0
t^oC	100	100	100	100	100	100	100	120	120	120	103	103	103	103	103	103
hrs.	169	103	103	64	100	64	48	100	84	48	150	100	87	100	48	48
Preparation	L_1	L_2	L_1	L_2	L_1	L_2	L_2	L_2	L_1	L_2	L_2	L_2	L_2	T_1	T_2	T_2
X-ray result	L	L	G	A	G	A	PH	A	L+G	A	not distinguished.		A	OFF +	G	A
Electron Microscopy.	Well formed flaky crystals.	Flakes and small % of hammers.	Wheat sheath crystals.	-	Wheat sheath crystals.	-	Small square crystals.	Irregular forms	Irregular flakes surrounded with amorphous material	-	Corn shaped crystals		-	Large rods and traces of flakes.	Wheat sheath crystals.	-

L - Zeolite L; ER - Erionite; G - Gibbsite; PH - Phillipsite; A - Amorphous.
L_1 and L_2 - see Table 7. OFF - Offretite
T_1, T_2 and T_3 - see Table 7.

TABLE 9. Series II.

Order number of Experiment	1"	2"	3"	4"	5"	6"	7"	8"	10"	11"	12"	13"	14"	15"	16"
Preparation	L_1	L_1	L_1	L_1	L_2	L_2	L_2	L_2	L_1	L_1	L_1	L_1	L_1		
Variation of the composition.	-	-	-	-	-	-	9.0gNaOH added	9.0gNaOH added	LiOH instead KOH	LiOH instead KOH + 7gNaOH	LiOH instead KOH + 7gNaOH	6gLiOH + 5gNaAlO$_2$ added	6gLiOH + 5gNaAlO$_2$ added	15gKOH 12gLiOH 5.6gAL(OH)$_3$ 20cm^{3}H$_2$O 130g "SYNTON".	15gKOH 12gLiOH 5.6gAL(OH)$_3$ 20cm^{3}H$_2$O 130g "SYNTON".
X-ray result.	L	L	L	G	L + ER + OFF	ER + L + OFF	PH	PH	G + not identified	G		G + PH	G + L not identified.	Not identified. + L	
Electron Microscopy.	Flaky crystals	Flaky crystals	Flaky crystals	Wheat-sheath crystals	Flakes, rods and hammers.	Rods and hammers.	Crystal clusters	Crystal clusters	As 4".	As 4"	-	-	Uniform granular crystals.		
hrs.	300	300	260	140	260	400	200	200	140	120	120	230	230	250	400
Notes	NS	NS	OS	OS	NS	NS	NS	OS	OS	NS	OS	NS	NS	NS	OS

NS - new "SYTON". OS - old "SYTON". Other symbols - see Tables 7 and 8.

Fig. 14, x 12000. L, preparation 1'.

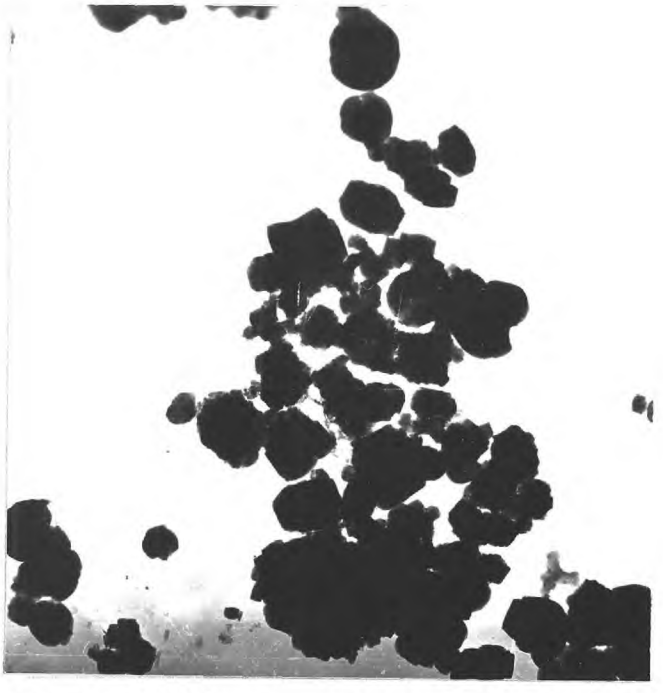

Fig. 15, x 13000. L, prepared by Union Carbide.

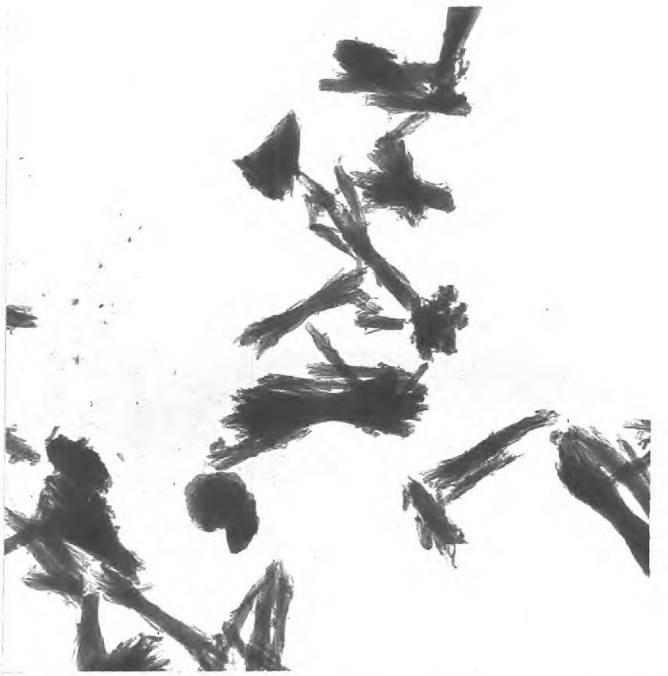

Fig. 16, x 17000. Gibbsite, preparation 3'.

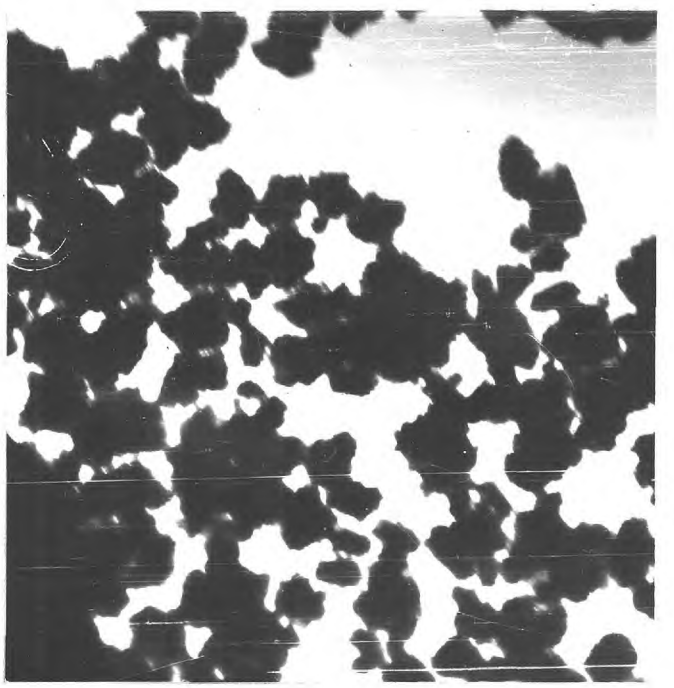

Fig. 17, x 14000. Phillipsite, preparation 8".

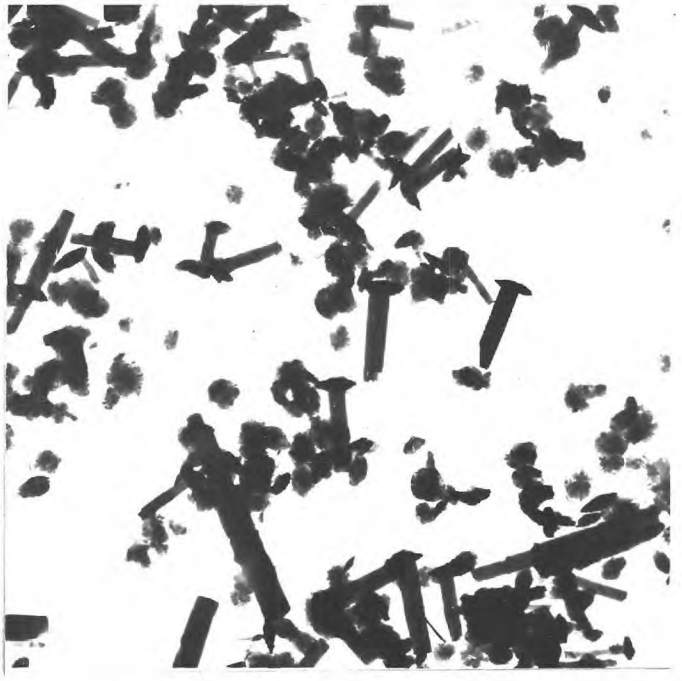

Fig. 18a, x 28000. L-IC, prepared by M. Damm.

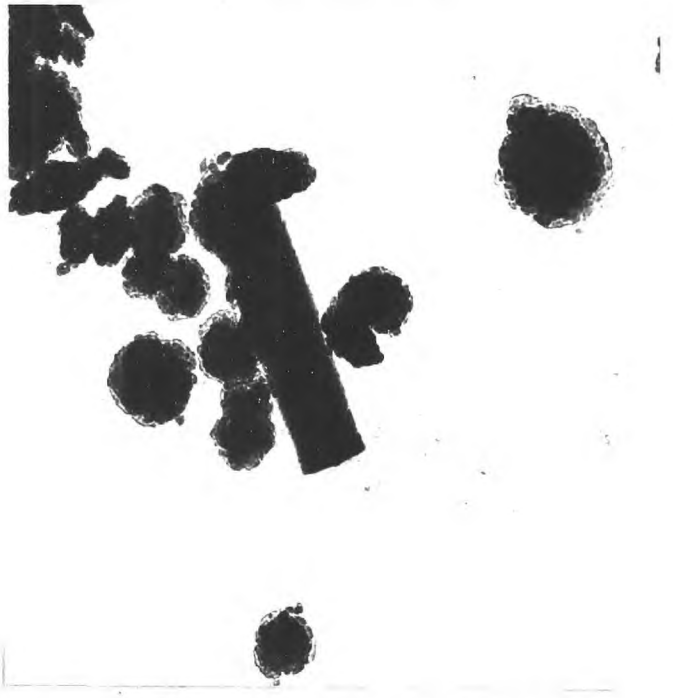

Fig. 18b, x 16000. L, preparation 2'.

Fig. 18c, x 20000. L, preparation 6".

Fig. 19, x 12000. Offretite (contd. by L), preparation 17'.

18b and 18c). Sample L-IC was the first to be shown to be a mixed phase. Presence of different species was revealed by examination of its X-ray powder pattern (Table 10). Reflections additional to those of pure L(11) were d = 4.82 Å, associated with gibbsite, and d = 11.4, 6.60, 3.71 and 3.58 which are typical of erionite and offretite.

Formula T, yielded offretite with traces of L. The crystals were well formed, large pods (Fig. 19).

Two new phases which could not be identified were also obtained. The first was named Na_1K-BB (13' and 14') and second, Li_1K-VV (14", 15", 16"). Table 11 and Figs. 20a and 20b present their X-ray powder patterns and electron micrographs respectively.

The results of the above two series of syntheses showed that lack of sodium cations favours crystallisation of L (p. 84), while the converse favours crystallisation of erionite and/or offretite. (It is difficult to distinguish erionite and offretite in a mixed phase - see p.95). It was of interest to find whether a further increase of the sodium content would result in pure erionite or offretite. A third series of syntheses was performed for this purpose.

The results are given in Table 12. Pure offretite was obtained only in case 8"', but was poorly crystalline. Pure erionite was not obtained,

An increase of the sodium content above the limits set by the formulae for preparation of zeolite T(33) led to crystallisation of a) chabazite, from concentrated solutions ($H_2O/(Na_2O + K_2O) = 26.4$) - cases 3" and 4"; and b) faujasite, from more dilute solutions ($H_2O/(N_2O + K_2O) = 52$) - cases 5"' and 6"'

TABLE 10

X-ray powder patterns of L-IC, L, Erionite and Gibbsite.

L-IC		L		Erionite		Gibbsite	
d Å	intensity	d Å	intensity	d Å	intensity	d Å	intensity
16.0	vs	16.0	vs	-	-	-	-
11.4	w	-	-	11.4	vs	-	-
-	-	-	-	9.16	m	-	-
7.90	w	7.90	w	-	-	-	-
7.52	s	7.52	s	7.50	s	-	-
6.60	w	-	-	6.60	s	-	-
-	-	-	-	6.29	m	-	-
6.02	m	6.02	m	-	-	-	-
5.82	m	5.82	m	-	-	-	-
-	-	-	-	5.62	m	-	-
-	-	-	-	5.37	m	-	-
4.82	w	-	-	-	-	4.82	vs
4.61	vs	4.61	vs	4.60	s	-	-
4.40	m	4.40	m	-	-	-	-
-	-	-	-	-	-	4.38	s
4.33	m	4.33	m	4.34	s	4.36	m
-	-	-	-	4.16	m	-	-
3.91	vs	3.91	vs	-	-	3.75	w
3.71	w	-	-	3.71	s	3.62	w
3.65	m	3.65	m	-	-	3.39	w
3.58	w	-	-	3.58	vs	2.44	m
3.48	m	3.48	m	-	-		
-	-	-	-	3.30	m		
3.29	m	3.29	m	3.28	s		
3.19	s	3.19	s	3.18	m		
-	-	-	-	3.16	vs		

TABLE 11.

X-ray powder patterns of samples Na, K-BB and Li, K-VV

Na, K-BB		Li, K-VV	
d Å	intensity	d Å	intensity
9.80	w	8.20	w
4.90	w	8.00	w
3.20	s	7.50	w
3.08	vs	6.30	m
2.77	w	5.90	s
2.75	m	5.60	m
2.64	vs	5.30	m
2.58	w	4.65	m
2.44	m	4.08	m
2.41	w	3.88	w
2.25	m	3.78	w
2.14	w	3.60	w
2.04	m	3.36	s
2.03	m	3.30	w
1.99	w	3.24	m
1.96	w	3.15	m
1.88	w	3.05	m
1.77	m	3.02	w
1.74	m	2.99	m
1.72	w	2.88	m
1.67	w	2.68	w
1.66	m	2.65	w
1.64	w	2.55	w
1.59	w	2.46	w

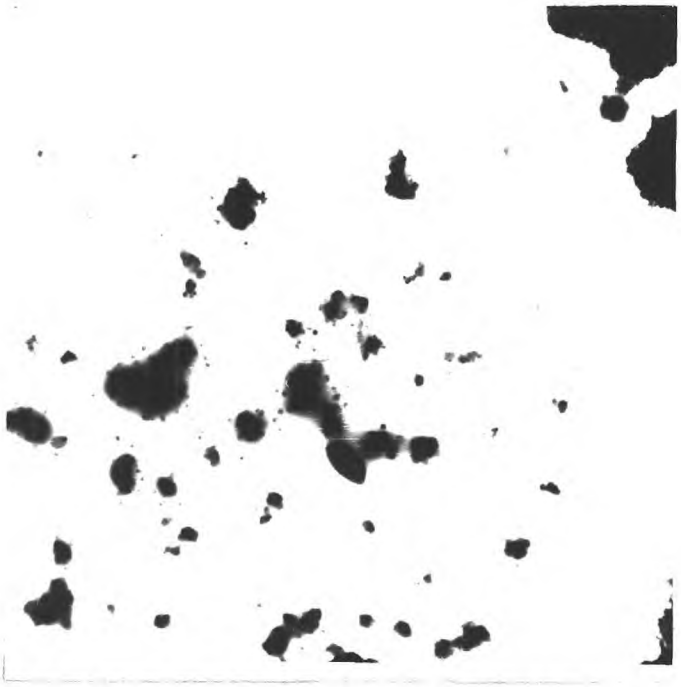

Fig. 20a, x 16000. Na, K-BB, preparation 14'.

Fig. 20b, x 12000. Li, K-VV, preparation 16".

TABLE 12

Composition and conditions of syntheses - Series III

Order number of experiment										
	1''' and 2'''		3''' and 4'''		5''' and 6'''		7''' and 8'''		9''' and 10'''	
preparation.	L_2		T_1		T_2		T_1		T_2	
hrs.	168		178		168		168		172	
$Na_2O/(N_2O+K_2O)$	0.60		1.03		0.98		0.80		0.78	
$(Na_2O+K_2O)/SiO_2$	0.40		0.30		0.14		0.38		0.46	
Si_2O/AL_2O_3	20.30		20.00		21.27		20.17		21.27	
$H_2O/(N_2O+K_2O)$	15.5		26.36		51.96		20.58		17.07	
X-ray result	PH	PH + CH	PH + CH		FAUJ		A	OFF	PH	PH + CH

CH - Chabazite.

FAUJ - Faujasite.

For the meanings of the other symbols, see Tables 7 and 8.

1.2 CO-CRYSTALLISATION AND INTERGROWTH OF ZEOLITE L, ERIONITE AND OFFRETITE.

The data from the previous section showed (samples L-IC, 2', 5", 6" and 17') that zeolite L, erionite and offretite tend to grow together. It was also found that Linde T contains small amounts of zeolite L, shown by the presence of the reflection d = 16.00, which belongs to L(11).

Before considering further the problem of co-crystallisation of the three zeolites, it is necessary to discuss the possibility of distinguishing between erionite and offretite. It had previously been reported that X-ray powder patterns of the two zeolites were identical(24), and more recently that they could be distinguished by single-crystal X-ray or electron diffraction, but with less certainty by the X-ray powder technique(12). In the present work with synthetic samples it was found, however, that three fairly strong diffraction arcs occurred only in fully ordered erionite: 101 (d = 9.16), 201 (d = 5.37) and 211 (d = 4.16). These could be used for purposes of distinction. Fig. 21 presents the X-ray powder photographs.

The co-crystallisation of the three zeolites was detected by the X-ray powder technique, but as the latter is not easily able to detect the presence of small amounts of impurities, the samples were further examined in the electron microscope. All samples showed, in different proportions, the presence of flakes, rod-like crystals and hammer-shaped crystals as well as conglomerates of these (Figs. 18a, b and c and 19). Electron micrographs on a scanning microscope* (Fig. 22) and carbon replica micro-

---

* obtained by D. Mainwaring.

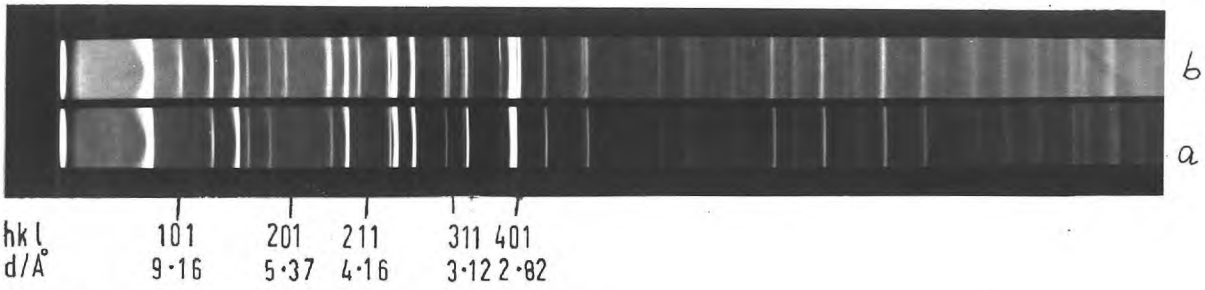

Fig. 21, X-ray powder pattern.

a) offretite. b) erionite.

Fig. 22, x 41,000 . L, preparation 6".

Fig. 23, x 20000. L, preparation 6".

Fig. 29, x 28000. L, preparation 5".

graphs (Fig. 23) give information about three-dimensional shape of the crystals: The flaky crystals were disc-like agglomerates and the rod-shaped crystals were cylindrical. The head of each hammer was a smooth continuation of the shaft, thus showing that each hammer is formed by epitaxy (see reference 138).

Electron diffraction patterns of the various particles were interpreted by comparison of measured spot spacings (p. 38) with those calculated from the known unit cells of offretite, erionite and zeolite L (Table 13). Though it was difficult to obtain an electron diffraction pattern from a single flaky crystal, a few such patterns were successfully recorded (Fig. 24) and were found to correspond with that expected from a crystal of L lying on its basal plane.

Figure 25 shows an electron diffraction pattern from a rod-like crystal which was identified as a faulted erionite. There are streaks running parallel to c, and the spots corresponding to ℓ odd are weaker than those for ℓ even. This suggests the occurrence of stacking faults (p. 39) in layers normal to c resulting in small regions of offretite within the crystal. In fact this pattern can be considered

TABLE 13.

Parameters / Zeolite	80 KV		100 KV		a Å	c Å
	a*mm	c*mm	a*mm	c*mm		
Zeolite L	1.32	2.81	1.19	2.53	18.4	7.5
Erionite	1.83_5	1.40	1.65	1.26	13.26	15.12
Offretite	1.83_5	2.79	1.65	2.51	13.26	7.56

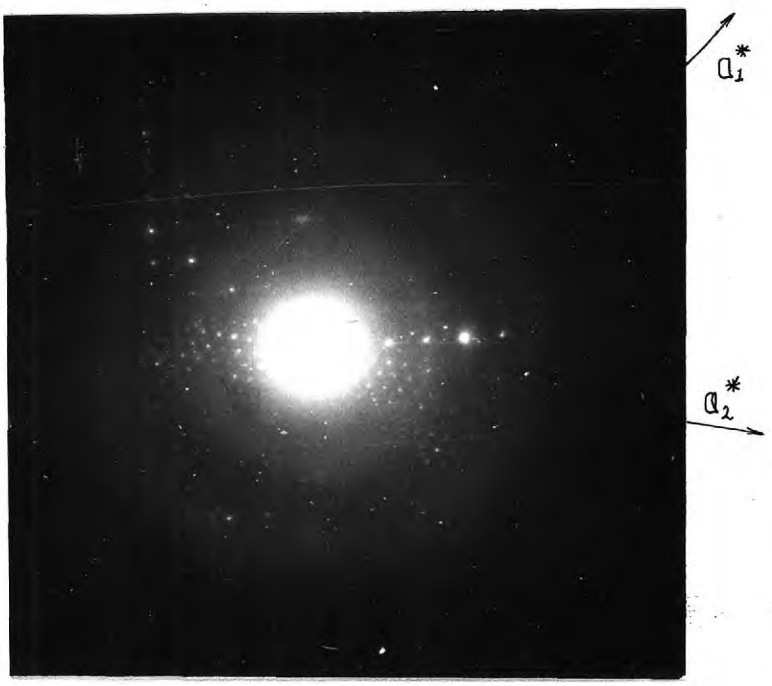

Fig. 24, ED pattern of L (beam parallel to c axis).

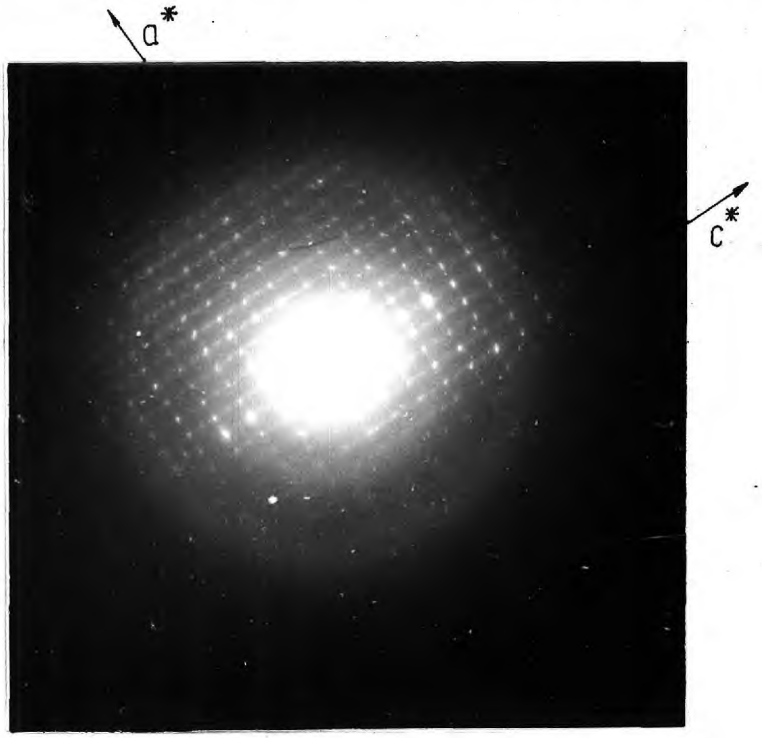

Fig. 25, ED pattern of a rod; faulted erionite.

as an intergrowth of erionite and offretite. The exact proportion is difficult to estimate although it seems likely that erionite forms the major part. Figure 26 is an electron diffraction pattern obtained from the shaft of a hammer-shaped crystal. The pattern is interpreted as a faulted offretite with c parallel to the shaft. This pattern differs from that in Fig. 25 in that the spots referred to above with l odd, have now disappeared, but the streaks parallel to c still persist. Faults therefore occur in stacking layers normal to c. When electron diffraction was directed only at the head of the hammer, the pattern in Figure 27 was obtained which corresponds to that of a crystal of zeolite L with the c-axis in the direction of the shaft.

The relation between the a-axes of offretite of the shaft and zeolite L of the head was established by electron diffraction patterns taken to include both parts (reference 138). It was concluded that in the two phases both the a- and c-axes are parallel.

In order to explain the result just described it is necessary to look more closely at the crystal structures (Table 1). All are frameworks in which $(Si,Al)O_4$ tetrahedra join at their apices to form rings of 4, 6, 8 and 12 tetrahedra. Each structure has as building units 11-hedral cancrinite cages and hexagonal prisms. Identical layers, perpendicular to the c directions exist in erionite and offretite, whilst identical chains parallel to the c direction occur in the L and offretite structures. Using the notation in which six-membered rings centred on the three possible six-fold axes in the unit cell are labelled A, B and C, offretite follows an AAB sequence, whereas

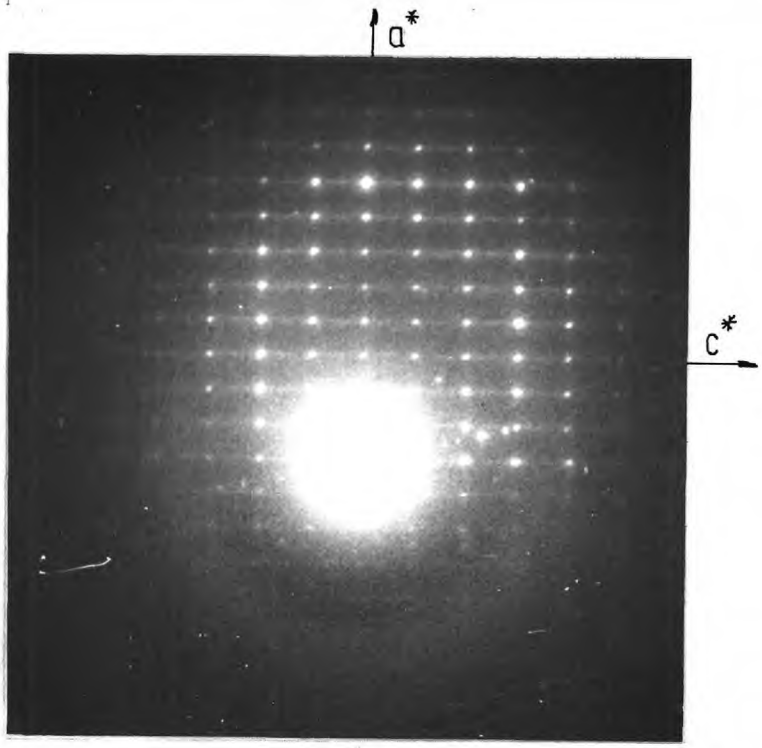

Fig. 26, ED pattern from the shaft of a hammer-shaped crystal; faulted offretite.

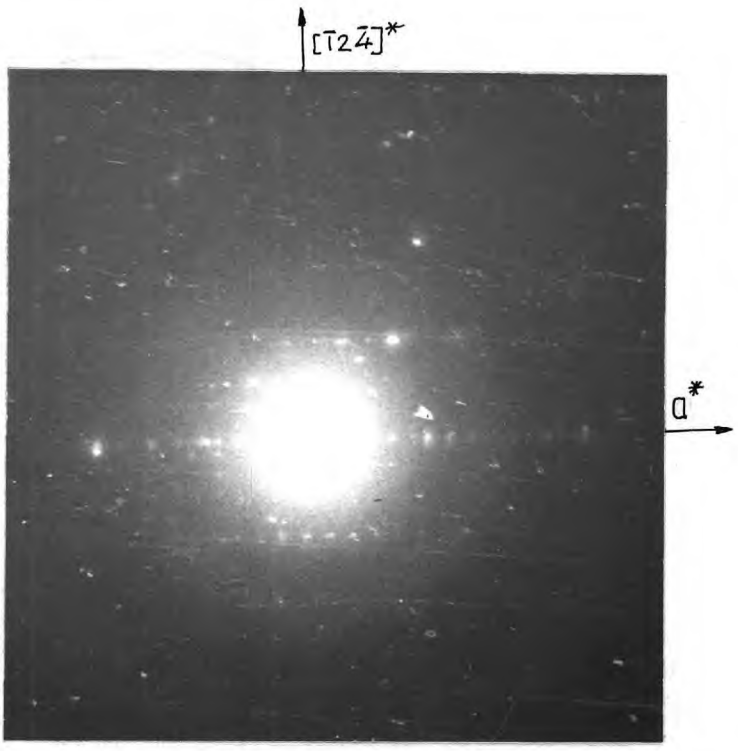

Fig. 27, ED pattern of head of hammer-shaped crystal, zeolite L.

erionite has a longer AABAAC sequence. The faulting of offretite and erionite can be appreciated when the similarity of the two structures, differing only in stacking sequence, is considered. Faulting will occur where the regular sequence is broken by the occurrence of a random layer, A, B or C. Erionite shows a tendency towards three layer repetition and therefore intercalates regions of offretite. The offretite intercalation is made manifest by the weaker l odd reflections in the pattern on Fig. 25.

On the other hand faulted offretite shows no tendency for higher periodicity than 3 and so remains essentially an offretite with frequent faults. In general these kinds of faulting will entail the presence of A, B and C layers in comparable number, with consequent blocking of the main channels and alteration of the molecular sieve behaviour. However, other kinds of faulting can occur in offretite. This faulting may be easily visualised by generating the framework structure of offretite through a symmetry operation involving chains of four-membered rings, similar to those occurring in some other zeolites having non-intersecting, parallel main channels, for example zeolite L, cancrinite and gmelinite(11). Periodic variations from the ideal offretite chain are possible, which can introduce kinds of faulting that do not obstruct the main channel. These types of faulting cannot be distinguished by electron diffraction from those which block the channels, but the molecular sieve behaviour of faulted crystals should serve to differentiate between them.

The hammer-shaped crystals probably owe their peculiar shape to epitaxial growth between a head composed of zeolite L and a handle of offretite. Since both structures contain identical chains, similarly orientated with respect to their unit cells, the epitaxy may be explained by some

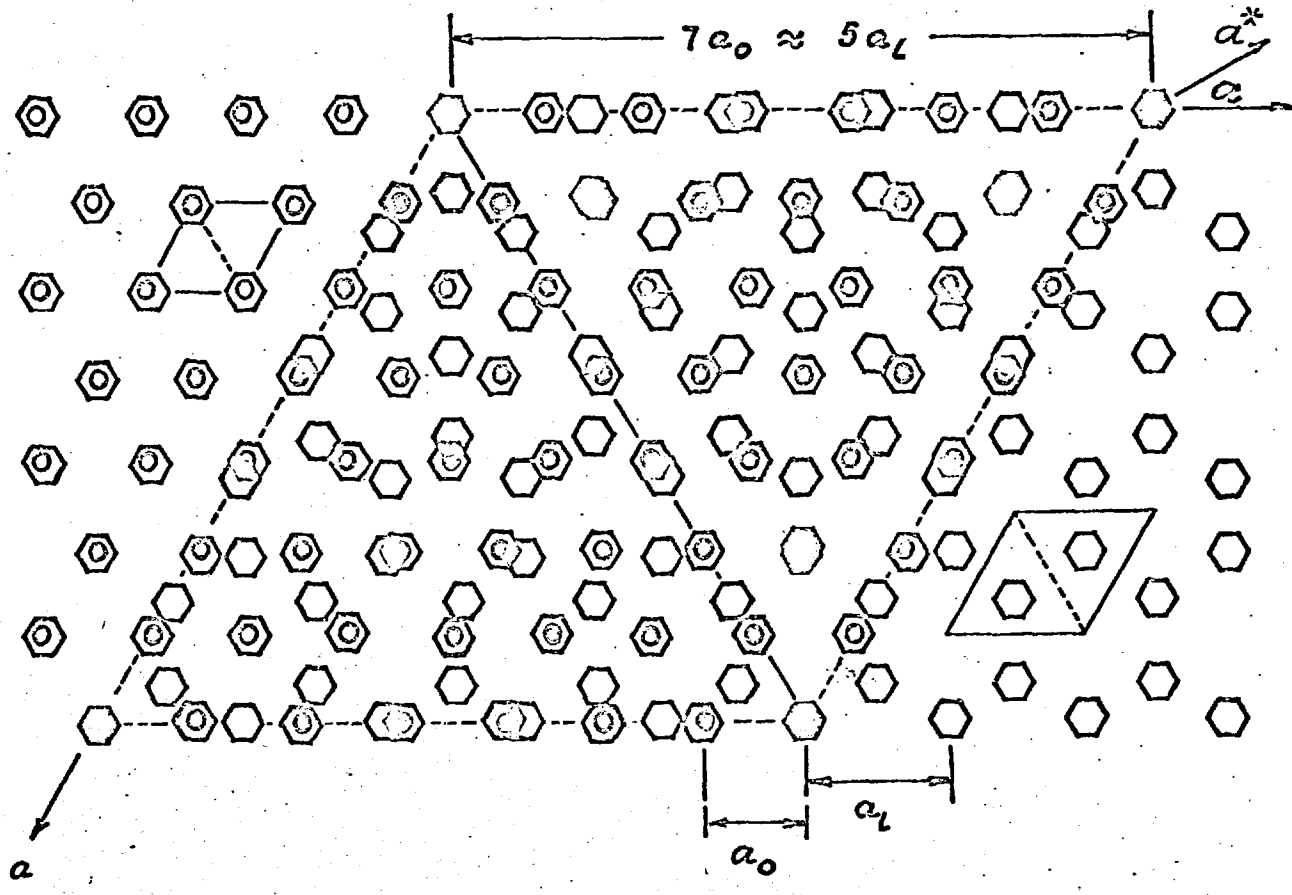

Fig. 28 Projection down c axis

of the chains passing through the interface and effecting a firm union between the two crystals. It would also be necessary for there to be an approximate lattice fit for not one, but a whole array of linking chains. Figure 28 shows a projection down the c-axis of the chains in offretite and zeolite L upon which certain indicated chains nearly coincide. A coincidence would result in a ratio $a_L/a_O = 1.4$, which is close to the experimental value 1.388 and within the limits set by Wilman(141). A question which naturally arises here is whether the offretite or the zeolite L was present first. However, a careful examination of the electron micrographs has revealed several hammers with two shafts(138) - an example is given in Fig. 29 - p.97. whereas double-headed hammers have not so far been observed. These facts seem to indicate that offretite shafts have grown on heads of zeolite L.

From the foregoing observation it can be concluded that zeolite L grows predominantly in the a direction in a flaky habit, whilst offretite and erionite have a preference for growing in the c direction in a rod-like habit. The structural causes of the favoured platy habit of zeolite L, in spite of the presence of the chains accounting for the fibrous, acicular or prismatic habits of offretite and erionite, are not known.

X-ray powder diffraction fails to distinguish between offretite and structural intergrowths such as zeolite T, in which there is a fairly high proportion of erionite stacking. The appearance of hammer-shaped crystals in a given sample is an indication of the presence of both offretite and zeolite L and can be used as such when the X-ray powder method fails to show their presence (sample 2'). Hammer-shaped crystals have been encountered previously but not identified(78). It is always advisable to examine

specimens of offretite and erionite by electron diffraction to detect whether faulting occurs. This is particularly important when samples are intended as sorbents. The data in section 4.1.2 reveal that K-erionite does not sorb Ar, in contrast to the Na-form. A sample of K-offretite, faulted by erionite, will not sorb Ar, but the corresponding non-faulted form will. Thus, in case of faulting of offretite by erionite, sieving properties are determined by the erionite layers. However, faulted and unfaulted samples of offretite will have virtually the same X-ray powder patterns.

The data in section 4.1 gives the following sequence of the saturation capacities for Ar at 77.3°K:

$$N_{\text{sat H-OFF}} > N_{\text{sat H-ER}} > N_{\text{sat HL}}$$

Accordingly, the presence of offretite and erionite in L will result in higher adsorption capacity than that of pure L. The saturation capacities of Ar found on L-IC confirmed this (Table 30). Capacities for Ar of L samples contaminated by K-erionite would, however, be expected to be lower than those for pure L. In fact, the capacity of Ar on KL-IC was found to be higher than that of KL (Table 30) demonstrating that erionite is the minor contaminant and the offretite faulting is of a type that does not obstruct the channel (p.102). Quantitative conclusions are not possible as neither the erionite/offretite ratio nor the degree of faulting is known.

1.3 EFFECTS OF SECONDARY BUILDING UNITS ON CO-CRYSTALLISATION.

The simultaneous growth of zeolite L, erionite and offretite, all of which possess common building units (cancrinite cages and hexagonal prisms) suggests that such

units may form in solution as precursors to nucleation of crystal growth. Such units may well originate from chains and rings of SiO_4^{-4} and AlO_4^{-5} tetrahedra, surrounding a cation in solution. Condensation-polymerization of polygonal and polyhedral ions, as discussed before(75) may then result in formation of stable nuclei. This mechanism is supported by the fact that cations are included within these units in the final structures(11,14). The idea that the initial orientation around the cations may be of decisive importance for directing the process of crystallisation of zeolite L, erionite and offretite is supported further by the following observations: The value of the $Na_2O/(Na_2O + K_2O)$ ratio was the only essential difference in the patented compositions for syntheses of L and T (Table 7). It was found in the present work that compositions without Na^+ are most favourable for obtaining pure L, and also that the ratios $Na_2O/(Na_2O + K_2O)$ together with $H_2O/(Na_2O + K_2O$ are determining for erionite/offretite, chabazite and faujasite preparations. (Tables 8, 9 and 12).

The co-crystallisation of zeolite L, erionite and offretite conveniently illustrates the tendency of phases which possess common building units to co-crystallise. Where domains of the structures are common to each structure, limiting cases of co-crystallisation are observed, such as the epitaxy of offretite and L (common chains - p. 12) and the intergrowth of erionite and offretite (common layers, p 16).

Co-crystallisation of zeolites cannot always be attributed to the presence of common building units, but this appears to be true for a number of cases. Table 3 summarises some co-crystallising phases found by other authors. The following cases taken from this table further illustrates this point:

co-crystallising phases	common building units
faujasite/sodalite	sodalite cages
zeolite A/sodalite	sodalite cages
faujasite/chabazite	hexagonal prisms
chabazite/erionite	hexagonal prisms
epistilbite/hormotome	layers of four-membered rings, joined by eight-membered rings.
epistilbite/heuleudite	

Four and eight (or six)-membered rings are common for many co-crystallising phases of Table 3 - chabazite/phillipsite, erionite/phillipsite, analcite/mordenite, analcite/cancrinite, but as such small building units are incorporated into the majority of zeolites, their presence cannot be considered as decisive for co-crystallisation. A more probable reason for the above cases is the presence of common chains of four-membered rings of the type described in(11). Examination of the data in Table 3 shows that analcite and phillipsite frequently co-crystallise. It is possible to consider that these two zeolites are formed in the initial stages of crystallisation and are then transformed, partially or fully, into other phases. An application of the simplexity principle, proposed by Goldsmith(139) explains the prior initial formation of analcite and phillipsite, as their structures are more highly disordered (with higher entropy) than the phases with which they co-crystallised. Transformation of one structure into another in the mother liquor should be considered as a special case of co-crystallisation, involving a reorganisation of structures already formed. In such cases, a correlation between the

secondary building units of the initial structure (most disordered one) and that to which it transforms will be of significance. The fact that the synthetic zeolites are not necessarily equilibrium phases and that Ostwald's rule(79) sometimes applies to the zeolite crystallisation processes (p. 46) makes the variety of the simultaneously existing phases large and generalisation difficult.

2. ION-EXCHANGE

Ion-exchange was used to prepare modified zeolite sorbents. The extent of ion-exchange towards different cations at room temperature and concentrations near saturation was determined for zeolite L and erionite. In the present section the results of these ion-exchange experiments will be considered. Analytical and X-ray characteristics of each ion-exchanged form will also be discussed.

2.1 CHEMICAL CHARACTERISTICS OF THE ION-EXCHANGED FORMS OF ZEOLITE L ERIONITE AND H-OFFRETITE.

The samples of L, L-IC, ER and OFF described on p. 68 were used for ion-exchange. Table 14 gives the total chemical composition of L, ER and OFF.

TABLE 14

Chemical composition of the original samples of zeolite L, erionite and offretite

Sample	% relative to the hydrated weight							idealised oxide formula
	K_2O	Na_2O	CaO	$(TMA)_2O$	Al_2O_3	SiO_2	H_2O	
L	14.03	0.70	-	-	15.20	59.06	10.90	$K_2O_{0.9}Na_2O_{0.1}$ $Al_2O_3 6SiO_2 4H_2O$
ER	3.90	5.05	0.63		14.76	64.39	11.90	$Na_2O_{0.6}K_2O_{0.3}CaO_{0.}$ $Al_2O_3 7SiO_2 5H_2O$
OFF*	5.96	-	-	11.60	13.82	61.45	8.10	$(TMA)_2O_{0.6}K_2O_{0.4}$ $Al_2O_3 7SiO_2 3H_2O$

* results provided by Dr. R. Aiello.

Results of analyses of the ion-exchanged forms of L, ER and OFF are given in Table 15. Samples having the following unit cell compositions were used as references, for determining the degree of ion-exchange: $K_9Al_9Si_{27}O_{72}$ for L; $Na_6K_3Al_9Si_{27}O_{72}$ for ER and $K_4Al_4Si_{14}O_{36}$ for OFF. Both the residual potassium and the entering cation were determined spectrophotometrically (see p.79) for each form of L, except HL and LiL, where only the residual potassium was determined.

For the erionites the degree of ion-exchange was estimated by measuring (spectrophotometrically) the amount of potassium and sodium on each sample; and for H-OFF by measuring the amount of potassium only.

From the degree of ion-exchange (Table 15) the following characteristics were calculated: compositions of the unit cells; weights of the unit cells and the numbers of unit cells per gram of dehydrated sample.

Water contents (Table 15) were determined from the weight losses on ignition. For the decationated forms however, this loss includes hydroxyl water. The latter was calculated from the degree of ion-exchange for each of the samples. The values obtained, expressed as a percentage of the dehydrated weight are 4.6% (HL); 5.3%(H-ER) and 4.3%(H-OFF). The amount of hydroxyl water for the metal-cation exchanged forms (e.g. for $Na_2HK_6Al_9Si_{27}O_{72}$) was below 0.5% and was neglected. On the basis of the zeolitic water in each sample, the numbers of water molecules per unit cell were determined (line 6 in Table 15).

Originally the amount adsorbed was calculated in cc(STP) of sorbate per gram of dehydrated sorbent ($a\frac{cc}{g}$). It was considered (p.158) to be more convenient if the amount adsorbed was expressed as the number of molecules of sorbate per unit cell of dehydrated sorbent ($N\frac{m}{u.c}$).

TABLE 15

Chemical characteristics of the ion-exchanged forms of zeolite L, erionite and offretite.

Characteristic \ Sorbent	HL	LiL	NaL	KL	CsL	BaL	LaL	K-ER	Na-ER	H-ER	H-OF
H_2O% referred to dehydr. weight.*1	27.5*2	24.6	15.8	12.3	11.5	16.6	17.3	13.5	17.1	21.9*2	20.
Degree of ion-exchange, % equiv.	82.3	31.4	32.5	9.8	32.6	33.6	34.7	43.8	11.6	86.5	78.1
Idealised formula of unit cell.	H_8KR*4	Li_2HK_6R	Na_2HK_6R	K_8HR	Cs_2HK_6R	$BaHK_6R$	$LaHK_6R$	K_7Na_2R	Na_7K_2R	H_8KR	H_3KR_1
Weight of unit cell.	2199.3	2403.0	2434.0	2466.1	2654.3	2525.0	2488.9	2472.5	2395.0	2200.6	1115.
Number of u.c.per gram, 10^{20}.	2.74	2.50	2.48	2.44	2.27	2.38	2.41	2.42	2.52	2.74	5.3
H_2O molecules per unit cell*3.	27.4	33.0	21.4	16.9	17.0	23.0	23.9	18.2	22.1	20.4	10.2
k, coeff.for transfer a $\frac{cc}{g}$ into $N\frac{m}{u.c.}$	0.098	0.107	0.108	0.110	0.117	0.116	0.115	0.108	0.106	0.098	0.0

*1 estimated as loss of weight by ignition.

*2 hydroxyl water included.

*3 estimated on the basis of the zeolitic water.

*4 $R = Al_9Si_{27}O_{72}$; $R_1 = Al_4Si_{14}O_{36}$.

A coefficient $\underline{k}$ for converting a $\frac{cc}{g}$ into $N\frac{m}{u.c.}$ for each sorbent is given on line 7 of Table 15 and can be used for recalculation of the adsorption data where necessary.

Several points arising from the data of Table 15 deserve attention:

1. The extent of ion-exchange of zeolite L towards different metal cations is restricted to values in the range 31-34%. As about 38% of the cations are thought to be sited in the main channel(11), it seems that under the present experimental conditions only these ions are available for exchange. This confirms and extends to different cations the results of Barrer and Villiger who found by structural analyses(11) that after an exchange at room temperature, the channel is occupied by K^+ (in potassium enriched form of zeolite L) and by Na^+ (in the sodium enriched form).

Breck and Flanigen(15) have reported a variety of degrees of ion-exchange of L towards different cations: av. 25% (Zn^{2+} and Ce^{3+}); av. 40% (Li^+, Na^+, Sr^{2+}, Mg^{2+}) and as high as av. 72% for Ba^{2+} and Ce^{2+}. The ion-exchange procedure was the usual one of mixing the original sample at room temperature with solutions of the corresponding chloride, sulphate or nitrate and washing the product obtained with distilled water. The mixtures were vigorously stirred and this, together with the differences in solution concentrations, are the only differences between the procedure of reference 15 and that of the present work. The high value of 73.2% exchange found by Breck and Flanigen is difficult to explain on the basis of the structure of zeolite L. Of the eight samples investigated by Breck and Flanigen, four gave about 40% exchange which is close to the percentage of cations in the main channel.

However, as adsorption in zeolite L takes place in the

main channel, only the exchange of the cations sited there is relevant when preparing samples for adsorption.

2. Zeolite L undergoes partial decationation during the ion-exchange, as a result of which a deficiency of about one cation per unit cell is present in all metal cation-exchanged forms studied. A decationation during washing of newly synthesised samples of L has also been reported by Breck and Flanigen(15), although numerical data are not available. In the ion-exchange of L carried out by Barrer and Villiger(11) decationation was not observed. Their procedure included washing of the product with a weak solution of NaOH, which explains the absence of decationation.

3. The ion-exchange of natural erionite also shows a restriction on the number of the original cations that can be replaced. It can be concluded, from comparison of the composition of the original sample and of the K-ER and Na-ER prepared from it, that four of the nine cations per unit cell cannot be exchanged. This corresponds to 45% cation equivalents. Limitation in the degree of exchange of up to 40% has been reported by Peterson et al(28) and of up to 50% by Eberly(27). All these results can be related to the work of Gard et al(14) who located one cation position in the middle of the cancrinite cage. As there are four such sites per unit cell, the number of cations sited there is equal to the number of cations which do not undergo ion-exchange. Similarly, ion-exchange in L suggests that the cations in the cancrinite cages do not undergo exchange at room temperature. Cations in the cancrinite cages appear to be trapped at low temperatures in L and erionite structures.

The exchangeable cations in erionite are thought to be in the large cavities. There are two large cavities per unit cell and there will be about five such cations per cell.

The cation distribution in erionite will be further discussed on the basis of the adsorption data in a later section (4.1.2).

4. The extents of ion-exchange for decationated forms, via the NH_4-forms, of L and ER are almost twice those found for the metal-cation forms (line 2, Table 15). Barrer and Kanellopoulos(19) prepared NH_4L at 100°C and also found an extensive exchange(84%). They attributed this to exchange of all cations in the unit cell except those in the cancrinite cages. The calculated value for this exchange is 78% which is in approximate agreement with the experimental value. The same explanation can be accepted for the present data, but the reason for the special behaviour of NH_4^+, compared with the metal cations, is not clear. The ion size is not the cause, as NH_4^+ (radii 1.42 Å(123)) is larger than the alkali metal ions used (Table 16).

For H-ER the observed high degree of ion-exchange for NH_4^+ makes it necessary to consider the possibility of exchange of the cations in the cancrinite cages.

As only a single sample of offretite was investigated no conclusions based on the degree of ion-exchange could be made. This case has been discussed elsewhere(126).

2.2 X-RAY EXAMINATION OF THE ION-EXCHANGED FORMS OF L.

It was of interest to investigate the effect of different cations on the structure of zeolite L. For this purpose X-ray powder patterns were taken at room temperature on a Guinier camera for all ion-exchanged forms and used to compute the unit cell. Sharp lines of medium intensity, each corresponding to a single reflection(11) were selected and their position accurately measured on a Vernier scale. The lines selected were 001, 210, 220, 310, 301, 221, 311 and 321. $Pb(NO_3)_2$ was used as a standard. Corrected d spacings

were calculated by applying a computer program Delkor(127). With the d values so obtained the unit cell dimensions of each form were calculated. For this purpose a computer program CDLS(128) was used. The results are listed in Table 16.

TABLE 16

Unit cell and cation dimensions for ion-exchanged forms of zeolite L.

Sorbent	a $\mathring{A}$	c $\mathring{A}$	V $\mathring{A}^3$	R cation* $\mathring{A}$	V cation $\mathring{A}^3$	V_2 cations unit cell $\mathring{A}^3$/u.c.
HL	18.357	7.597	2217.12	-	-	-
LiL	18.409	7.551	2216.11	0.60	0.90	1.80
NaL	18.485	7.514	2223.43	0.95	3.58	7.16
KL	18.450	7.529	2219.84	1.33	9.83	19.65
CsL	18.447	7.545	2223.67	1.68	19.80	39.60
BaL	18.436	7.528	2215.69	1.35	10.27	10.27
LaL	18.349	7.527	2194.69	1.15	6.35	6.35

* the data obtained from (123).

Table 16 also gives the radius and volume of each cation together with the total volume of cations per unit cell.

The dependence of the unit cell axes on the cation size is presented graphically on fig. 30. We can divide the investigated cations into two families: cations with the same valence but different size (Li^+, Na^+, K^+ and Cs^+); and cations with different valence and hence cation density per unit cell, but of approximately the same size (K^+, Ba^{2+} and La^{3+}). Fig. 30 shows that both a and c cell dimensions

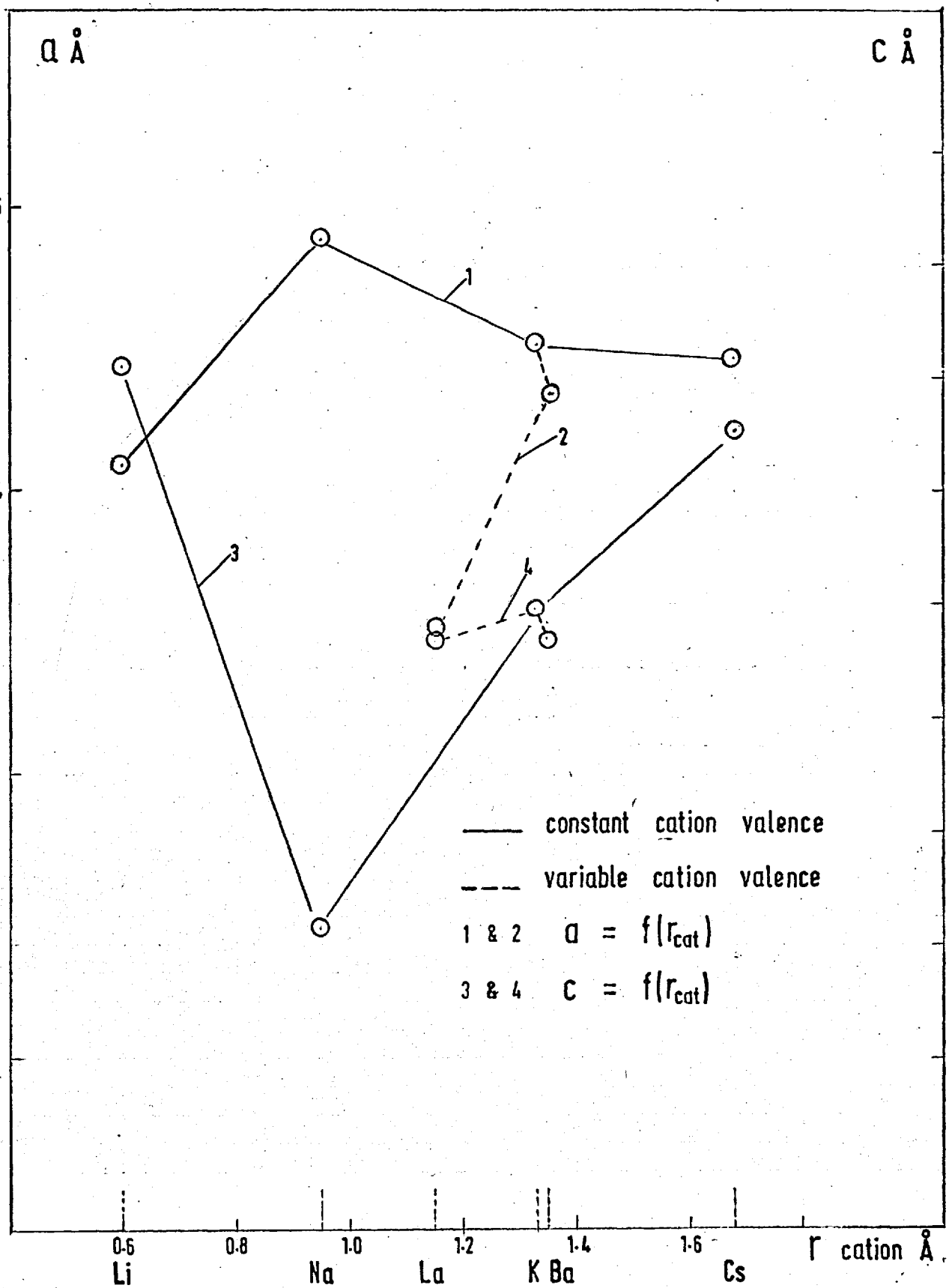

Fig. 30 UNIT CELL CONSTANTS vs r cation

are dependent on the cation size as follows:

$$a_{Li} < a_{Na^+} > a_{K^+} > a_{Cs^+}$$

$$c_{Li} > c_{Na^+} < c_{K^+} < c_{Cs^+}$$

Thus with the exception of LiL the increasing cation size resulted in contraction of a and expansion in c. The valence of the cations mainly influences the a dimension (curve 2 on Fig. 30) - the higher the valence the lower the a value - but no measurable effect of valence was observed on the c dimension.

The dependence of the volume of the unit cell on the volume of cations per unit cell is shown in Fig. 31. Constant cation valence corresponds to constant volume of the unit cell, which is thus independent of the size of the cation, LiL again being slightly exceptional. Decreasing cation valence is followed by an increase of the volume of the unit cell. One might attribute this behaviour to the differences in the volumes occupied per unit cell by the cations of different valence. An examination of column 7 of Table 16 shows, however, that the differences in the corresponding volumes for cations of different valence are smaller than those for cations of constant valence (for example KL, LaL vs CsL, NaL or vs CsL, KL). Such an explanation, therefore is not tenable.

The distribution of the cation charge in the main channels of L may also be considered as a cause. For monovalent cations, three electrostatic charges are sited at distances apart of 5.58 Å(11) which is the separation between neighbouring sites in the main channels. For cations of higher valency such a distribution is no longer possible, the limiting case being La^{3+}, where all the charges will be

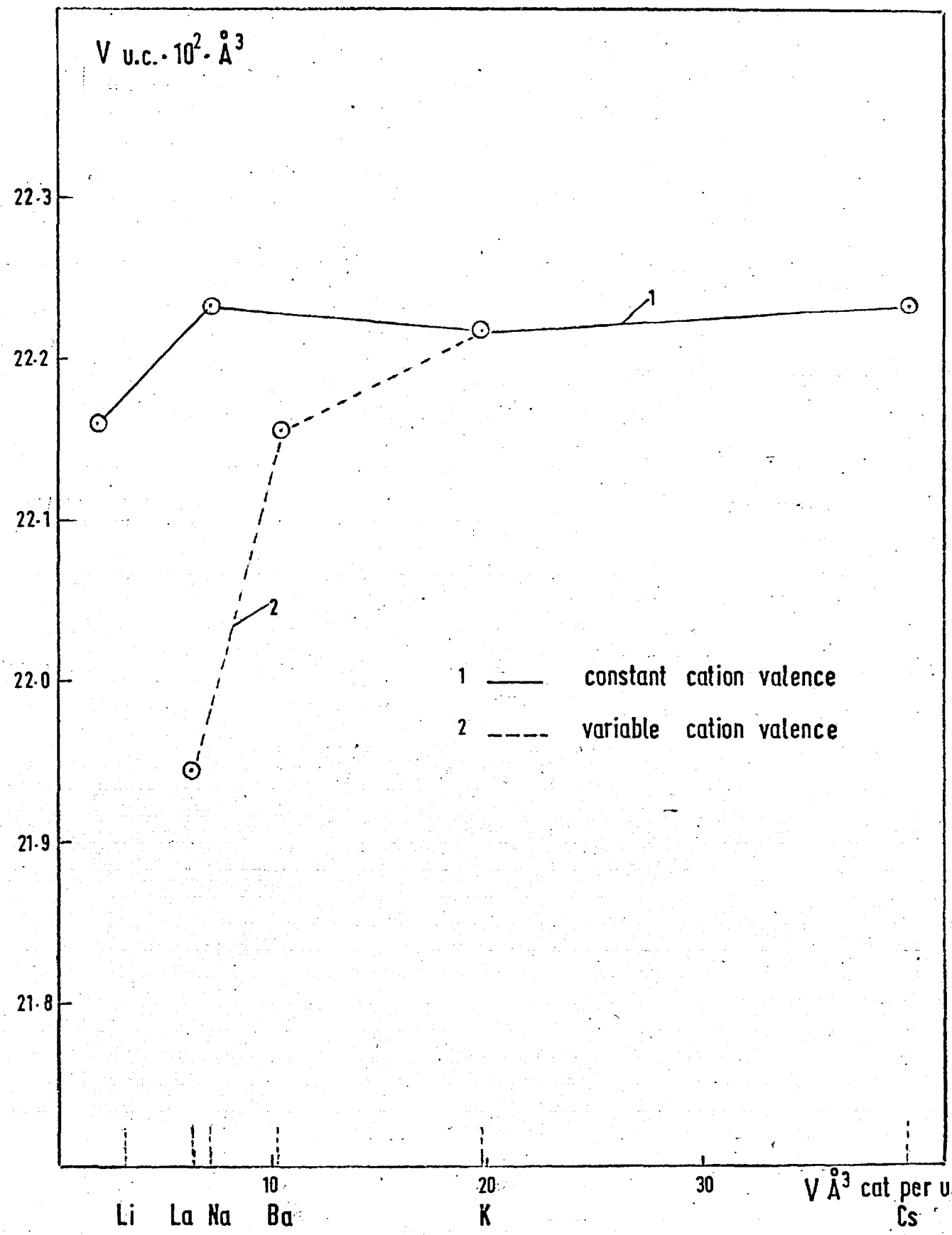

Fig. 31 V u.c. vs V cations per u.c.

concentrated at the location of La^{3+}. Such different charge distribution may deform the unit cell differently.

The computed unit cells for all ion-exchanged forms of L were used to calculate the d spacings for each form using a computer program Apol(129). From the obtained powder patterns of each ion-exchanged form the d spacings were also directly measured by Guinier ruler. The intensities were visually estimated and the data are given in Tables 17 and 18. The patterns of LiL, NaL and KL showed almost identical intensities of the corresponding lines and only the KL pattern is therefore tabulated. The only exceptions were the reflections 300 and 201 which are observed as weak lines on patterns of LiL and NaL, but are absent for KL.

By comparison the intensities in the CsL pattern are considerably different; reflections 210, 001, 111, 301 and 321 being absent, whereas in the other patterns they have strong or medium intensity (see Table 17). The presence of reflection 201 for HL alone, and absence of 111 from CsL, BaL and LaL, represent significant differences in the patterns. Other minor differences can be found by directly comparing each pair of patterns.

TABLE 17.

X-ray powder patterns* at room temperature of HL, KL and CsL

HL			KL			CsL		
d $\AA^{-1}$	hkl	I/I_o	d $\AA^{-1}$	hkl	I/I_o	d $\AA^{-1}$	hkl	I/I_o
15.90	100	vs	15.98	100	vs	15.98	100	vs
9.18	110	w	9.22	110	w	9.20	110	m
-	-	-	7.99	200	w	8.00	200	w
7.60	001	m	7.53	001	s	-	-	-
6.00	210	s	6.04	210	s	6.04	210	w
5.85	111	m	5.83	111	m	-	-	-
5.49	201	w	-	-	-	-	-	-
4.59	220	s	4.61	220	vs	4.61	220	s
4.41	310	w	4.43	310	m	4.43	310	m
4.35	301	m	4.35	301	m	-	-	-
3.93	221	s	3.93	221	vs	3.93	221	s
3.69	-	s	3.66	-	vs	3.67	-	m
3.51	-	s	3.48	-	vs	3.49	-	m
3.29	321	m	3.29	321	s	-	-	-
3.18	-	s	3.19	-	vs	3.20	-	m
3.09	-	m	3.07	-	vs	3.08	-	m
2.92	222	s	2.92	222	vs	2.91	222	m
-	-	-	2.80	421	m	-	-	-
2.65	600	m	2.66	600	vs	2.65	600	w
2.63	-	w	2.62	-	m	2.63	-	m
-	-	-	2.56	-	m	-	-	-
-	-	-	2.48	-	m	2.49	-	m
-	-	-	2.43	-	m	-	-	-
-	-	-	2.20	-	s	2.20	-	w
1.89	-	w	1.89	-	s	1.89	-	m
-	-	-	1.82	-	m	-	-	-
-	-	-	1.78	-	w	1.79	-	w
-	-	-	1.69	-	m	-	-	-
-	-	-	1.53	-	m	-	-	-

* Lines found to be weak in all patterns are omitted.

TABLE 18.

X-ray powder patterns* at room temperature of BaL and LaL

BaL			LaL		
d A^{o-1}	hkl	I/I_o	d A^{o-1}	hkl	I/I_o
15.97	100	vs	15.89	100	vs
7.53	001	s	7.53	001	s
-	-	-	6.80	101	w
6.04	210	s	6.01	210	s
-	-	-	-	-	-
4.61	220	s	4.59	220	m
4.43	310	w	4.41	310	m
4.35	301	w	4.33	301	m
3.93	221	vs	3.92	221	vs
3.82	311	w	-	-	-
3.67	-	m	3.70	-	s
3.49	-	s	3.49	-	s
3.29	321	m	3.28	321	w
3.19	-	s	3.19	-	s
3.07	-	s	3.07	-	s
2.94	501	m	-	-	-
2.92	222	s	2.91	222	vs
2.80	421	w	-	-	-
-	-	-	2.73	402	w
2.68	511	vw	2.67	511	w
2.66	600	m	2.65	600	m
2.62	-	w	2.62	-	vw
2.42	-	w	-	-	-
-	-	-	2.20	-	m
1.89	-	m	1.89	-	m
-	-	-	1.81	-	w
-	-	-	1.78	-	w
1.57	-	m	1.57	-	m
1.53	-	m	1.53	-	m

* Lines found to be weak in both patterns are omitted.

3. BEHAVIOUR ON HEATING.

The behaviour of zeolite L on heating was studied by DTA, TGA, electron microscopy and X-ray techniques. The aim was to characterise the dehydration process and to investigate possible alteration of the structure during and after heating. A partical investigation by TGA and X-ray techniques was also made on samples of erionite and offretite.

3.1 DIFFERENTIAL THERMAL ANALYSES (DTA).

DTA data for LiL, NaL and CsL are presented on Fig. 32 and for KL, BaL and LaL - on Fig. 33. All ion-exchanged forms of monovalent cations showed similar DTA curves with a wide endothermal peak starting at about 100°C and ending at 300°C. Each main peak is made up of two narrow endothermal peaks, of poorer definition, positioned respectively at 130°C and 220°C (LiL); 125°C and 205°C (NaL); 125°C and 200°C (KL) and 130°C and 210°C (CsL). These narrow peaks are sharper for the cases of small cations - LiL and NaL, than for KL and CsL (Figs. 32 and 33). It is well known(66,119) that an endothermal peak in the interval 100°C-400°C in DTA curves of zeolites corresponds with dehydration. The presence of several individual endothermal peaks is reasonably attributed(66,119) to the presence of different types of zeolitic water, i.e. to the existence of energetically different sites for water molecules in the structure. The better the definition of the peaks, the greater the difference in binding energy of the water sites. It can be assumed, therefore, that two energetically well defined water sites exist in LiL and HL, but they are les differentiated in KL and CsL. The separation in case of small cations may be due to their larger hydration energy as shown in Table 19.

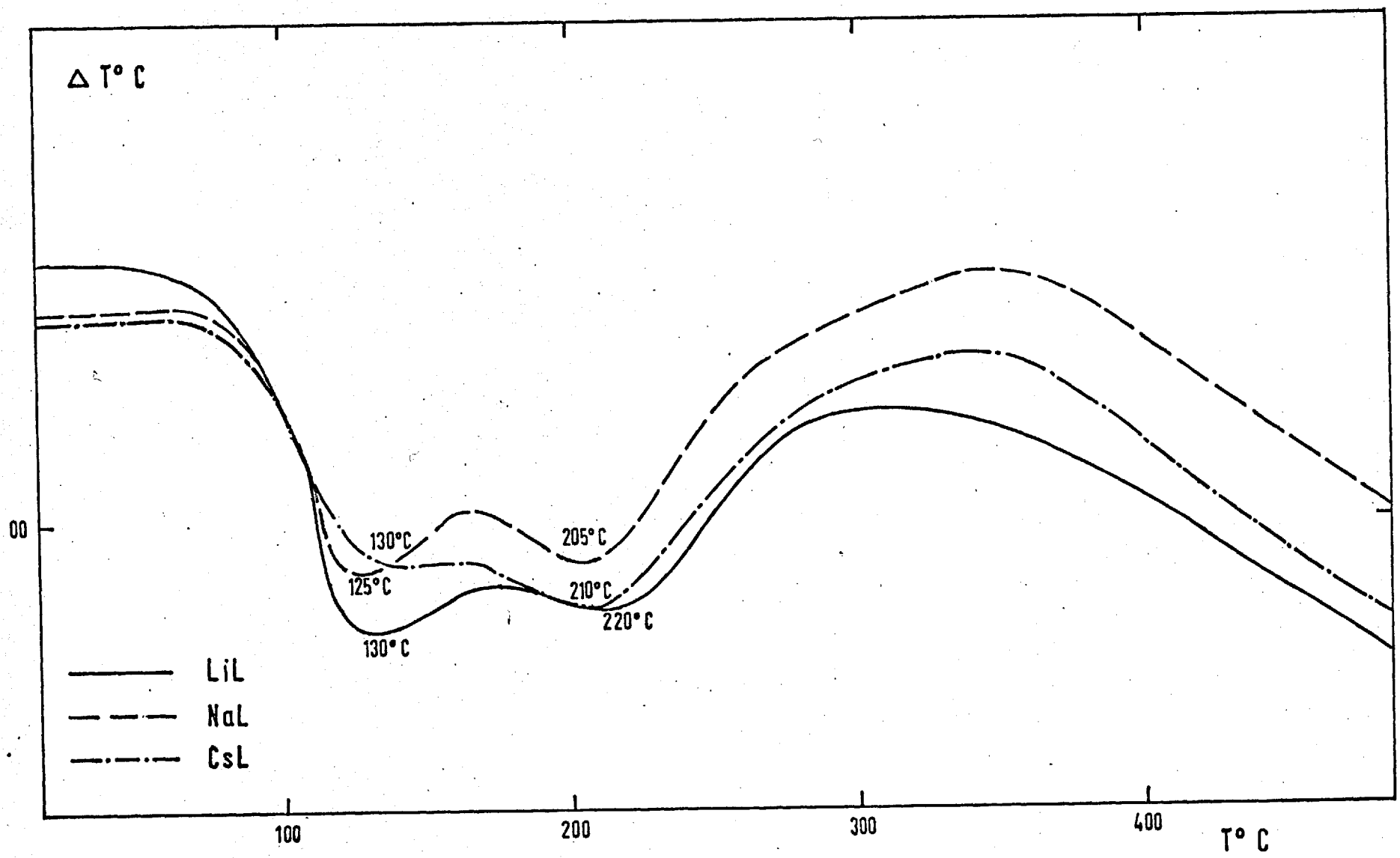

Fig. 32 DTA CURVES for LiL, NaL and CsL.

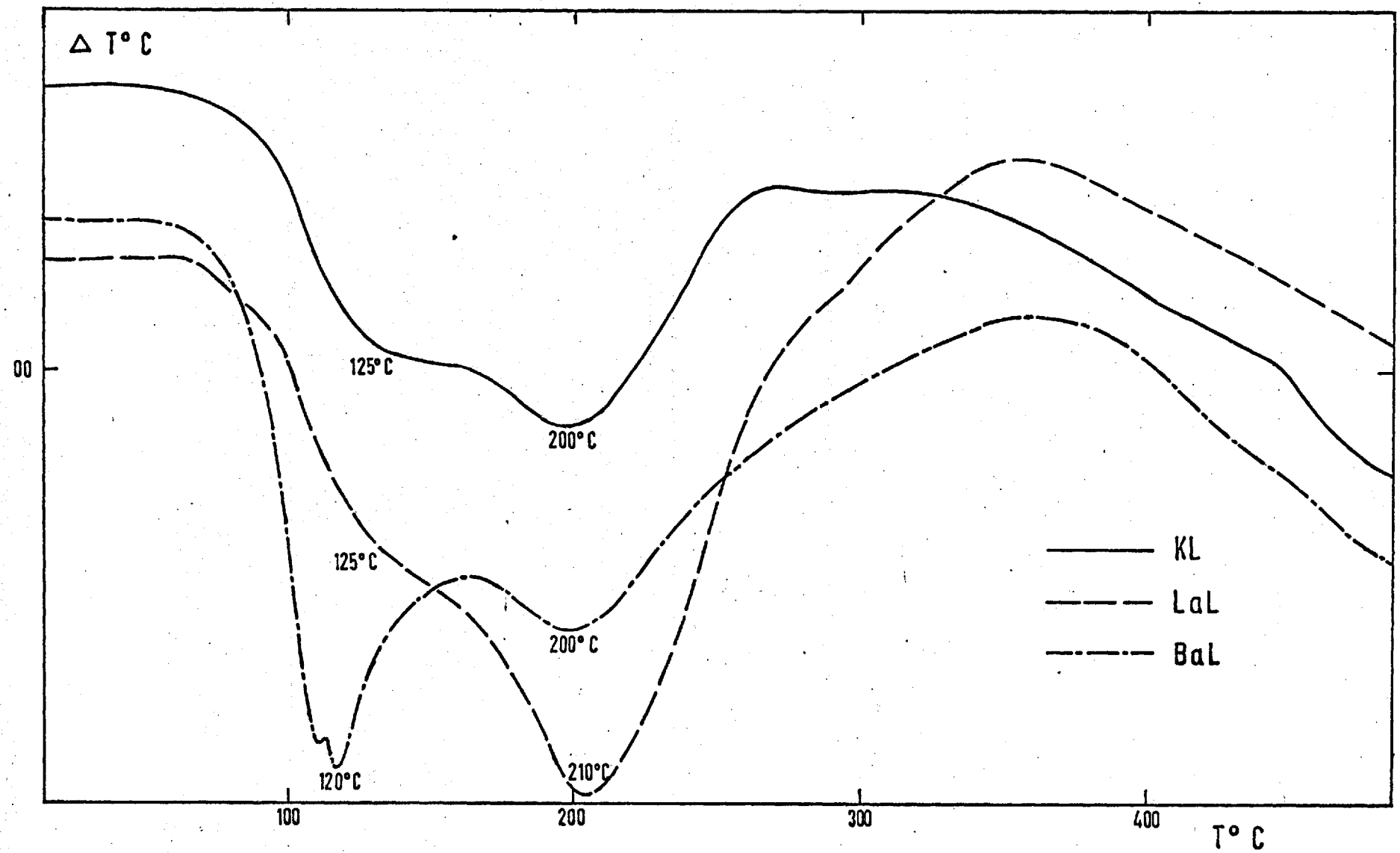

Fig. 33 DTA CURVES for KL BaL and LaL

TABLE 19

Heats of hydration of cations in k cal/g ion (124)

Li^+	Na^+	K^+	Cs^+	Ba^{2+}
136	114	94	80	376

The water molecules in the main channels of zeolite L can be divided into those mainly concentrated around the cations and those more nearly free of the cations. In accordance with Table 19 the smaller alkali metal cations would, therefore, be expected to have the observed more distinct DTA peaks.

DTA curves of BaL and LaL also show wide endothermal peaks in the same temperature interval as in the previously discussed cases, but these peaks are different in shape. For BaL a deep sharp peak at 120°C and a flat one at 200°C are observed while for LaL one distinguishes a narrow peak at 210°C and a badly defined one at 125°C. This difference can again be attributed to the different heats of hydration of the cations. The narrow endothermal peaks, much deeper than in the case of monovalent cations, are probably due to water from strongly bonded clusters around Ba^{2+} and La^{3+}.

3.2 THERMOGRAVIMETRIC ANALYSES (TGA).

TGA analysis served mainly to estimate the loss of weight for the sorbents. TGA curves were obtained for all samples of L, for K-ER and for the original sample of

offretite. (The latter contains TMA*).

The TGA data are presented in Figs. 34 and 35. The loss of weight is calculated relatively to the hydrated weight. The TGA curves of HL, LiL and OFF show continuous loss of weight up to 1000°C. For all other sorbents, well defined plateaux are observed. The temperature of the beginning of each plateau and the corresponding loss of weight are given in Table 20. The loss of weight in the table is calculated relatively to the dehydrated weight for convenient comparison with the data of Table 15.

TABLE 20

Data from TGA

Sorbent	NaL	KL	CsL	BaL	LaL	K-ER
Loss weight %	12.8	12.0	9.9	14.1	15.4	11.2
t°C.	500	520	500	520	530	400

A comparison of the data in the above table and in Table 15, line 1, reveals that the loss of weight estimated by ignition exceeds the corresponding values estimated from TGA curves. However, the order obtained for the different ion-exchanged forms is the same:

$$LaL > BaL > NaL > KL > CsL$$

This order is in good agreement with the cation size and cation densities of Table 16. The ion-exchanged forms of L which have the highest weight losses in Table 15 are those for which TGA curves showed continuous loss of weight - HL and LiL. The effects on HL could be understood in terms of the dehydroxylation process (p. 42) continuing up

* TMA - tetramethyl ammonium cation.

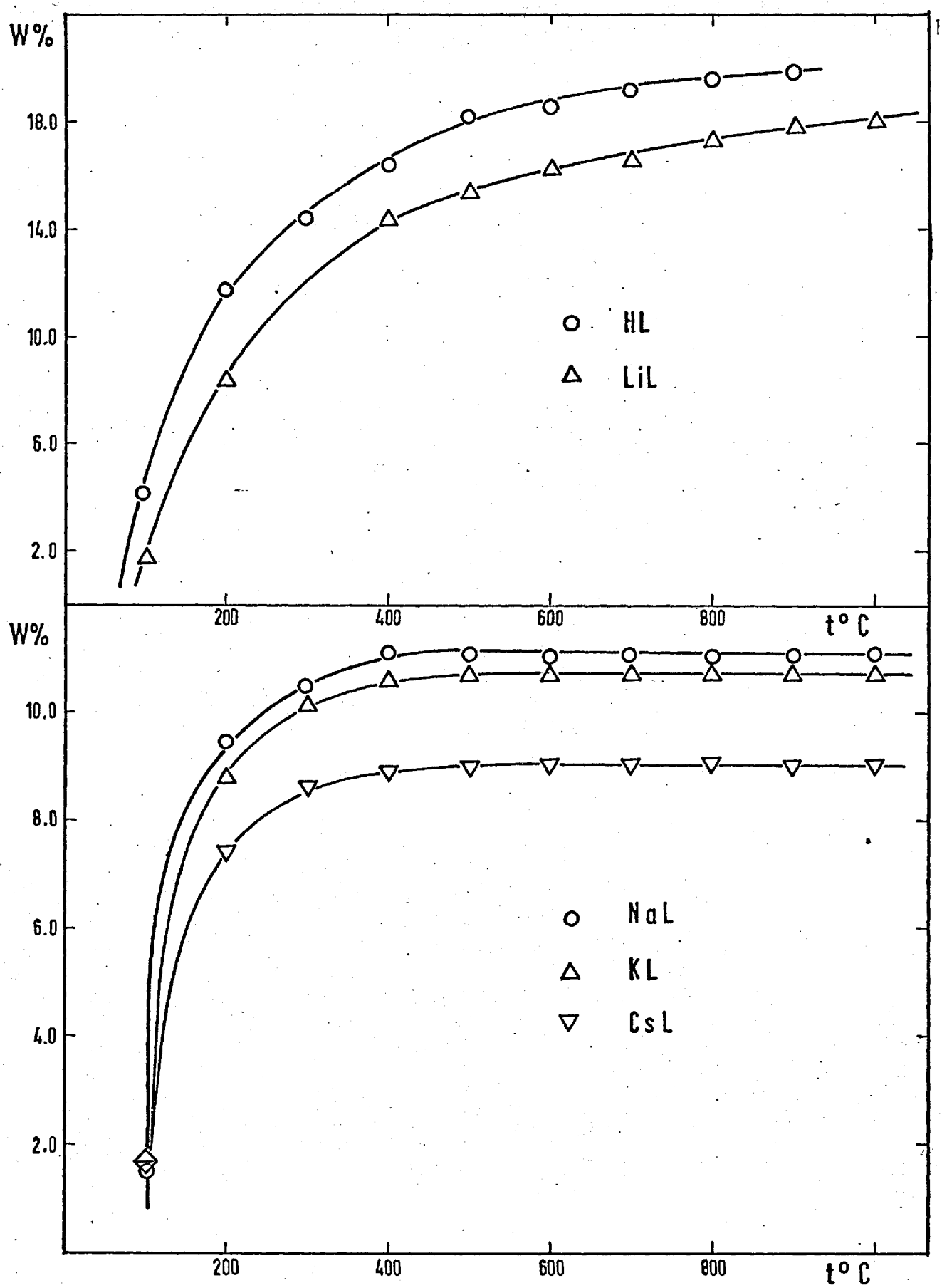

Fig. 34 Loss of weight – TGA data

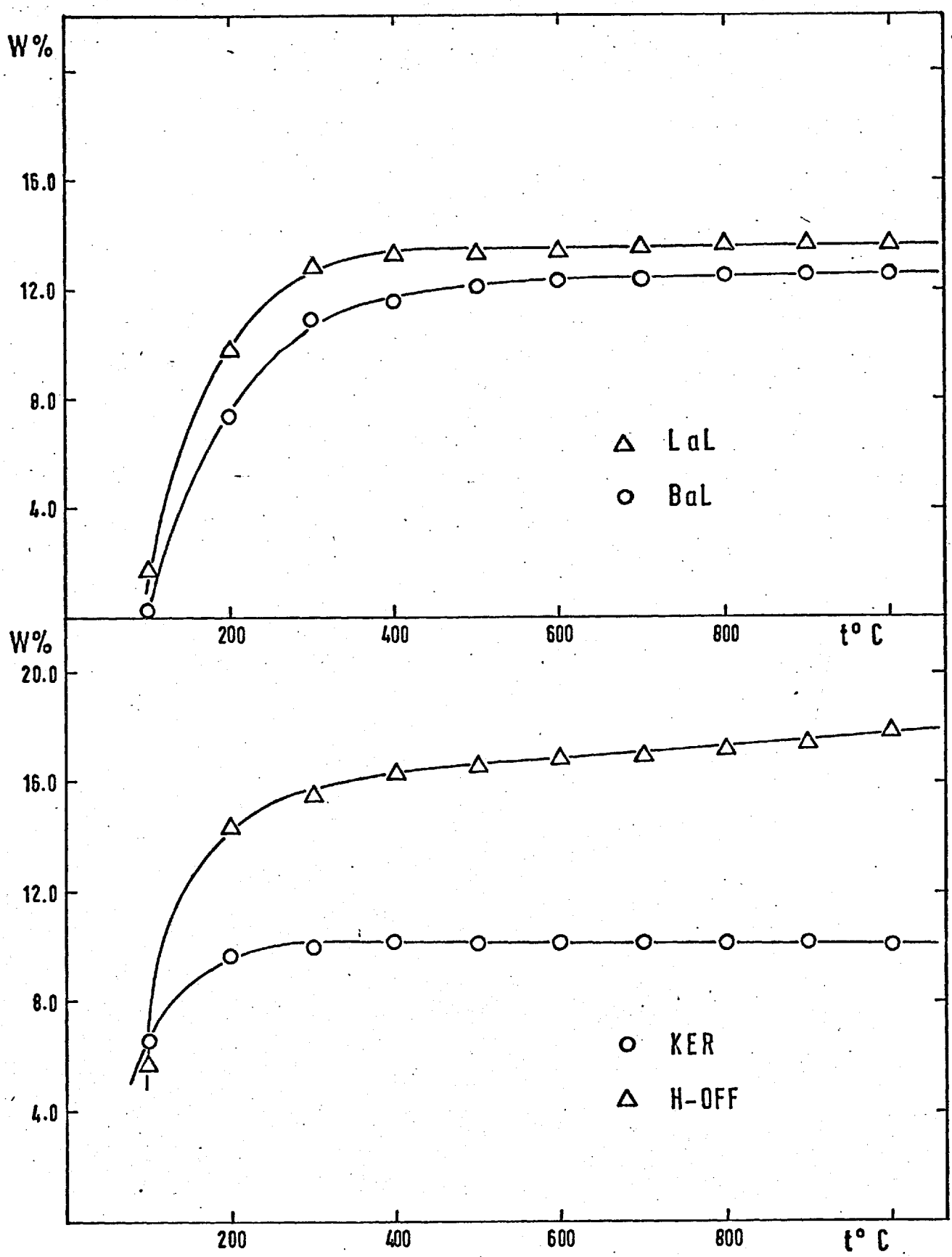

Fig. 35 Loss of weight – T G A data

to high temperature. For the case of LiL, we could suppose that during the heating the sample undergoes partial hydrolysis to give some LiOH and hydrogen zeolite. Decomposition of LiOH occurs at 610°C at atmospheric pressure(123).

As mentioned previously, the TGA curve of OFF is obtained on the original sample containing TMA. Decomposition of TMA during heating (p. 71) is obviously the reason for the continuous loss of weight. This result cannot be related to the data of Table 15 as in the sample there used the TMA is already burned out.

3.3 X-RAY INVESTIGATION OF THE SORBENTS DURING HEATING.

For all the sorbents the structural alterations, if any, were investigated during and after outgassing. The hydrated structures at room temperature were used as references. Deviations from the reference state were determined quantitatively by measuring the unit cell dimensions and qualitatively by visual estimation of change in the intensity of the lines in the X-ray powder patterns. Each fully hydrated sorbent was X-rayed at room temperature; the temperature was then increased slowly and the sample continuously X-rayed until fully dehydrated. The investigations were carried out on a X-ray powder camera with heating - Lenné (p.77). A platinum holder was used and on each pattern the platinum lines are observed (d spacings 2.27, 1.96, 1.38 and 1.18 (130)). For most of the samples the dehydration process during heating under atmospheric pressure was practically completed at about 500°C, (section 3.2) and heating was therefore stopped at 550°C. Each sample, except KL, was heated 30 hrs. The time for cooling is given in Table 21.

TABLE 21.

Time for cooling of the samples on Lenné camera.

Sorbent	HL	LiL	NaL	KL*	CsL	BaL	LaL*
$\mathcal{T}$ cooling hrs.	9	8	12	-	37	10	-

Sorbent	H-ER	Na-ER	K-ER	H-OFF
$\mathcal{T}$ cooling hrs.	16	36	16	16

* Conditions further described on Figs. 40 and 43.

Heating up to temperatures where a collapse of structure occurs and thus estimating the limits of the thermal stability was of interest, but experimental difficulties prevented this. After the collapse of the structure a glass-like substance was formed that damaged the Pt mesh of the sample-holder. For this reason, heating up to 1200°C was performed only once - on KL. It was found that the structure persists until 700°C (Fig. 36).

3.3.1 Data on ion-exchanged forms of L.

In Figs. 37-43 X-ray patterns of all the ion-exchanged forms of L are presented. Each pattern was indexed according to the computed unit cell at room temperature using program Apol(129). The measurements for estimation of the unit cell dimensions at different temperatures were made

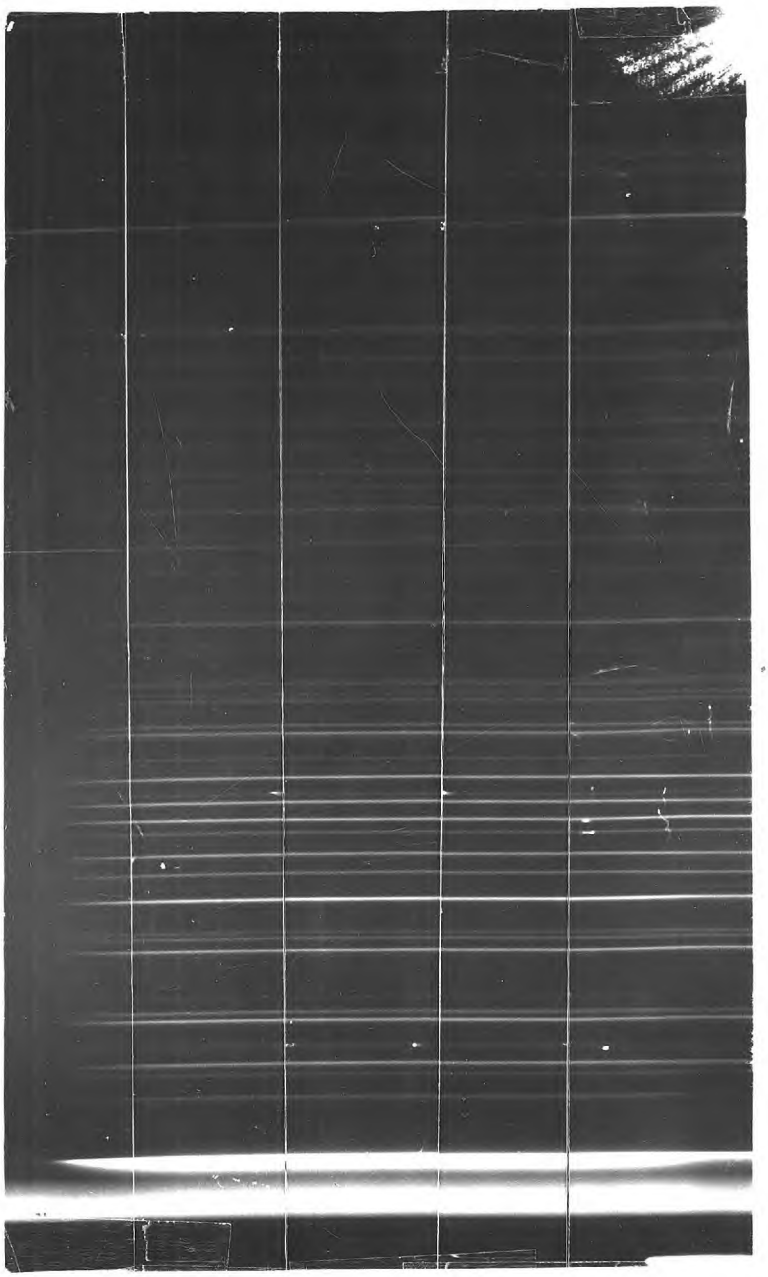

Fig. 36 KL

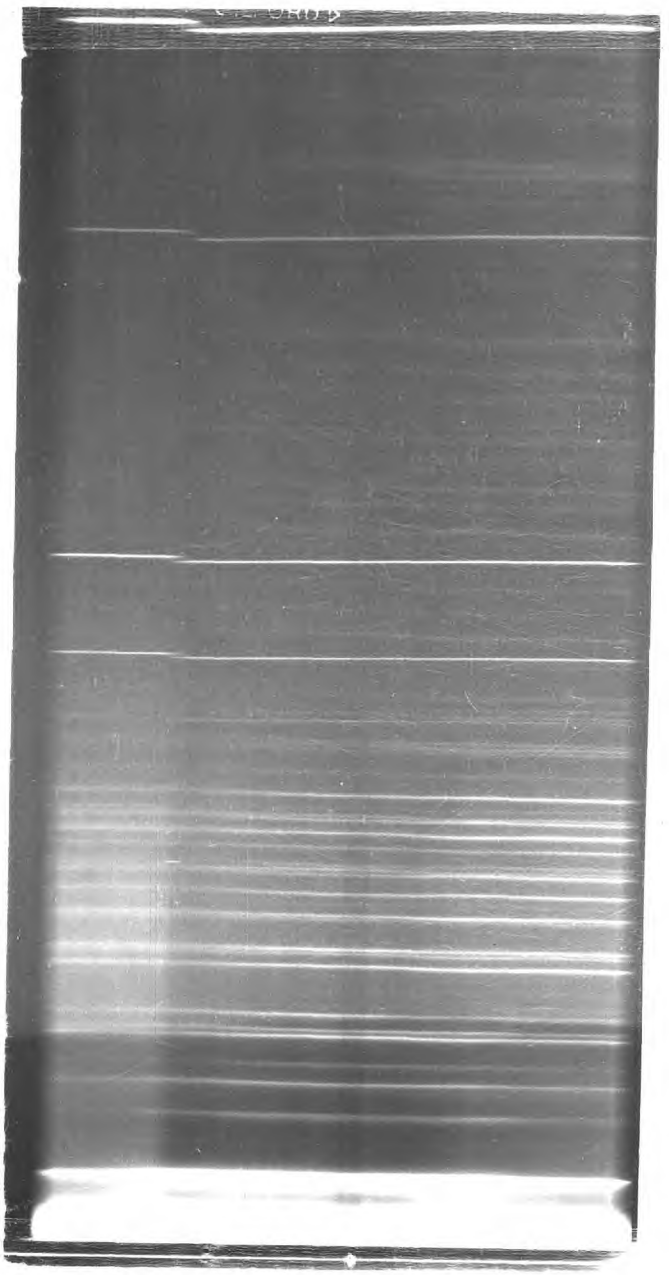

Fig. 37 HL

Fig. 38 LiL

using a Guinier ruler. A standard could not be used because of the single sample-holder in the Lenné camera. The above technique is that usually used in such cases(126).

The reflections measured were 200, 210, 220, 310, 001 and 301. They were selected according to the requirements described previously (p.113) and with the additional condition of convenient $hk\ell$ values for manual computation of the unit cell (p. 28). At a given temperature each value was measured at least three times and the mean value of $d_{hk\ell}$ estimated.

No alteration of the unit cell with the temperature was found for CsL and noticeable, but small, alterations were observed for LiL, NaL and KL. For the latter three samples data for selected temperatures only are presented in Table 22. There is a slight expansion of the unit cell constants of LiL.

Much larger alterations of the unit cell constants with the temperature were found for HL, BaL and LaL - Fig.44 Table 22. For almost all the sorbents an increase of a value is accompanied by a decrease in c value. At about 200°C the values of a go through a maximum and the values of c through a minimum. At about 500°C both a and c constants of BaL and LaL have regained their original values at R.T.*, while those of HL are contracted.

On the pattern of HL (Fig. 37) one can see a merging at about 200°C of line 112 (d = 3.51) with 410 (d = 3.47) and of line 302 (d = 3.08) with 330 (d = 3.06). The lines split again after 250°C. These effects on the pattern can be well understood from considerations of the unit cell dimensions at these temperature intervals.

It is remarkable that the alterations of the unit cell

---

* R.T. = room temperature.

Fig. 39 NaL

No cooling Heating time 42 hrs.

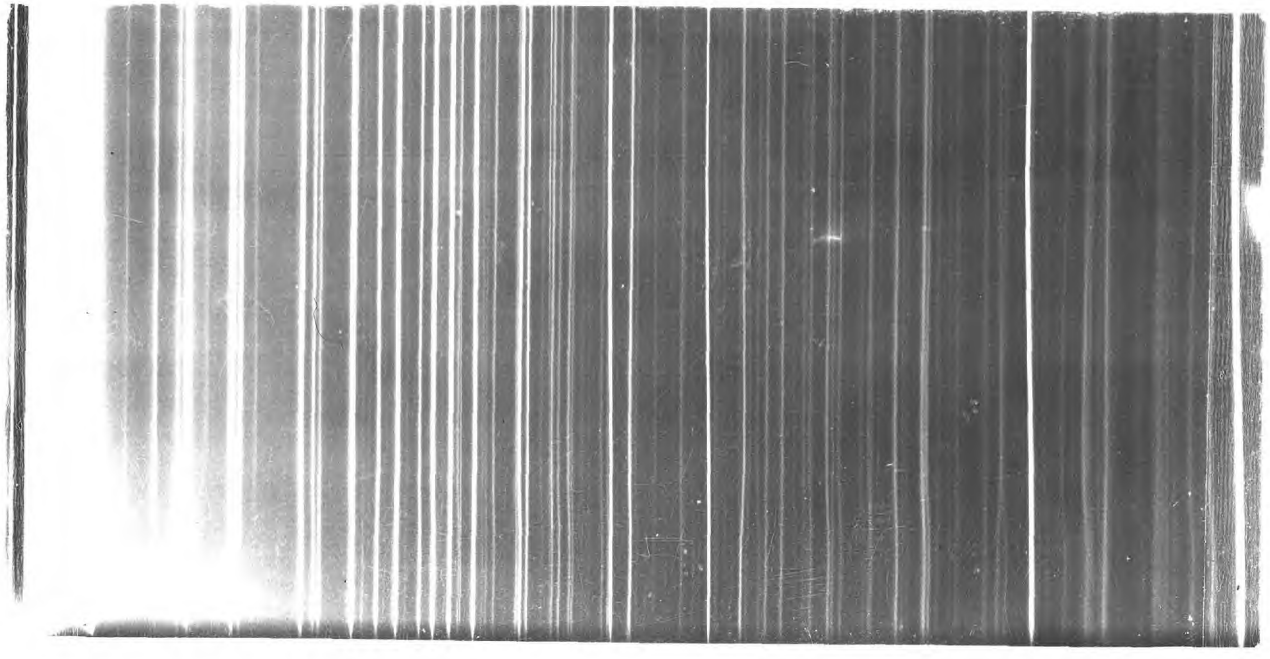

Fig. 40 KL

Fig. 41 CsL

Fig. 42 BaL

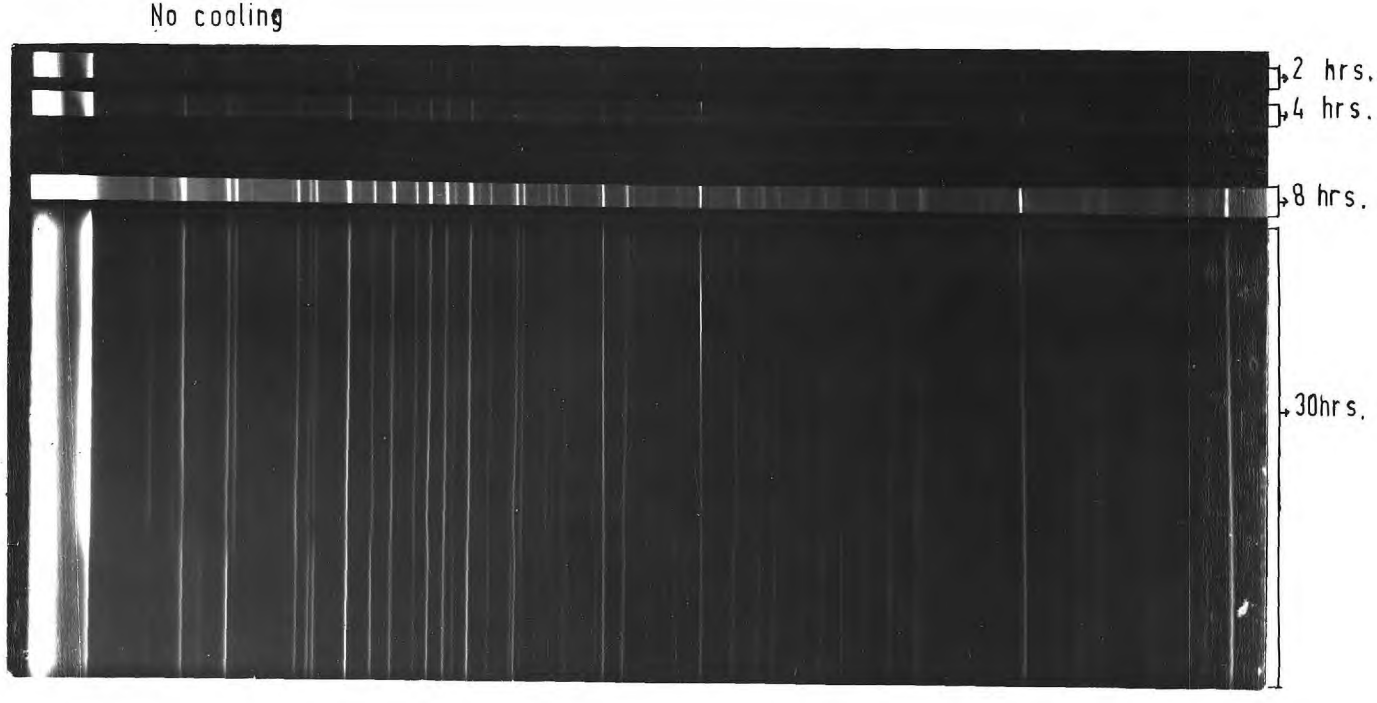

Fig. 43 LaL

TABLE 22.

Alteration of the unit cell constants during heating for ion-exchanged forms of zeolite L

t°C	HL		BaL		LaL	
	a Å	c Å	a Å	c Å	a Å	c Å
RT	18.36	7.60	18.44	No alteration found	18.35	7.53
100	18.36	7.60	18.44		18.36	7.53
150	18.38	7.55	18.47		18.42	7.51
200	18.42	7.50	18.53		18.47	7.52
250	18.40	7.51	18.48		18.42	7.52
300	18.30	7.52	18.46		18.38	7.53
400	18.24	7.52	18.44		18.36	7.53
500	18.24	7.52	18.44		18.35	7.53
	LiL		NaL		KL	
RT	18.41	7.55	18.48	7.51	18.45	7.53
200	18.43	7.55	18.49	7.50	18.46	7.52
500	18.42	7.57	18.51	7.50	18.46	7.52

TABLE 23.

Alteration of the volume of the unit cell during heating for ion-exchanged forms of zeolite L

t°C	HL	LiL	NaL	KL	BaL	LaL
RT	2217.1	2216.1	2223.4	2219.8	2215.7	2194.7
200	2203.7	2220.8	2220.5	2219.2	2239.0	2224.0
500	2166.6	2224.3	2225.3	2219.2	2215.7	2194.7

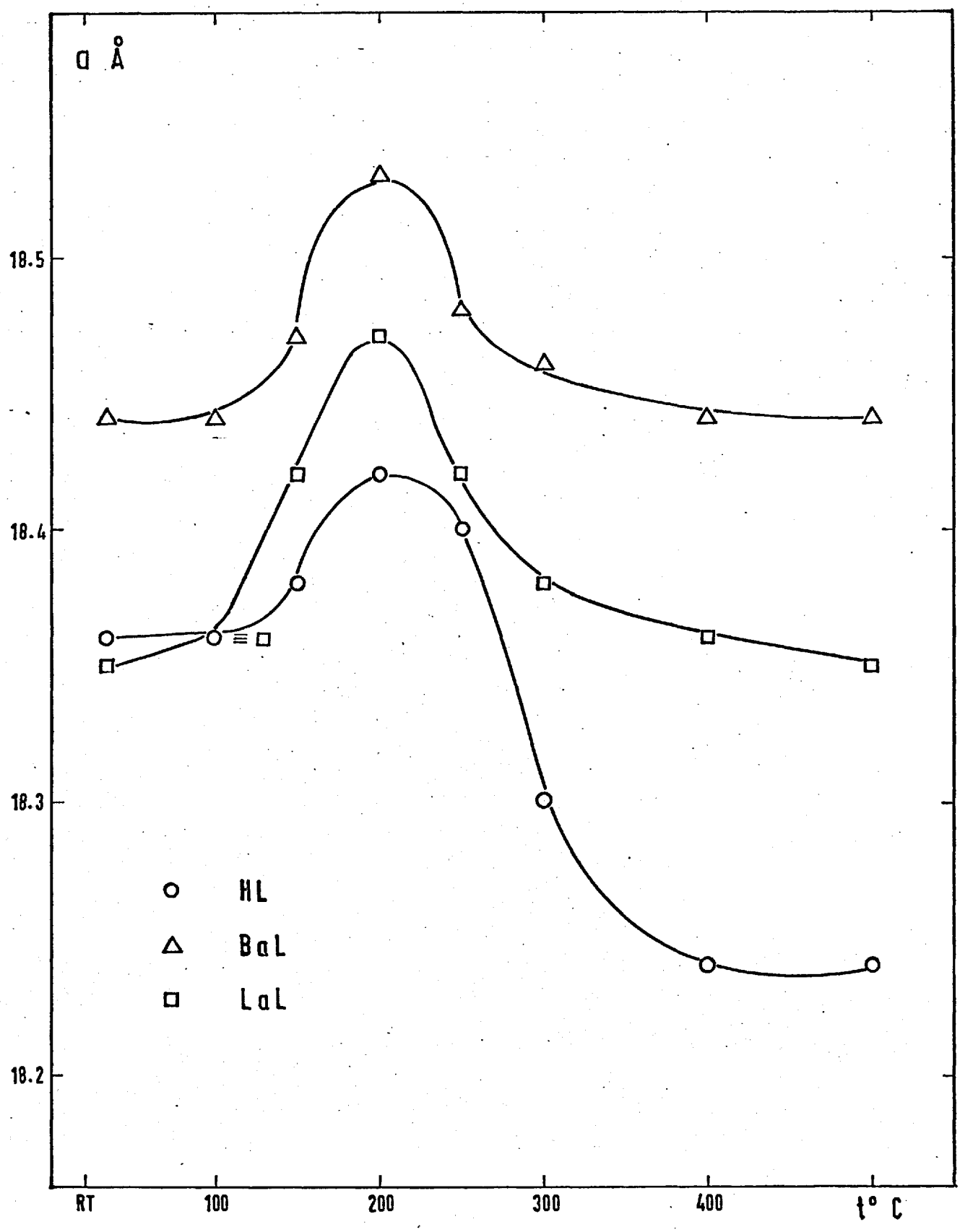

Fig. 44 a constant vs temperature

TABLE 24.

Alteration of the intensity during heating in the X-ray powder patterns of ion-exchanged forms of zeolite L.

SAMPLE	hkl	t°C	I*
HL	100	140	i
	110	140	i
	001	140	i
	101	140	i
LiL	100	150	i
	110	150	A
	200	150	i
	201	200	A
	311	160	D
NaL	100	150	i
	110	150	i
	201	150	A
	311	150	D
	200	200	i
KL	100	130	i
	110	130	A
	200	130	i
	201	160	A
	311	150	D
CsL	100	150	i
	110	150	i
	200	150	i
	311	150	d

SAMPLE	hkl	t°C	I*
BaL	100	150	i
	110	150	A
	101	150	D
	200	100	A
	200	200	D
	001	180	i
	501 or 420	200	d
	501 or 420	300	i
	600	100	d
	600	300	i
	600	500	d
LaL	100	180	i
	110	180	i
	200	190	A
	200	300	D
	101	190	D
	111	180	i
	201	200	A
	201	300	D
	211	180	D
	310	180	i
	301	180	i

* Legend for the intensity alteration:

i - increasing

d - decreasing.

A - a line appears.

D - a line disappears.

dimensions of HL, BaL and LaL are largest at a moderate temperature (200°C) and almost negligible at high temperature. Apparently, therefore, it is not the temperature which alters the unit cell dimensions, but the loss of zeolitic water which occurs largely in the interval around 200°C (see section 3.1).

On the basis of the calculated unit cell dimensions the volumes of the unit cells of all samples were computed for each ion-exchanged form. The results for three selected temperatures are presented in Table 23. The unit cell of HL is essentially contracted at high temperature; that of LiL - slightly expanded; BaL and LaL show fairly strong maxima at about 200°C, but at 500°C the volumes are virtually the same as those at R.T.

In contrast to the above results an examination of the line intensities showed persisting changes with the temperature for all ion-exchanged forms. The data are presented in Table 24. As the intensity of the lines is directly related to the position and nature of the atoms in the unit cell (p. 27), the intensity alterations during heating must be due to migration of ions and water in the structure and to loss of water. It was of interest to distinguish which reflections are affected by water and which by cation migration. From the data in Table 24 we can select reflections such as 100 and 110 for which the intensity increase during heating is common for all the ion-exchanged forms, including HL. For all the samples this increase occurs in the interval between 130-180°C. The intensity alteration of these reflections, therefore, could be attributed to water migration and loss (see section 3.1 and 3.2).

Common for all the metal-ion-exchanged forms, but not for HL, is an increase of the intensity of the 200 and 201

reflections attributable to cation migration during outgassing and heating. Further we find (from the data of Table 24) that a decrease of the intensity of 311 is common for all ion-exchanged forms of monovalent cations. For polyvalent cations (BaL and LaL) alteration is observed in the intensity of a greater number of reflections (501, 600, 310, 311).

3.3.2 Data on ion-exchanged forms of erionite and on H-OFF

On Figs. 45-48 the Lenné camera X-ray patterns for K-ER, Na-ER, H-ER and H-OFF are presented.* The lines measured for estimation of the alteration of the unit cell of erionite were 100, 200, 300, 400, 002 and 006, and for offretite, 100, 200, 300, 400, 001 and 002. The unit cell constants are presented on Table 25. The data for erionite are plotted on Fig. 49. A monotonic decrease of $\underline{a}$ and increase of $\underline{c}$ is observed for all the sorbents. As a result of the opposing alterations of $\underline{a}$ and $\underline{c}$, neighbouring reflections with large $\underline{\ell}$ index and those of large $\underline{h}$ and $\underline{k}$ indices merge together above 200°C. This is best seen on the pattern of Na-ER, Fig. 46: line 204 (d = 3.14) merges with 310 (d = 3.18) and line 214 (d = 3.85) merges with 400 (d = 3.86). These lines remain merged at high temperature (compare with HL, Fig. 37).

The volumes of the unit cells calculated at R.T. and 500°C are given in Table 26. A contraction of the unit cell is common for all the samples, being largest for K-ER and almost negligible for H-OFF.

The results of examination of line intensities are

---

* In erionite patterns, two weak lines, d = 5.05 $\mathring{A}^{-1}$ and d = 7.20 $\mathring{A}^{-1}$, were found to belong to inpurity in the natural sample (ER) - see p. 68.

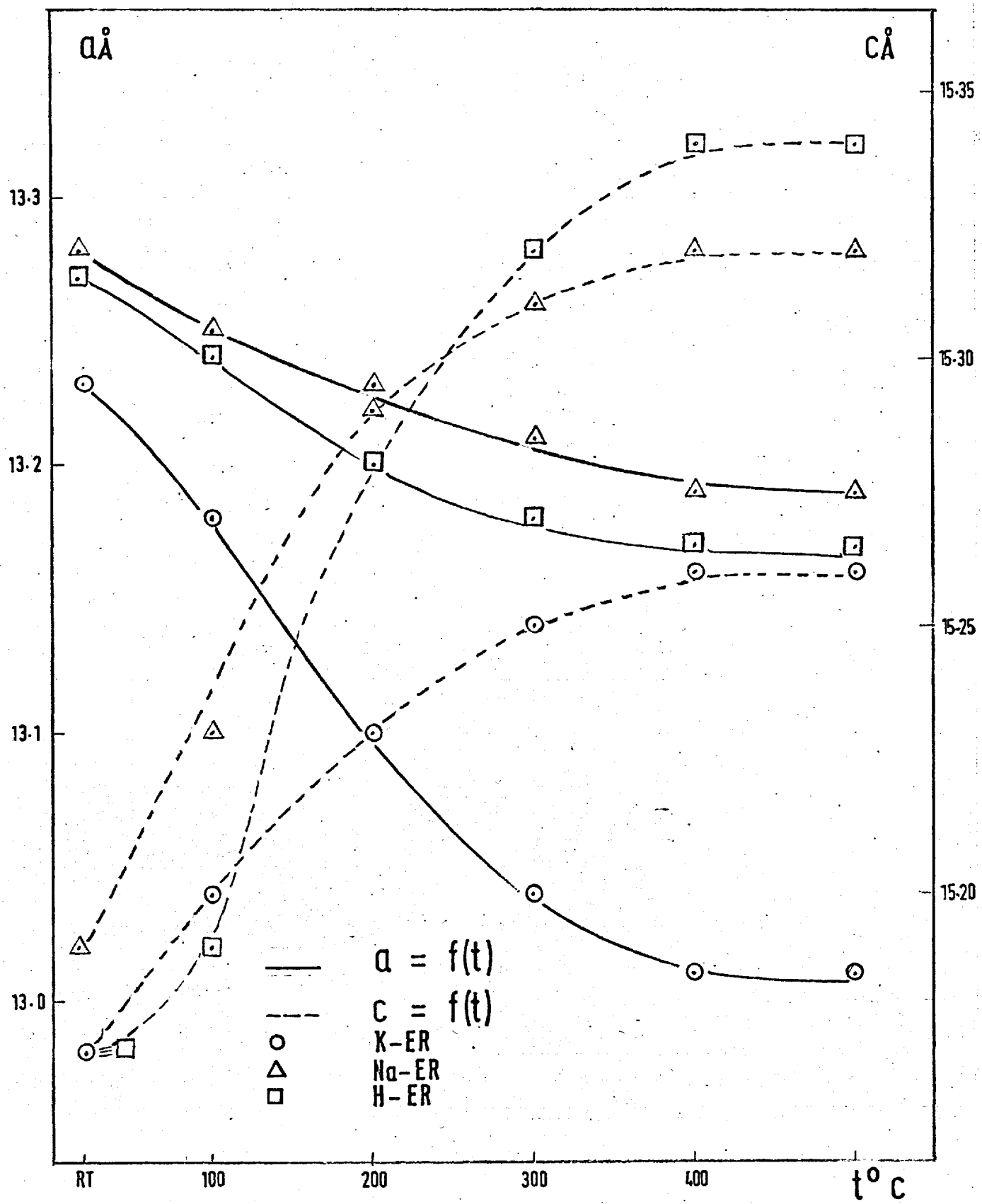

Fig. 49 UNIT CELL CONSTANTS vs TEMPERATURE

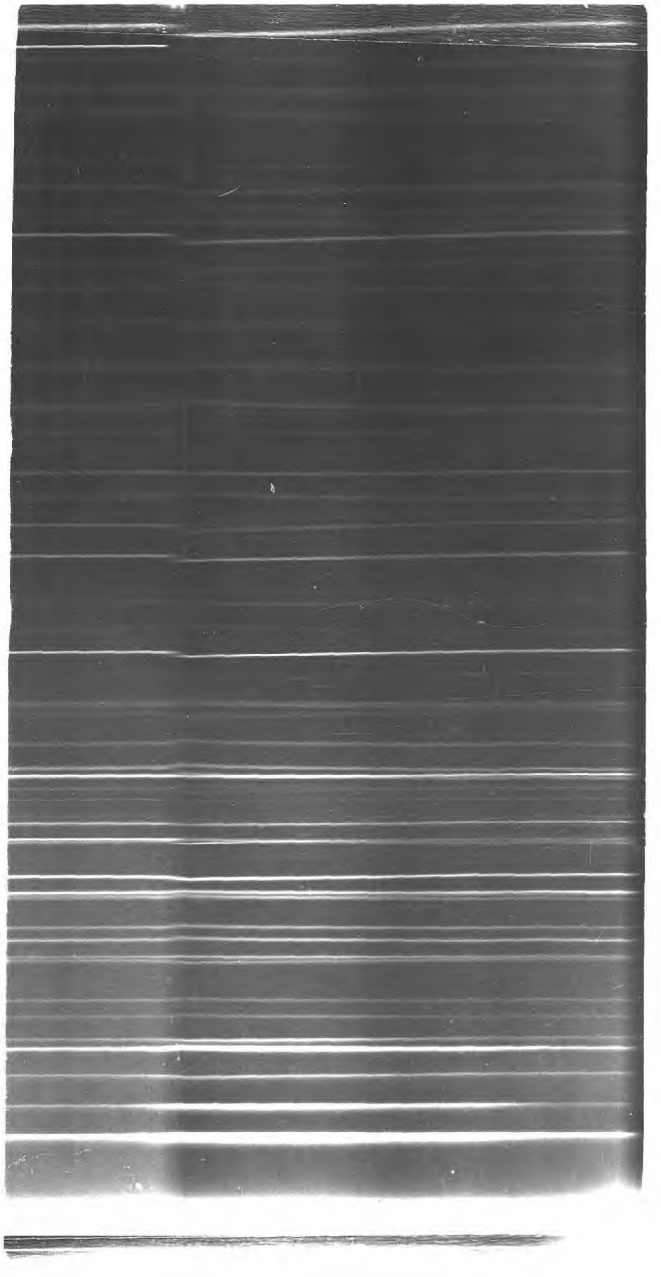

Fig. 45 H-ER

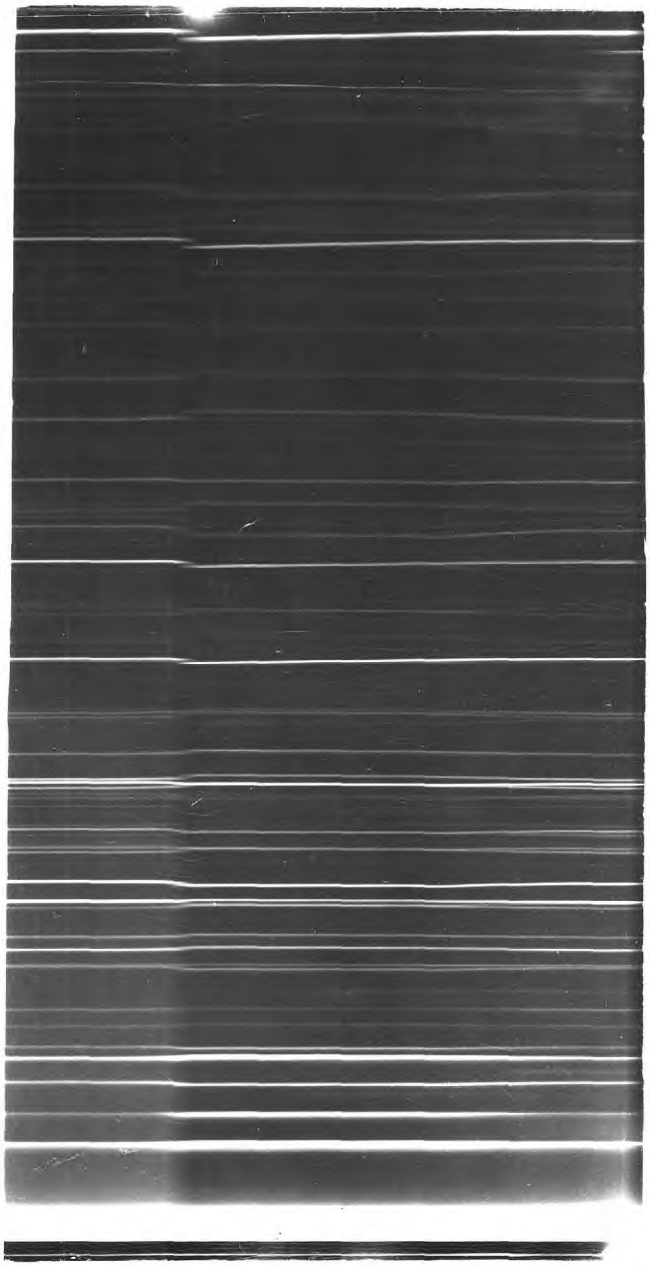

Fig. 46 Na-ER

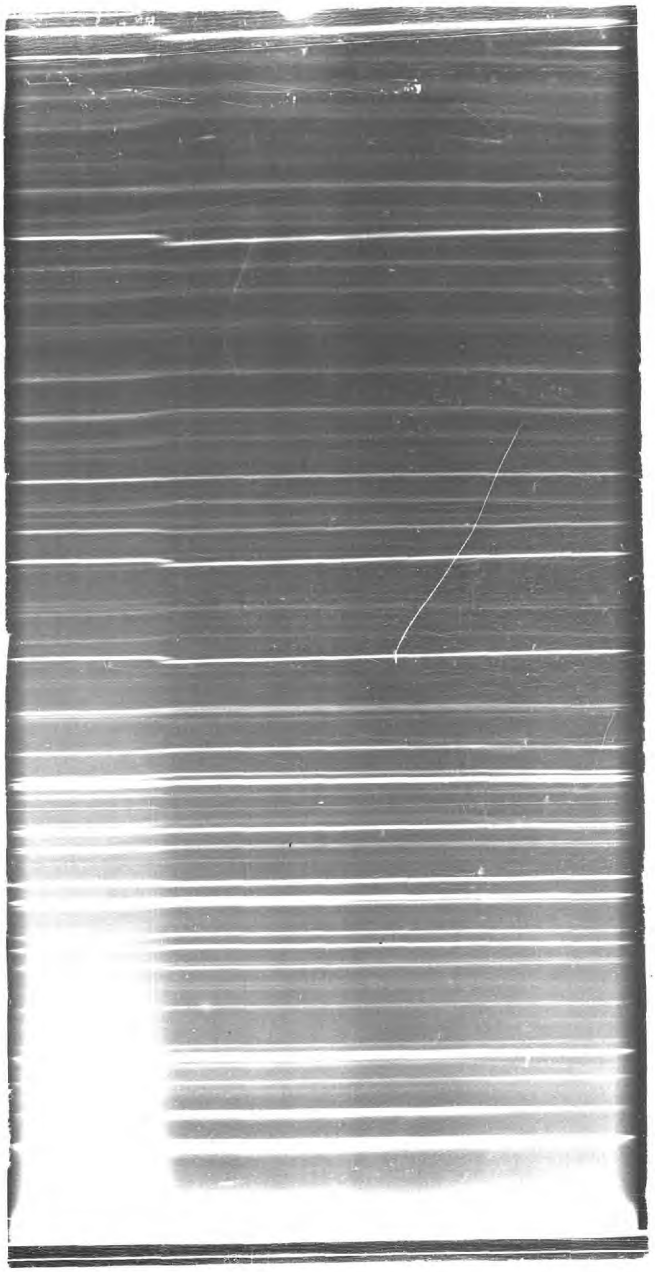

Fig. 47 K-ER

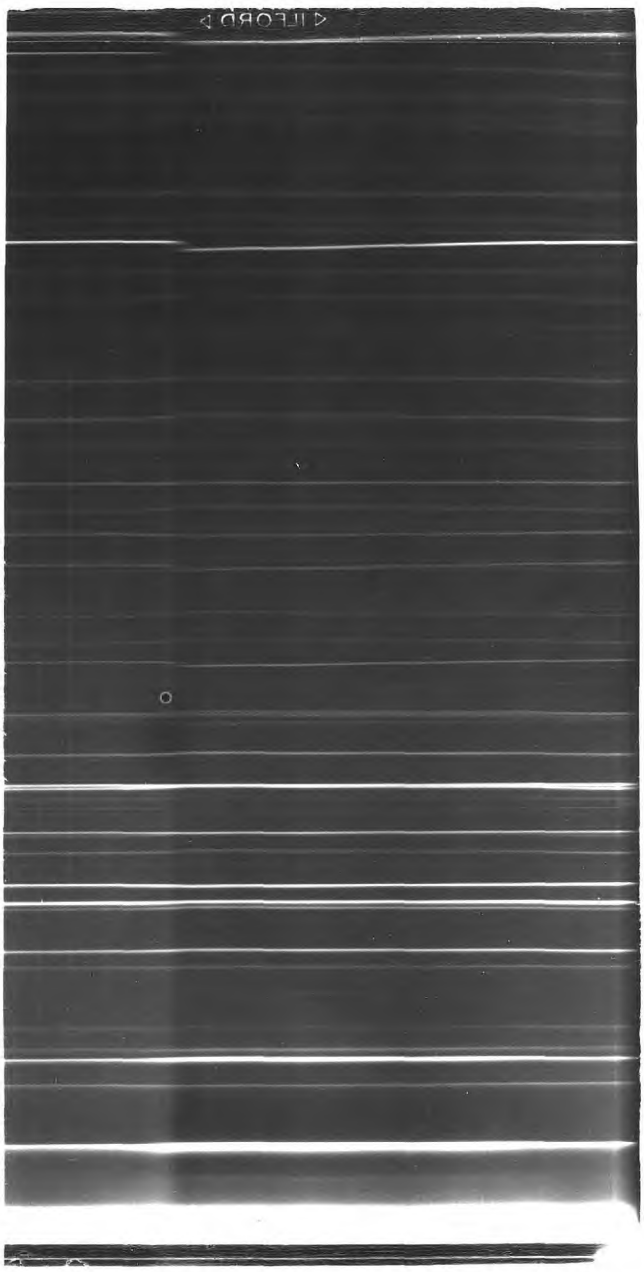

Fig. 48 H-OFF

TABLE 25.

Alteration of the unit cell constant during heating for ion-exchanged forms of erionite

t°C	K-ER		Na-ER		H-ER		H-OFF	
	a Å	c Å	a Å	c Å	a Å	c Å	a Å	c Å
RT	13.23	15.17	13.28	15.19	13.27	15.17	13.24	7.53
100	13.18	15.20	13.25	15.23	13.24	15.19	13.23	7.53
200	13.10	15.23	13.23	15.29	13.20	15.27	13.20	7.55
300	13.04	15.25	13.21	15.31	13.18	15.32	13.20	7.56
400	13.01	15.26	13.19	15.32	13.17	15.34	13.19	7.57
500	13.01	15.26	13.19	15.32	13.17	15.34	13.19	7.57

TABLE 26.

Volumes of the unit cells of ion-exchanged forms of erionite and H-OFF at room and high temperature

t°C Sample	K-ER	Na-ER	H-ER	H-OFF
RT	2299.3	2320.6	2313.4	1142.0
500	2237.1	2308.2	2304.2	1140.3

TABLE 27.

Alteration of the intensity during heating of X-ray powder patterns of ion-exchanged forms of erionite and H-OFF

K-ER			Na-ER			H-ER			H-OFF		
hkl	t°C	I*	hkl	t°C	I*	hkl	t°C	I*	hkl	t°C	I*
100	180	i	100	160	i	100	150	i	100	120	i
101	180	i	101	160	i	101	150	i	001	120	i
110	180	i	110	160	i	110	150	i	110	120	i
201	170	d	201	300	d				200	300	d
200	170	D							201	300	d

I* see the legend for Table 24.

presented in Table 27. An increase in the intensities of the 100, 110 and 101 reflections is common for all erionite samples and can be attributed (see p.141) mainly to water migration and removal. The intensity increase of the 100 and 110 lines is common for all ion-exchanged forms of L, ER and for H-OFF, implying that water removal affects the three structures in the same way. It is probable that the population of the planes 100 and 110 is altered in all structures.

3.4 STRUCTURE REFINEMENT FOR DEHYDRATED BaL AT HIGH TEMPERATURE.

Fourier syntheses were made to refine the structure of BaL after dehydration. The main aim was to determine the position of Ba^{2+} after dehydration. The refinement is still in progress. The results so far obtained are given on p.281 in the Appendix. At the present stage the reliability factor found is R = 0.241, and it is certain that barium cation migrates during dehydration from the position 0, 0.3, 0 to the position 0.19, 0.38, 0.

3.5 THERMAL STABILITY

Interest in the thermal behaviour of zeolite L originated from early adsorption experiments on KL-IC and NaL-IC, which indicated that different conditions of outgassing altered the adsorption capacities. Both KL-IC and NaL-IC showed about 20% lower adsorption of Ar at 90.4°K after a second outgassing (40 hrs. at 360°C). The effect was investigated in detail on KL-IC: repeated heatings in vacua were performed and after each run an Ar adsorption isotherm at 77.3°K was determined. The conditions of outgassing between the runs are given on Table 28 and the

isothermsare plotted on Fig. 50.

TABLE 28.

Sorbent	Isotherm No.	Vacua during heating mm Hg	Outgassed at t°C	Outgassing time (hrs)	Rate of heating	Rate of cooling
KL-IC	1	-	360	50	75°C/hr	150°C/hr
	2	3.10^{-6}	360	20	50°C/hr	100°C/hr
	3	2.10^{-6}	360	16	80°C/hr	80°C/hr
	4	3.10^{-6}	350	58	150°C/hr	80°C/hr
	5	2.10^{-6}	360	15	80°C/hr	70°C/hr
CsL	1	3.10^{-6}	360	20	50°C/hr	50°C/hr
	2	2.10^{-6}	200	10	50°C/hr	60°C/hr
	3	4.10^{-6}	360	20	80°C/hr	60°C/h
	4	2.10^{-6}	360	16	350°C/hr	300°C/ 10 min.
	5	5.10^{-6}	360	20	40°C/hr	300°C/ 10 min.

Outgassing conditions also modified the adsorption capacity in the case of Ar at 77.3°K on CsL (Table 28 and Fig. 51). A low rate of heating, maintaining a high vacuum at 360°C and low rate of cooling were found to favour reproducible sorption capacities. This was confirmed on BaL for which good reproducibility was obtained for four separate isotherms of Ar at 77.3°K. The adsorption capacity was always checked after a series of isotherms on a given ion-exchanged form and found to be satisfactorily reproduceable for all forms of sample L supplied by UC (see p.68). It was found (p.90) that L-IC was contaminated with erionite, offretite and gibbsite and also was finer (Figs. 15 and 18a). The Guinier patterns and

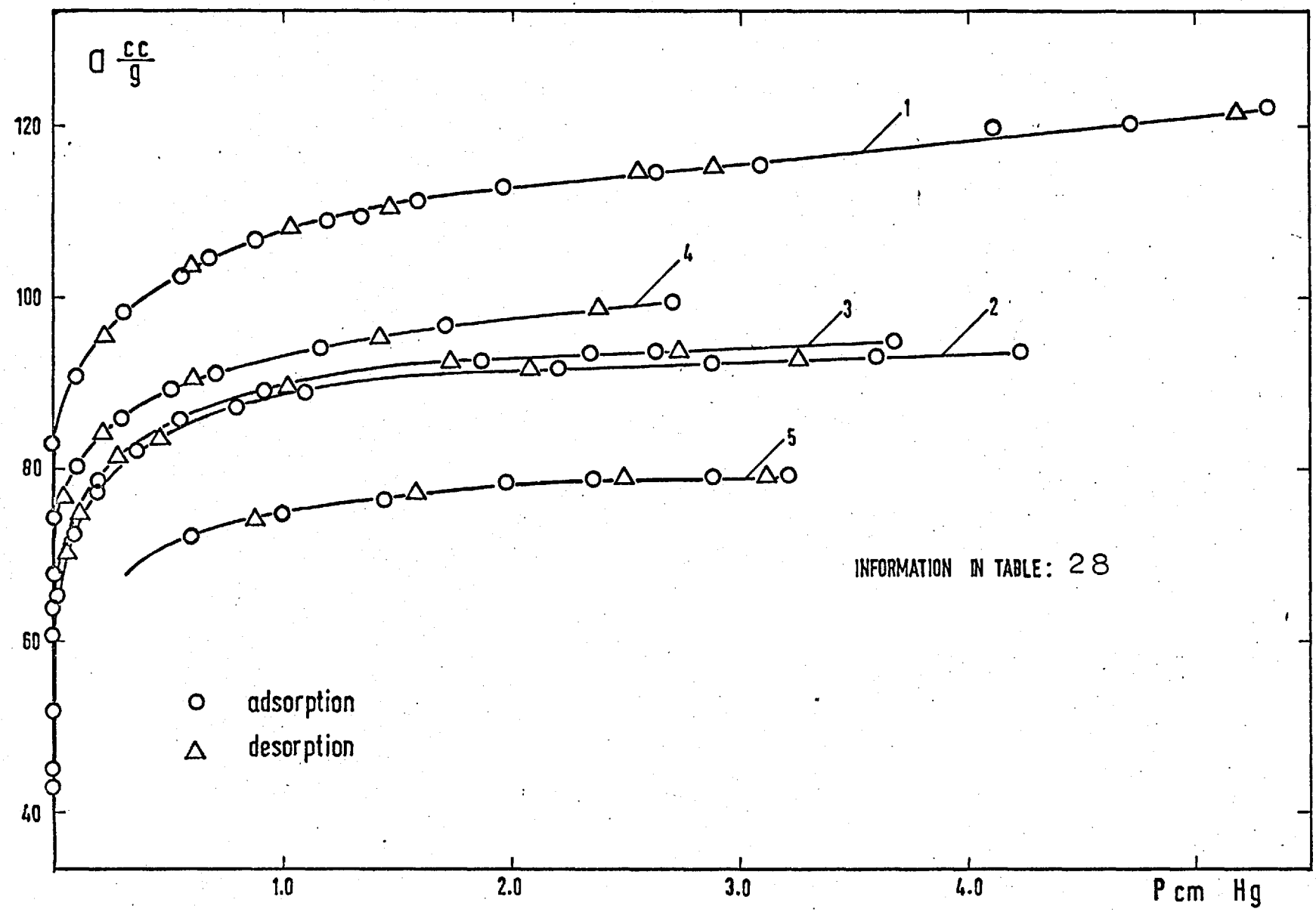

Fig. 50 Ar on KL-IC at 77.3° K

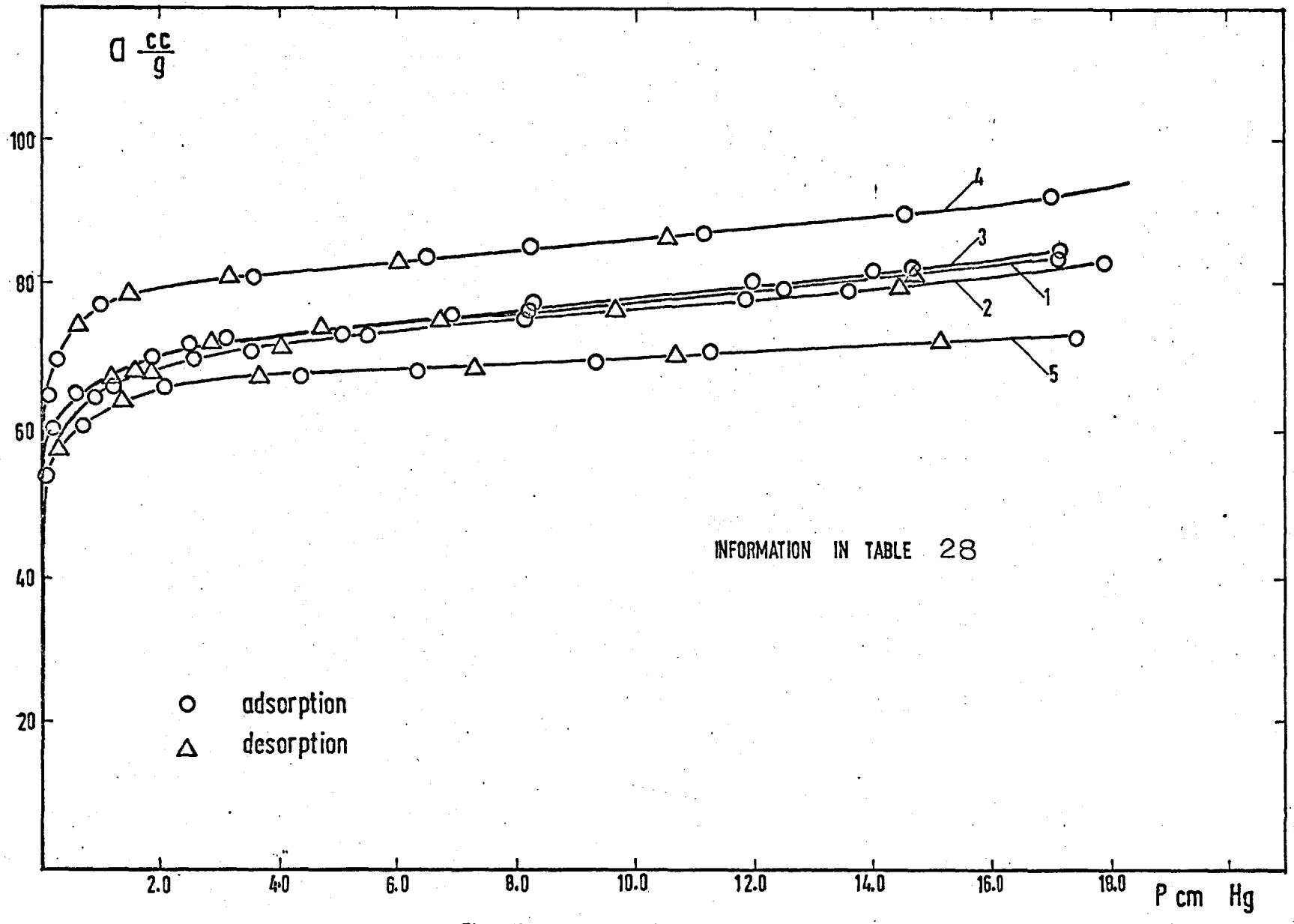

Fig. 51 Ar on CsL at 77.3° K

diffractometer charts of K-IC and NaL-IC before and after heating showed that heating destroyed the gibbsite (line d = 4.72 Å which belongs to gibbsite vanished) and that the intensities of the lines - 111, 210, 301, 311 and 002 were drastically altered.

The observed behaviour of KL-IC on heating was not fully explained, but several factors may be relevant. In section 3.3.2 it was found that the unit cell of erionite always contracts as a result of heating and outgassing, while the unit cell of L remains essentially the same. This suggests that, as well as the gibbsite, erionite in L-IC may suffer irreversible damage during heating.

The influence of the heating and cooling rates, found both on KL-IC and on CsL, could be related to the location of cations in non-equilibrium position. The migration of cations considered in sections 3.4 and 3.3.1 makes the above argument credible.

4. ADSORPTION.

4.1 ADSORPTION OF Ar AT 77.3 AND 90.4°K.

Baths of liquid nitrogen and oxygen respectively were used for sorption measurements at 77.3°K and 90.4°K. Although equilibrium was practically established after 30 minutes, forty minutes to one hour were allowed before taking a reading.

Isotherms of Ar at 77.3°K were measured on each of the investigated samples. All isotherms were reversible, and with the exception of some ion-exchanged forms of L-IC - all were reproducible. Reversibility was checked by desorption measurements either after completing the whole isotherm or by desorption at intermediate pressures. Reproducibility was confirmed by measuring parts or all of each isotherm after an interval of a few weeks.

The adsorption of Ar on each sorbent at 77.3°K was used to determine the apparent saturation capacities(89) for Ar at this temperature, the micropore volume(99) and the affinity of sorption. These characteristics are a convenient basis for comparing the sorbents.

Adsorption of Ar at 90.4°K was measured on a few samples of L and L-IC, and affinities and apparent saturation capacities were derived therefrom, although the results for Ar at 77.3°K provided similar and sufficient information.

4.1.1 Data on ion-exchanged forms of L.

Isotherms of Ar at 77.3°K on ion-exchanged forms of L are plotted on Fig. 52 and the numerical data are given on p.258. The amount adsorbed is expressed in cc(STP) argon per gram of dehydrated sorbent. All isotherms were rectangular and most were of type I in the BDDT classification(89).

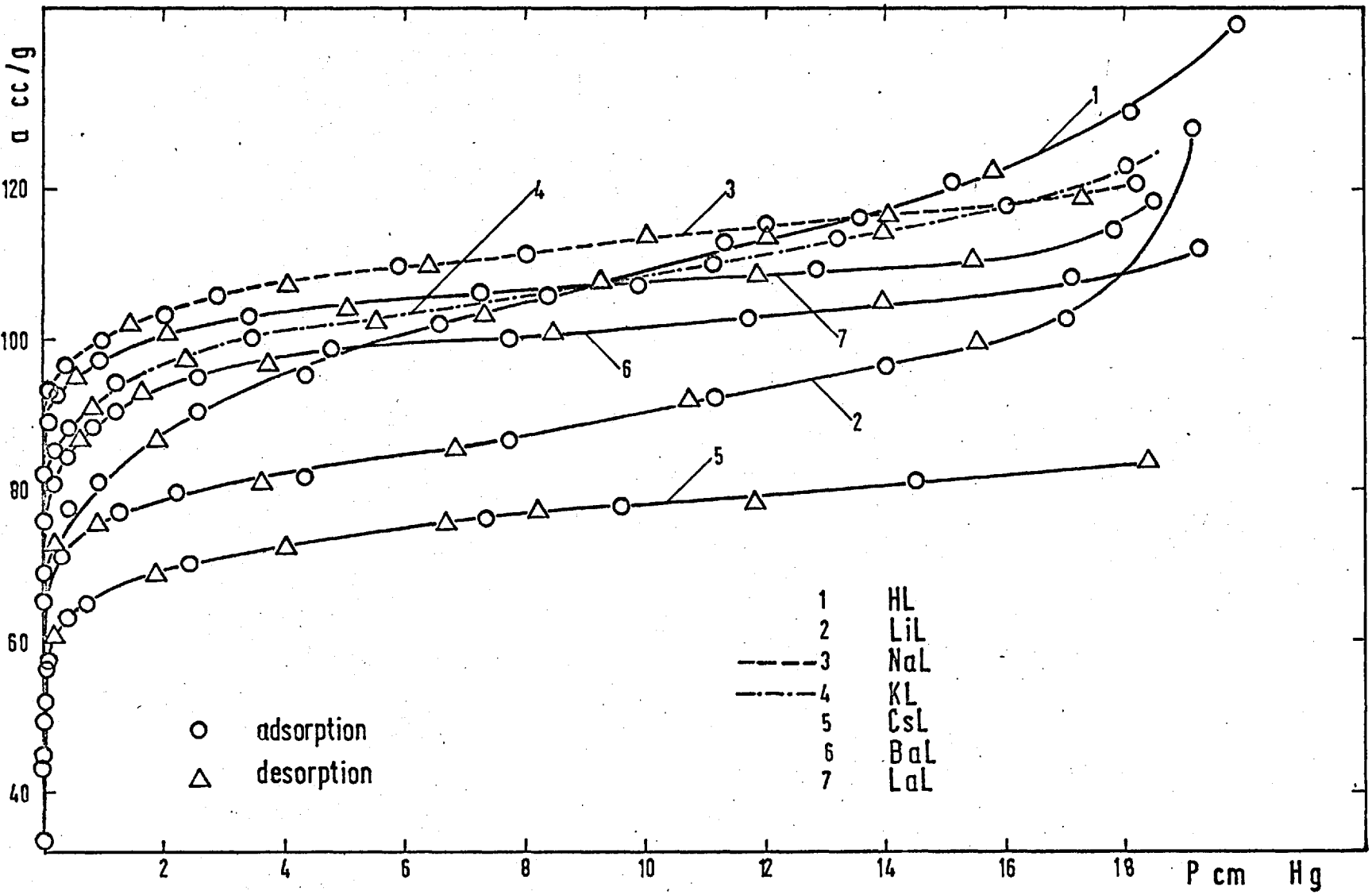

Fig. 52 Ar at 77.3 °K

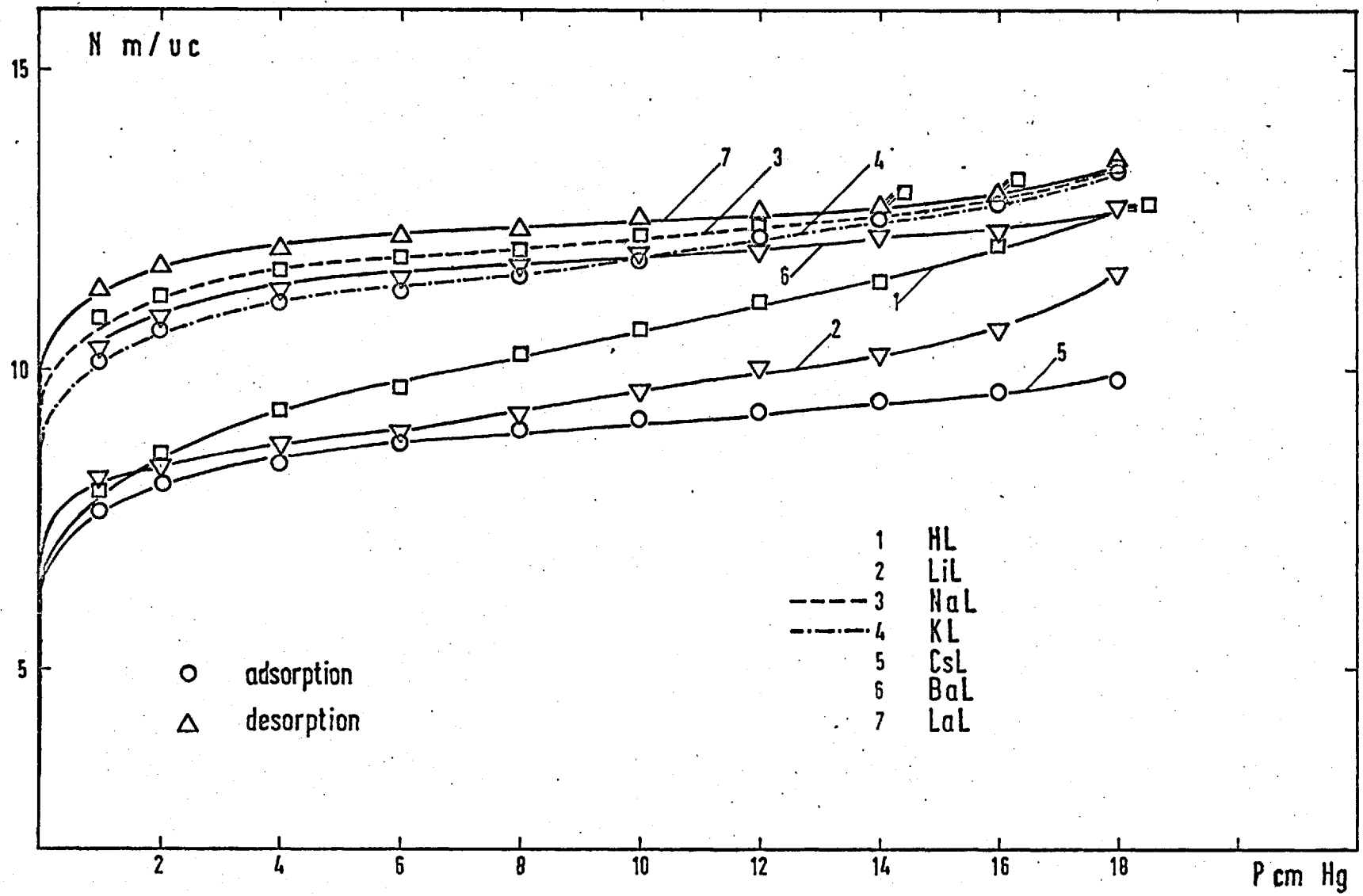

Fig. 53 Ar at 77.3° K

The isotherms in HL and LiL are less rectangular in shape from the others, for which saturation is already approached at pressures as low as 4 cm Hg. The isotherm in HL and LiL in form approach those of type II(89). The absence of cations in the cavities of the HL structure, and the small size of Li^+, probably well recessed into the anionic oxygen framework, may account for the isotherm contours.

As a result of the difference in atomic weight and valency of the cations in the different forms, a gram of dehydrated crystals contains a different number of unit cells in each case (Table 15, line 5). Therefore equal weights of different ion-exchanged forms possess different free volumes even if the free volume per unit cell for all ion-exchanged forms is the same. In Fig. 53 the same adsorption data as that on Fig. 52 is presented, expressing the amount adsorbed as the number of molecules of sorbate per unit cell of dehydrated sorbent, $N\frac{m}{u.c.}$. The new relative position of the isotherm of HL is notable. Contrary to Fig. 52, there is not on Fig. 53 any pressure region where the adsorption of Ar in HL exceeds that in NaL, KL, BaL and LaL. Alterations of the order of the isotherms in LaL, NaL, KL and BaL at low pressure can also be seen. The most remarkable changes are those observed for HL and CsL because the differences between their unit cell volumes is the greatest. To facilitate correct comparison almost all subsequent isotherms will be presented in coordinates $N\frac{m}{u.c.}$ vs P cmHg.

The apparent saturation capacities for Ar at 77.3°K were calculated for all ion-exchanged forms by plotting $\frac{P}{N}\frac{\text{cmHg u.c.}}{\text{molecules}}$ vs P cmHg, the limiting slopes then being $\frac{1}{N_{SAT}}$(72).

The results are given in Table 29. With the exception of LiL and CsL all the capacities are similar, decreasing in the order:

$$NaL > KL > LaL > HL > BaL > LiL > CsL$$

TABLE 29.

Apparent saturation capacities for Ar at 77.3°K.

Sorbent	HL	LiL	NaL	KL	CsL	BaL	LaL
N_{SAT} m/u.c.	13.2	11.7	14.2	13.5	9.7	12.8	13.3

NaL has the highest capacity although one would have expected higher values for HL, LiL, LaL and BaL. Estimated water contents by ignition and by TGA (Table 15 and Table 20 respectively) follow in the expected order HL>LaL>BaL>NaL. In a brief note on adsorption properties of ion-exchanged forms of L, Breck and Flanigen(78) also found that the capacity of NaL exceeds that of BaL and CsL.

For forms containing monovalent ions only, one finds a surprisingly low saturation capacity for LiL, compared with NaL and KL. A similar anomaly for the Li form has been found for adsorption of O_2 at 90.4°K on Li-chabazite(83) Adsorption of Ar and O_2 at 90.4°K has also been found(68) to be lower on Li-faujasite than on Na-faujasite for pressure below 30 cm.Hg.

The order expected is usually based only on cations radii and valences. Decreases in their size and numbers would be accompanied by an increase in the free volume per unit cell in absence of other alterations. From section 2.2, Figs. 30 and 31, it is known that the decrease in cation density is accompanied by a contraction of the unit cell .

volume. There are, therefore, two competing factors connecting the free volume of the unit cell in zeolite L with the decreasing cation density. These qualitative considerations make the sequence of saturation capacities reasonable for all forms save HL and LiL.

Information relevant to the low saturation capacities found in HL and LiL can be found in the TGA data (section 3.2) and structural results at high temperature (section 3.3) In the TGA curves of HL and LiL no plateau is observed, in contrast to the other forms of L. The completeness of dehydration of HL and LiL under the experimental conditions (p. 75) is therefore not certain. Higher temperatures for outgassing are not practicable, because of the danger of damage to the structure. HL and LiL were the only forms which showed irreversible alteration of the unit cell on heating (Tables 22 and 23). HL, in addition, is the only sample which exhibits signs of crystal collapse before 550°C (Fig. 37). In which way each of these factors contributes to the poor saturation capacities of HL and LiL it is not known. However, it is not surprising that these two samples display unusual adsorption behaviour.

A few isotherms of Ar at 90.4°K are presented on Fig. 54. The samples used are NaL, KL, BaL and NaL-IC, KL-IC and CaL-IC. The apparent saturation capacities are here expressed in cc(STP) per gram dehydrated sorbent, and given in Table 30.

TABLE 30.

Apparent saturation capacities of Ar at 90.7°K.

Sorbent	NaL-IC	CaL-IC	KL-IC	NaL	BaL	KL
a_{SAT} $\frac{cc}{g}$	112.0	109.2	94.8	102.6	92.3	89.3

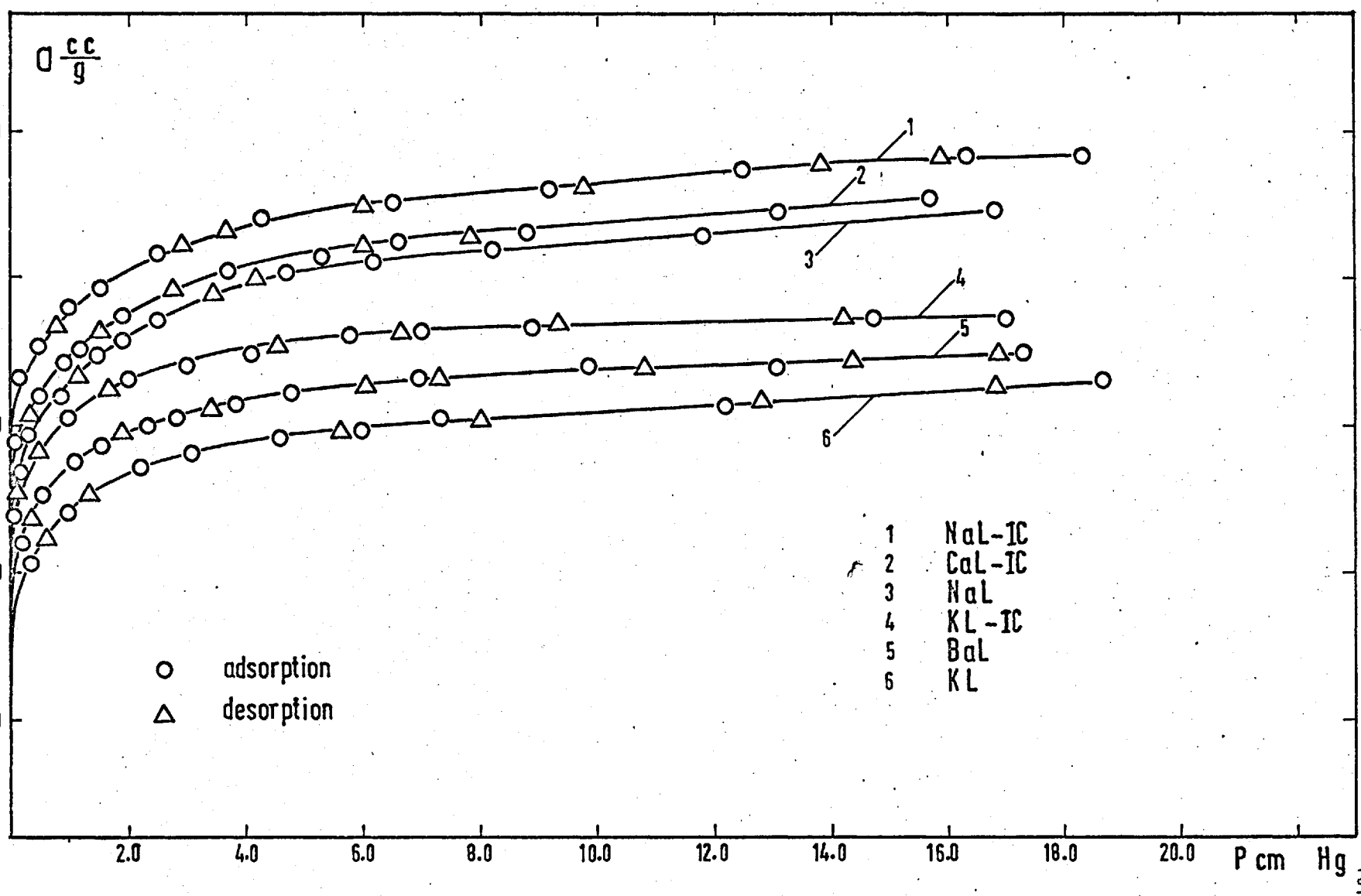

Fig. 54 Ar at 90.5° K

The results conveniently demonstrate the greater adsorption of ion-exchanged forms of L-IC compared with the corresponding samples of L. This is due to the presence of erionite and offretite in the L-IC sample. (Fig. 56)

4.1.2 Ion-exchanged forms of erionite and H-OFF. Comparison with the data on L.

In Fig. 55 and 56 (p.260) are given isotherms of Ar at 77.3°K in H-ER, Na-ER, K-ER and H-OFF, together with those in HL, NaL and KL for comparison. Isotherms in H-ER and H-OFF are rectangular compared with that in HL. Of the three sorbents, H-OFF exhibits the highest sorption at all pressures in the interval investigated.* K-ER practically excludes Ar and the extremely low uptakes observed (less than one tenth of that for Na-ER and H-ER) is attributable, in part at least, to adsorption on the external surface. The apparent capacities obtained are given in Table 31.

TABLE 31.

Apparent saturation capacities of Ar at 77.3°K.

Sorbent	K-ER	Na-ER	H-ER	H-OFF
N_{SAT}^{m}/u.c.	1.4	13.10	13.40	15.0*

A comparison of Tables 29 and 31 reveals the following order of decreasing saturation capacities for corresponding

---

* As the unit cell of offretite is exactly half that of erionite (p.13), the amount adsorbed on offretite is presented on Fig. 56 in $N^{m}/2u.c.$.

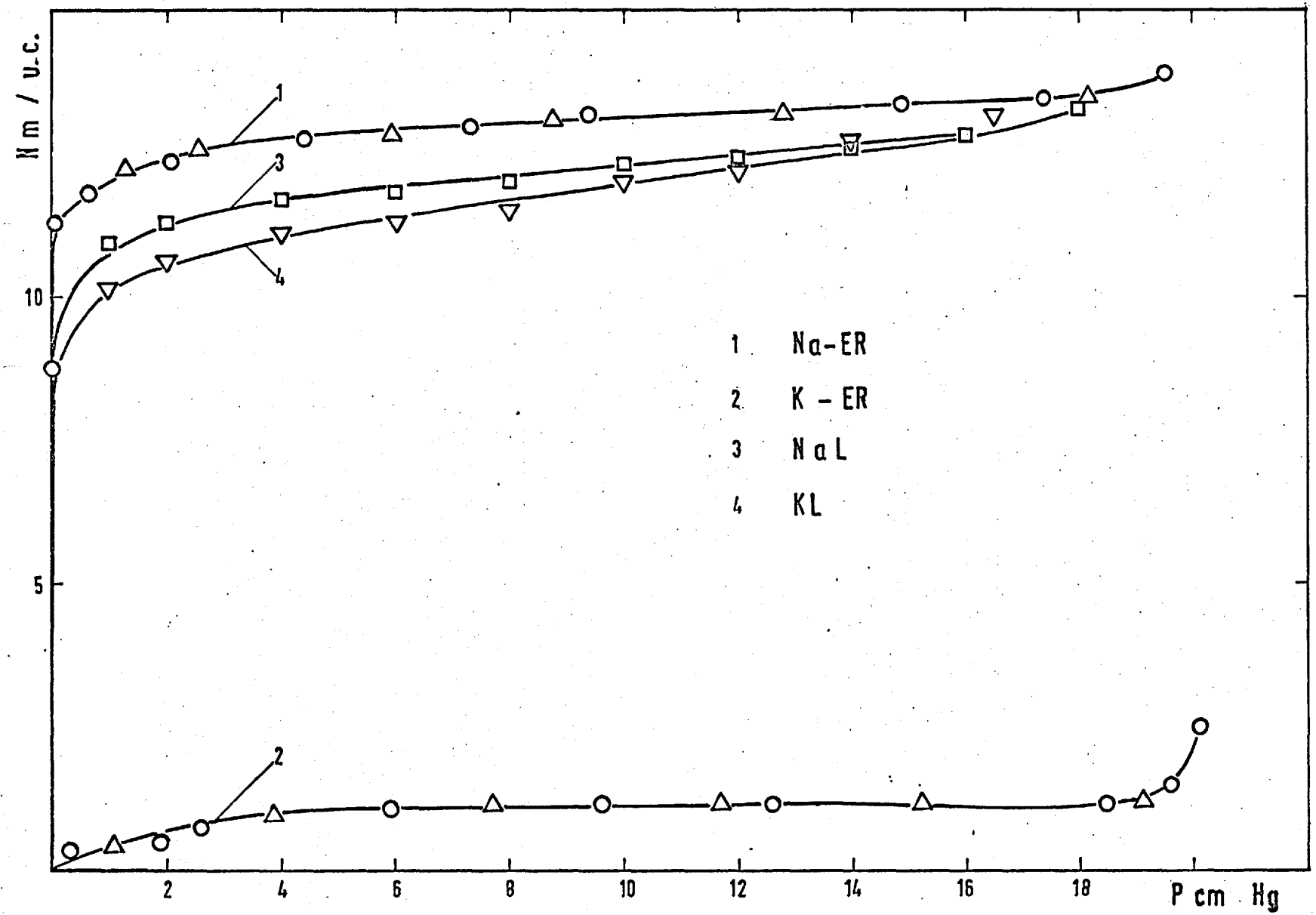

Fig. 55 Ar at 77.3° K

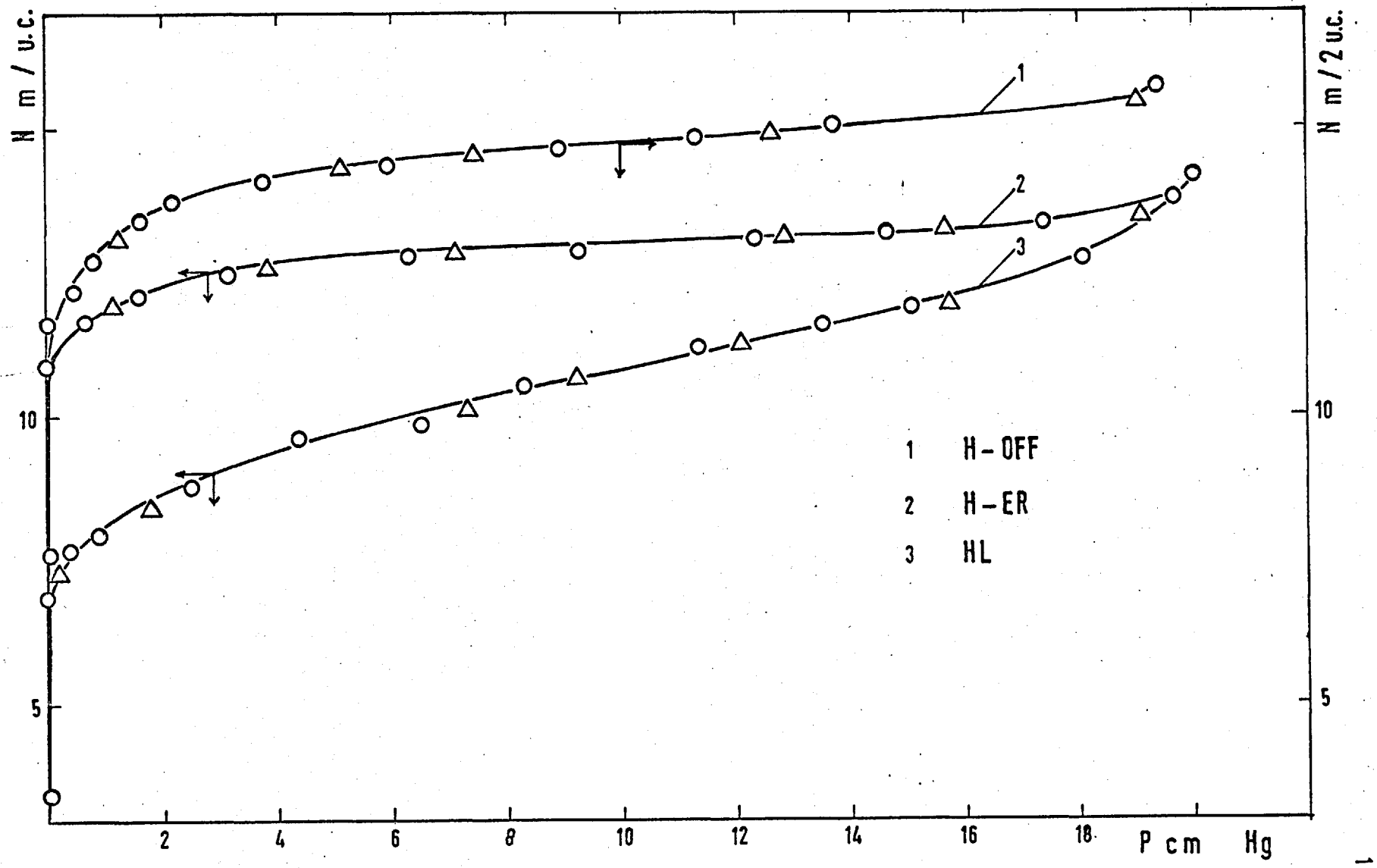

Fig. 56 Ar at 77.3° K

ion-exchanged forms:

$$\text{H-OFF} > \text{H-ER} \geqslant \text{HL}$$
$$\text{Na-ER} < \text{NaL}$$
$$\text{K-ER} \ll \text{KL}$$

Considering the free volumes per unit cell for each of the investigated zeolites (Table 1, p.13) one would expect H-OFF and H-ER to exhibit approximately the same saturation capacities, which would be higher than that of HL. In fact H-ER exhibits considerably lower capacity than H-OFF. However, the erionite sample (see p.68) was found (p.143) to contain some impurities. Also the data of section 3.3.2, Table 26, show a considerable contraction for erionite during and after heating, but a negligible alteration for offretite. This could mean poorer thermal stability for erionite and, hence, a lower adsorption capacity. Finally the packing of sorbate molecules in continuous offretite channels and in the finite cavities of erionite may be different.

Information in the literature on sorption by K-ER is contradictory, since rejection of Ar by K-ER has been reported(27) as well as considerable adsorption(28). At the time of the above publications, the distinction between the structures of offretite and erionite was not known, and the contradiction may be due to incorrect mineralogical identification. Possibly in reference 28 the sample contains offretite.

The results of the present work and of reference 27 on K-ER suggest that a cation is positioned in such a way as to prevent the entry of Ar molecules ($d = 3.8_{3}$ Å). The aperture of the eight-membered ring (3.5 Å - 4.7 Å), through which the molecules must pass, could easily be blocked by a potassium cation ($d = 2.60$ Å) sited nearby.

Fig. 55 clearly shows the effect of the same cations (Na^+ and K^+) on two different frameworks - zeolite L and erionite. While for zeolite L the replacement of K^+ by Na^+ does not cause any essential alteration of the adsorption behaviour, on erionite this replacement involves a shift from a non-sorbing to a strongly adsorbing form. The explanation is certainly the presence of a large (twelve-membered ring) aperture for passage of the sorbate molecules in L, and a small one (eight-membered ring) for erionite.

It was of interest to find out if K-ER and Na-ER possessed sieving properties towards rare and permanent gases. Adsorption of oxygen did not occur within K-ER at 77.3°K and 195.2°K, whereas Na-ER was at 273.2°K capable of including even xenon.

4.1.3 Estimation of micropore volumes of ion-exchanged forms of L, ER and of H-OFF.

The data of the previous sections, 4.1.1 and 4.1.2, showed that often the apparent saturation capacities depart from those expected from a consideration of the unit cell volumes and the size and valence of the cations. Wherever possible, an explanation for the abnormal cases has been sought from the results of sections 2.2, 3.2 and 3.3. However, the saturation capacity must be a direct function of the free volume per unit cell. It was therefore of interest to attempt to estimate, for each case, this free volume and relate it to the saturation capacities found. For this purpose Dubinin's method for determination of the micropore volume of sorbents(99) was employed (p.57). Equation 3.3-4 from Chapter I can be presented in logarithmic form as

$$\ell g x = \ell g W_o \rho + \frac{k}{\beta^2} \left(2.303\ RT\ \ell g \frac{P_o}{P}\right)^2 \quad \ldots\ (4.1\text{-}1)$$

At constant temperature

$$\frac{k}{\beta^2}\ (2.303\ RT)^2 = \text{const} = n \qquad \ldots\ (4.1\text{-}2)$$

and so

$$\ell_{gx} = \ell_g\ W_o\rho + n\left(\ell_g \frac{P_o}{P}\right)^2 \qquad \ldots\ (4.1\text{-}3)$$

Plots of ℓ_{gx} vs $\left(\ell_g \frac{P_o}{P}\right)^2$ should give straight lines and the value of the intercept will give the micropore volume, W_o. The amount adsorbed $\underline{x}$ was expressed in grams of sorbate per gram of dehydrated sorbent; the densities ρ were taken in g/cc, so that the micropore volume W_o was directly determined in cc/g. The density of liquid argon used for the present computation was $\rho_{Ar}^{77.3^oK} = 1.41$ g/cc(131) The saturation vapour pressure P_o was calculated from the following formula(132):

$$\ell_g P_{mm} = \frac{0.05223A}{T} + B$$

where

$$A = -6826.0$$
$$B = 6.9605$$

Figs. 57-61 show the Dubinin plots. At pressures near saturation, a deviation of the points from a straight line is observed on all the graphs. Similar deviations have been observed(133) for the adsorption of nitrogen on activated carbons at 77.3°K. In general, it is believed(99) that the method is more accurate for regions of low pressures. However, the technique used in the present work (p.76) does not provide satisfactory accuracy at low pressure, so

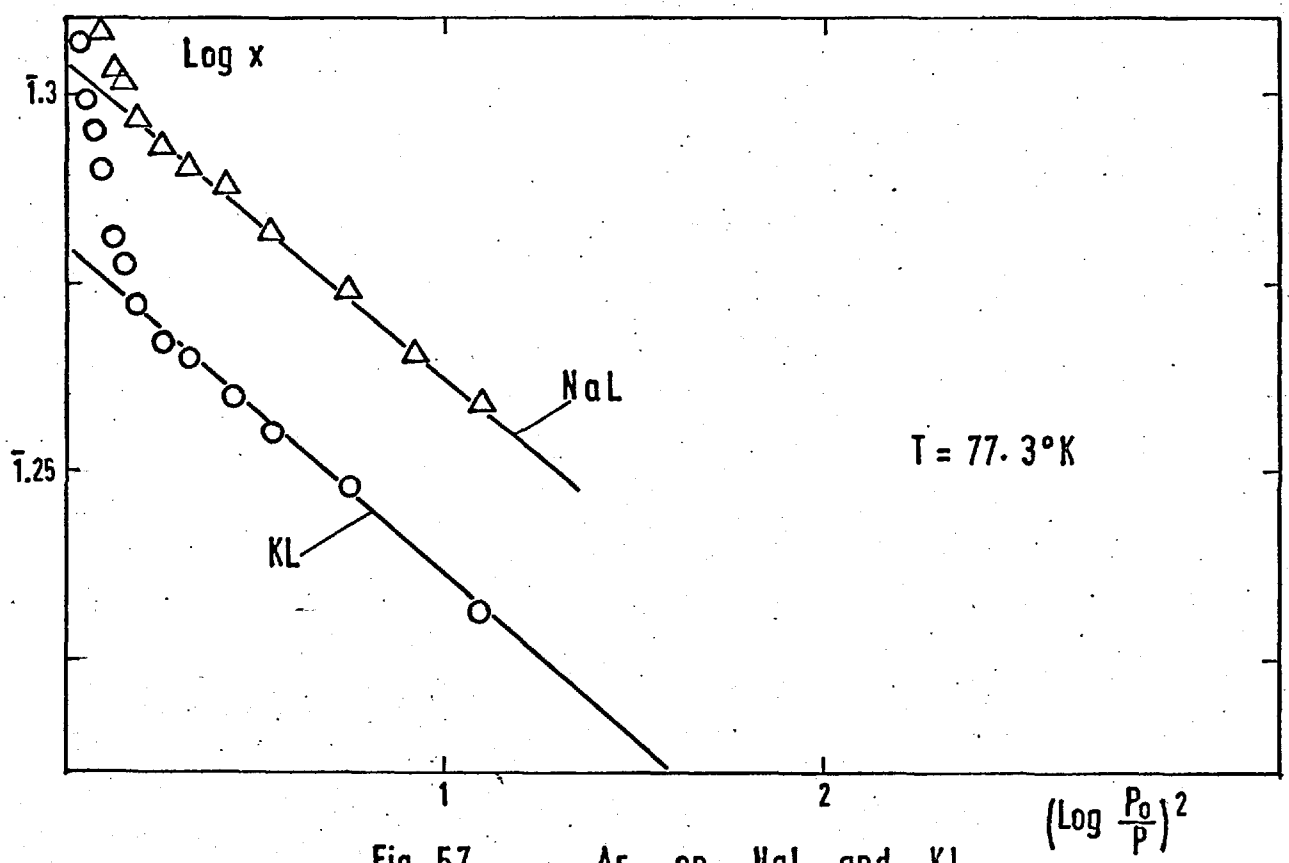

Fig. 57 Ar on NaL and KL

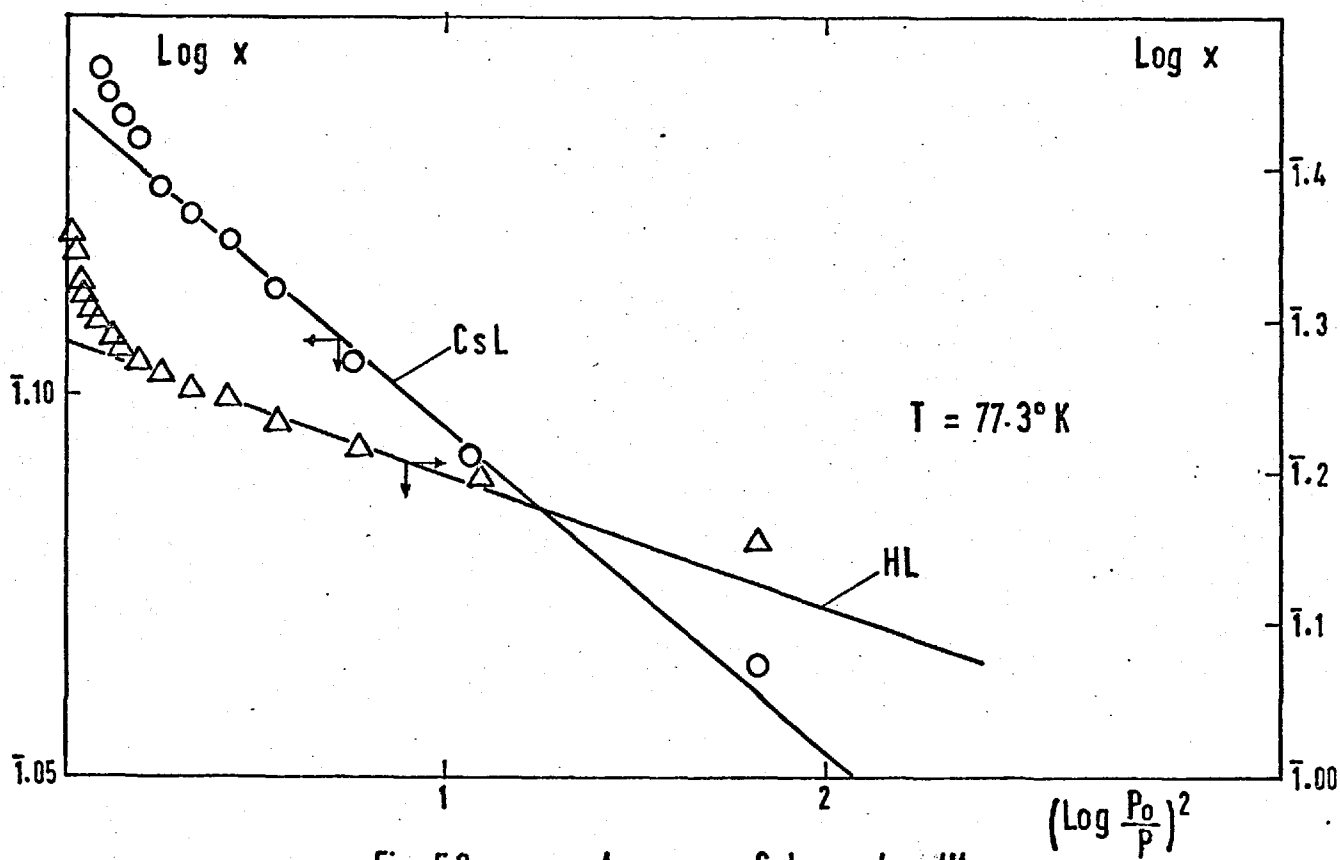

Fig. 58 Ar on CsL and HL

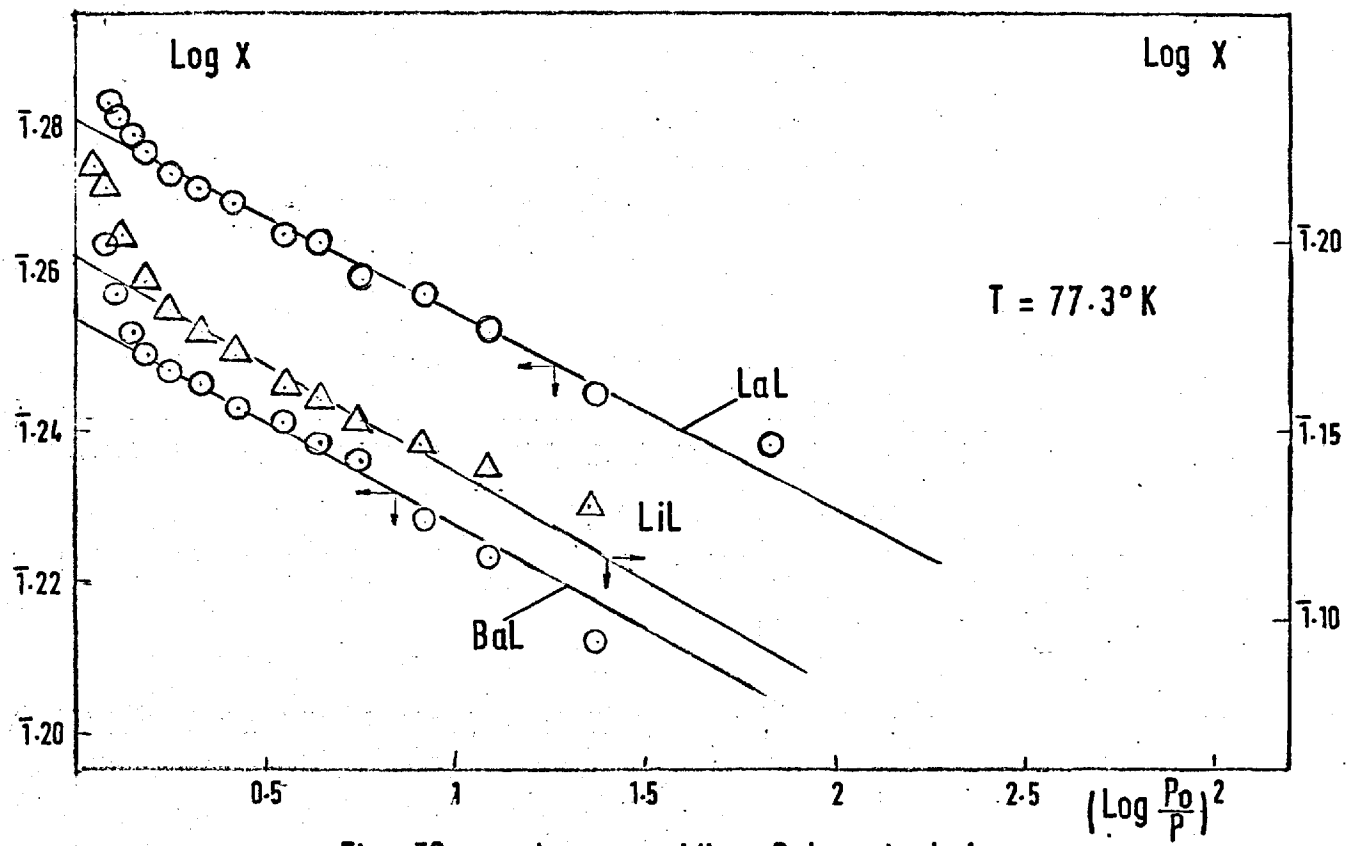

Fig. 59 Ar on LiL, BaL and LaL

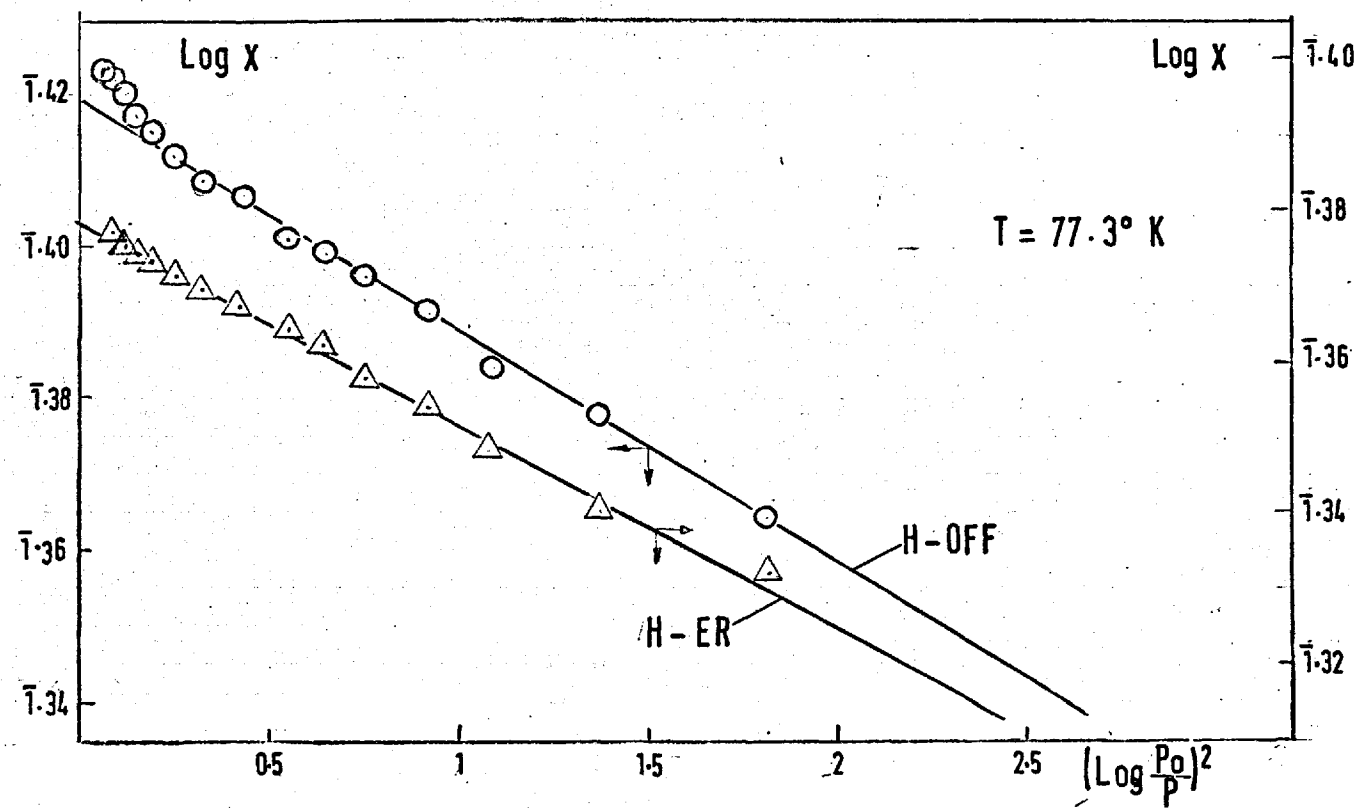

Fig. 60 Ar on H-OFF and H-ER

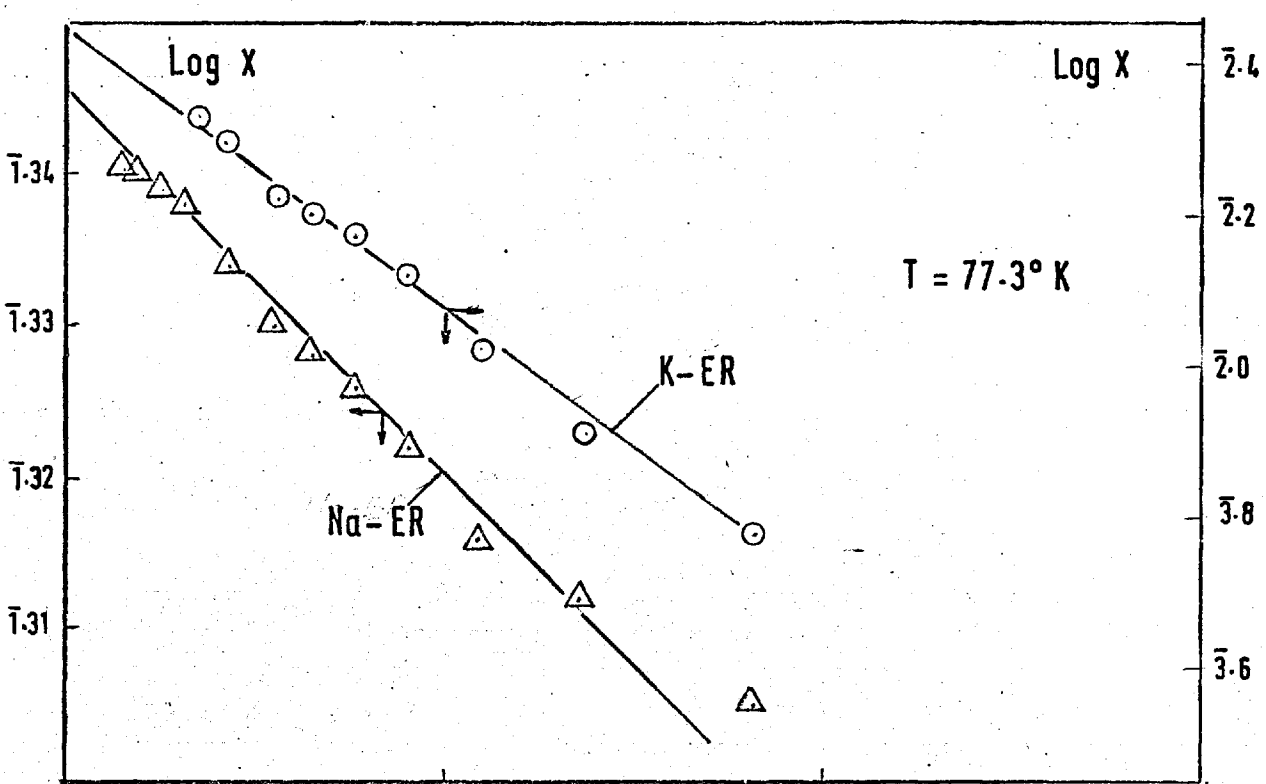

Fig. 61 Ar on Na-ER and K-ER

the complete isotherms were used and the most probable straight lines drawn. The values of the micropore volumes per gram dehydrated sorbent, W_o cc/g, are presented in Table 32. Also included are the values of the micropore volume per unit cell, W_o', expressed in $Å^3$.

TABLE 32.

Micropore volumes of ion-exchanged forms of L.

Sorbent	HL	LiL	NaL	KL	CsL	BaL	LaL
W_o cc/g	0.137	0.110	0.143	0.135	0.097	0.128	0.138
$W_o' Å^3$/u.c.	500	450	580	540	430	530	570

TABLE 33.

Micropore volumes of ion-exchanged forms of erionite and of H-OFF.

Sorbent	H-ER	Na-ER	K-ER	H-OFF
W_o cc/g	0.179	0.157	0.019	0.187
$W_o' Å^3$/u.c.	650	630	70	690

The values found for LiL and CsL are much smaller than those for the rest of the samples in Table 32. This is in a good agreement with the saturation capacities found (Table 29). The micropore volume of HL is less than those of NaL, KL, LaL and BaL, which again agrees with the sequence of the saturation capacities, with the exception of BaL. Also of note are the very similar micropore volumes of NaL and LaL on the one hand and of KL and BaL on the other. The

latter pair shows, in agreement with the saturation capacities, that the free volume of an ion-exchanged form containing a polyvalent cation is not necessarily larger than that of a monovalent cation of the same size.

The values of Table 33 agree well with the values of the saturation capacities of the sorbents involved (Table 31).

The free volume of zeolite-sorbents is frequently estimated on the basis of water content(68;109). In the present study the high values of water content found for LiL and HL (Table 15) are in disagreement with the observed adsorption behaviour. This method of estimating the free volume is therefore not fully satisfactory and illustrates the usefulness of Dubinin's alternative method.

4.1.4 Affinity of sorption

A quantitative measure of the affinity of a sorbate for a certain sorbent is the decrease in the chemical potential, $-\Delta\mu$, when the gas is transferred reversibly and isothermally from the gas phase at standard pressure P_o = 1 atm into an infinite amount of sorbent-sorbate mixture at equilibrium pressure P:

$$-\Delta\mu = RT \ln \frac{P_o}{P}$$

The above equation was used to calculate the affinity of Ar at different amounts adsorbed for all sorbents investigated. The plots for the ion-exchanged forms of L are shown in Fig. 62, and those for ion-exchanged erionite and H-OFF in Fig. 63. The same curves in HL and NaL are repeated in Fig. 63.

In Fig. 62 LaL, NaK, BaL and KL have higher affinity

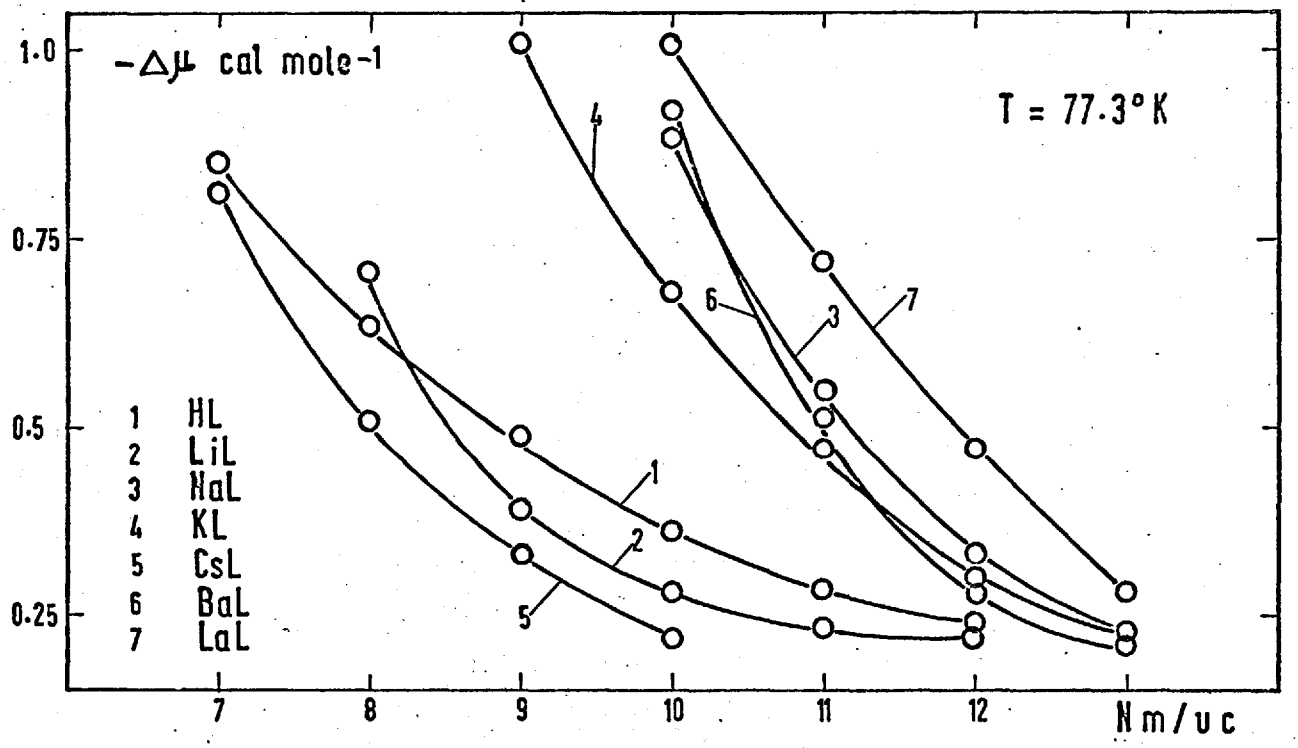

Fig. 62 Ar on ion-exchanged L

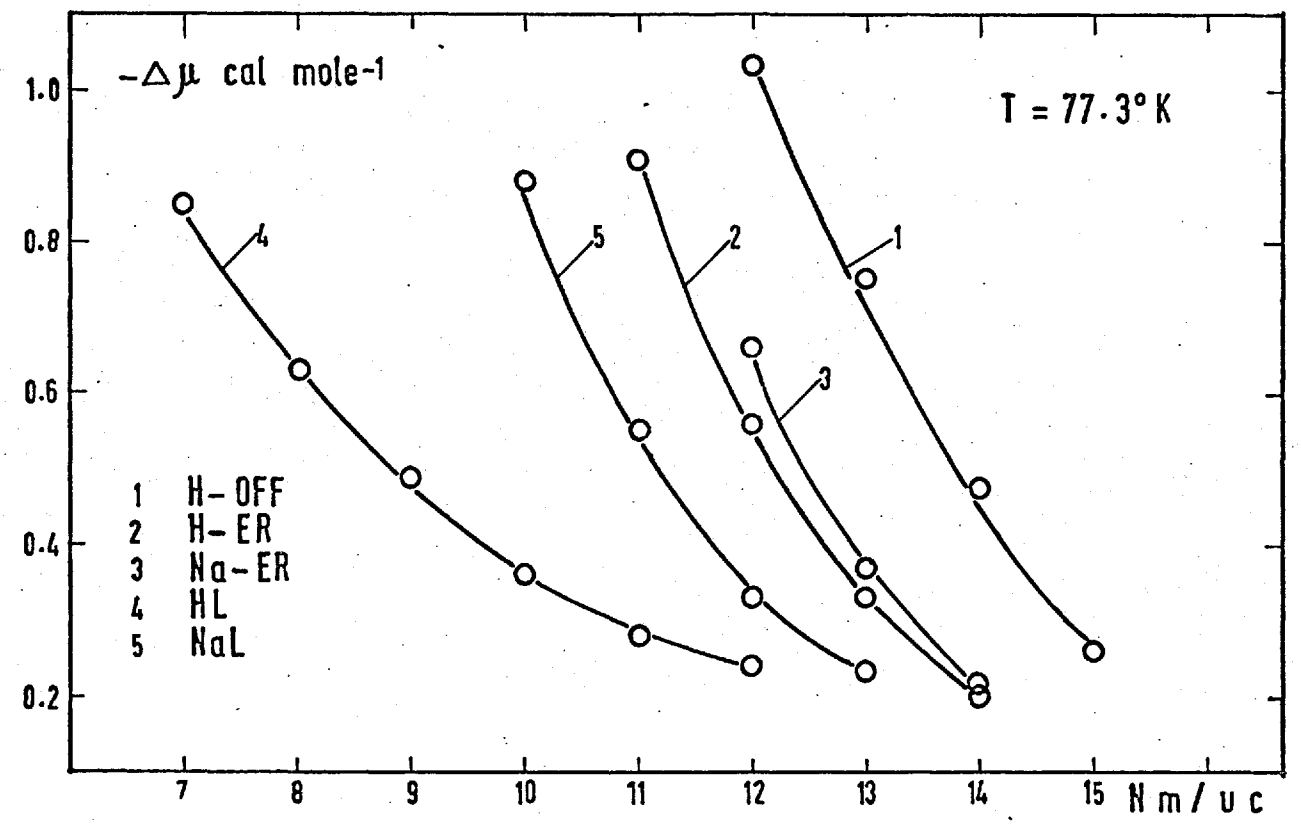

Fig. 63 Ar on ion-exchanged L ER and OFF

for Ar and HL, LiL and CsL, a lower affinity. The sorbents of the first group are those with the larger micropore volumes (Table 32). A comparison of the affinity of Ar towards the decationated forms of L, ER and OFF shows that the affinity is greatest for H-OFF and lowest for HL. The order of the affinity of these samples is the same as the order of the calculated micropore volumes (Tables 32 and 33).

Fig. 64 gives the affinity curves of three selected samples - NaL, NaL-IC and CaL-IC for Ar at 77.3°K and 90.4°K. The greater affinity for L-IC samples is attributable to the presence of erionite and offretite on L-IC.

4.2 ADSORPTION OF Kr IN THE TEMPERATURE RANGE 130°K - 240°K.

Krypton isotherms were measured for each sorbent at at least five temperatures in the range 130°K - 240°K. The equilibria served to determine isosteric heats, affinity of sorption, equilibrium constants and energy of adsorption in the standard states for all the systems studied. For ion-exchanged forms of L containing cations of different valency, (KL, BaL and LaL), the 'virial' coefficients required to describe the experimental isotherms were calculated, together with the thermodynamic properties of the standard states. For identical ion-exchanged forms of zeolite L, erionite and offretite - HL, H-ER and H-OFF - half standard entropies (p. 53) and entropies of the sorbed phase were calculated from the isosteric heats.

4.2.1 Isotherms.

All krypton isotherms were reversible and reproducible. Equilibrium was established in about 15 minutes; however, half an hour was allowed between readings. An outgassing

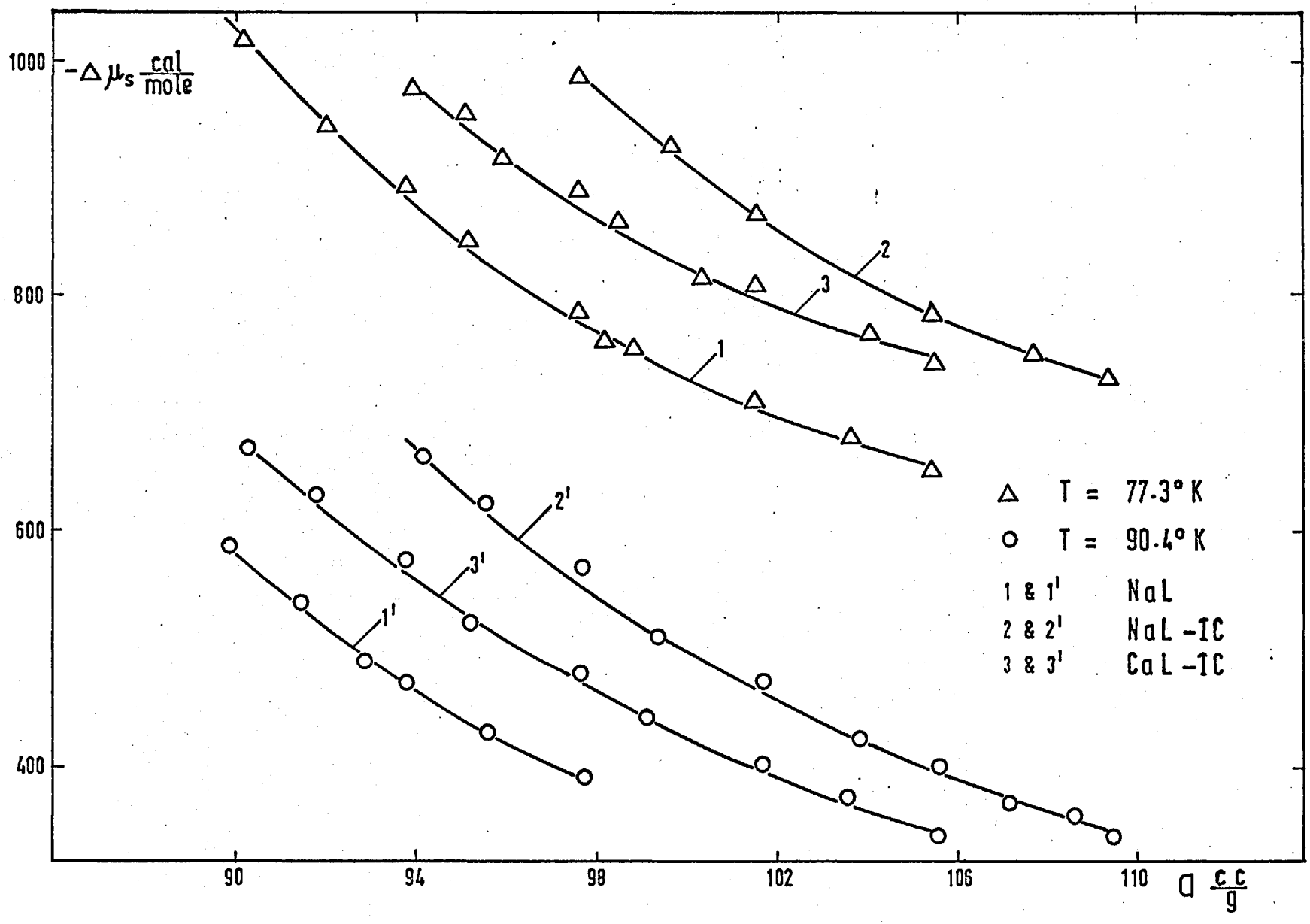

Fig. 64 Ar on NaL, NaL-IC and CaL-IC

temperature of 150°C was used between runs. Heating and cooling was carried out at rates not exceeding 50°C per hour. Outgassing under such conditions was sufficient for complete desorption.

The isotherms, expressed as numbers of molecules per unit cell vs pressure are given on Figs. 65-73 and the numerical data in the Appendix. All isotherms were of type I of the BDDT classification(134). Among the isotherms on ion-exchanged forms of zeolite L, those containing only monovalent cations were generally less rectangular than the corresponding ones on BaL and LaL. Thus a relatively stronger sorbate/sorbent interaction is present on the forms containing polyvalent cations.

Although, as previously indicated, argon isotherms at 77.3°K on the HL and LiL (Fig. 53) were significantly different in shape from the rest of the series, with krypton such differences were not apparent.

Krypton isotherms in H-ER and H-OFF were similar and more rectangular than those in HL (Fig. 65, 72 and 73). This was also observed for argon adsorption at 77.3°K on the three sorbents and was attributed to stronger sorbate-sorbent interactions in H-ER and H-OFF. These differences for both argon and krypton can be related to differences in structures of the sorbents (p. 13). In the channels of offretite (and cavities of erionite) of free diameter d = 6.3 Å, the adsorption fields and binding energies should be stronger than in the wider chennels of zeolite L, with d = 7.1-7.8 Å. (The sequence of the values of the isosteric heats of Kr on HL, H-ER and H-OFF confirm this. (p.192))

A comparison of Figs. 65, 72 and 73 reveals also that for corresponding temperatures and pressures the amounts adsorbed on HL are much lower than on H-ER and H-OFF. This

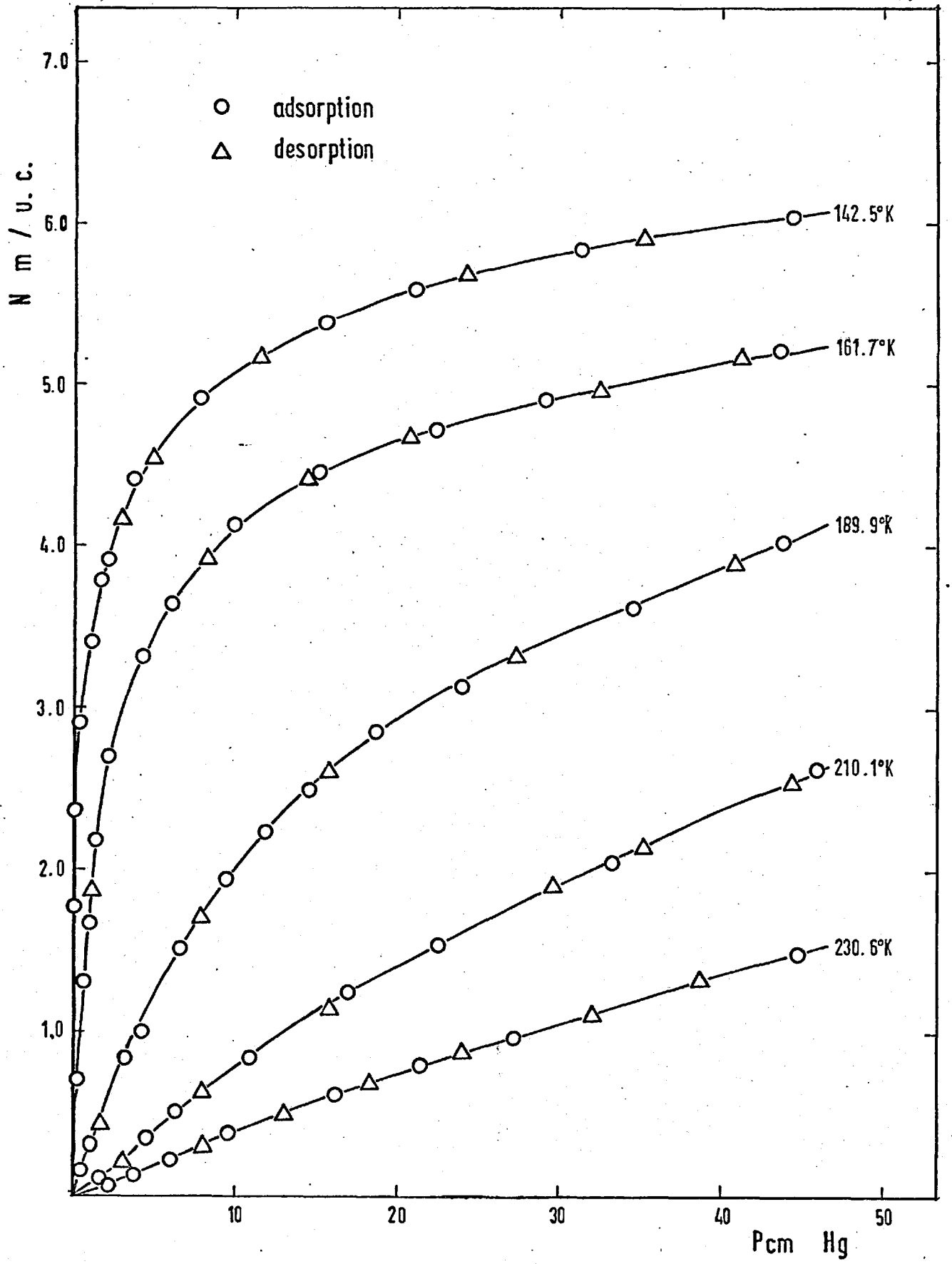

Fig. 65 Kr on HL

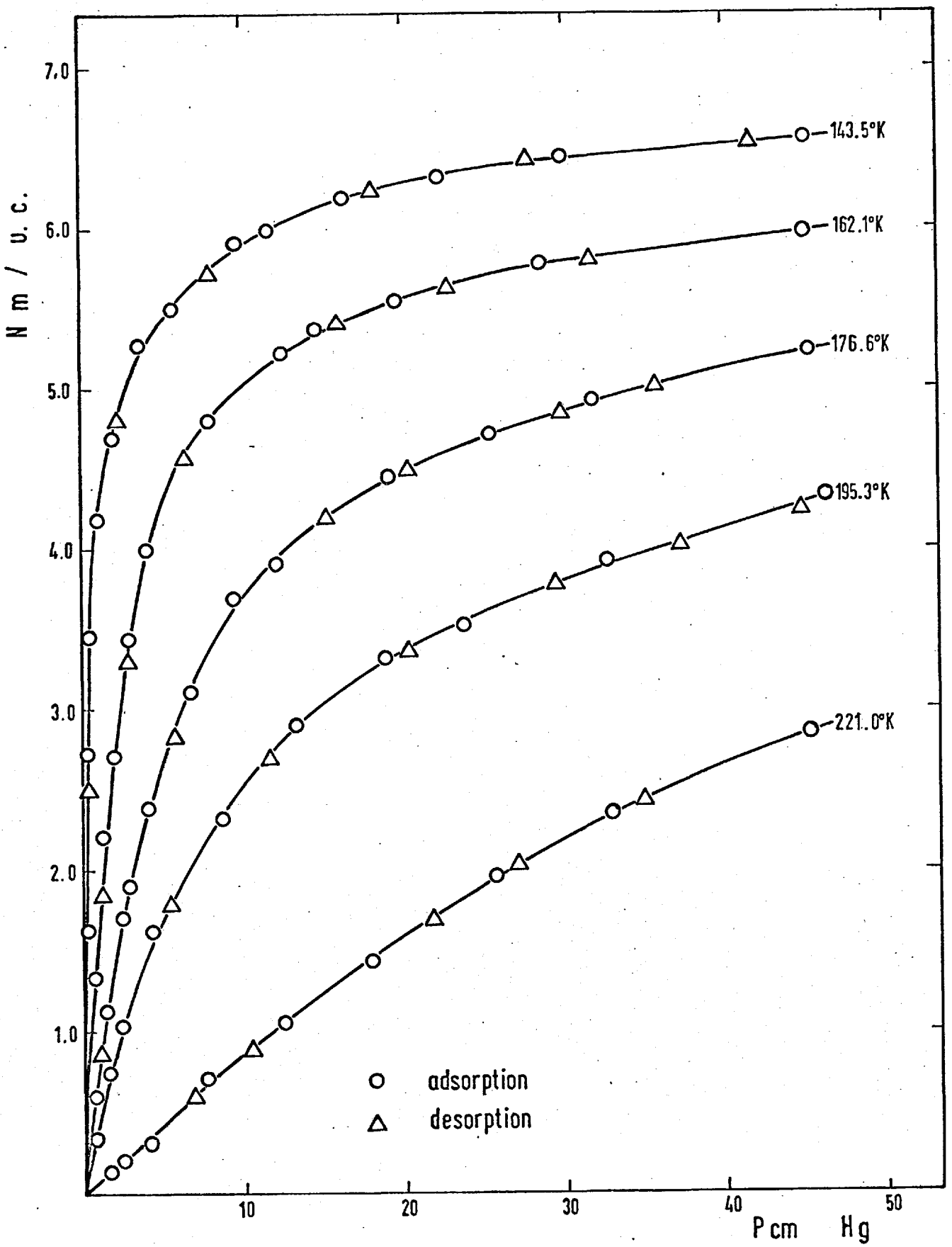

Fig. 66 Kr on LiL

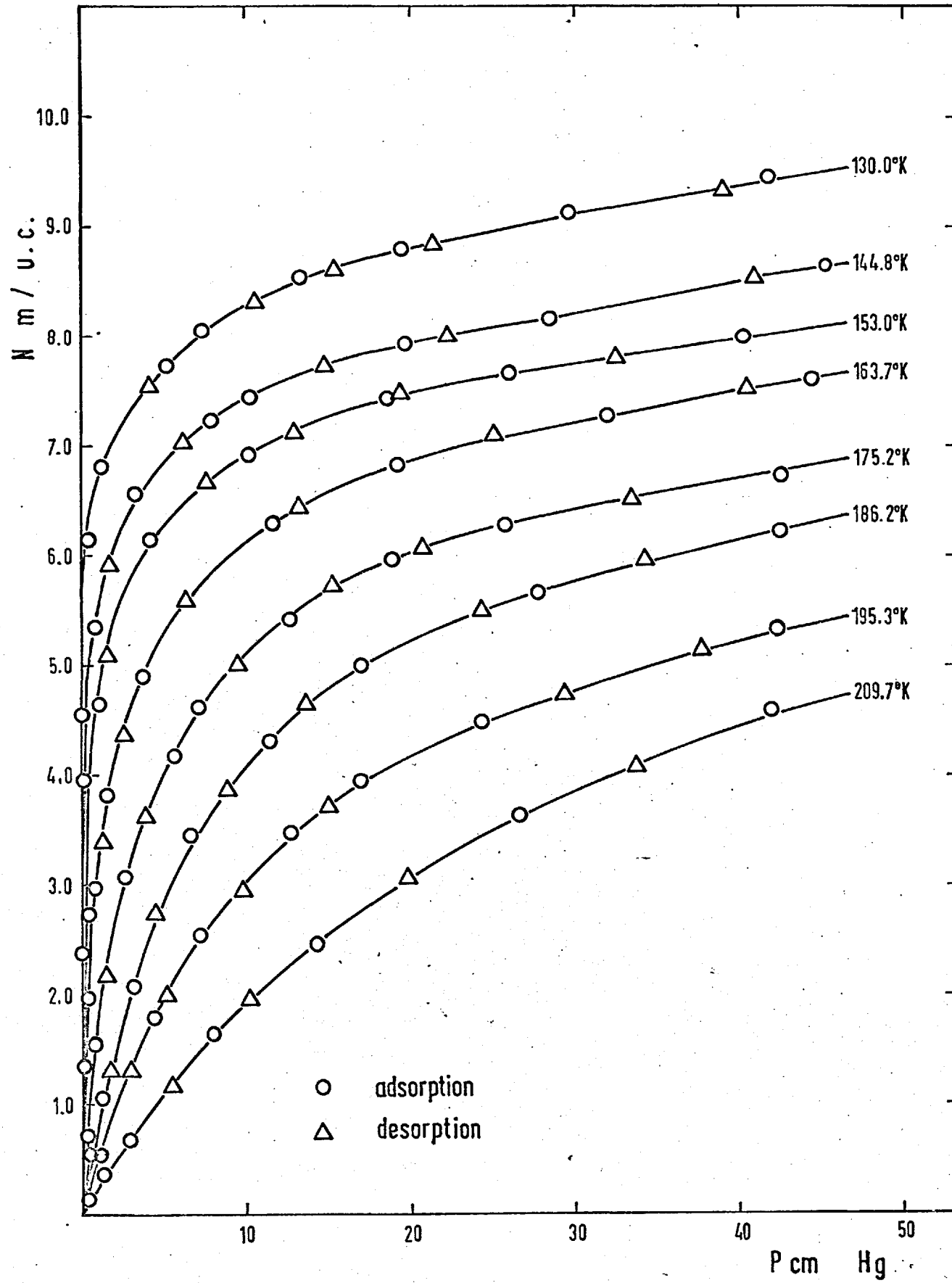

Fig. 67 Kr on NaL

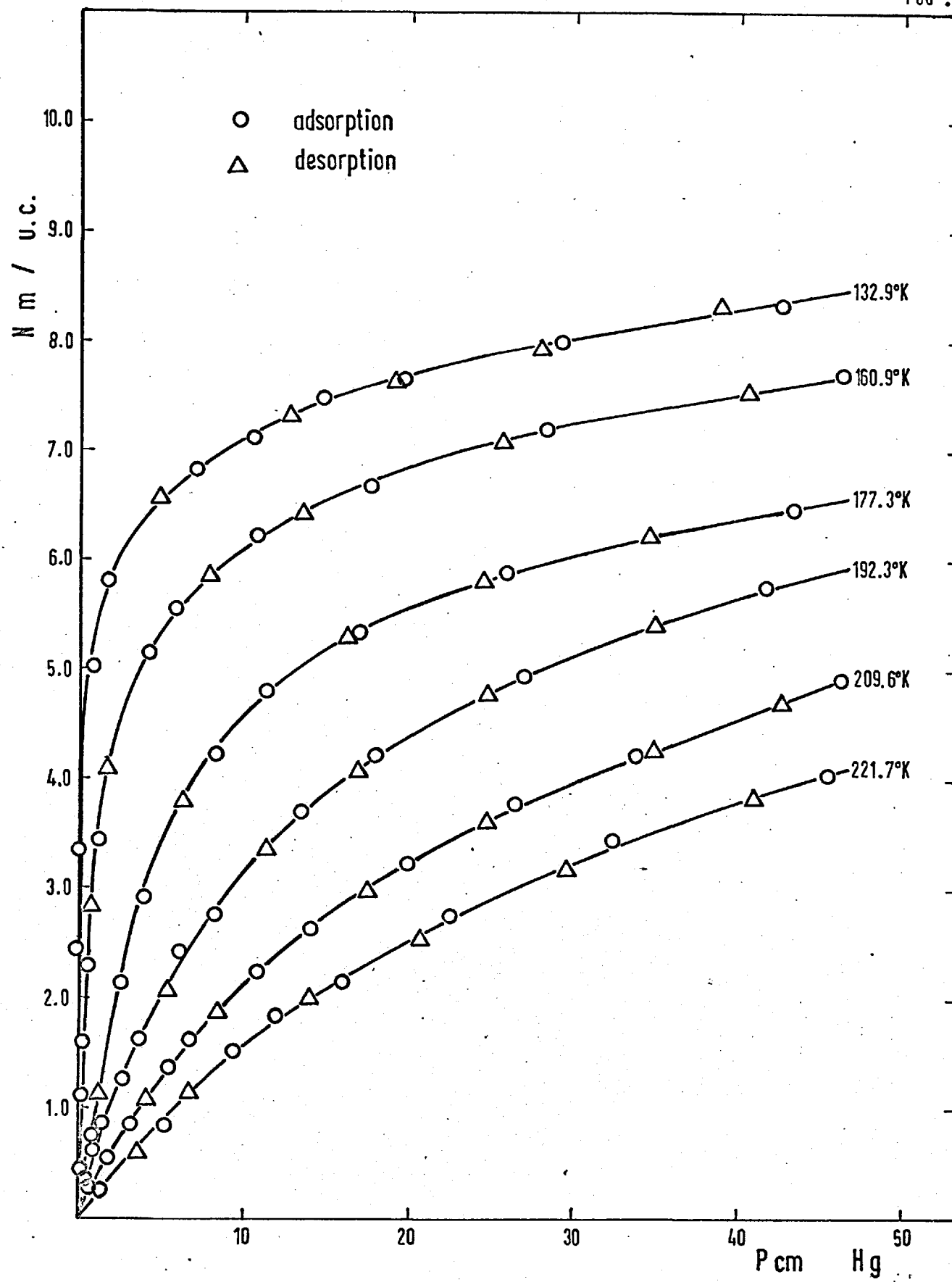

Fig. 68 Kr on KL

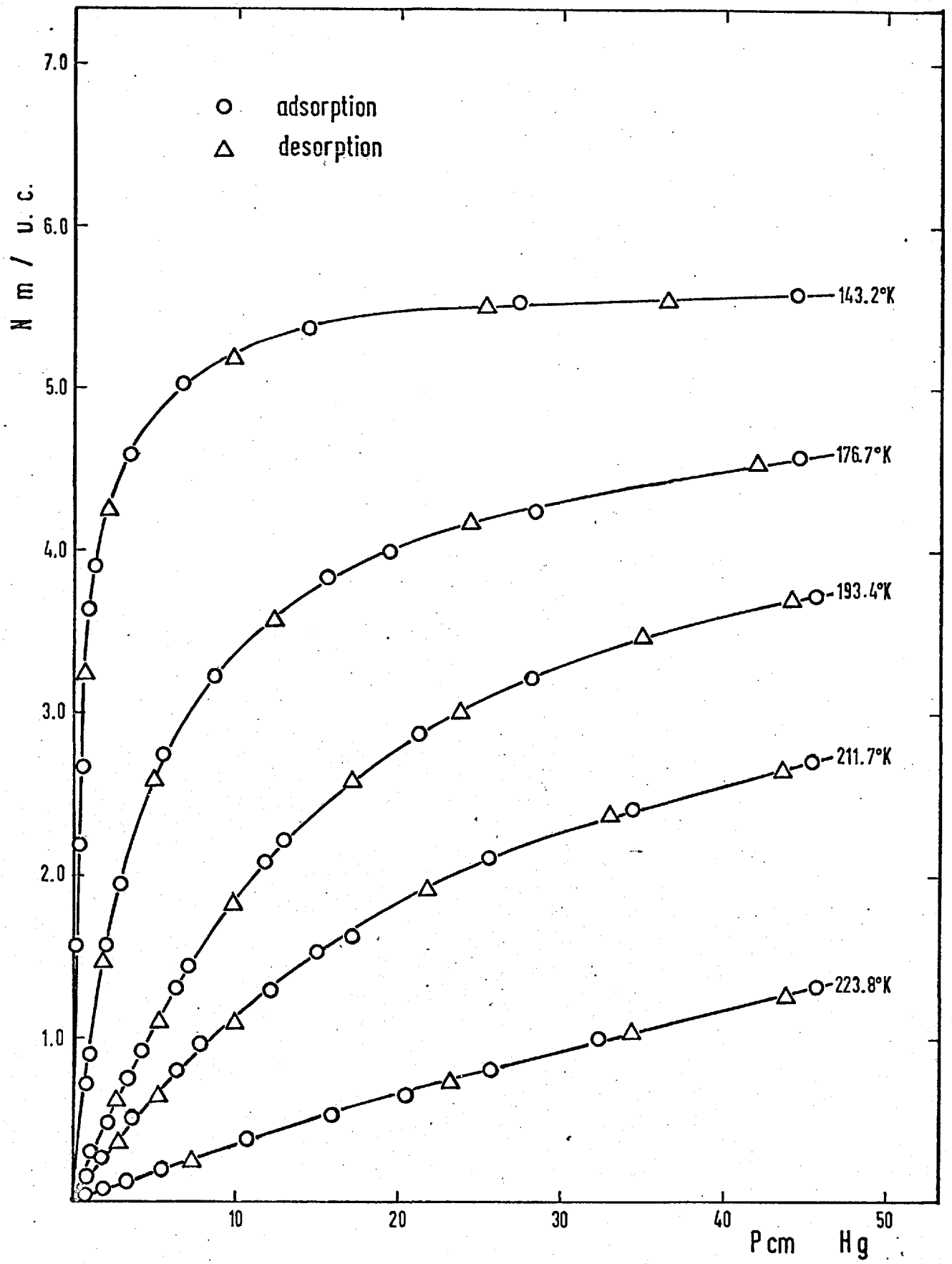

Fig. 69 Kr on CsL

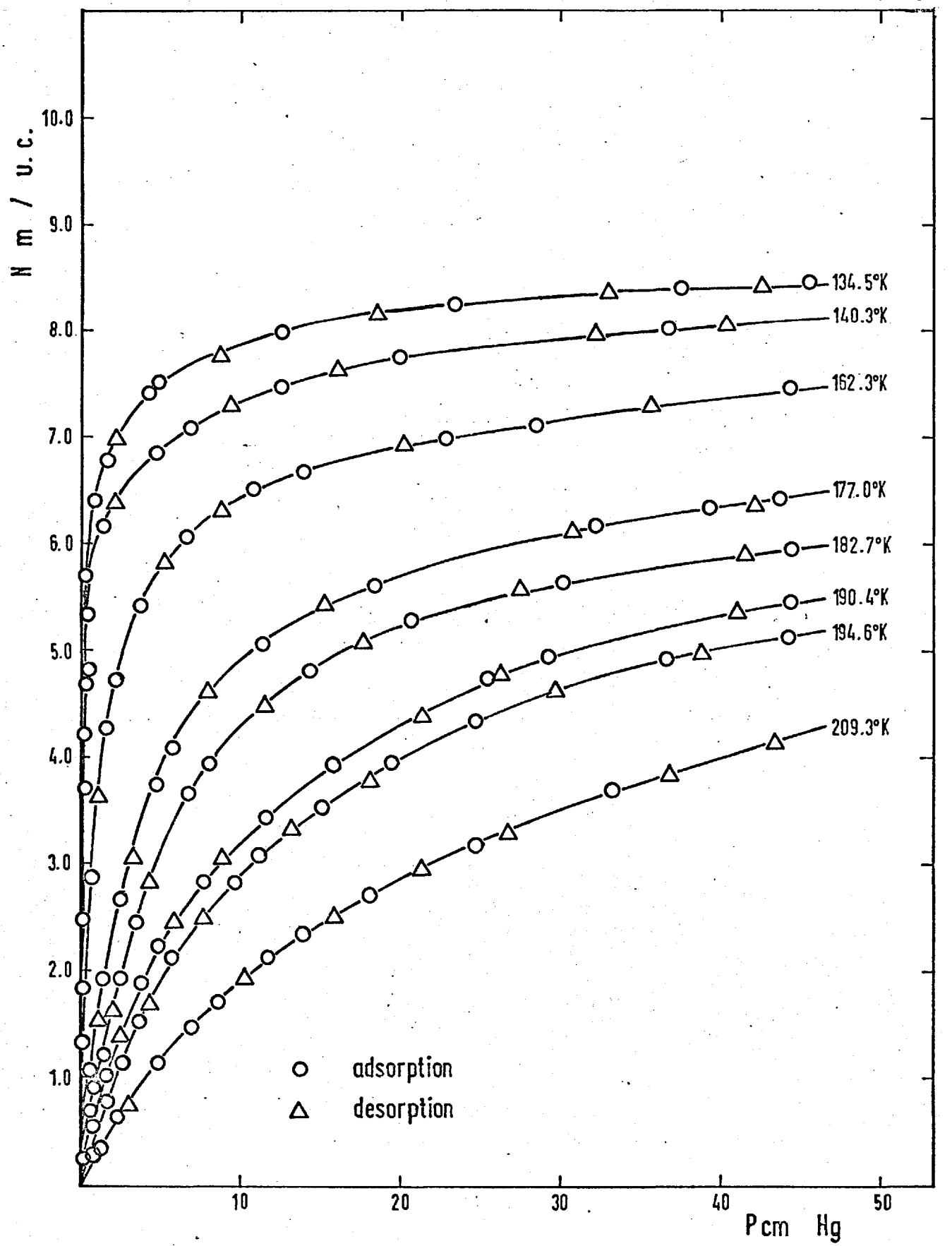

Fig. 70 Kr on BaL

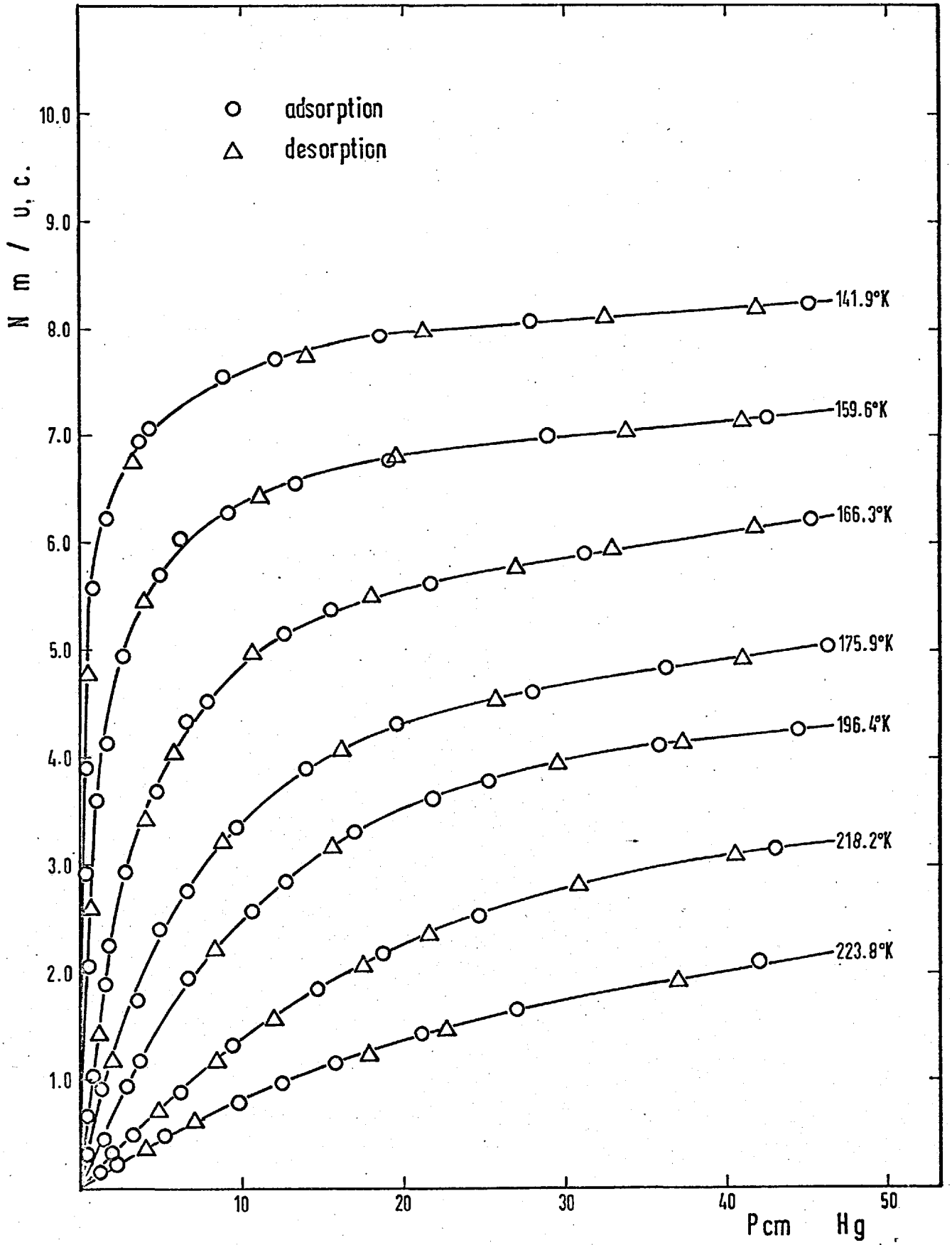

Fig. 71 Kr on LaL

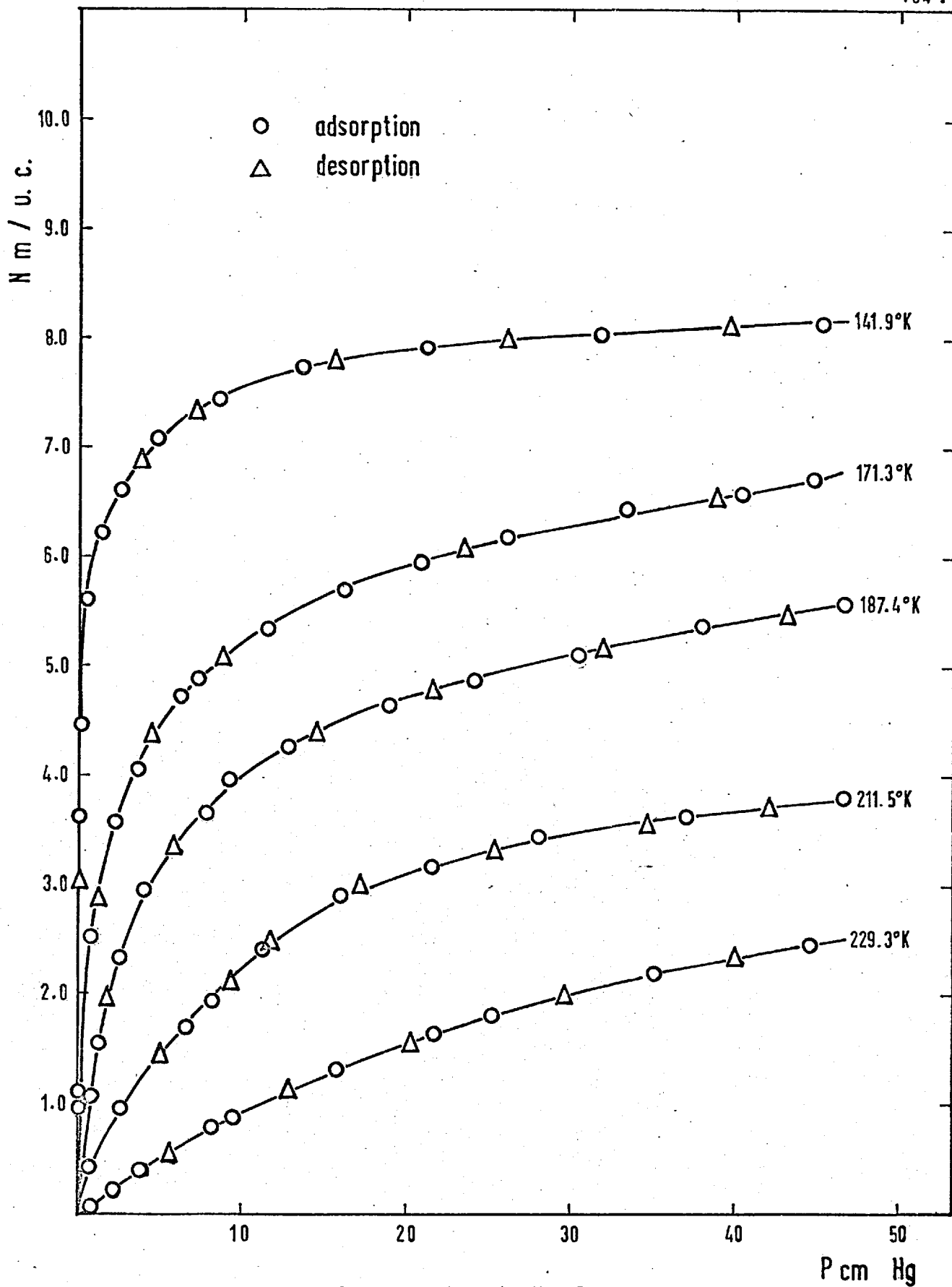

Fig. 72 Kr on H-ER

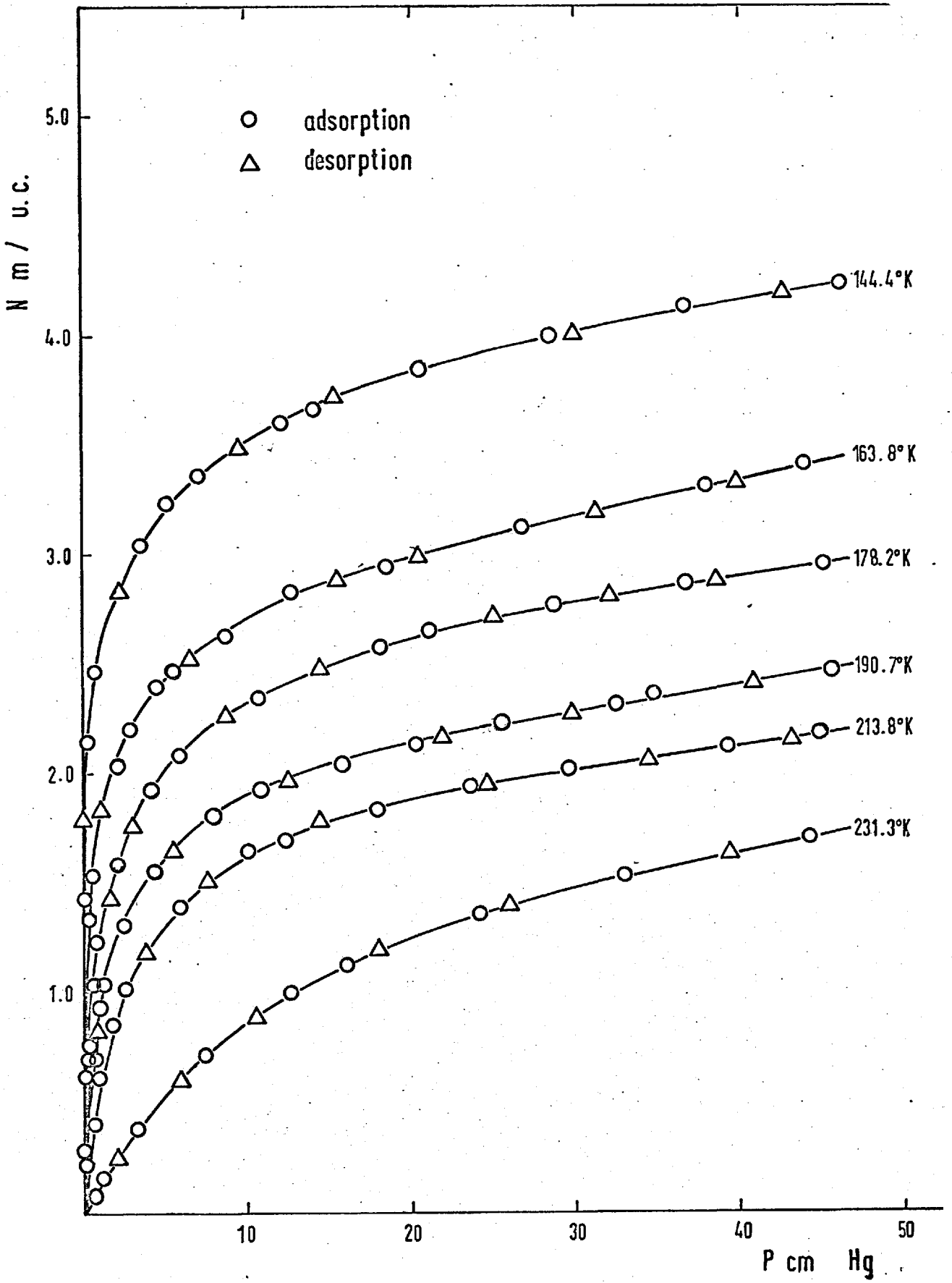

Fig. 73 Kr on H-OFF

could be attributed to the smaller free volume (Tables 32 & 33) as well as the weaker sorbate/sorbent interaction of HL compared with H-ER and H-OFF.

4.2.2 Isosteric heats.

Isosteric heats of sorption (p.52) were determined using the integral form of the Clausius-Clapeyron equation:

$$\ell g \frac{P_1}{P_2} = - \frac{\Delta \bar{H}_1}{2.303R} \left[\frac{1}{T_1} - \frac{1}{T_2} \right] \quad \ldots (4.2\text{-}1)$$

or $$\ell g\, P = - \frac{\Delta \bar{H}_1}{2.303R} \cdot \frac{1}{T} + \text{const.} \quad \ldots (4.2\text{-}2)$$

For the purpose of finding $\Delta \bar{H}_1$, three types of plot were used: those of $\ell g P$ vs $\frac{1}{T}$ for constant $\underline{a}$ and for each of a series of temperatures those of $\ell g P$ vs $\underline{a}$ and of $\ell g \frac{P}{a}$ vs $\underline{a}$ (P is the pressure in cmHg and $\underline{a}$ is the uptake in cc(STP) per gram dehydrated sorbent). Average values of $\Delta \bar{H}_1$ from the first two methods only were estimated, unless a significant discrepancy occurred, in which case the values of the third method were taken into account. In this way values of $\Delta \bar{H}_1$ were obtained with a maximum deviation from the mean curve of $\pm$ 0.15 kcal/mole.

No evidence of a temperature dependence of $\Delta \bar{H}_1$ was found within the limits of the experimental error. Barrer and Stuart(68) have also found, for argon adsorption on zeolite X, that the isosteric heats were not, within the error, functions of temperature.

In Table 34 the average isosteric heats are tabulated for different ion-exchanged forms of L. The heats were graphed both as functions of uptake $\underline{a}$ (cc(STP) of sorbate per gram of dehydrated sorbent) in Fig. 74 and of uptake η.

TABLE 34.

Isosteric heats ($-\Delta\bar{H}_1$ kcal/mole) of Kr on ion-exchanged forms of L.

a cc/g	HL		LiL		NaL		KL		CsL		BaL		LaL	
	η	$-\Delta\bar{H}_1$	η	$-\Delta\bar{H}_1$	η	$-\Delta\bar{H}_1$	η	$-\Delta\bar{H}_1$	η	$-\Delta\bar{H}_1$	η	$-\Delta\bar{H}_1$	η	$-\Delta\bar{H}_1$
5	36	4.56	46	4.75	35	5.00	37	4.60	-	-	39	4.75	-	-
10	73	4.30	91	4.50	70	4.98	74	4.39	103	4.81	78	4.71	-	-
15	109	4.20	136	4.39	105	4.88	111	4.29	154	4.59	117	4.70	108	5.23
20	146	4.01	182	4.23	140	4.80	148	4.14	206	4.43	156	4.63	145	5.11
25	182	3.95	223	4.10	175	4.71	185	3.98	258	4.32	195	4.60	182	5.28
30	220	3.81	272	4.01	210	4.67	222	3.80	310	4.25	234	4.52	218	5.02
35	256	3.68	318	3.90	245	4.52	260	3.59	360	4.17	274	4.49	254	5.06
40	292	3.42	364	3.74	280	4.34	296	3.32	410	3.98	312	4.43	290	4.85
45	328	3.19	410	3.55	315	4.19	334	3.03	-	-	352	4.41	326	4.65
50	366	3.07	455	3.32	350	4.10	370	2.82	-	-	390	4.38	362	4.21
55	400	2.90	500	3.21	385	3.92	407	2.64	-	-	430	4.23	398	3.82
60	-	-	-	-	420	3.70	445	2.40	-	-	470	4.13	435	3.79
65	-	-	-	-	455	3.56	-	-	-	-	508	4.01	-	-
70	-	-	-	-	490	3.36	-	-	-	-	546	3.79	-	-
75	-	-	-	-	525	3.21	-	-	-	-	-	-	-	-

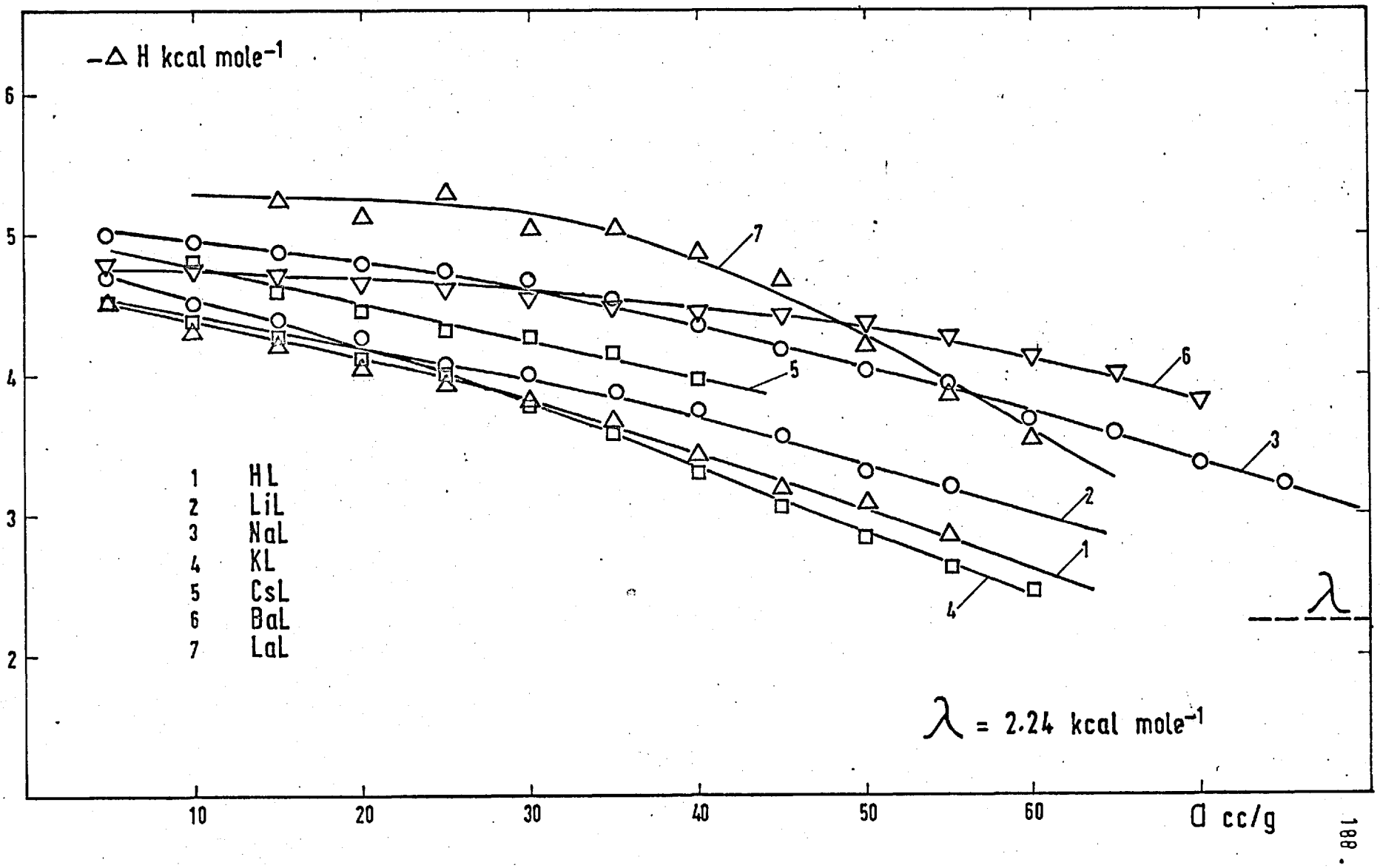

Fig. 74 ISOSTERIC HEATS of Kr

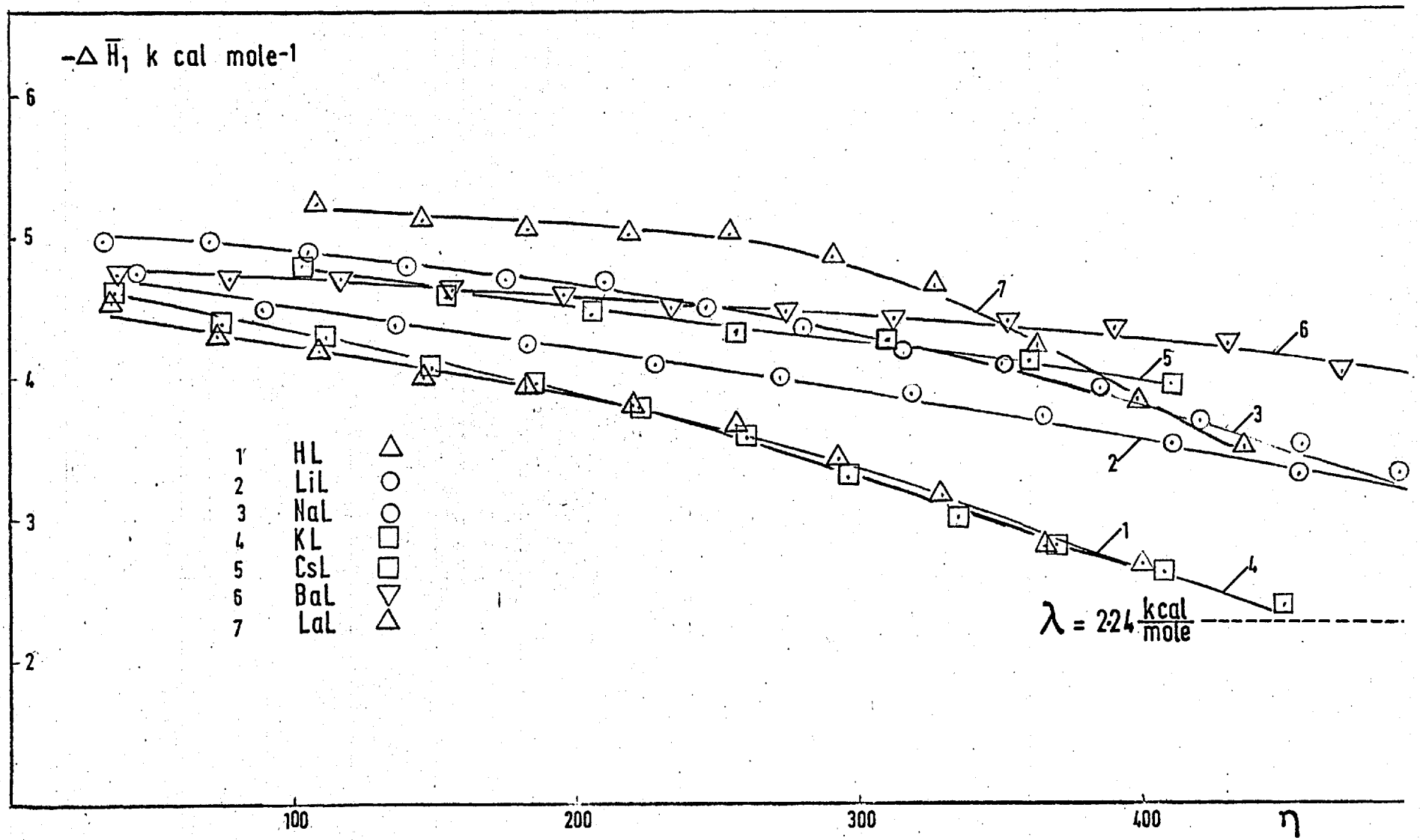

Fig. 75 ISOSTERIC HEATS of Kr

(cc(STP) of sorbate per unit free volume of the sorbent) in Fig. 75. The scale η was introduced to remove the dependence of $\Delta\bar{H}_1$ on the free volume*. Changes in relative position of the curves of CsL and LiL - both sorbents with lowest free volumes - are noted when Figs. 74 and 75 are compared.

In Fig. 76 the isosteric heats of Kr on the decationated forms of zeolite L, erionite and offretite are presented. Isosteric heats are plotted vs η and some numerical values are given in Table 35.

In all the systems studied, the isosteric heats decreased with the increasing uptake, thus showing heterogeneity(89,135) towards Kr for all sorbents. A comparison of the slopes of the isosteric heat curves showed that the apparent heterogeneity was lowest for BaL and greatest for LaL and HL.

The initial isosteric heats of Kr on different ion-exchanged forms of zeolite L, with the exception of LaL, fall within a range of $\pm$ 0.3 kcal/mole. On the other hand the initial isosteric heats on identical ion-exchanged forms of the three structurally distinct sorbents used are widely different (Fig. 76). Also differences arise in the slopes of the curves of heat vs amount sorbed for all the forms of zeolite L (Fig. 75) in contrast with the similarity of the slopes for HL, H-ER and H-OFF (Fig. 76). From this observation one might conclude that, for the systems investigated, the sorbate/framework interaction determines the initial heats of adsorption, while sorbate/cation interaction causes much of the energetic heterogeneity of the sorbent towards a given non-polar sorbate. The experimental evidence presented here is consistent with this conclusion, but is insufficient to prove it. Investigation of a variety of cation-

---

* the values of micropore volumes are used (Table 32).

TABLE 35.

Isosteric heats ($-\Delta\bar{H}_1$ kcal/mole) of Kr on H-ER and H-OFF

a $\frac{cc}{g}$	H-ER		H-OFF	
	η	$-\Delta\bar{H}_1$	η	$-\Delta\bar{H}_1$
5	28	5.42	-	-
10	56	5.28	-	-
15	84	4.95	-	-
20	112	4.92	110	5.53
25	140	4.70	137	5.50
30	168	4.62	165	5.39
35	196	4.45	192	5.22
40	224	4.39	220	5.17
45	252	4.35	248	5.03
50	280	4.25	274	4.81
55	308	4.12	302	4.70
60	336	3.80	330	4.58
65	364	3.76	358	4.41
70	-	-	385	4.30

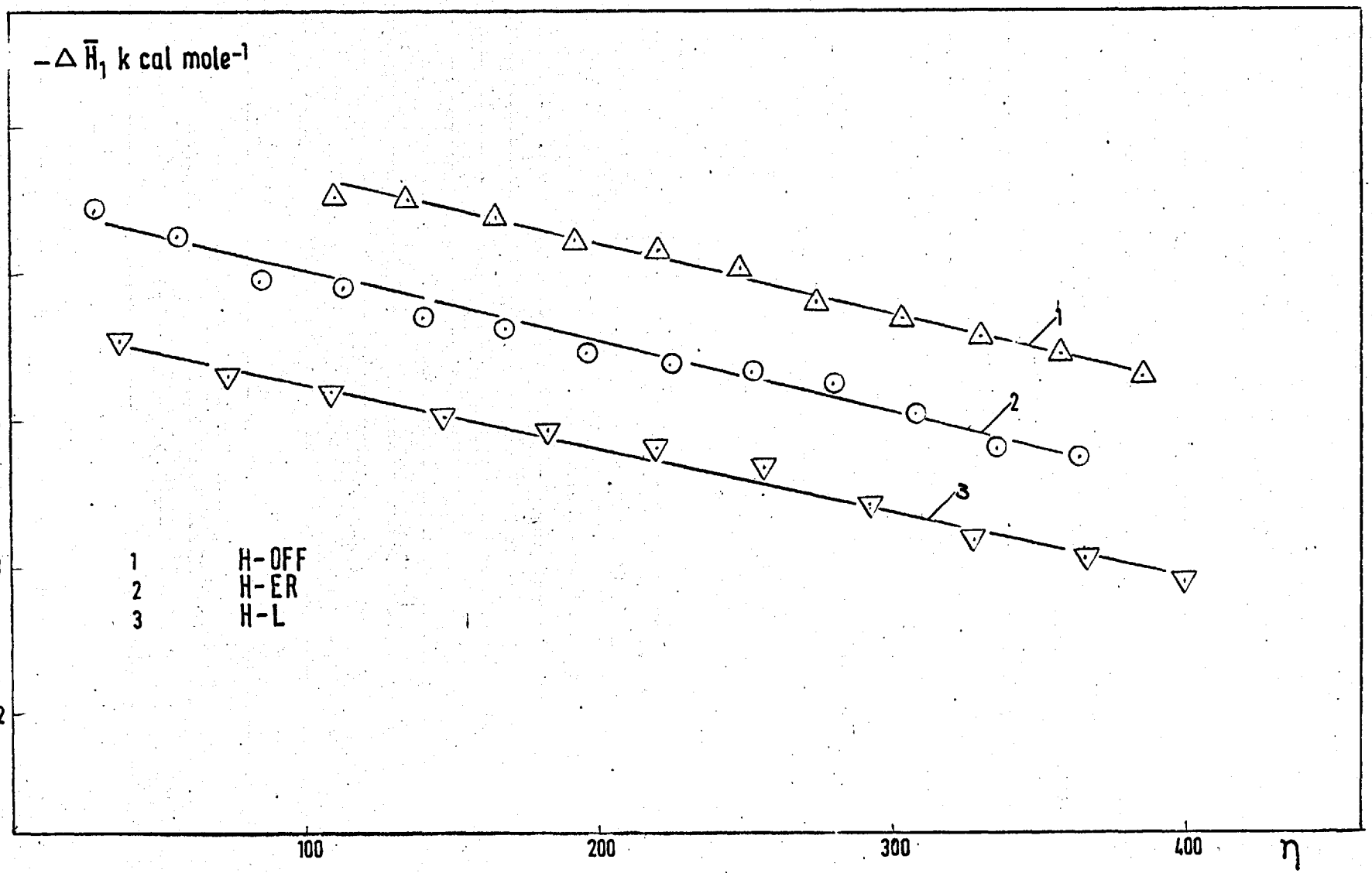

Fig. 76 ISOSTERIC HEATS of Kr

exchanged forms of erionite and offretite might provide further confirmation.

4.2.3 Affinity and selectivity

In section 4.1.4 the affinities of Ar at 77.3°K were calculated for all the sorbents. Affinities, $-\Delta\mu$, towards Kr were similarly calculated (cf section 4.1.4). For this purpose isotherms at the temperature closest to 140°K were selected. The results are presented on Figs. 77 and 78

The groups of sorbents of high (LaL, BaL, NaL and KL) and low (HL, LiL and CsL) selectivity are still distinguishable (see section 4.1.4), but less clearly so. Considerable alteration of the relative positions of the curves of sorbents of the first group was observed, NaL and BaL having the highest affinity for Kr, instead of LaL as found for Ar at 77.3°K. The order of HL and LiL in the second group has been reversed. However, the sequence of decreasing magnitudes of $-\Delta\mu$ for Kr on different sorbents still tends to follow the sequence of the decreasing micropore volumes (Table 32). The less clear distinction for Kr between the two groups of sorbents may be explained in terms of the distance from saturation. Micropore volumes should be more decisive in their influence as saturation is approached.

4.2.4 Empirical isotherm equations.

An empirical isotherm equation may be derived by a thermodynamic argument if one assumes that an equation of virial form relates pressure and mean concentration of sorbate within the zeolite (p.60-). The equation serves to evaluate the equilibrium constants for the distribution of sorbate between gas phase and crystals, and the energies of sorption in the standard states. These equilibrium constants are significant

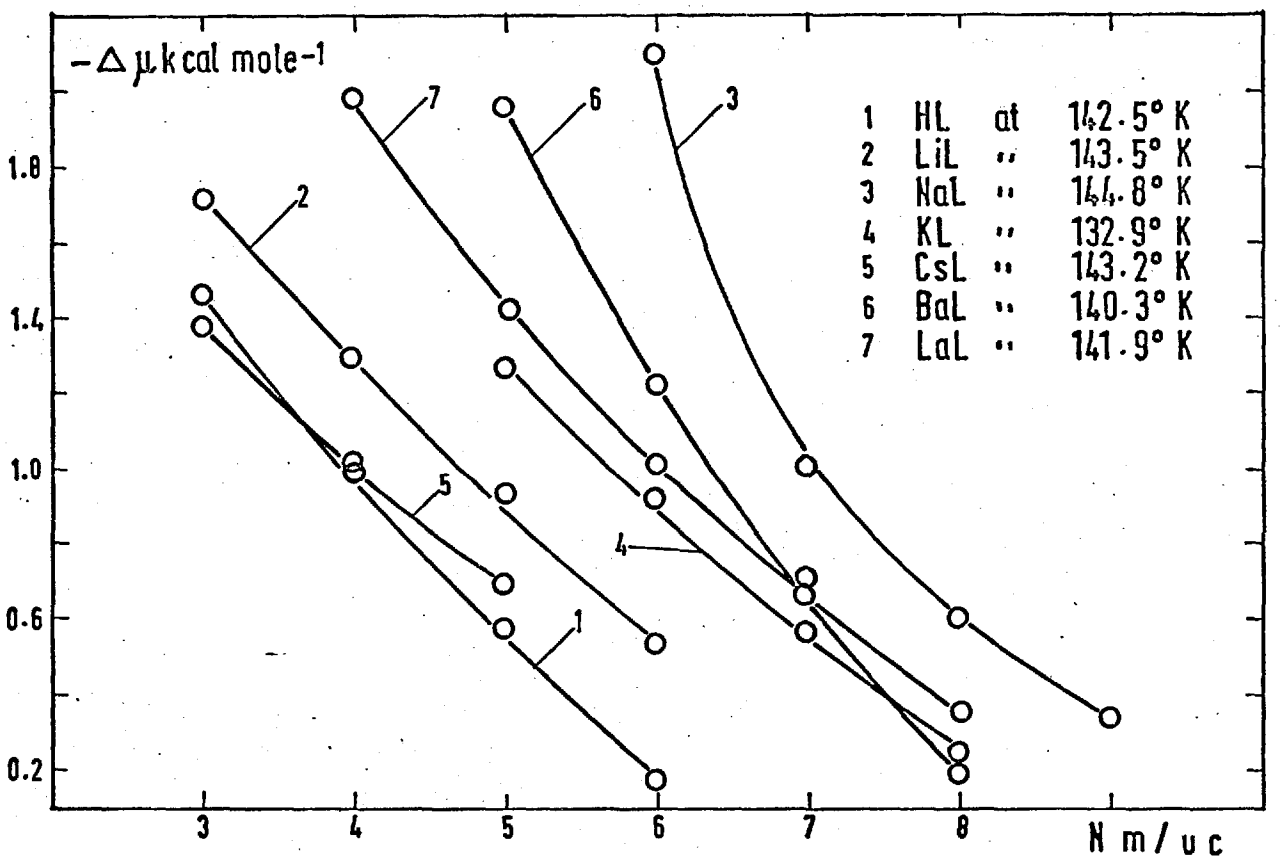

Fig. 77 Kr on ion-exchanged L

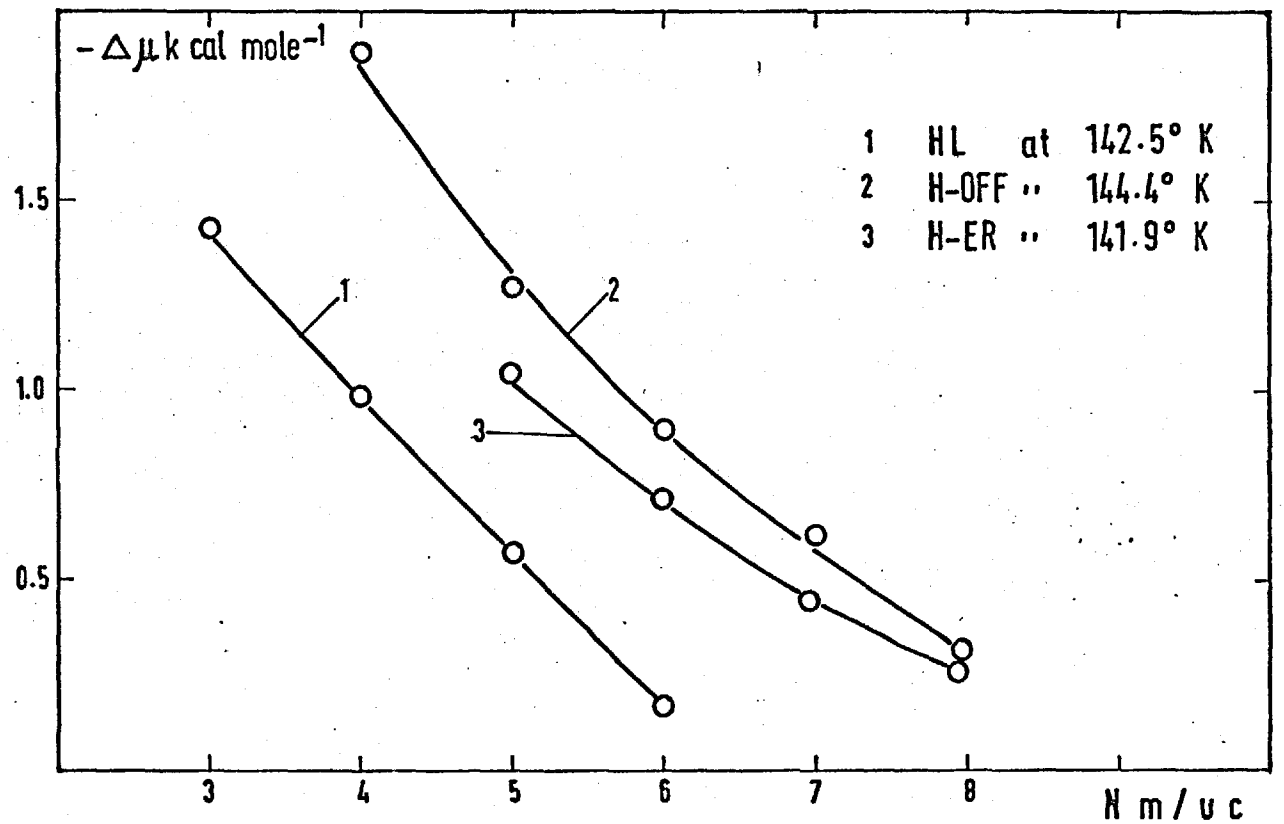

" "-ER and H-OFF

for comparing different sorbate/sorbent systems.

Equation 3.4-9 from Chapter I (p.62) can be written as

$$\ln K = \ln \frac{C_s}{P} + 2A_1 C_s + \frac{3}{2} A_s C_s^2 + \frac{4}{3} A_3 C_s^3 + \cdots \quad \ldots(4.2\text{-}3)$$

Depending on the definition of the parameters the above equation can be written in either of the following two forms:

1. Concentration in number of molecules sorbate per unit cell of dehydrated sorbent ($N\frac{m}{u.c.}$) and the pressure in cmHg (P cmHg):

$$\ln K' = \ln \frac{N}{P} + 2A'_1 N + \frac{3}{2} A'_2 N^2 + \cdots \quad \ldots (4.2\text{-}4)$$

2. Concentration in moles sorbate per litre of free volume of the zeolite ($C_s m'/\ell$) and the pressure can be replaced by concentration of the sorbate in the gas phase in moles per litre ($C_g\ m'/\ell$):

$$\ln K'' = \ln \frac{C_s}{C_g} + 2A_1^\circ C_s + \frac{3}{2} A_2^\circ C_s^2 + \cdots \quad \ldots (4.2\text{-}5)$$

The equilibrium constant K" is dimensionless and has the advantage that the thermodynamic functions calculated from it are independent of the chosen units of pressure and concentration. K' has the advantage of being more readily calculated from the experimental data.

As explained previously (p. 62) the equilibrium constant, K, can be estimated taken as the intercept (at $C_s = 0$) of plots $\ln\frac{C_s}{P}$ vs C_s. At this limit: $K' = \ln\frac{N}{P}$ and $K'' = \ln\frac{C_s}{C_g}$. Plots of $\ln \frac{N}{P}$ vs N were used for estimation of K'. Figs. 79, 80 and 81 illustrate such curves

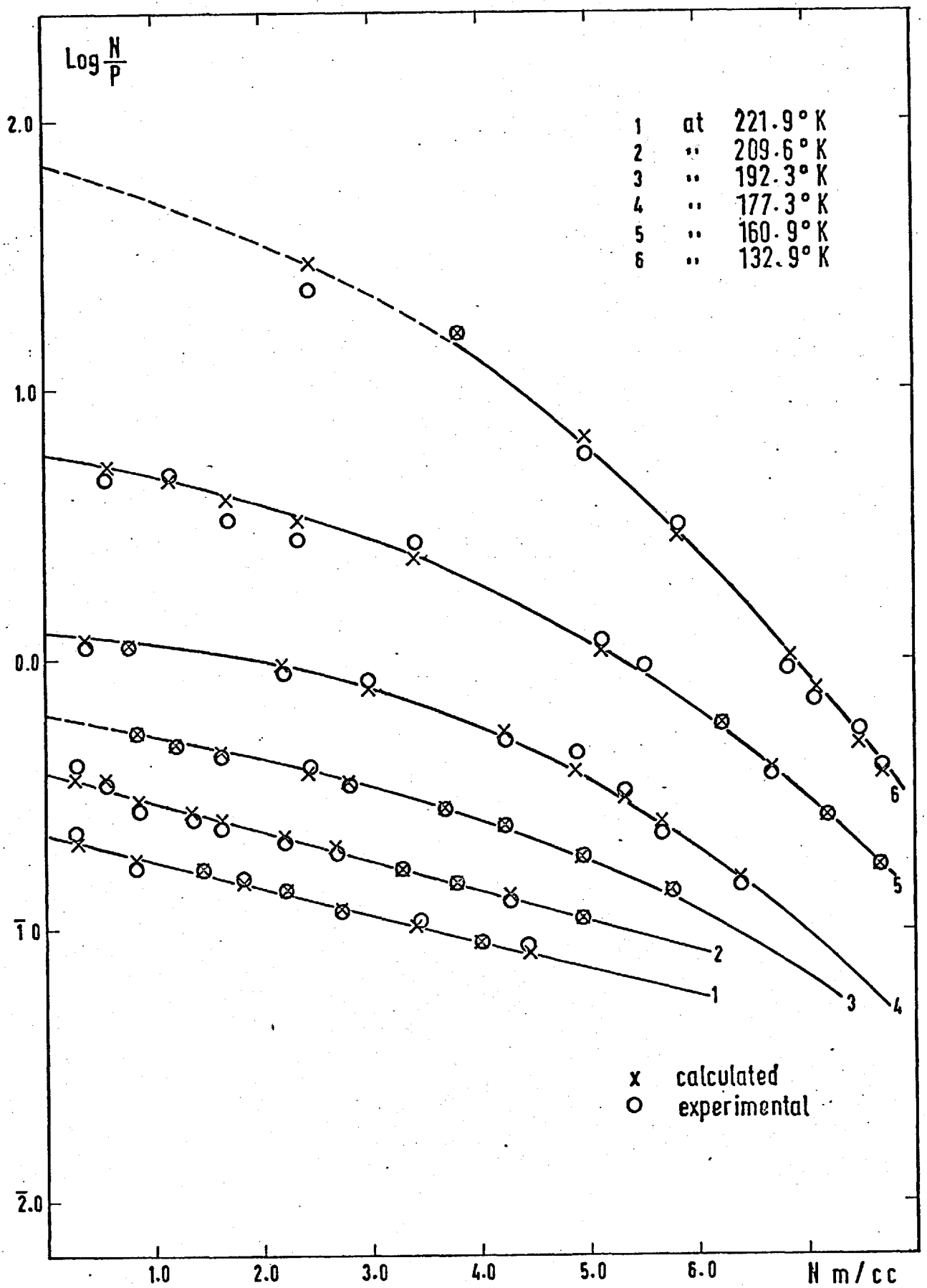
Log N/P
2.0
1.0
0.0
1̄.0
2̄.0
1 at 221.9° K
2 " 209.6° K
3 " 192.3° K
4 " 177.3° K
5 " 160.9° K
6 " 132.9° K
x calculated
O experimental
1.0
2.0
3.0
4.0
5.0
6.0
N m/cc

KL

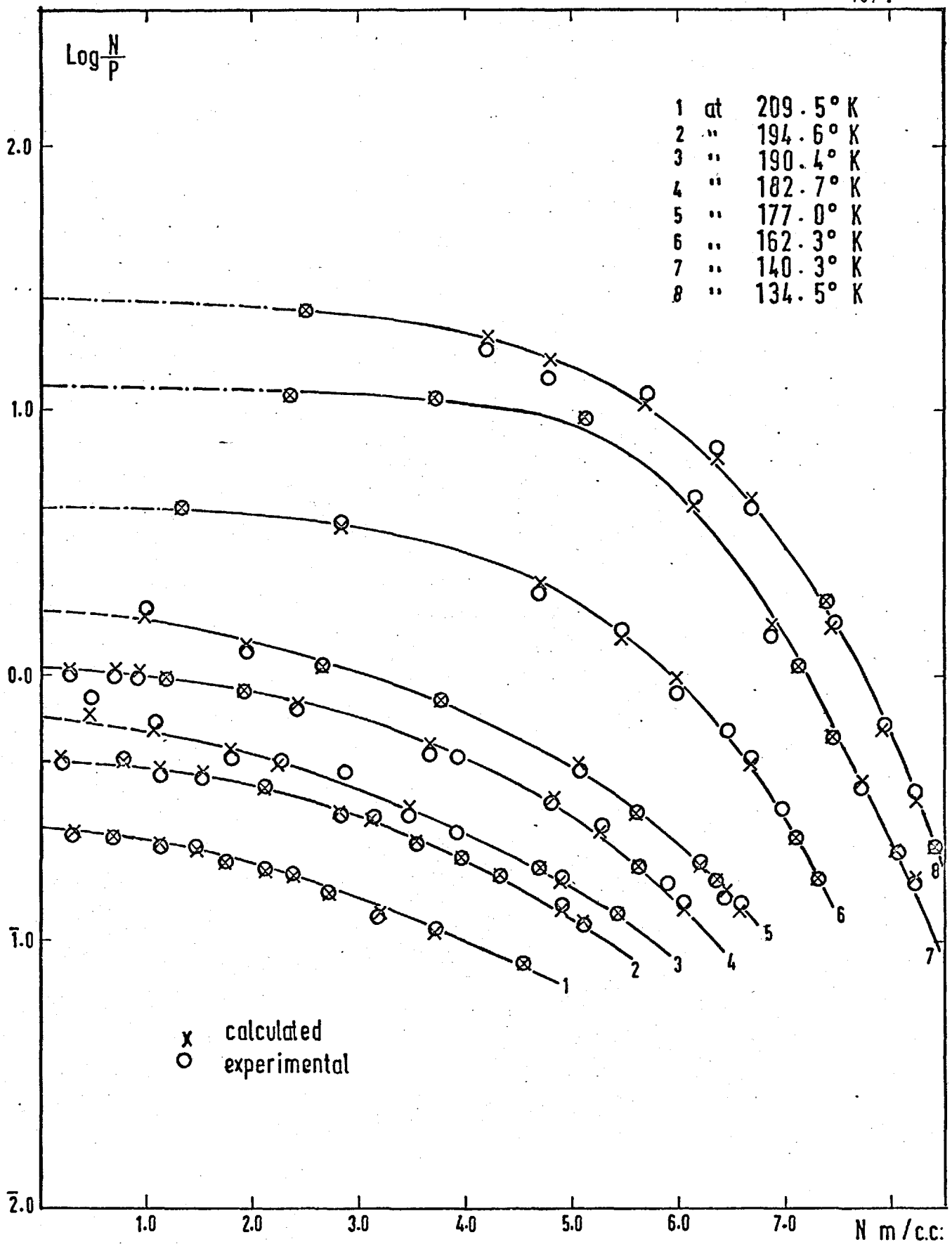

Fi 80 Kr on BaL

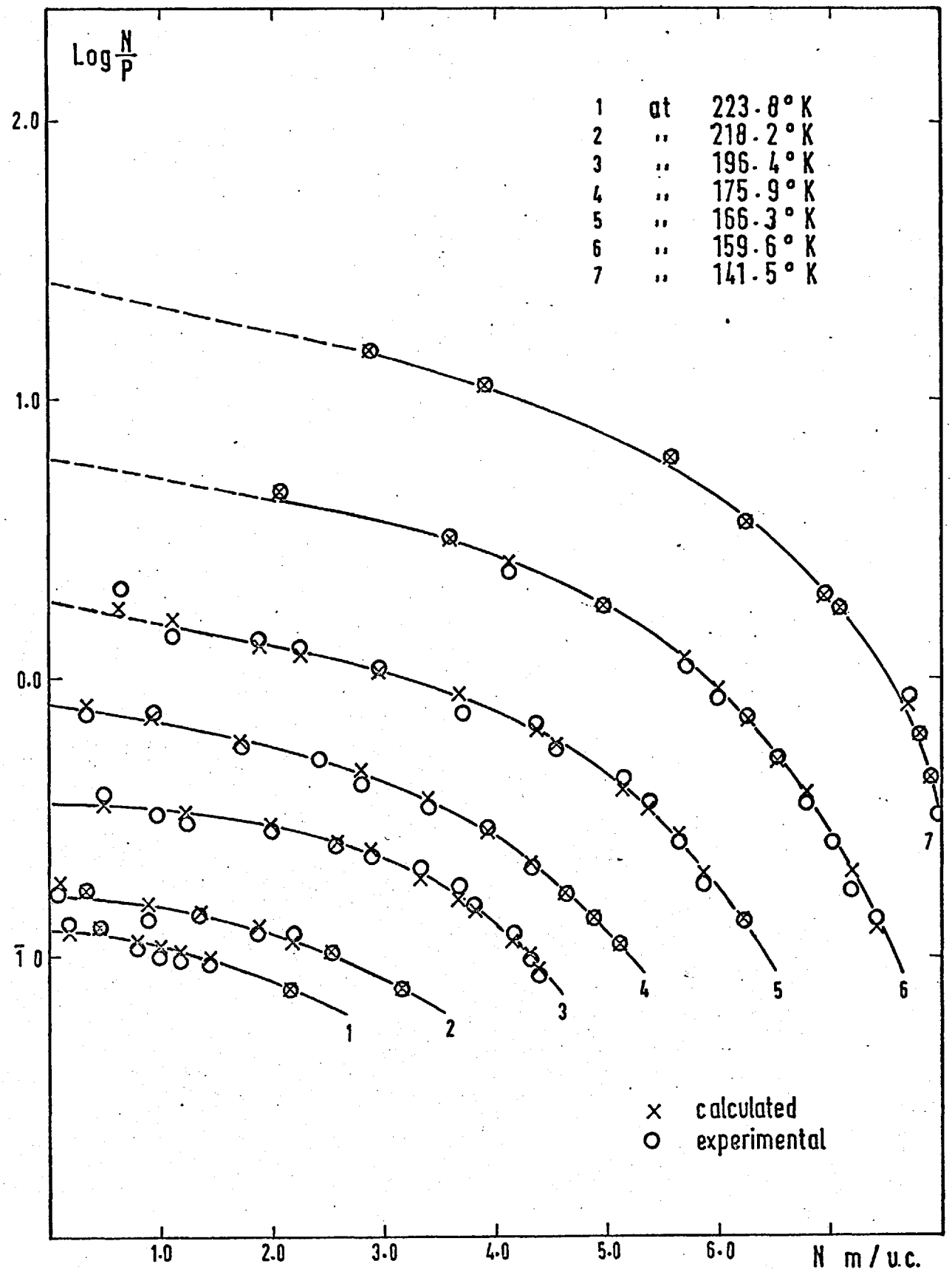

Fig. 81 Kr on LaL

for Kr in NaL, BaL and LaL. The best smoothed curve based on the experimental values of $\ell g \frac{N}{p}$ vs N was obtained by computer, using a best fit polynomial program(136).

The values of K" were derived from those of K'. However, plots $\ell g \frac{N}{p}$ vs N for rectangular isotherms require long extrapolation (see Figs. 79, 80 and 81). For such cases K' or K" should not be considered as the equilibrium constants, but as coefficients defined by the virial isotherm equation (p.195) applicable only over the experimental range of concentrations.

From the equilibrium constant K", the standard energy of sorption, ΔE^{o}, can be obtained from Van't Hoff's isochore

$$\frac{d \ell n\, K''}{dT} = - \frac{\Delta E^{o}}{RT^{2}}$$

For all the sorbents, plots of ℓg K" vs $\frac{1}{T}$ are given on Figs. 82, 83 and 84. The values of ΔE^{o} were estimated from the slopes of the straight lines obtained. For each experimental temperature a corrected value of the equilibrium constant, K"*, was read from the graph. In Tables 36 and 37 values of the equilibrium constant, K"* and the standard energy of sorption, ΔE^{o} are given for LiL, NaL, CsL and for HL, H-ER and H-OFF respectively. In Table 40 corresponding values for KL, BaL and LaL could be found. For an improved comparison between all investigated sorbents, an equilibrium constant, K''_{a}*, at an arbitrary temperature of 166.6°K was read from each graph. The values are given in Table 38.

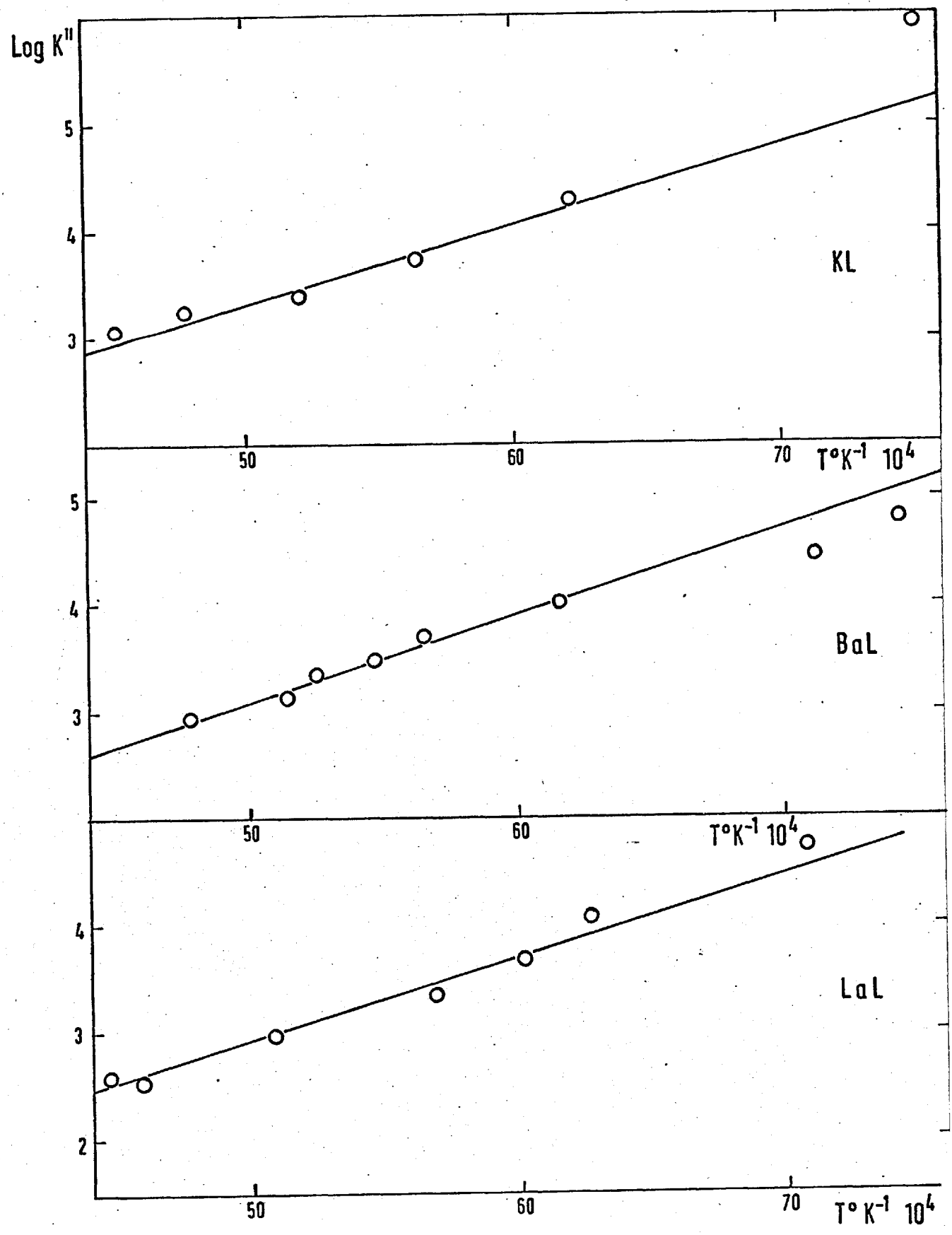

Fig. 82 Kr on KL BaL & LaL

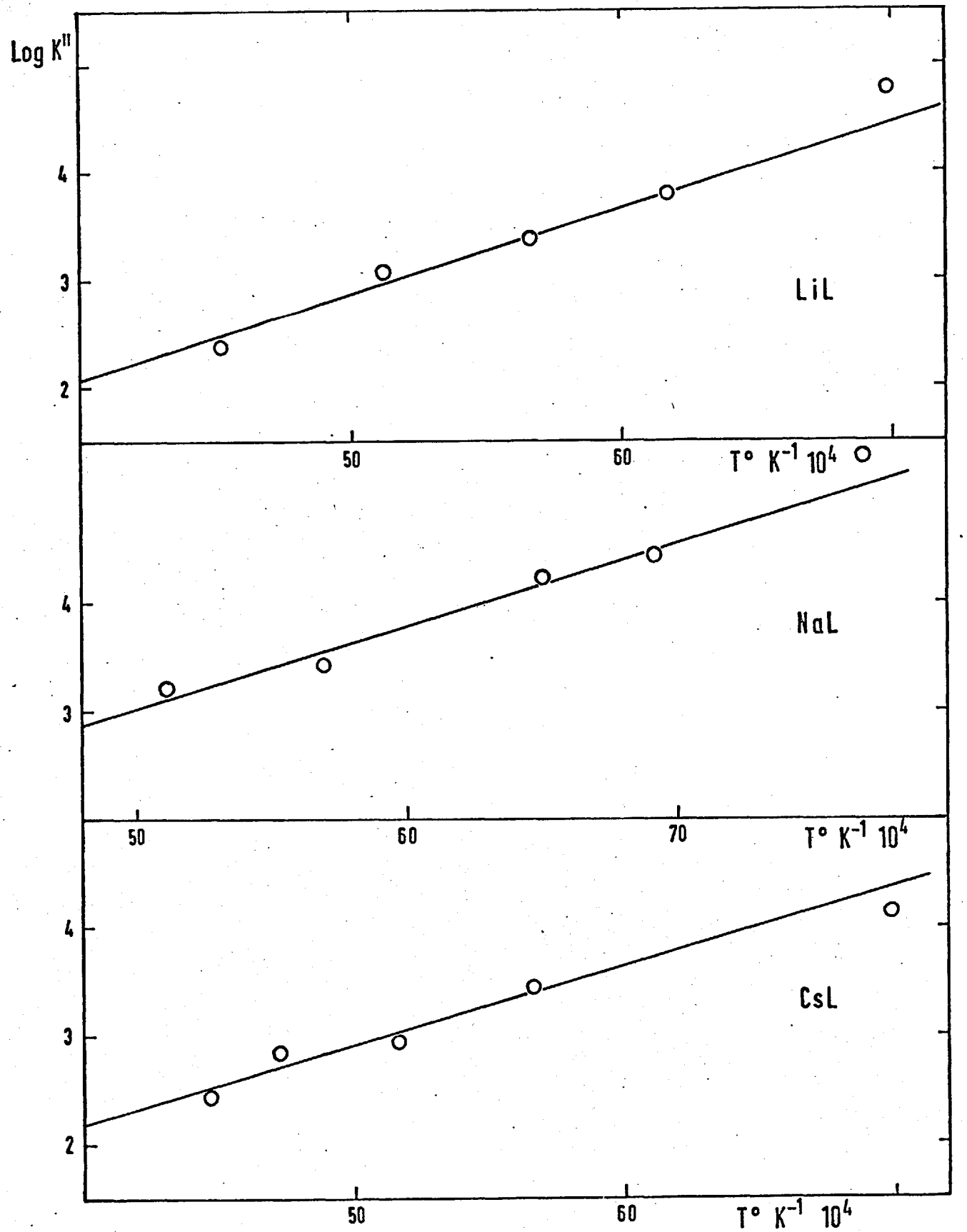

Fi-. 83 Kr on LiL, NaL & CsL

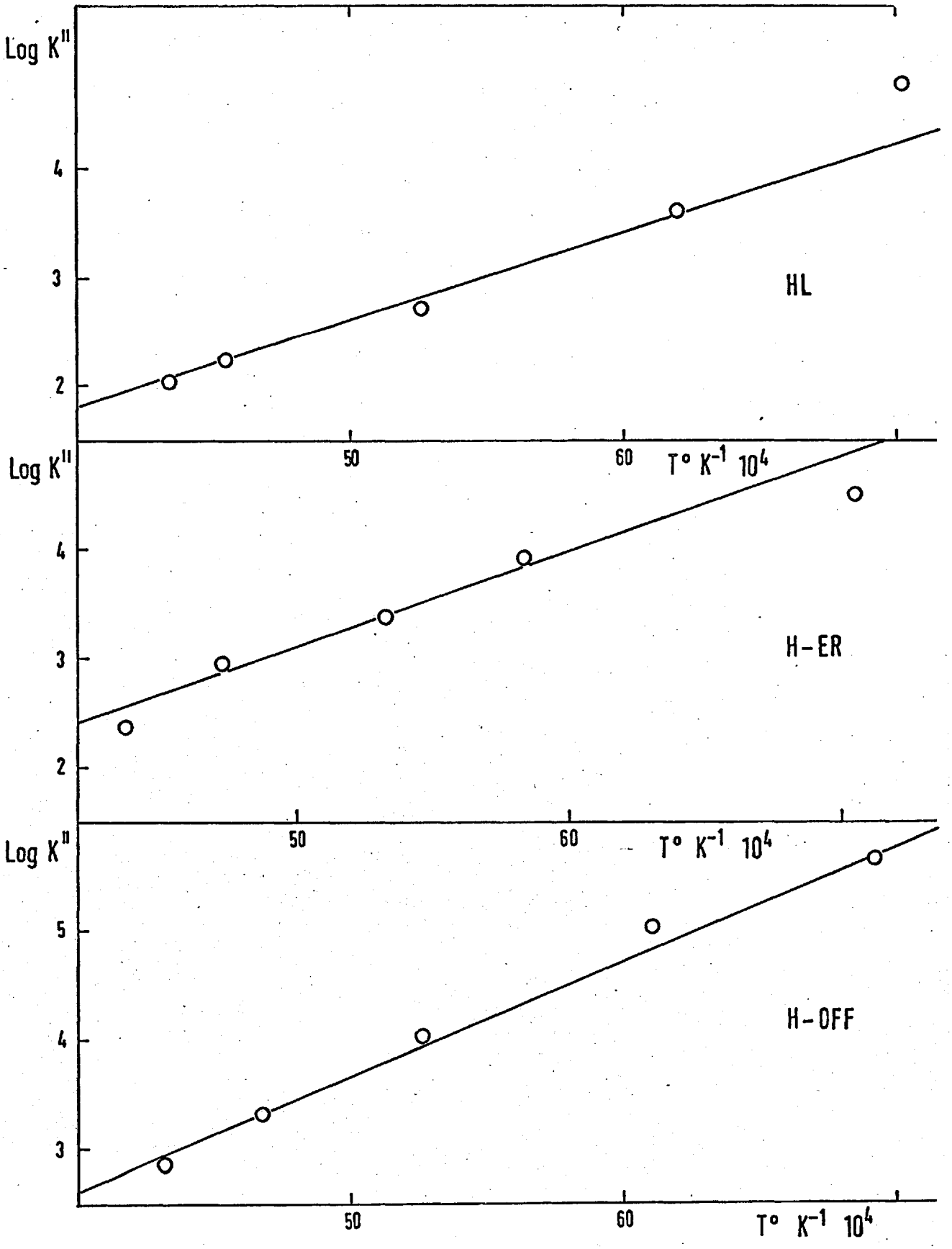

Fig. 84 Kr on HL, H-ER & H-OFF

TABLE 36.

Equilibrium constants (K"*) and standard energy (ΔE^{o}) for adsorption of Kr in ion-exchanged forms of L.

LiL $\Delta E^{o} = -3.6$ kcal/mole^{-1}.

$T^{o}K$	143.5	162.1	176.6	195.3	221.0
$lgK"$	4.784	3.779	3.375	3.041	2.392
K"*	$2.64.10^{4}$	$6.08.10^{3}$	$2.40.10^{3}$	$9.14.10^{2}$	$3.09.10^{2}$

NaL $\Delta E^{o} = -3.5$ kcal/mole^{-1}.

$T^{o}K$	130.0	144.8	153.6	175.2	195.3
$lgK"$	5.370	4.431	4.271	3.443	3.231
K"*	$1.16.10^{5}$	$3.13.10^{4}$	$1.45.10^{4}$	$3.55.10^{3}$	$1.27.10^{3}$

CsL $\Delta E^{o} = -3.5$ kcal/mole^{-1}

$T^{o}K$	143.2	176.7	193.4	211.7	223.8
$lgK"$	4.123	3.474	2.962	2.833	2.425
K"*	$2.32.10^{4}$	$2.46.10^{3}$	$1.04.10^{3}$	$5.07.10^{2}$	$3.22.10^{2}$

TABLE 37.

Equilibrium constant (K"*) and standard energy of adsorption (ΔE^{o}) for Kr in decationated L, ER and OFF.

HL ΔE^{o} = -3.60 kcal/mole^{-1}

$T^{o}K$	142.5	161.7	189.9	210.1	230.6
ℓg K"	4.785	3.607	2.732	2.225	2.019
K"*	$1.78.10^{4}$	$4.05.10^{3}$	$6.92.10^{2}$	$1.68.10^{2}$	$1.21.10^{2}$

H-ER ΔE^{o} = -4.00 kcal/mole^{-1}

$T^{o}K$	141.9	171.3	187.4	211.5	229.3
ℓg K"	4.513	3.929	3.390	2.972	2.397
K"*	$4.68.10^{4}$	$7.02.10^{3}$	$2.45.10^{2}$	$7.24.10^{2}$	$1.80.10^{2}$

H-OFF ΔE^{o} = -4.60 kcal/mole^{-1}

$T^{o}K$	144.4	163.8	190.7	213.8	231.8
ℓg K"	5.676	5.011	4.030	3.342	2.856
K"*	$4.74.10^{5}$	$6.61.10^{4}$	$8.61.10^{3}$	$2.19.10^{3}$	$8.81.10^{2}$

TABLE 38.

Equilibrium constants, $K_a''^*$, for adsorption of Kr at arbitrary temperature T_a = 166.6°K.

Sample	HL	LiL	NaL	KL	CsL
$K_a''^*$	$2.64.10^3$	$4.62.10^3$	$6.11.10^3$	$1.15.10^4$	$4.28.10^3$

Sample	BaL	LaL	H-ER	H-OFF
$K_a''^*$	$7.90.10^3$	$4.79.10^3$	$9.44.10^3$	$5.15.10^4$

The order of decreasing magnitudes of the arbitrary equilibrium constants $K_a''^*$ is:

H-OFF > KL > H-ER > BaL > NaL > LaL > LiL > CsL > HL

Plots of $\ell g\ K''$ vs $\frac{1}{T}$ enable equilibrium constants at any temperature, in the experimental range to be read, while an extrapolation of these plots gives an estimate of the equilibrium constants outside this region.

The standard energies of sorption, ΔE°, are very close (from 3.4 $\frac{kcal}{mole}$ to 3.6 $\frac{kcal}{mole}$) for all forms of zeolite L. On the other hand the values for HL, H-ER and H-OFF are found to differ (3.6 $\frac{kcal}{mole}$ for HL vs 4.6 $\frac{kcal}{mole}$ for H-OFF). Analogous arguments to those made to explain the parallel effect on the initial isosteric heats leads to the conclusion that framework/sorbate interaction is the determining factor here too. (p.190).

4.2.5 Coefficients A' and the properties of the standard state for adsorption of Kr on NaL, BaL and KL.

Any isotherm can be expressed by an equation similar to 4.2-4 (this Chapter). By solving a system of simultaneous equations of the form of equation 4.2-4, for a number of different points along the curve of $\ell n \frac{N}{p}$ vs N, the coefficients A'_1, A'_2, A'_3, etc. can be obtained. A computer program(136) was used to evaluate these coefficients for krypton isotherms on KL, BaL and LaL (Table 39).

The degree of each polynomial, required to describe the corresponding isotherm, are also tabulated. By means of the coefficients found, each isotherm of Kr on KL, BaL and LaL was computed. The points obtained by computation are plotted on Figs. 79, 80 and 81. (Allowance is made for plotting in coordinates $\ell g \frac{N}{p}$ vs N). Using the values of ΔE° and K"*, the standard free energy, ΔA° and entropy of sorption ΔS° at standard state were calculated from

$$\Delta A^\circ = -RT \ell n K"* \qquad \ldots (4.2\text{-}6)$$

$$\Delta S^\circ = -\frac{\Delta A^\circ}{T} + \frac{\Delta E^\circ}{T} \qquad \ldots (4.2\text{-}7)$$

Values ΔA° and ΔS° for each temperature on a given sorbent are presented in Table 40. From differentiation of equation (4.2-7) with respect to the temperature we see that the standard entropy of sorption is independent of temperature $\left(\frac{\partial}{\partial T}\left(\frac{\partial \Delta A^\circ}{\partial T}\right) = 0\right)$. Table 40 illustrates the agreement, with the above, of the present data. The values of $-\Delta S^\circ$ for BaL and LaL are of the same order and a factor of two greater than that found for KL. This indicates that an

TABLE 39.

Virial coefficients from empirical isotherm equation for adsorption of Kr on KL, BaL and LaL.

$T^{o}K$	A'_1	A'_2	A'_3	A'_4	D*	
160.9	0.47	-0.23	0.05	0.01	4	KL
177.3	0.05	-0.01	0.01	-	3	
221.7	0.13	-0.01	-	-	2	
192.7	0.03	-0.02	-0.01	-	3	
209.6	0.35	-0.12	0.02	-	3	
134.5	1.45	-0.51	0.06	0.01	4	BaL
162.3	-0.82	0.49	0.10	-0.01	4	
177.0	0.62	-0.30	0.06	-0.03	4	
182.7	-0.16	0.18	-0.05	0.01	4	
190.4	0.39	-1.17	0.04	-0.01	4	
194.6	0.06	-0.01	-0.01	-	3	
209.3	-1.23	-0.96	0.17	-	3	
159.6	0.41	-0.08	0.01	0.01	4	LaL
175.9	0.64	-0.35	0.09	-0.005	4	
196.4	-0.07	0.07	-	-	2	
218.2	0.13	-0.11	0.03	-	3	
223.8	1.16	-1.03	0.29	-	3	
166.3	-0.34	0.12	-0.01	-	3	

* degree of the polynomial.

TABLE 40.

Computation of the thermodynamical functions on the basis of the virial isotherms.

Adsorption of Kr on KL.

$T^{o}K$	K'* mole $u.c.^{-1}\ cm^{-1}$	K"*	$-\Delta E^{o}$ cal $mole^{-1}$	$-\Delta A^{o}$ cal $mole^{-1}$	$-\Delta S^{o}$ e.u.	P^{o} cm	N^{o} molecules per u.c.	Cs^{o} mole litr
132.9	57.54	$1.48.10^{5}$	3390	3130	1.99	0.017	0.85	0.98
160.9	4.80	$1.59.10^{4}$	"	3080	1.97	0.21	0.85	0.97
177.3	1.73	$6.31.10^{3}$	"	3070	1.99	0.58	0.83	1.00
221.7	0.19	$8.71.10^{2}$	"	2970	1.92	5.21	0.85	0.95
192.3	0.72	$2.82.10^{3}$	"	3020	1.93	1.40	0.83	0.99
209.6	0.33	$1.32.10^{3}$	"	2980	1.98	3.07	0.86	0.96

Adsorption of Kr on BaL

134.5	56.10	$1.12.10^{5}$	3640	2950	4.11	0.018	0.90	1.00
140.3	30.34	$6.31.10^{4}$	"	2830	4.11	0.033	0.95	1.00
162.3	4.33	$1.05.10^{4}$	"	2770	4.15	0.231	0.98	0.95
177.0	1.54	$4.07.10^{3}$	"	2980	4.15	0.646	0.97	0.97
182.7	1.10	$2.95.10^{3}$	"	2850	4.15	0.902	0.98	1.00
190.4	0.75	$2.14.10^{3}$	"	2980	4.11	1.325	0.90	1.00
194.6	0.54	$1.59.10^{3}$	"	2800	4.16	1.825	0.90	0.95
209.3	0.26	$8.32.10^{2}$	"	2770	4.12	3.745	0.95	0.97

Adsorption of Kr on LaL

141.5	16.41	$5.01.10^{4}$	3530	2910	4.36	0.06	1.00	0.98
159.6	3.73	$8.91.10^{3}$	"	2830	4.36	0.27	1.00	0.95
175.9	1.10	$2.57.10^{3}$	"	2760	4.35	0.91	0.91	1.00
196.4	0.34	$7.08.10^{2}$	"	2670	4.36	2.94	0.90	0.99
218.2	0.12	$2.24.10^{2}$	"	2570	4.38	8.33	1.0	1.00
223.8	0.08	$1.78.10^{2}$	"	2550	4.38	12.5	0.95	0.93
166.3	2.06	$5.13.10^{3}$	"	2800	4.37	0.48	0.92	0.97

equilibrium transfer at standard state of a mole of sorbate from the gas phase into the sorbed phase is accompanied by a greater decrease of the disorder of the krypton molecules on BaL and LaL compared with KL. An explanation might lie in the difference in the polarisation energy of K^+, Ba^{2+} and La^{3+} and in the distribution of the cation electrostatic charge per unit cell for each case.

A useful characteristic of a given sorbate/sorbent system is the concentration of the sorbed phase in the standard state at a given temperature. As at standard state the activity of the sorbed phase is unity, the state associated with K'* will be defined by $\underline{a}_{s\text{-}u.c.} \frac{m}{} = 1$ (concentration $N^o \frac{m}{u.c.}$) and the state associated with K"* will be $\underline{a}'_{s\text{-}} \frac{m'}{\ell} = 1$ (concentration $C_s^o \frac{m'}{\ell}$). $\underline{N}^o$ can be obtained from plots $\underline{a}_{s\text{-}}$ vs N as the values of $\underline{N}$ corresponding to $\underline{a}_s = 1$. The values of $\underline{a}_s$ were calculated at a given uptake $\underline{N}$ from $\underline{a}_{s\text{-}} = K'^*.P$ (see p.61). Examples of curves a_s vs N are given in Figs. 85, 86 and 87 and the values of N^o obtained are tabulated in Table 40. The concentration C_s^o are also given (For calculation of C_s^o see p.280 in the Appendix). The accuracy of the estimated values of N^o is unsatisfactory as the curves $\underline{a}_{s\text{-}}$ vs N are exponential and the value of N^o lies in the most inaccurate part of the curves. N^o can be obtained indirectly from that equilibrium pressure, P^o, which corresponds to $a_s = 1$:

$$P^o = \frac{a_s}{K'} = \frac{1}{K'} \qquad \ldots (4.2\text{-}8)$$

From each plotted isotherm the value of N^o corresponding to P^o can be read with certainty provided the isotherms are not too rectangular. Mean values of N^o and C_s^o have been estimated in this way where possible.

The activity coefficients, γ, of the sorbed phase can

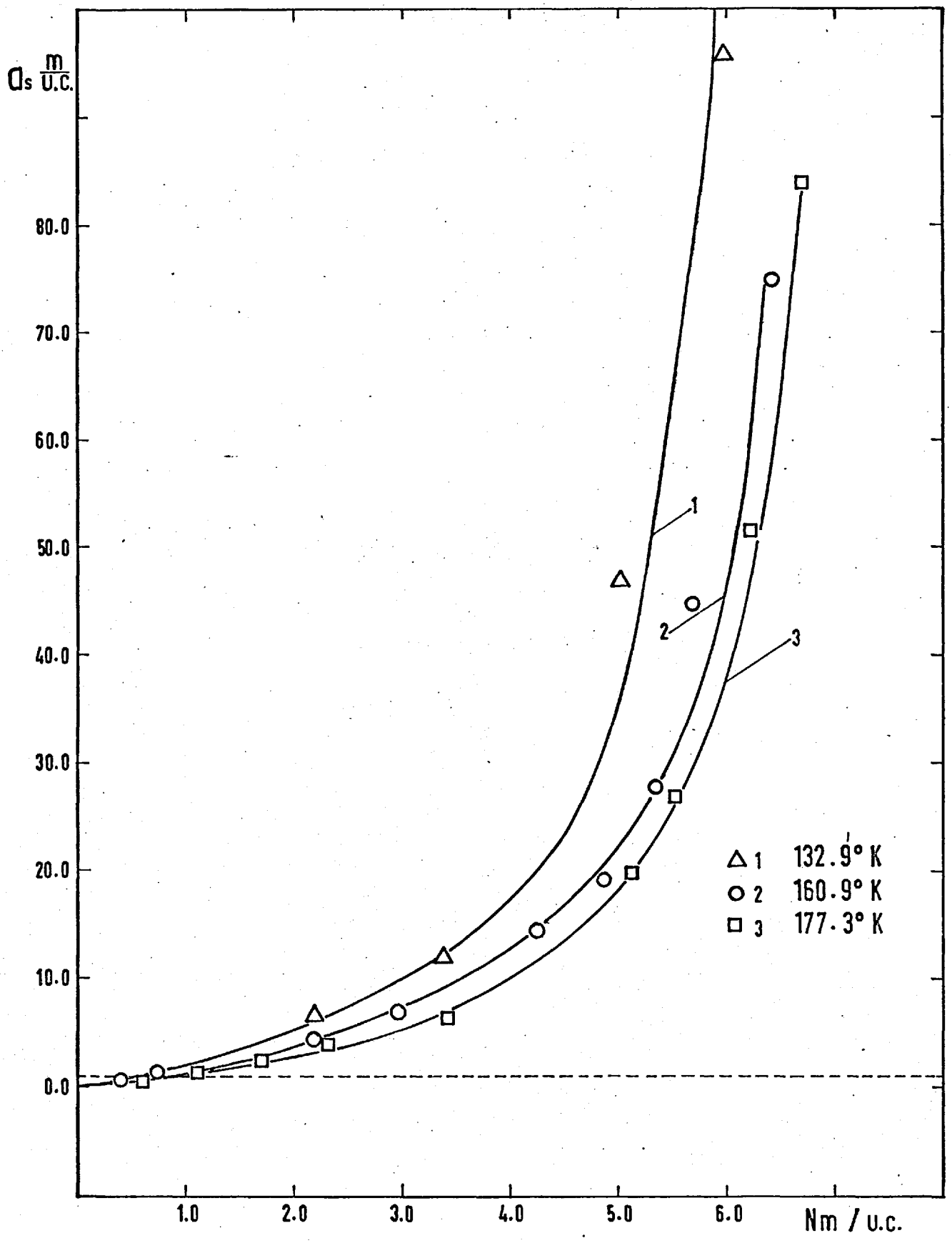

Fig. 85 Kr on KL

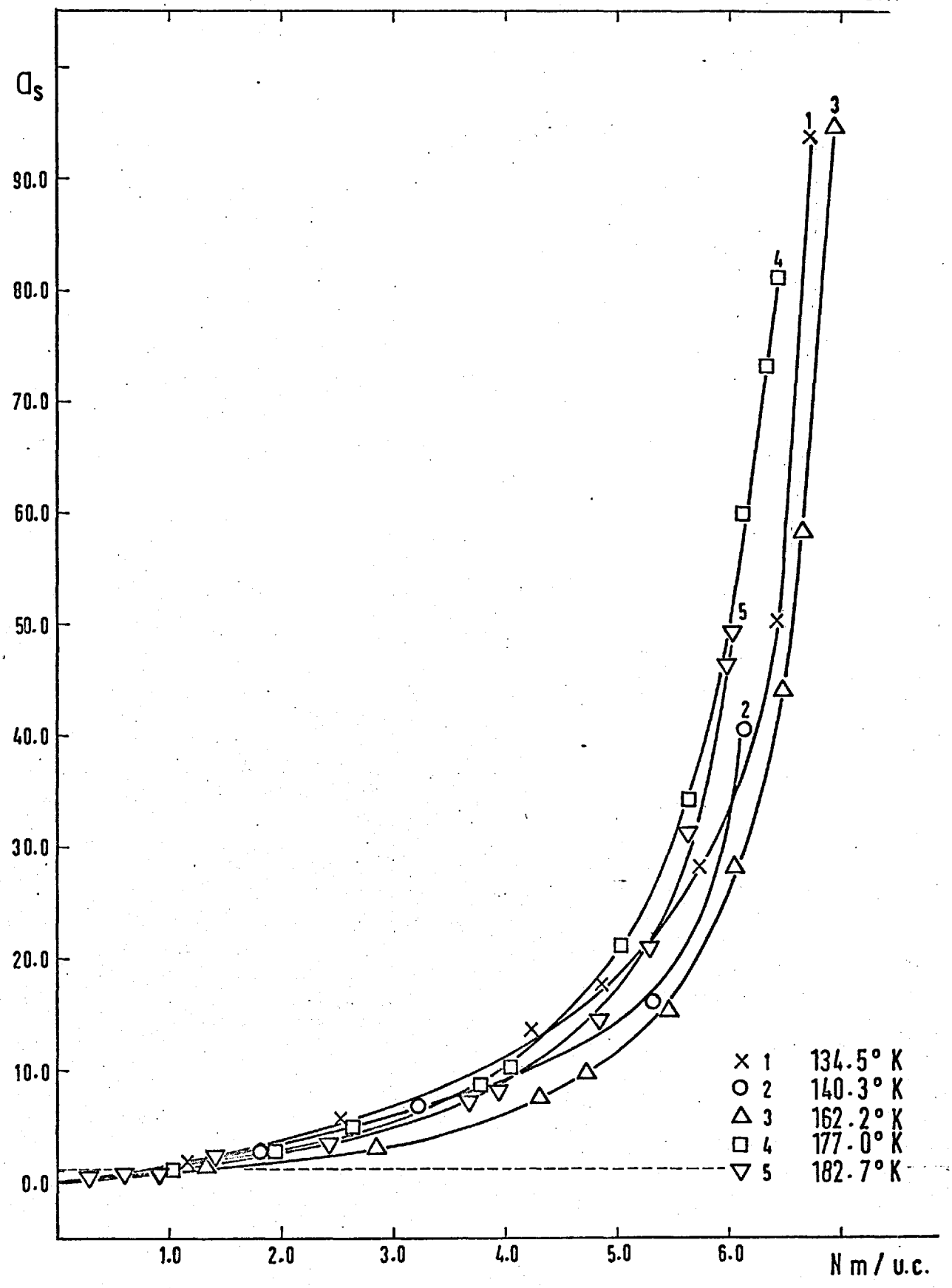

Fig. 86 Kr on BaL

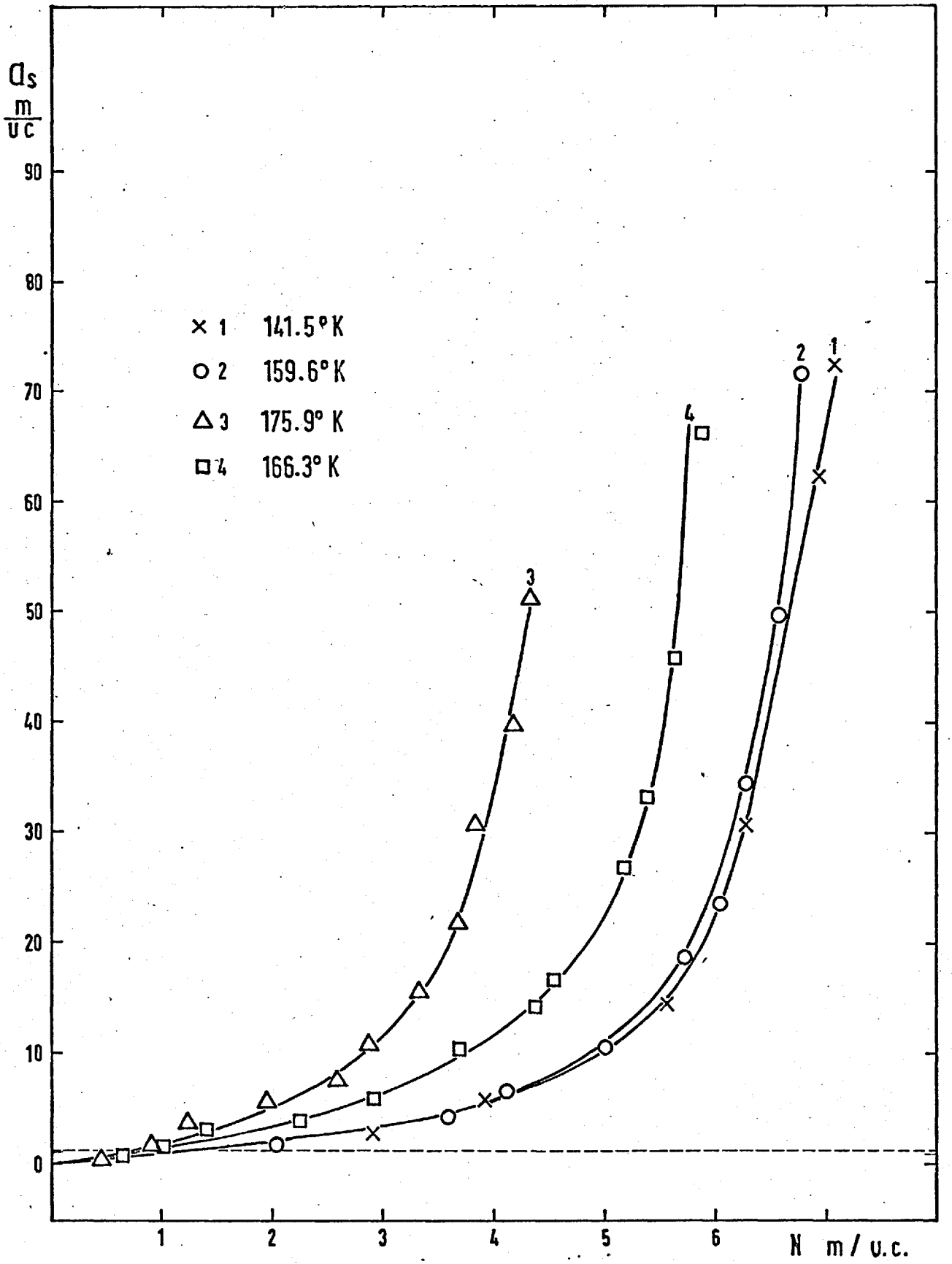

Fig. 87 Kr on LaL

obtained from $\gamma = \frac{K' P}{N}$ (p. 62). In Figs. 88, 89 and 90 the activity coefficient of Kr on KL, BaL and LaL are presented, as functions of the concentration, serving to further characterise the sorbed phase. For different temperatures at a given concentration, the values are the resultant of the opposing influences of the equilibrium constant, K', and the equilibrium pressure, P, because when

$$T_1 > T_2$$

one has

$$P_1 > P_2$$
$$K_1' < K_2'$$

4.2.6 Half standard entropies and entropies of the sorbed phase for Kr on HL, H-ER and H-OFF.

Differential entropies of sorption, $\Delta \bar{S}_1$, were calculated directly from the isosteric heats, $\Delta \bar{H}_1$, according to eq. 3.1-3 in Chapter I.

$$\Delta \bar{S}_1 = \frac{\Delta \bar{H}_1}{T}$$

The values were used to calculate the differential molar entropies of the sorbed phase, $\bar{S}_1$ (p. 53)

$$\bar{S}_1 = S_g^{\omega\, o} + R \ln \frac{P^o}{P} + \int_{T_o}^{T} Cp \frac{dT}{T} + \frac{\Delta \bar{H}_1}{T} \qquad \ldots\ (4.2\text{-}9)$$

where $S_g^{\omega\, o}$ = 39.2 e.u. for krypton at 298°K(125). The calculated differential molar entropies for the sorbed krypton on HL, H-ER and H-OFF at selected temperature are given in Table 41 and plotted as a function of the amount adsorbed, $N \frac{m}{u.c.}$, in Figs. 91, 92 and 93. In Fig. 94

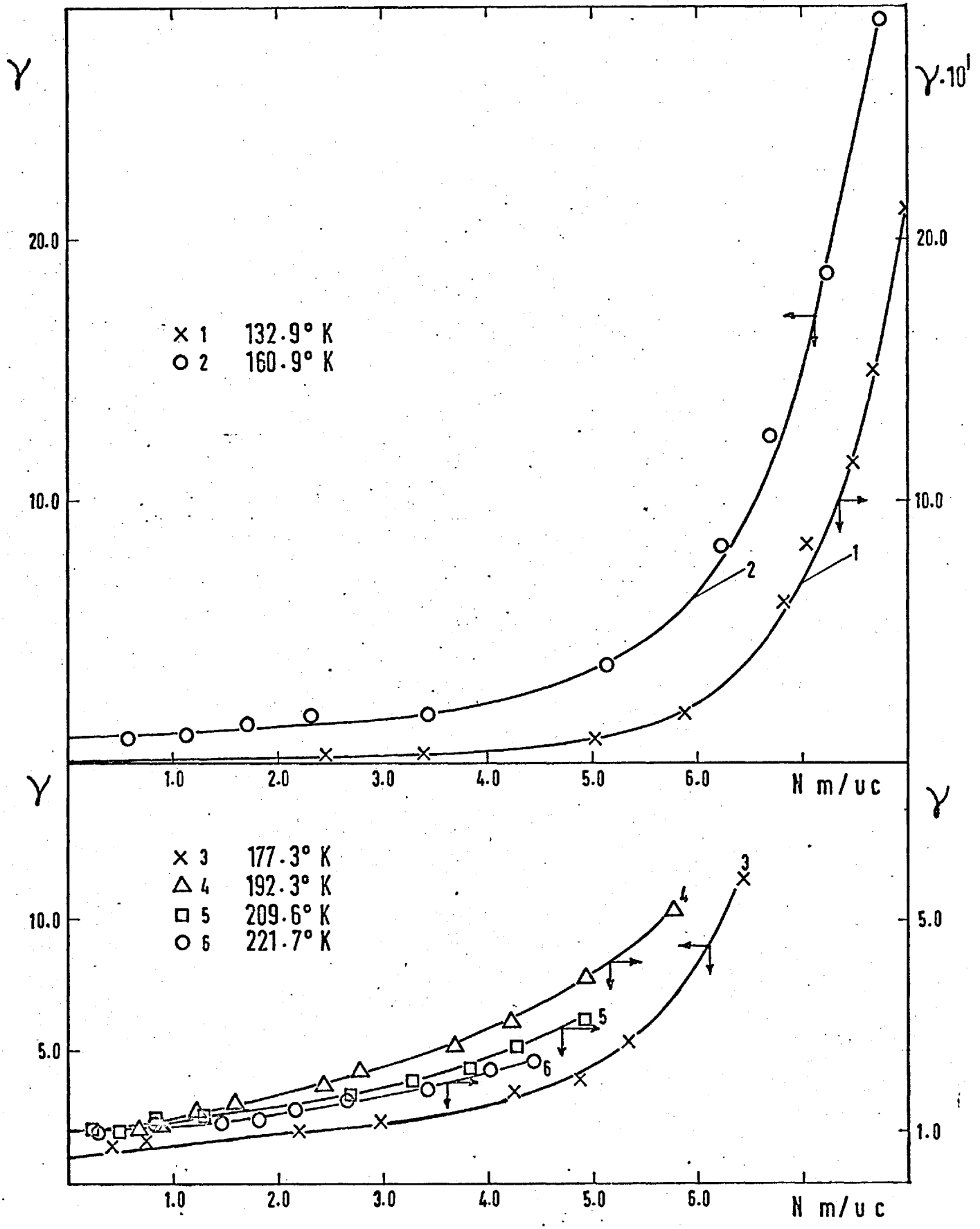

Fig. 88 Kr on KL

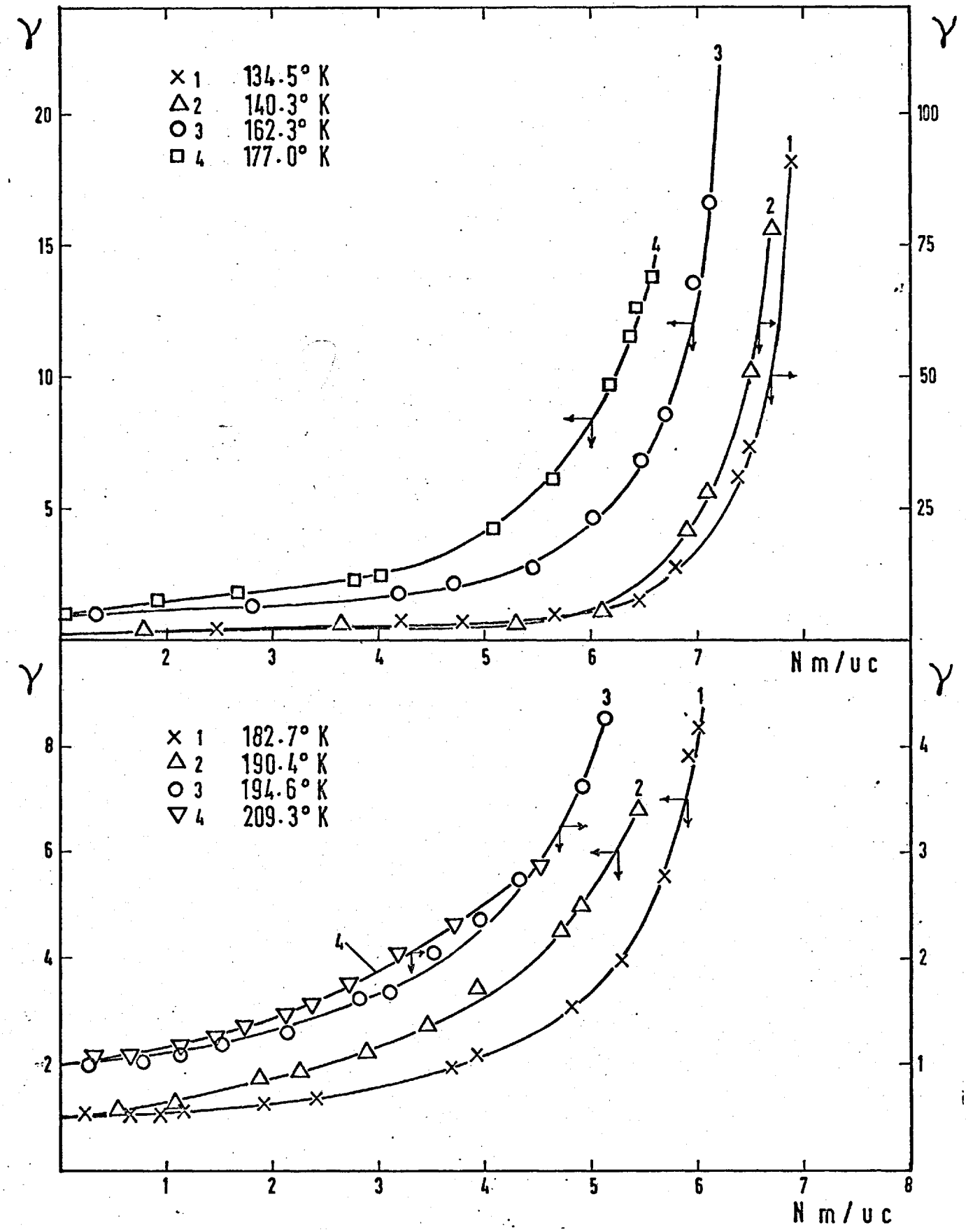

Fig. 89 Kr on BaL

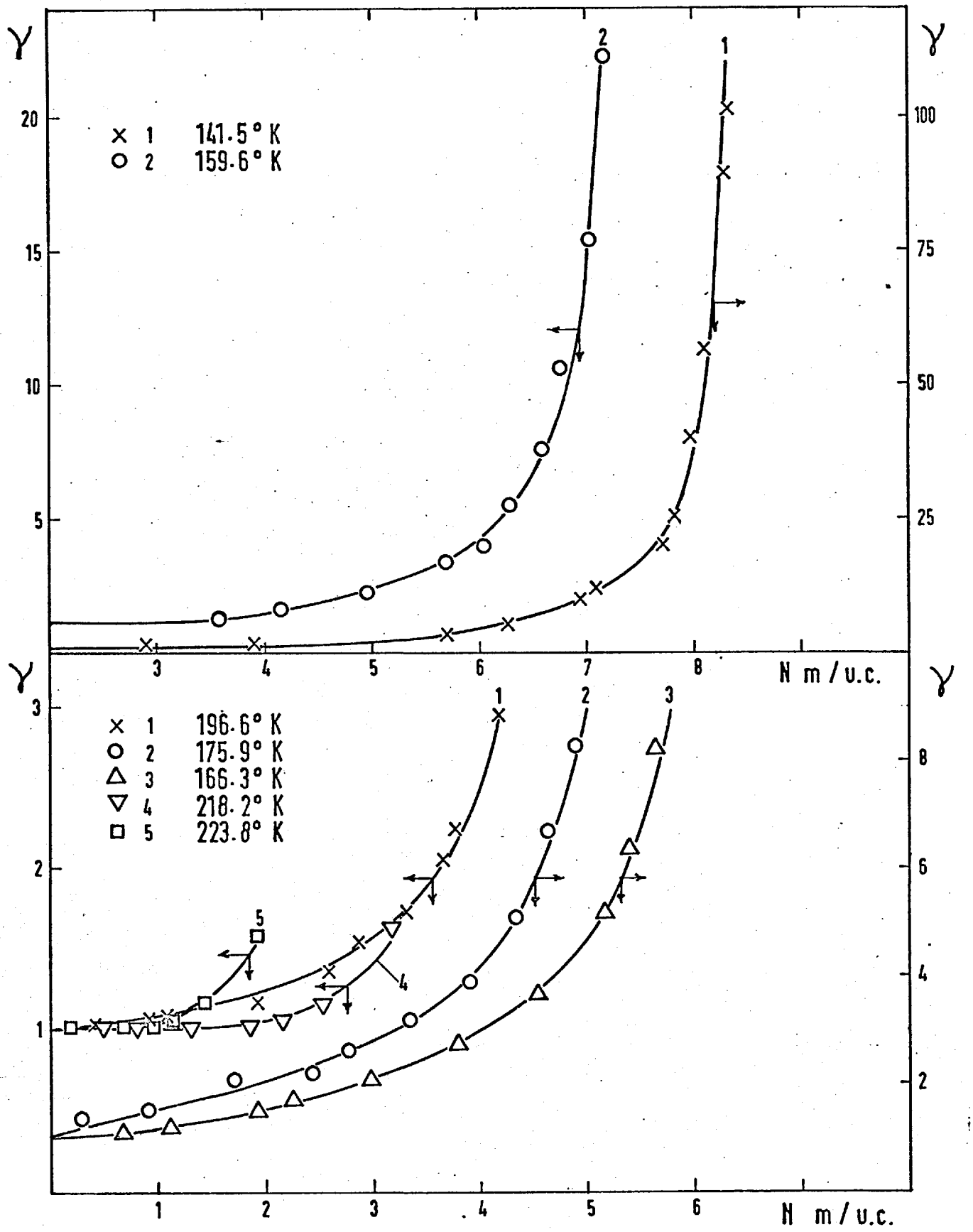

Fig. 90 Kr on LaL

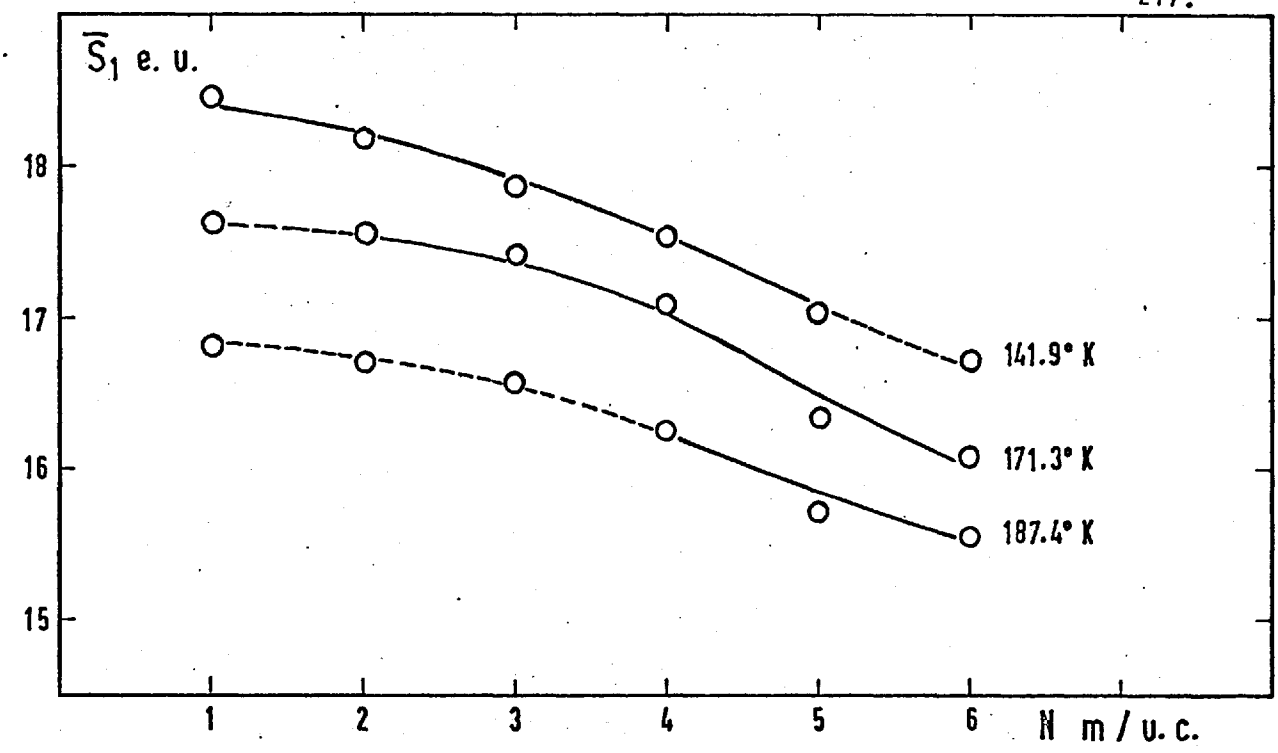

Fig. 91 Kr on H-ER

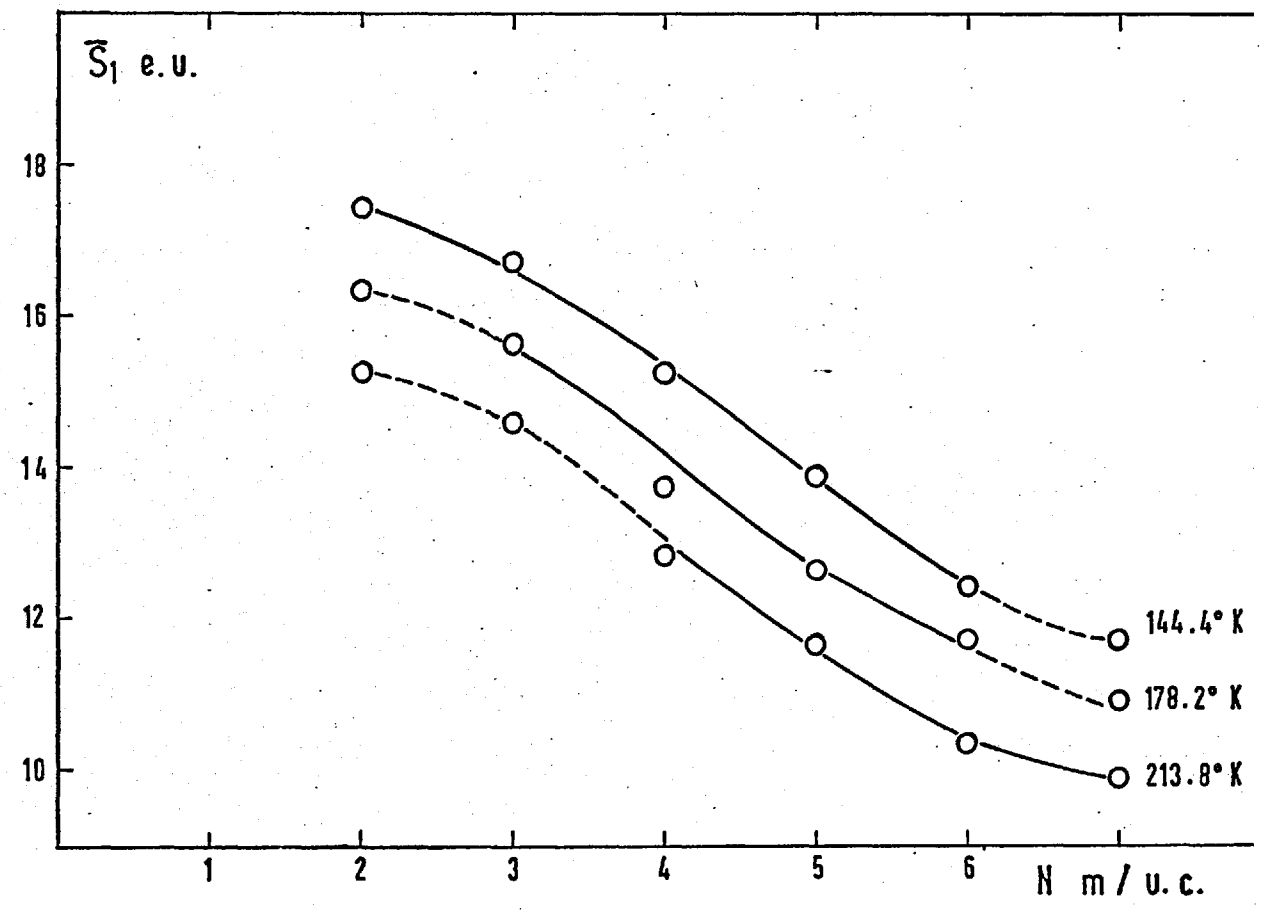

Fig. 92 Kr on H-OFF

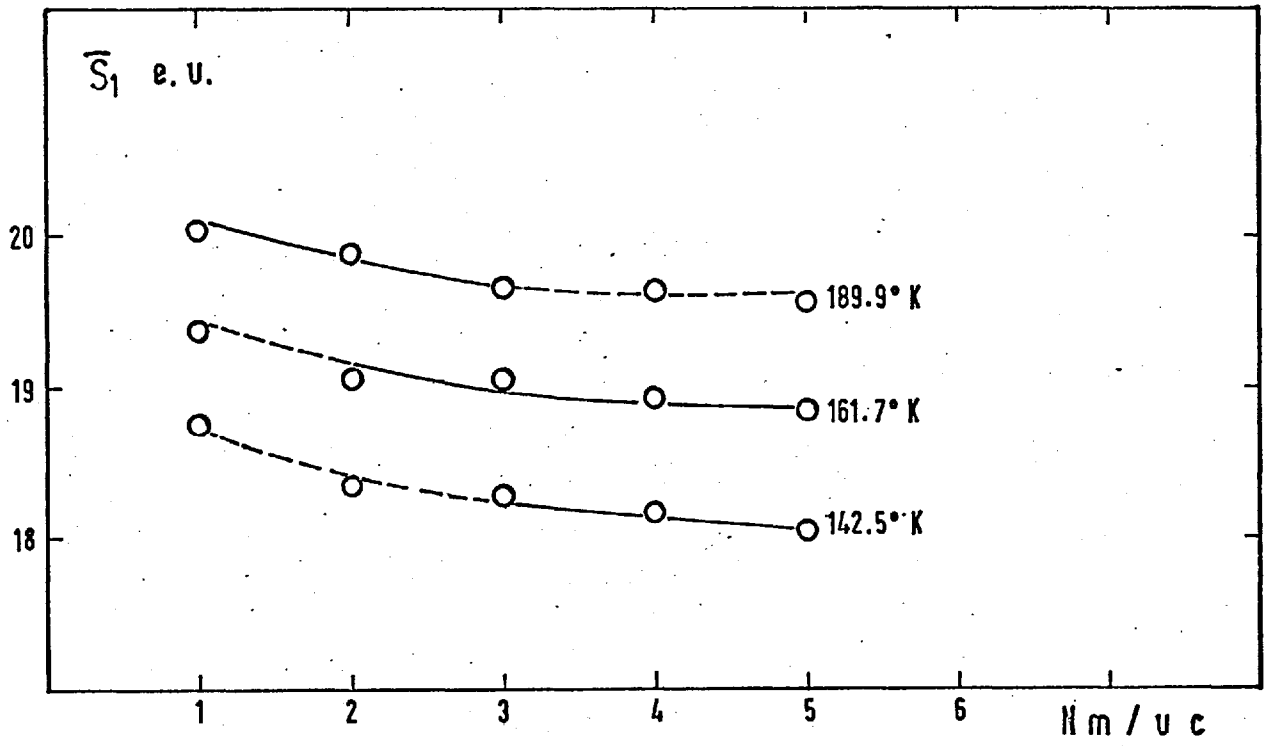

Fig. 93 Kr on HL

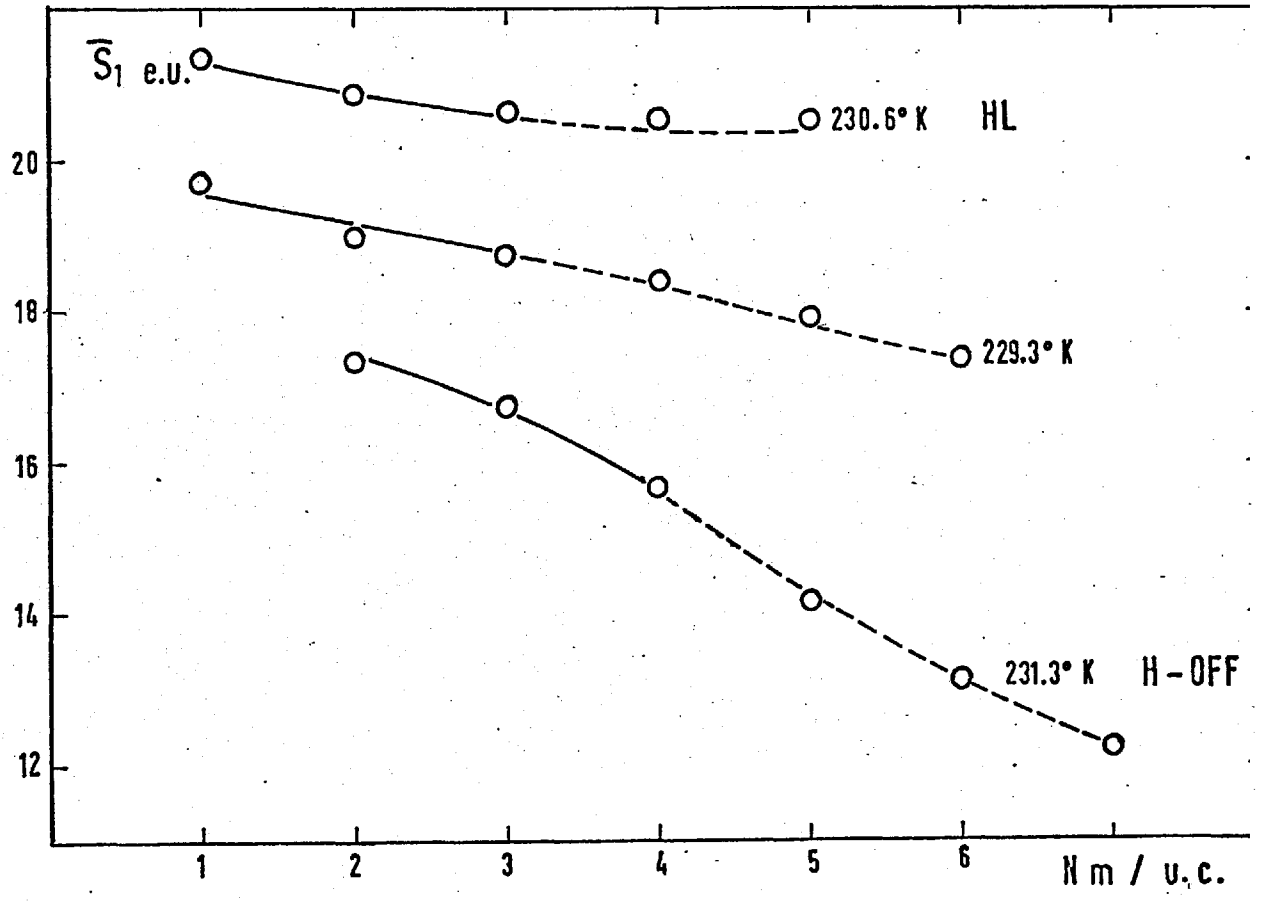

Fig. 94 Kr on HL, H-ER and H-OFF

TABLE 41.

Half standard entropies ($-\Delta\bar{S}_h$) and entropies of the sorbed phase ($\bar{S}_1$) for Kr on HL, H-ER and H-OFF.

N m/u.c.	$-\Delta\bar{S}_h$	$\bar{S}_1$	$-\Delta\bar{S}_h$	$\bar{S}_1$	$-\Delta\bar{S}_h$	$\bar{S}_1$	
	T^o = 142.5°K		T = 161°K		T = 189.9°K		
1	16.78	18.75	16.78	19.38	16.92	20.03	HL
2	17.19	18.34	17.09	19.07	17.08	19.87	
3	17.25	18.28	17.11	19.05	17.29	19.66	
4	17.37	18.16	17.24	18.92	17.32	19.63	
5	17.76	18.07	17.32	18.84	17.36	19.59	
	T = 141.9°K		T = 171.3°K		T = 187.4°K		
1	18.69	16.82	18.76	17.67	18.46	18.43	H-ER
2	18.74	16.77	18.89	17.54	18.72	18.17	
3	18.93	16.58	19.00	17.43	19.00	17.88	
4	19.24	16.27	19.31	17.12	19.34	17.55	
5	19.81	15.70	20.09	16.34	19.87	17.02	
6	19.93	15.58	20.35	16.08	20.14	16.75	
	T = 144.4°K		T = 178.2°K		T = 213.8°K		
2	20.38	15.23	20.30	16.34	20.13	17.72	H-OFF
3	21.01	14.60	21.13	15.51	20.78	16.77	
4	22.81	12.80	22.92	13.72	22.54	15.01	
5	23.91	11.70	23.99	12.65	23.70	13.85	
6	25.22	10.39	24.90	11.74	25.07	12.48	
7	25.69	9.92	25.66	10.98	25.67	11.78	

plots for different sorbents at similar temperatures are presented. The dotted parts of all entropy curves were calculated from the half standard entropy, $\Delta\bar{S}_h$, defined as:

$$-\Delta\bar{S}_h = {}^{\omega t}\bar{S}_g - \bar{S}_1 \qquad \ldots (4.2\text{-}10)$$

${}^{\omega t}\bar{S}_g$ - molar entropy of the sorbate in the gas phase at the equilibrium temperature of adsorption and pressure p^o = 1 atm.

Values $\Delta\bar{S}_h$ were obtained from the relationship:

$$-\Delta\bar{S}_h = \frac{\Delta\bar{H}_1}{T} + R\,\ell n\,\frac{p^o}{p} \qquad \ldots (4.2\text{-}11)$$

The half standard entropy of sorption should be independent of temperature, provided $\Delta\bar{H}_1$ can be taken within experimental error, to be independent of temperature. The constancy of $\Delta\bar{S}_h$ is proved by the data of Table 41.

An examination of the equation 4.2-9 shows that there are two terms only which depend on the uptake: $R\,\ell n\,\frac{p^o}{p}$ and $\frac{\Delta H_1}{T}$. The first decreases with the uptake, but remains always positive while the second is always negative. If we ignore the interaction between pairs of sorbate molecules, then, for homogeneous surfaces $\frac{\Delta H_1}{T}$ will be constant at each uptake until a monolayer is completed(90) and for heterogeneous surfaces $\frac{\Delta H_1}{T}$ will decrease (in absolute value) with the uptake. The following curves are given as an idealised illustration of three limiting cases:

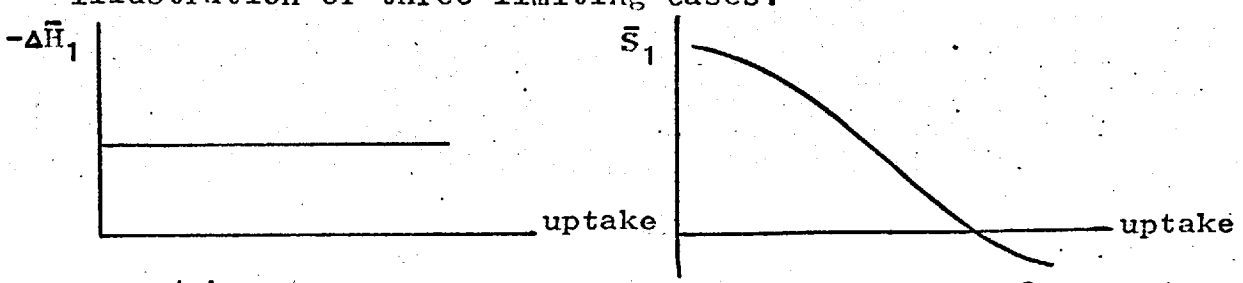

Case(a) - Monolayer adsorption on homogeneous surface.

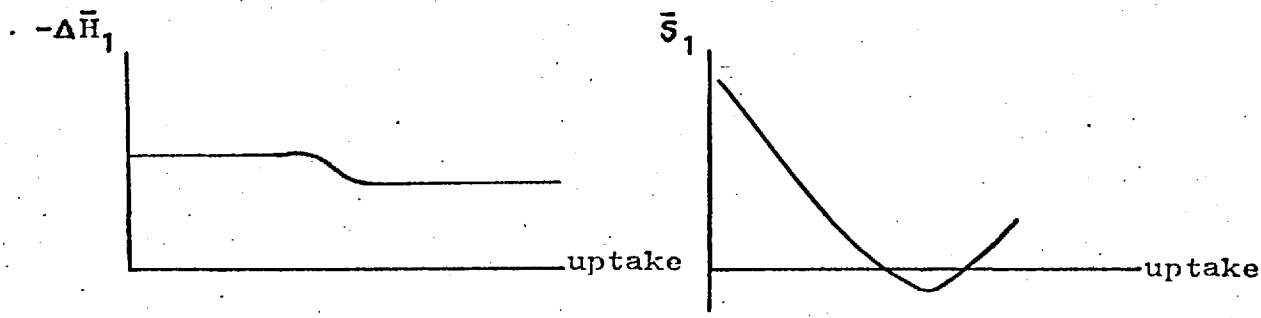

Case(b)- Multilayer adsorption on homogeneous surface.

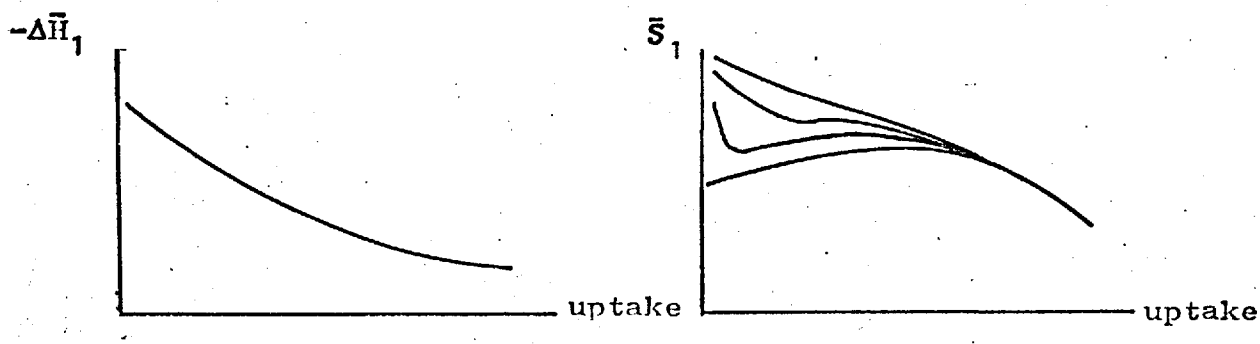

Case(c)- Monolayer adsorption on heterogeneous surface.

The experimental entropy curves found for Kr on HL, H-ER and H-OFF (Fig. 91,92,93 and 94) all decrease with the uptake. In section 4.2.2 it was shown that the above three sorbents are heterogeneous, but they are not so much so as to produce the maximum. For a homogeneous sorbent in which sorption is localised the equation for the configurational entropy is $\bar{S}_c = R\,\ell n\frac{1-\theta}{\theta}$ (p. 56). This will be assumed to be a first approximation to $(\bar{S}_1 - \bar{S}_{th})$ for the present systems. Examination of curves 91, 92, 93 and 94 shows that the order of decreasing entropy for the three sorbents at a given uptake is:

$$\bar{S}_{1\ HL} > \bar{S}_{1\ H\text{-}ER} > \bar{S}_{1\ H\text{-}OFF}$$

This order cannot be explained in terms of the micropore volumes, values of which are in reverse order: $W^{o}_{H\text{-}OFF} > W^{o}_{H\text{-}ER} > W^{o}_{HL}$ (p.171). Thus for a constant uptake, the order of θ for the three scrbents is as fóllows:

$$\theta_{H\text{-}OFF} < \theta_{H\text{-}ER} < \theta_{HL}$$

Substitution in equation for the configurational entropy, $\bar{S}_c$, leads1. when assuming the thermal entropies to be the same, to results contrary to those experimentally obtained, i.e. $\bar{S}_{1\ HL} < \bar{S}_{1\ H\text{-}ER} < \bar{S}_{1\ H\text{-}OFF}$ and 2. assuming $S_{th.HL} > S_{th.H\text{-}ER} > S_{th.H\text{-}OFF}$ to the order of $\bar{S}_1$ observed.

4.3 ADSORPTION OF Ar, Kr AND Xe ON NaL, KL AND BaL AT TEMPERATURES IN THE RANGE 120°K-273°K.

4.3.1 Isotherms.

NaL, KL and BaL were chosen for adsorption studies with Ar, Kr and Xe at a series of temperatures. Isotherms were measured at intervals of 10 to 25°K in the range 120°-200°K for Ar, 130°K-270°K for Kr and 170°K-273°K for Xe. The adsorption equilibrium was found to be established within 15-20 minutes and 30-40 minutes were allowed before reading each equilibrium pressure. The isotherms were reversible in all cases. After completing a series of isotherms for each gas the reproducibility was checked by repeating one of the isotherms of the series. Reproducibility was found to be satisfactory. As Xe condensed appreciably in the nitrogen trap the latter had to be removed, while pumping out the system, for short periods at regular intervals.

The isotherms of Ar, Kr and Xe obtained on NaL, KL

and BaL are given on Figs. 95-100 and 67, 68 and 70. A comparison of the isotherms of a given gas on each sorbent indicates more energetic sorbate-sorbent interaction(89) in BaL, than in KL and NaL.

All isotherms were type I in the BDDT classification(134) In contrast with the present results, in zeolite LiX, Kiselev et al (137) obtained upward inflections at low pressures for Xe adsorption.

One can compare the behaviour of Ar, Kr and Xe on a given sorbent, by taking isotherms for all gases at the same temperature. As such experiments were not performed, the comparison was made in the following manner: At an arbitrary pressure of 30 cmHg, the uptake for each gas at comparable temperatures was read from the graphs and tabulated in Table 42. The uptakes of Kr and Xe are similar and are approximately twice that of Ar.

TABLE 42.

Uptakes at pressure 30 cmHg

	NaL		KL		BaL	
	$T^{o}K$	N m/u.c.	$T^{o}K$	N m/u.c.	$T^{o}K$	N m/u.c.
Ar	162.0	4.7	169.4	3.6	164.9	3.6
Kr	163.7	7.2	160.9	7.2	162.3	7.2
Xe	169.4	6.9	169.3	6.1	171.2	6.4
Ar	189.7	1.8	188.4	1.7	185.8	1.8
Kr	186.2	5.8	209.6	4.0	182.7	5.6
Xe	181.0	6.0	210.9	4.3	187.5	6.1

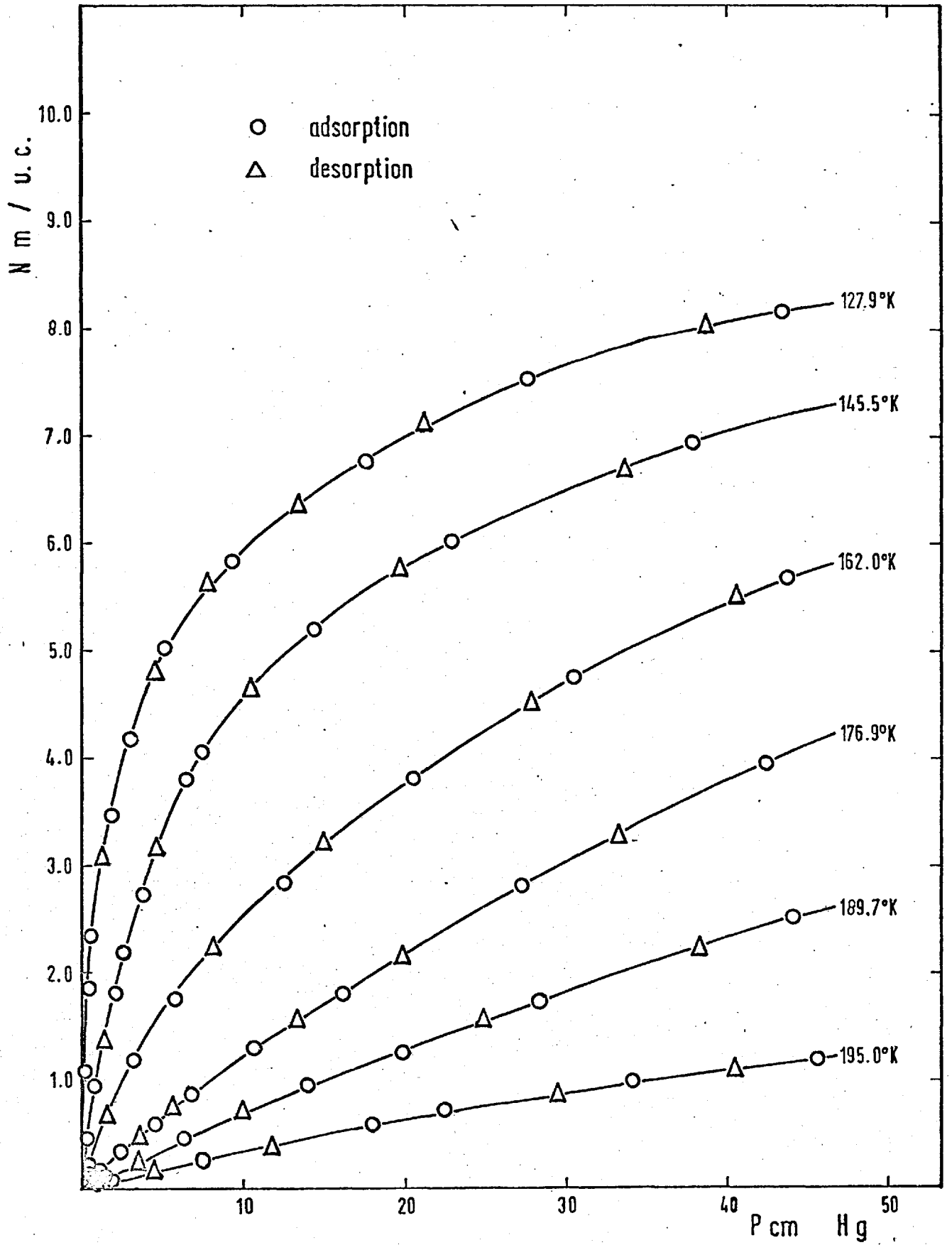

Fig. 95 Ar on NaL

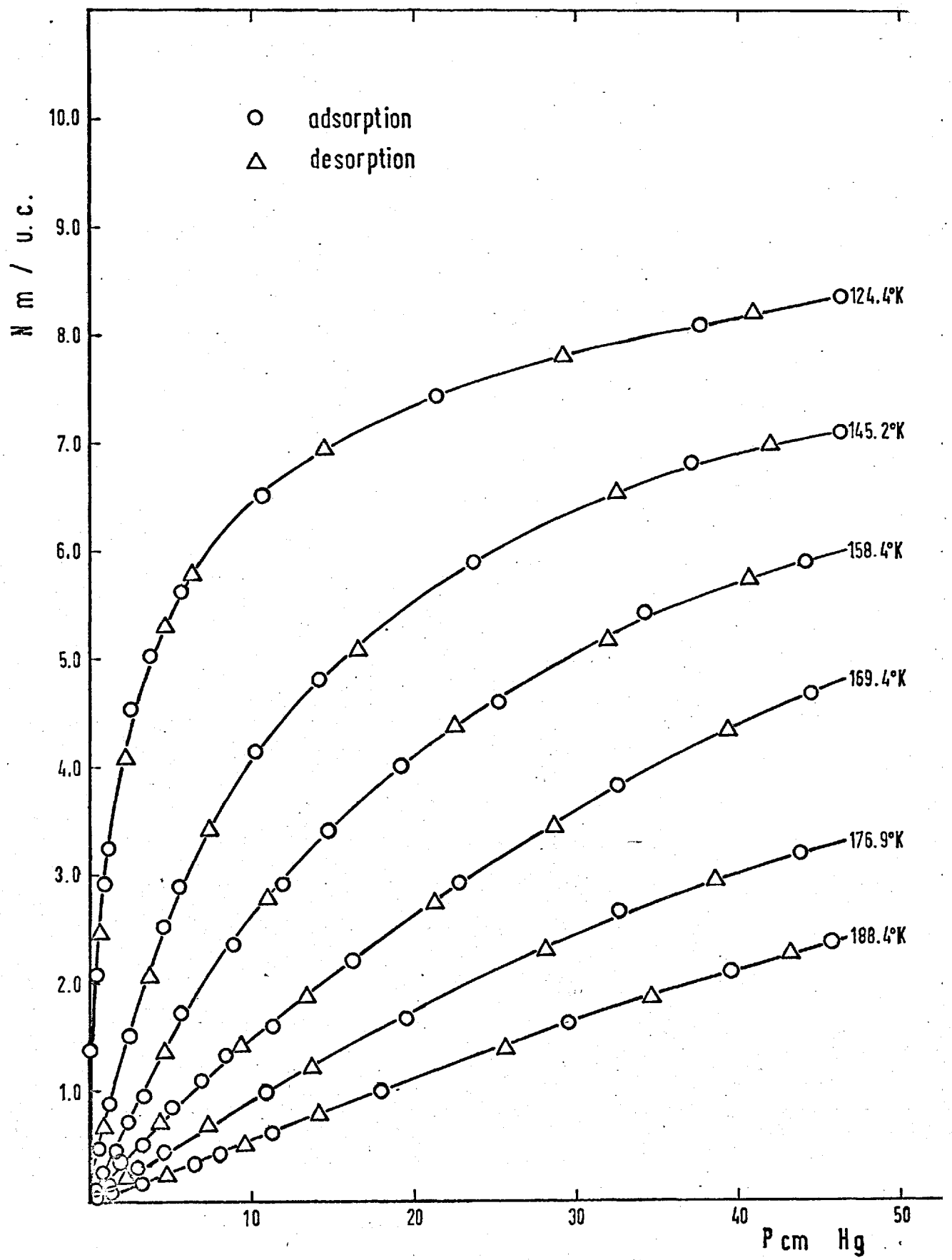

Fig. 96 Ar on KL

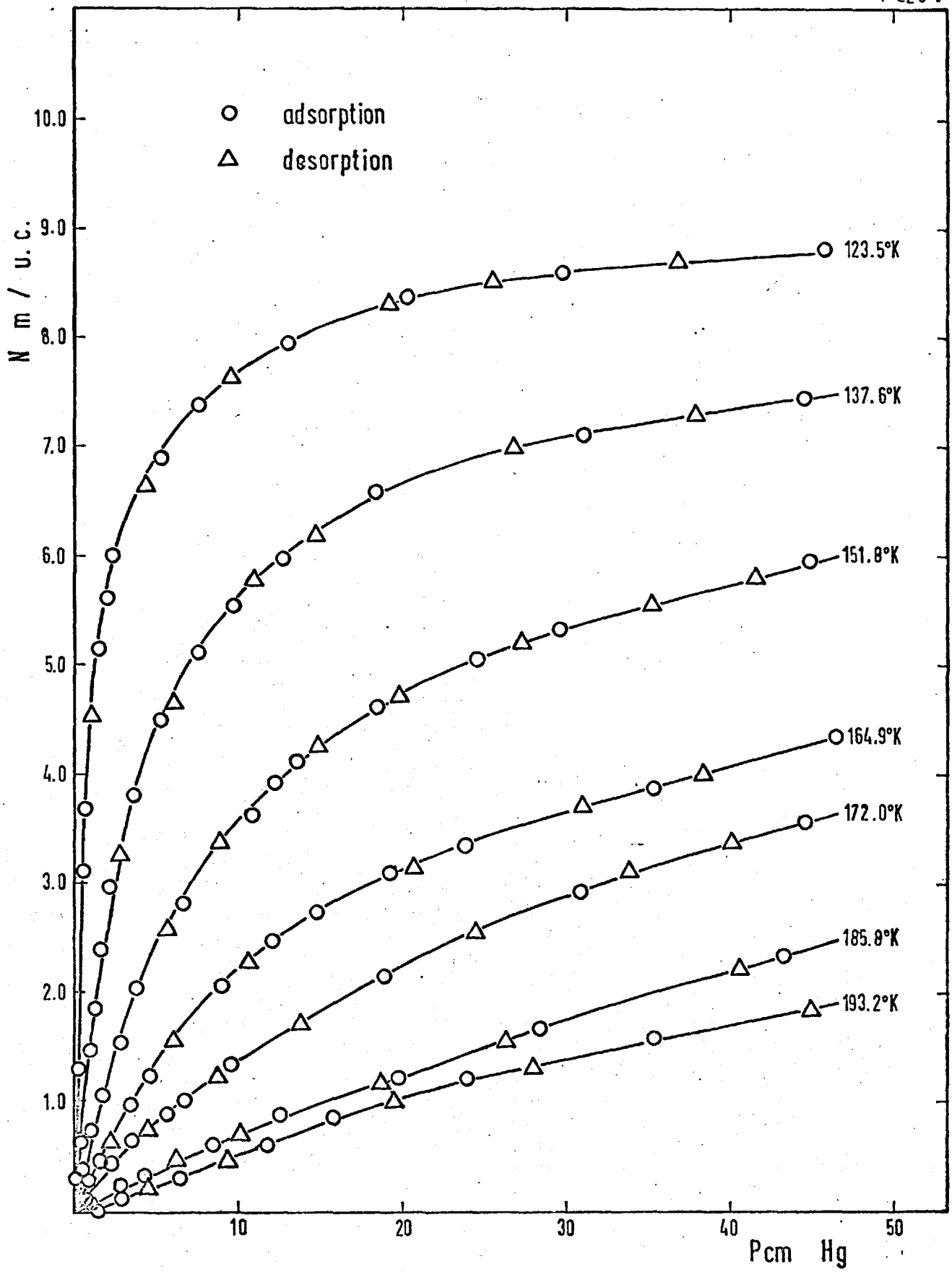

Fig. 97 Ar on BaL

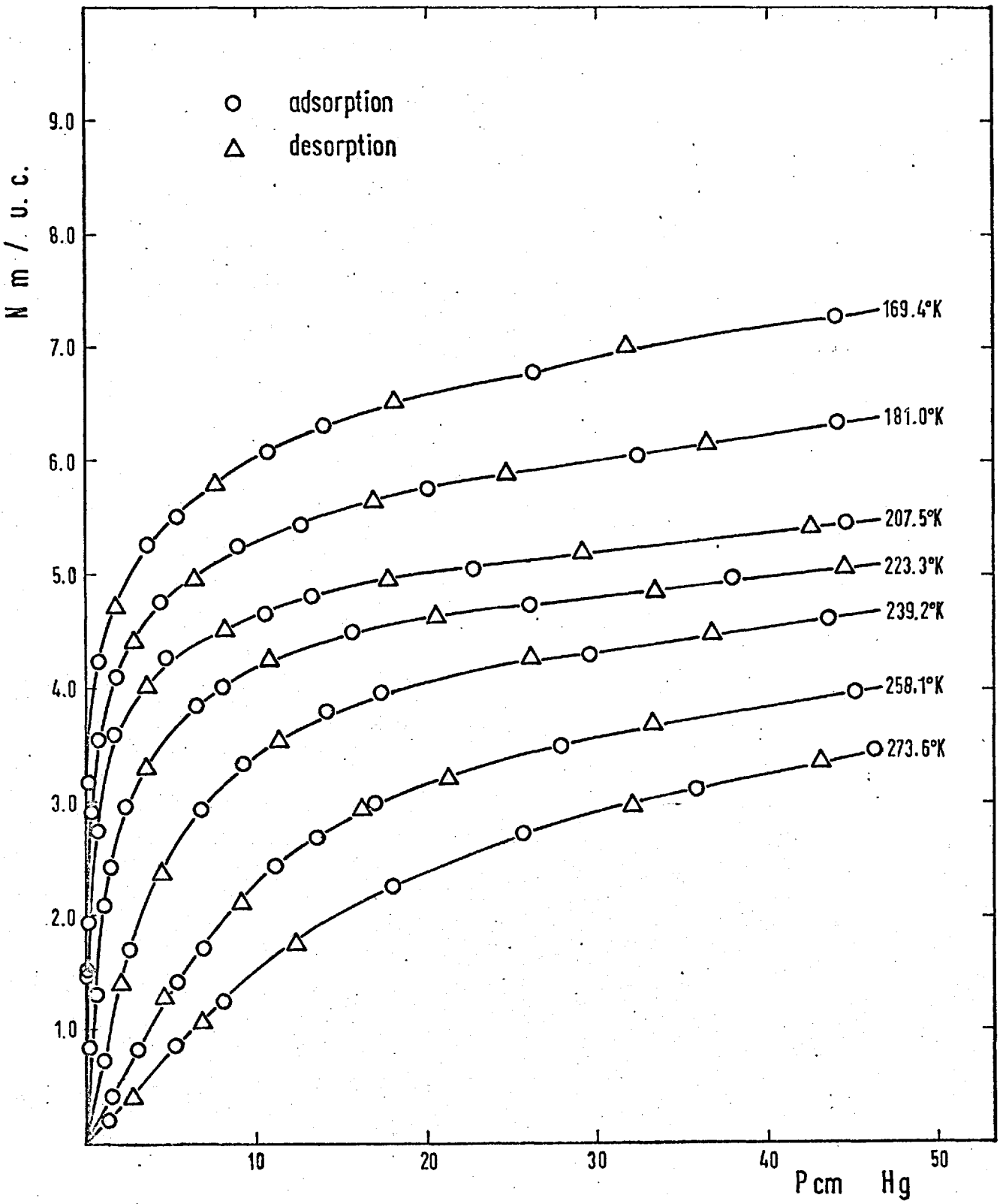

Fig. 98 Xe on NaL

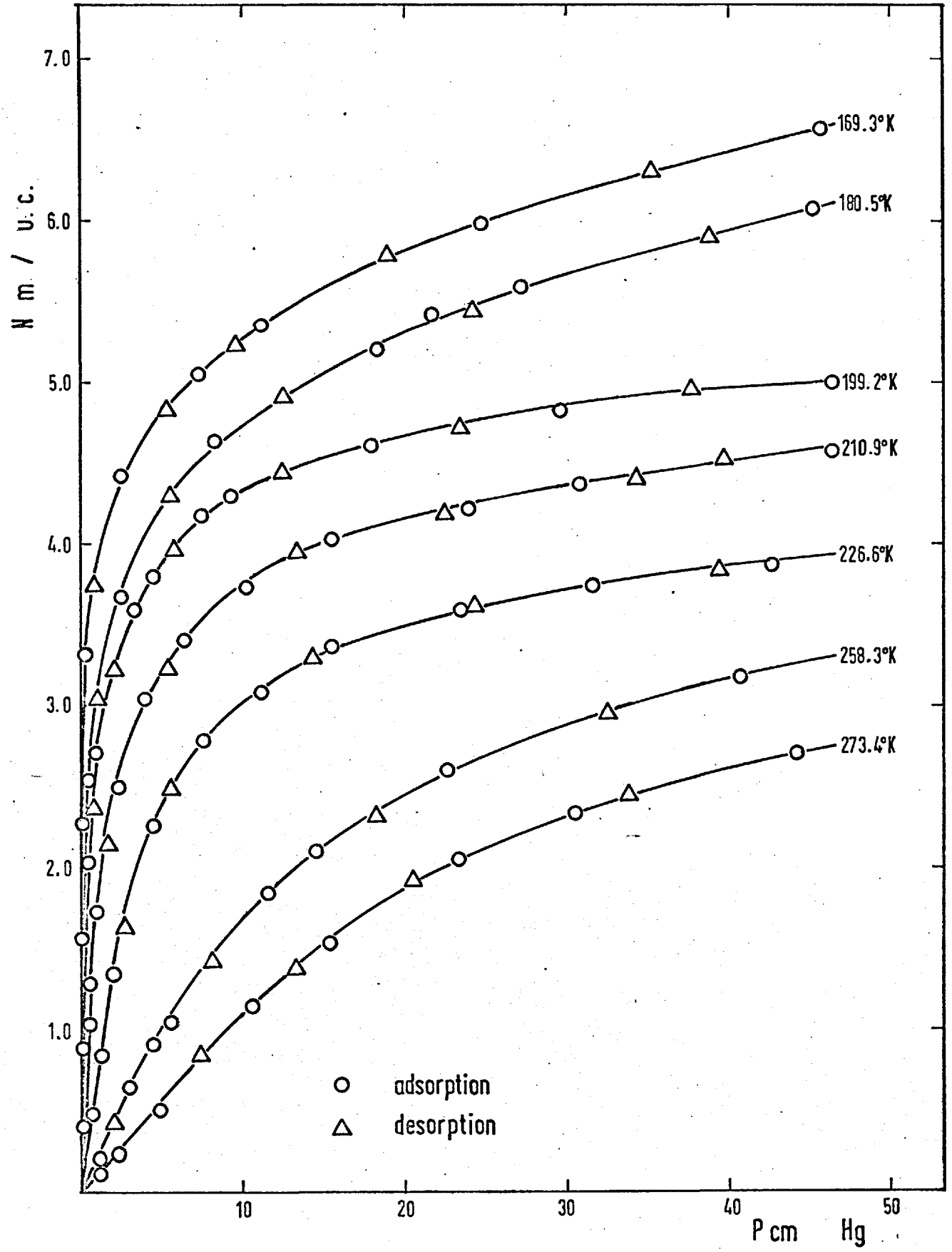

Fig. 99 Xe on KL

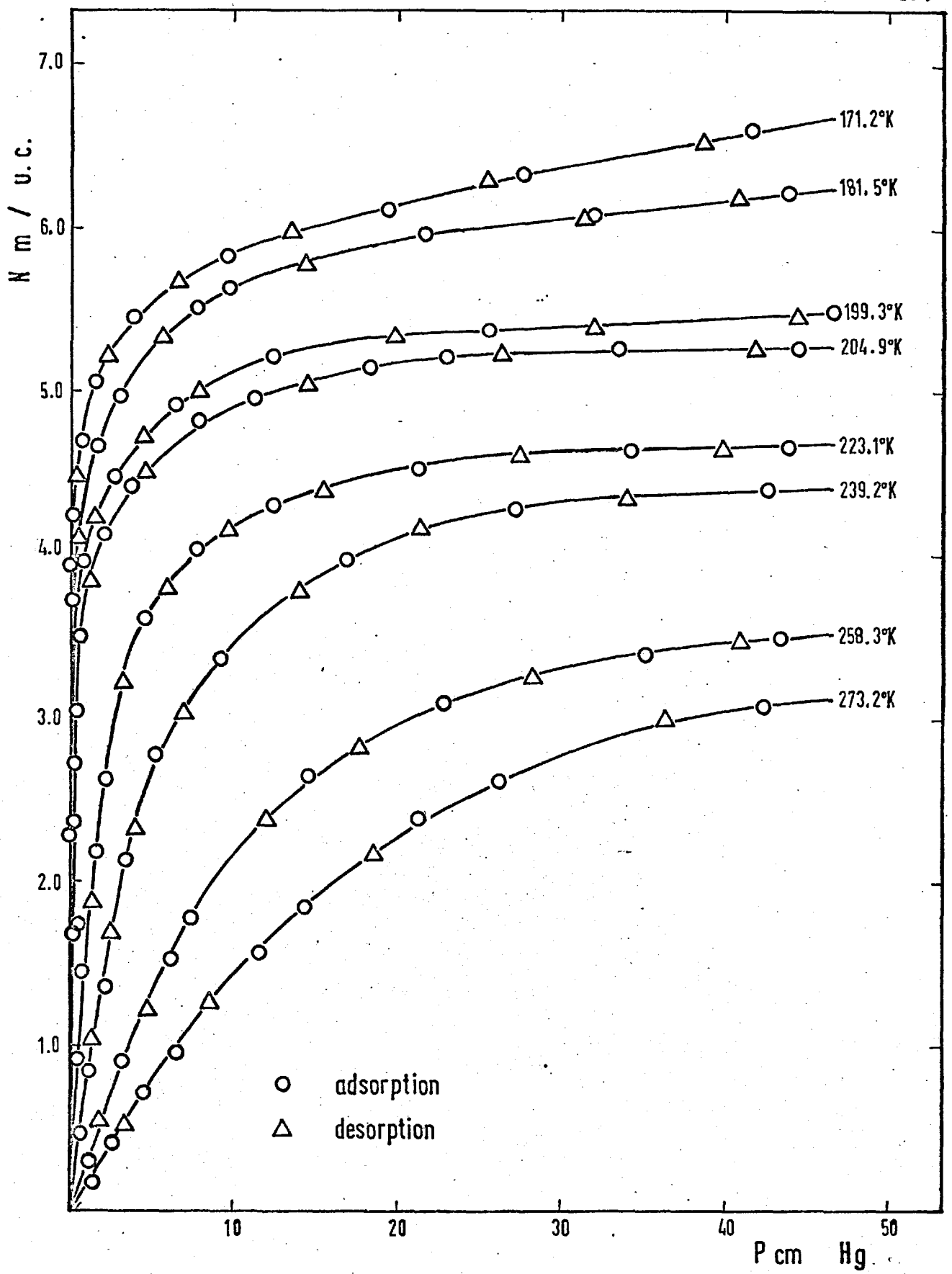

Fig. 100 Xe on BaL

4.3.2 Isosteric heats.

The isosteric heats of adsorption (p.52) of Ar, Kr and Xe on NaL, BaL and KL were determined from the isotherms by the three procedures previously indicated in section 4.2.4 (p.186). Examples are shown on Figs. 101, 102 and 103. The average values of isosteric heats obtained from each of the procedures were graphed to give the mean curves of $\Delta \bar{H}_1$ vs uptake. In Fig. 104 such curves for Ar on NaL, KL and BaL are presented and the points calculated by the different methods are distinguished. The numerical data are given on Table 43. For all other systems the curves of isosteric heats vs uptake are drawn using the average isosteric heats from the first two procedures and average of both plotted. An accuracy $\pm$ 0.15$\frac{kcal}{mole}$ was achieved. If appreciable discrepancy appeared then the third method was also used.

A better comparison between the three sorbents can be made if the isosteric heats are presented (Fig. 105) as a function of the common scale η (see p.190).

The isosteric heats of the three gases on NaL, KL and BaL were found to follow the normal order $\left|\Delta \bar{H}_1\right|_{Xe} > \left|\Delta \bar{H}_1\right|_{Kr} > \left|\Delta \bar{H}_1\right|_{Ar}$ at any one uptake η. Examination of the slopes of the plots of isosteric heat vs η indicates that the apparent heterogeneity towards Kr and Ar, in contrast to Xe persists over the whole interval of studied. The curves for Xe show a horizontal part in region of η 0-200, followed by a rapid decline in the region of η 200-400. This behaviour is compatible with energetic heterogeneity similar to that observed for Ar and Kr, offset by a sorbate-sorbate interaction which is larger for Xe and is sufficient at first to keep the isosteric

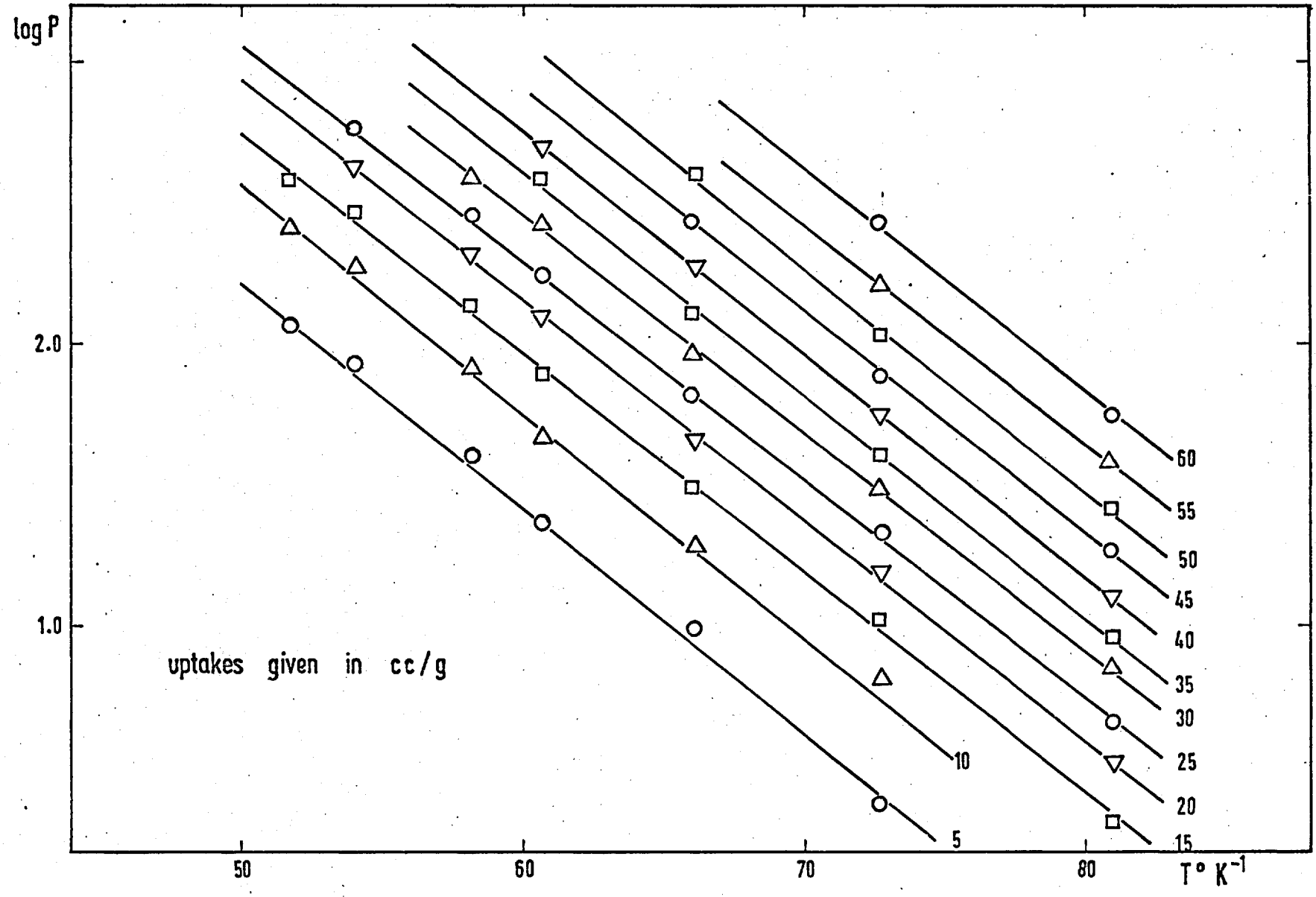

Fig. 101 ISOSTERS for Ar on BaL

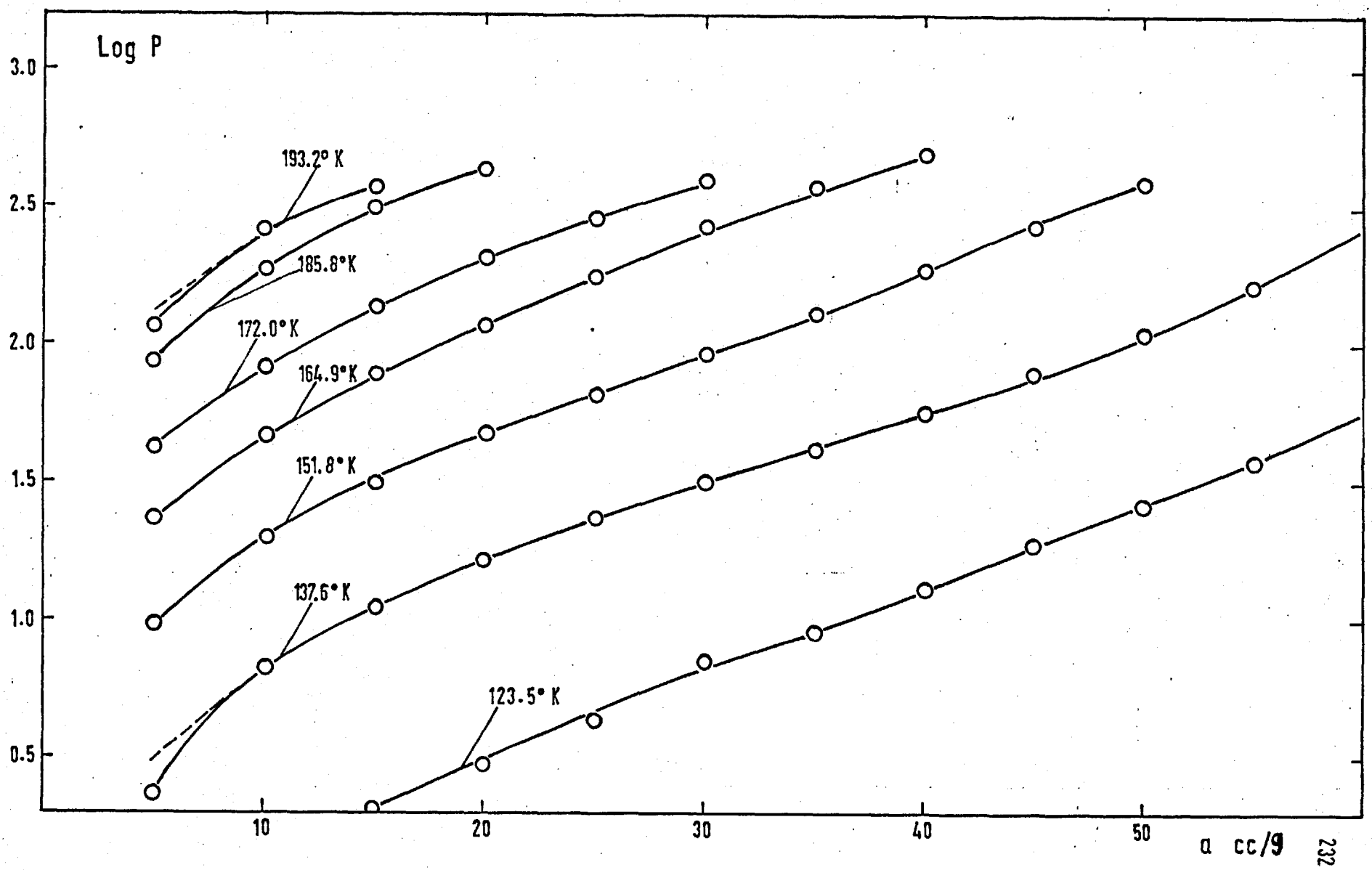

Fig. 102 Log P = f(a) for Ar on BaL

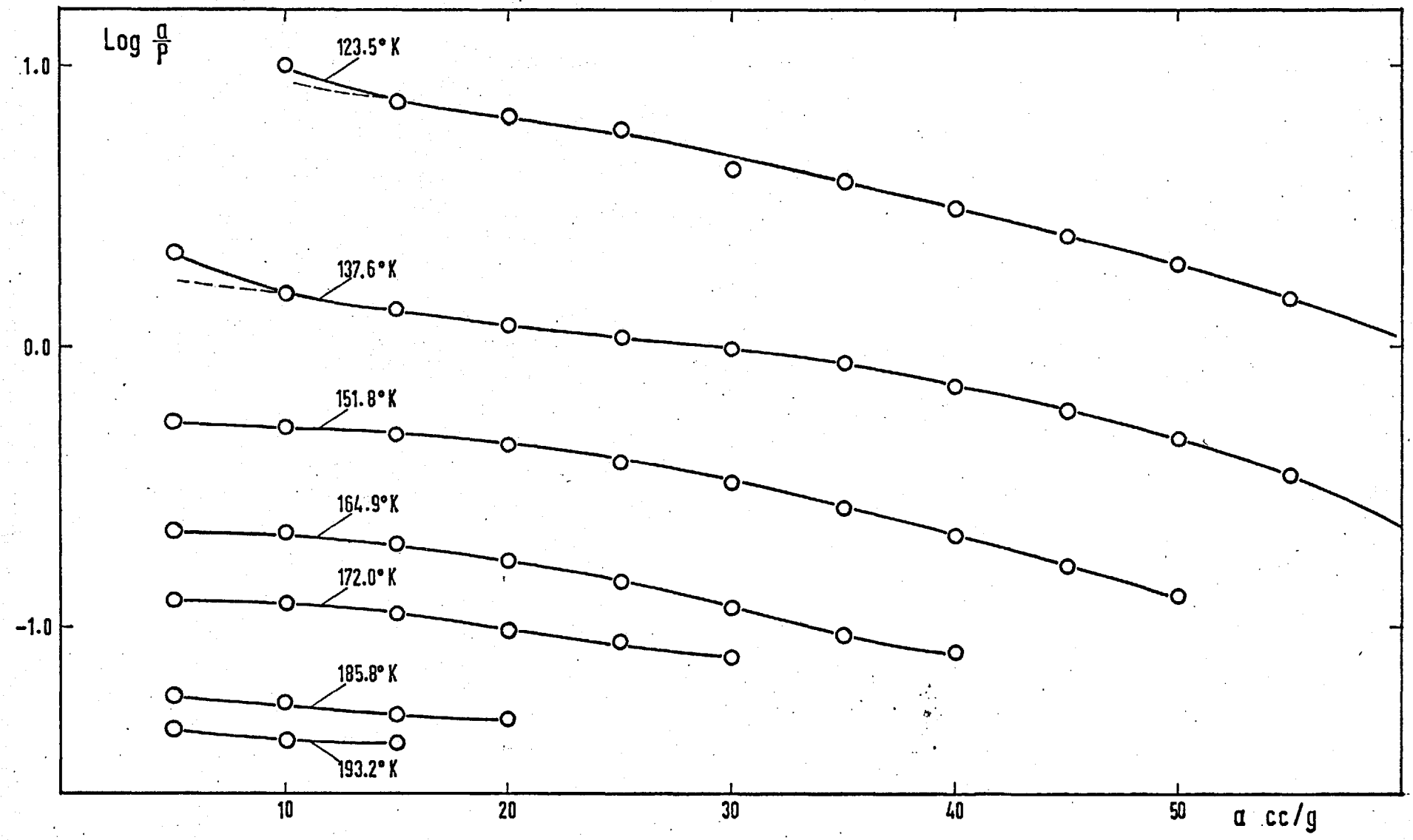

Fi-. 103 Lo- a/p = f'a' for Ar on BaL

TABLE 43.

Isosteric heats ($-\Delta\bar{H}_1$ kcal/mole) of Ar on NaL, KL and BaL.

$a\frac{cc}{g}$	NaL			KL			BaL		
	$-\Delta\bar{H}_1$ calculated from								
	ℓgP vs 1/T.	ℓgP vs a	ℓg P/a vs a	g P vs 1/T	g P vs a	g P/a vs a	g P vs 1/T	g P vs a	g P/a vs a
5	3.47	3.48	3.42	3.26		3.25	3.67		3.62
6			3.41					3.65	
0	3.43			3.16		3.10	3.67		3.75
15	3.38	3.41			3.17	3.07	3.15		3.67
16								3.60	
0	3.28		3.31	3.07		3.10	3.58		3.63
5	3.22	3.27			3.01	3.05	3.55		3.64
6								3.60	
0	3.17		3.12	2.90		2.97	3.53		3.62
5	3.06	3.01			2.97	2.85	3.60		3.61
6								3.60	
0	2.96		2.89	2.58		2.54	3.58		3.54
45	2.76	2.85			2.50	2.40	3.63		3.56
46								3.45	
50	2.72		2.65	2.29		2.33	3.51		3.48
55	2.49	2.56			2.20		3.47		3.45
56								3.45	
60	2.37		2.31	2.09		2.00	3.43		3.41

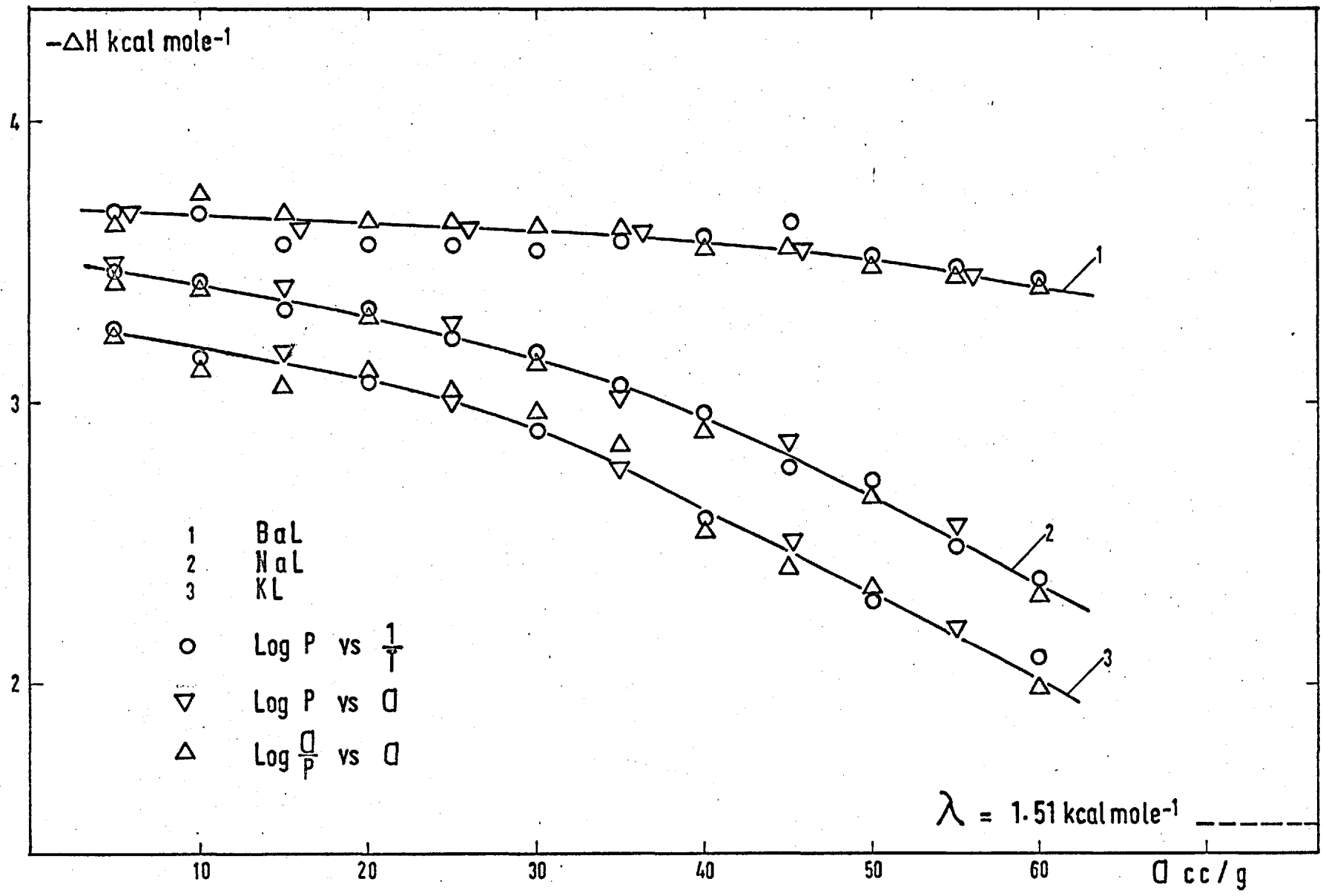

Fig. 104 ISOSTERIC HEATS of Ar

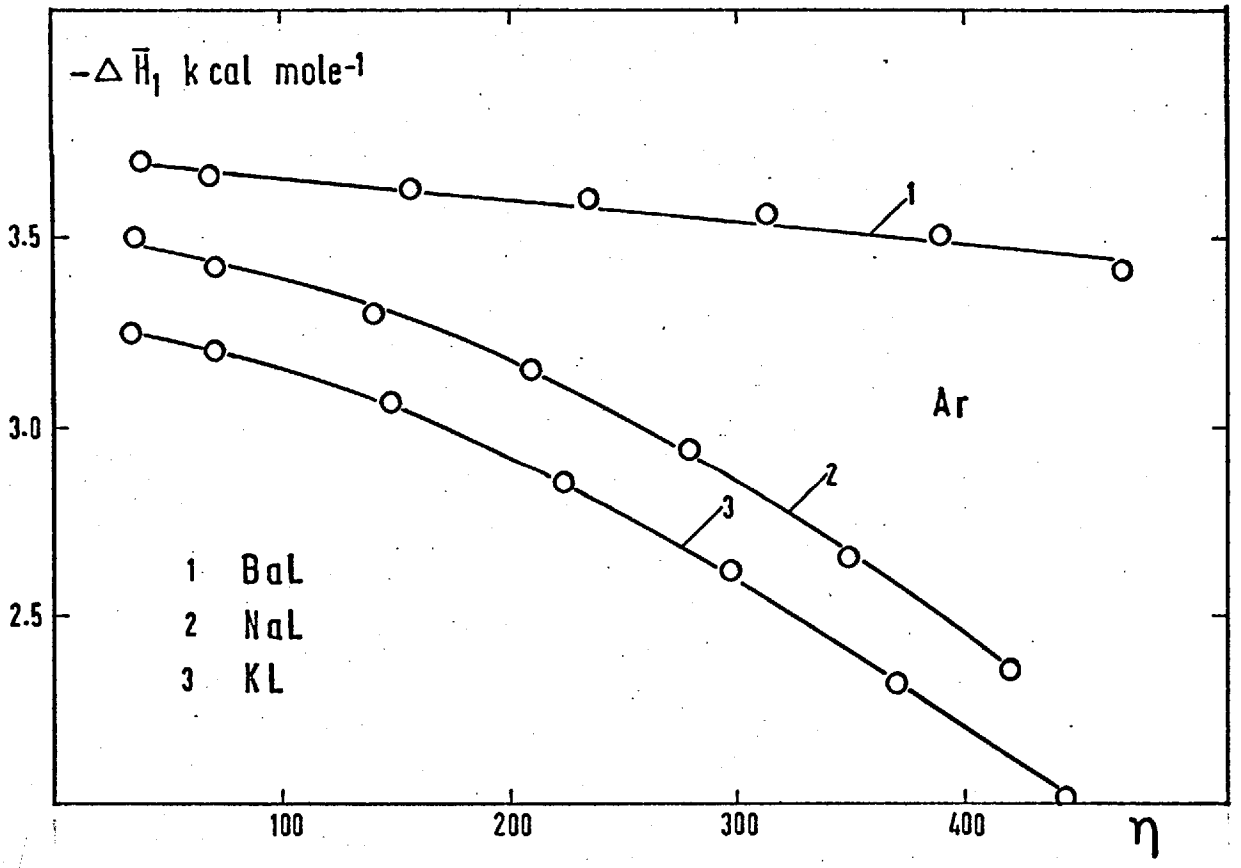

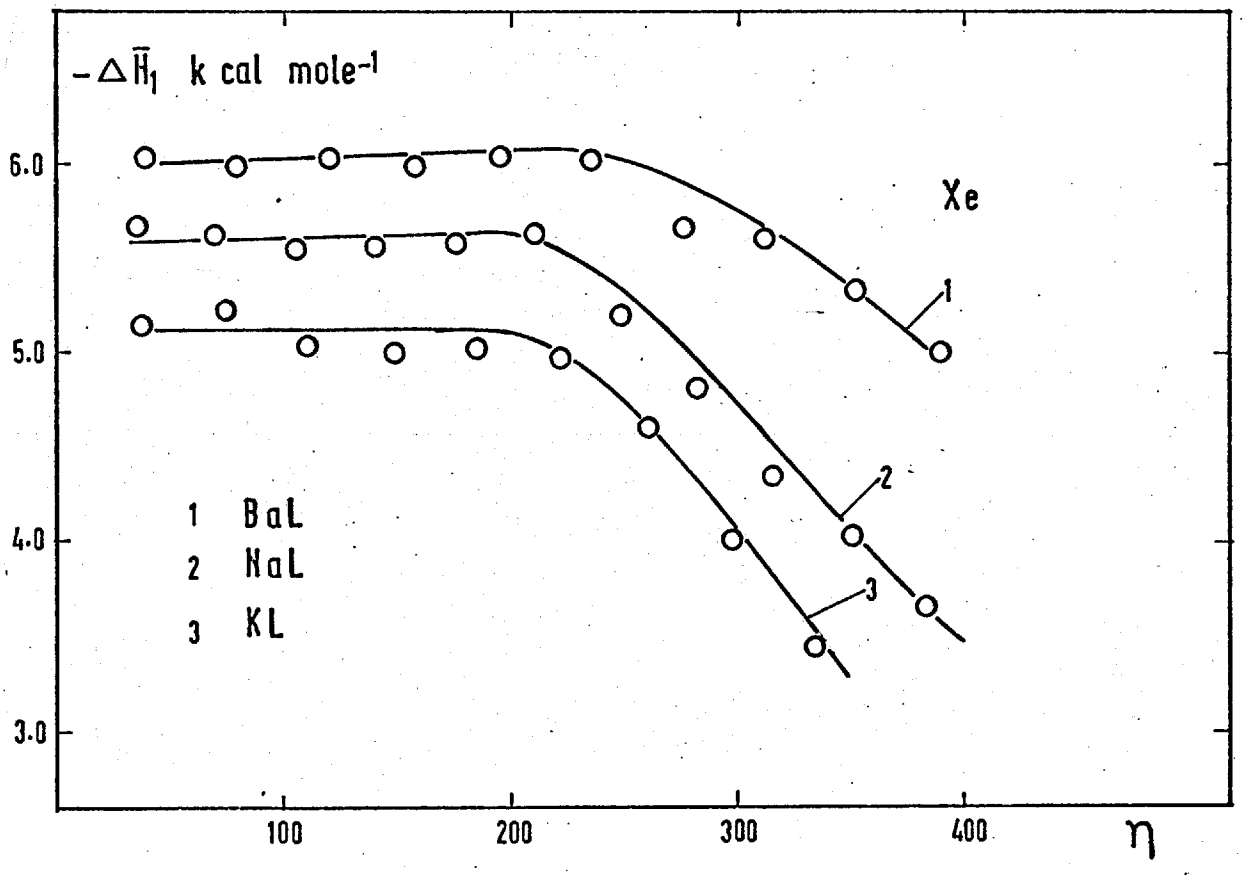

Fig. 105 $-\Delta \bar{H}_1$ vs η

heat nearly constant.

We can present the decrease in the isosteric heats from an arbitrary low η value (η_1 = 50) up to an equally arbitrary high η value (η_2 = 400) for all gases and sorbents. (Table 44). The values express the overall heterogeneity as a function of the nature of the sorbate and the sorbent.

TABLE 44.

Decrease in the isosteric heats ($\Delta \bar{H}_1$ kcal/mole^{-1}) of Ar, Kr and Xe on NaL, KL and BaL.

Sorbate	NaL			KL			BaL		
	$-\Delta \bar{H}_1$ at arbitrary η.								
	η_1	η_2	$\Delta(\eta_1-\eta_2)$	η_1	η_2	$\Delta(\eta_1-\eta_2)$	η_1	η_2	$\Delta(\eta_1-\eta_2$
Ar	3.40	2.40	1.00	3.25	2.12	1.13	3.69	3.58	0.11
Kr	5.00	3.90	1.10	4.40	2.65	1.75	4.70	4.38	0.32
Xe	5.60	3.46	2.14	5.10	3.20	1.90	6.00	4.80	1.20

The initial heats of a given sorbate are close in value for different sorbents as previously reported for Kr on all ion-exchanged forms of L(p.187) and now confirmed for the Ar and Xe. The same behaviour was found for Ar in Li, Na, K, Ba and Sr forms of zeolite X(68). Initial isosteric heats on Li, Na, K, Ba and Sr were all within a range of $\pm$ 0.5 kcal/mole.

In the case of krypton (p. 190) it was concluded that the initial isosteric heats are determined by the framework/sorbate interaction. The same argument can now be extended to the results from Ar and Xe and to the results for Ar in

zeolite X(68). The apparent heterogeneity on the other hand differs among the exchanged forms. For example in BaL $\Delta\bar{H}_1$ was nearly constant for both Ar and Kr, while NaL and KL exhibited noticeable heterogeneity toward the two gases. Barrer and Stuart (i.b.) have found that ion-exchanged forms of zeolite X, which were most energetically heterogeneous, contained cations which showed the greatest polarizing power and for non-polar sorbates, such as Ar, Kr and Xe, have attributed the heterogeneity to this property. Heterogeneity was much increased when the sorbates possessed permanent electric moments. For some cases of the present study (including those of Kr on all ion-exchanged forms) this explanation holds, (LaL exhibits the highest heterogeneity) but it cannot be applied to all cases (BaL vs NaL, KL for example). Close initial isosteric heats but distinctly different heterogeneities have also been found for adsorption of krypton on different forms of mordenite(92) and Ar on Na- and H-mordenite(108).

4.3.3 Entropy of adsorption.

The entropy of adsorption $\Delta\bar{S}_1$ (p. 53) for a given uptake and temperature, T, can be calculated from isosteric heats:

$$\Delta S_1 = \frac{\Delta\bar{H}_1}{T}$$

The entropy of adsorption will depend on the amount adsorbed in a manner similar to that of the isosteric heats, but this dependence will, in addition, be a function of temperature. The entropies of adsorption of Ar, Kr and Xe on NaL, KL and BaL at selected temperatures are given in Figs. 106, 107 and 108. For a particular sorbent/sorbate system, the lower the temperature the greater the decrease of the entropy when sorption occurs. One can consider the slope of

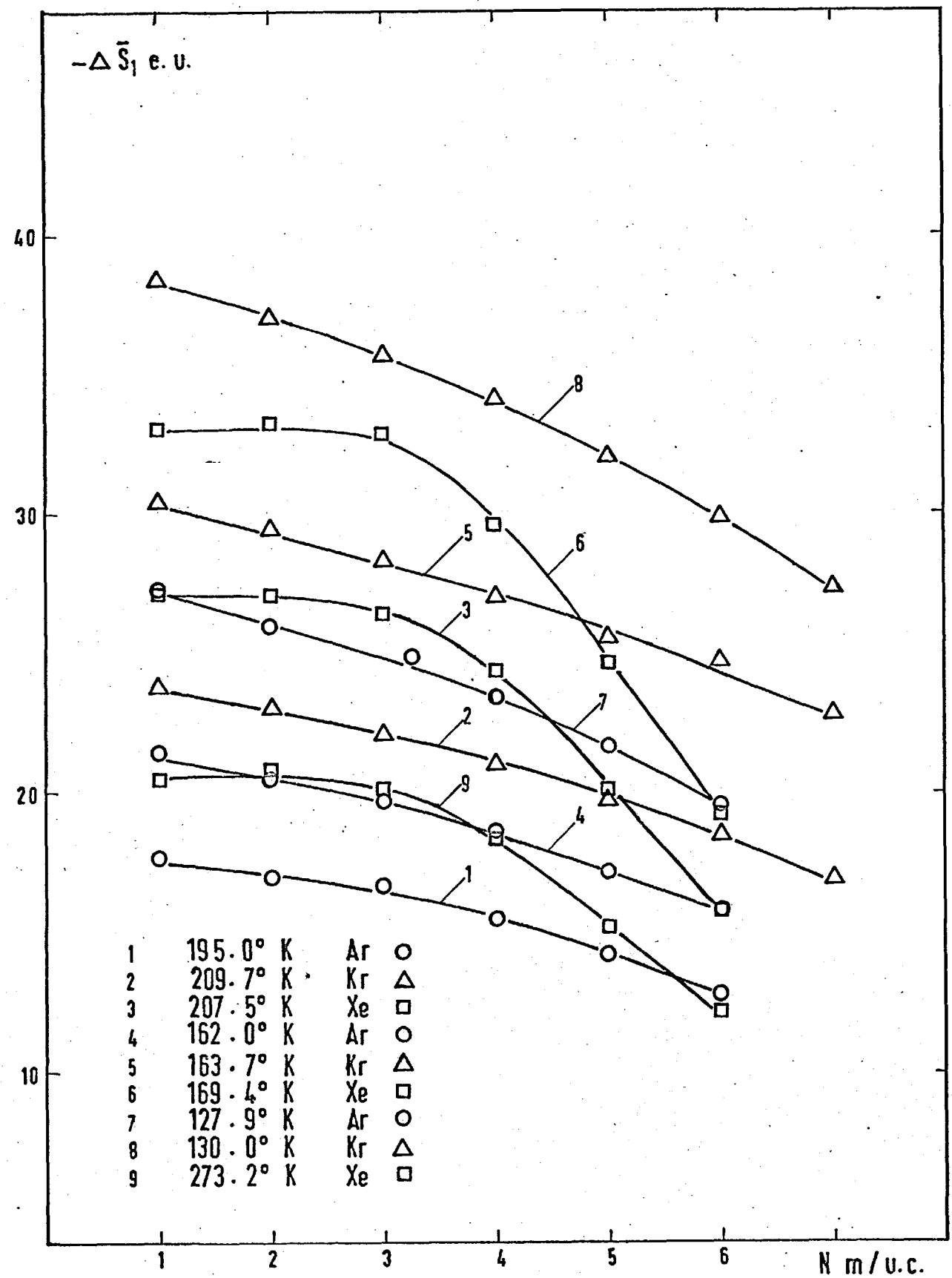

Fig. 106 Ar, Kr and Xe on NaL

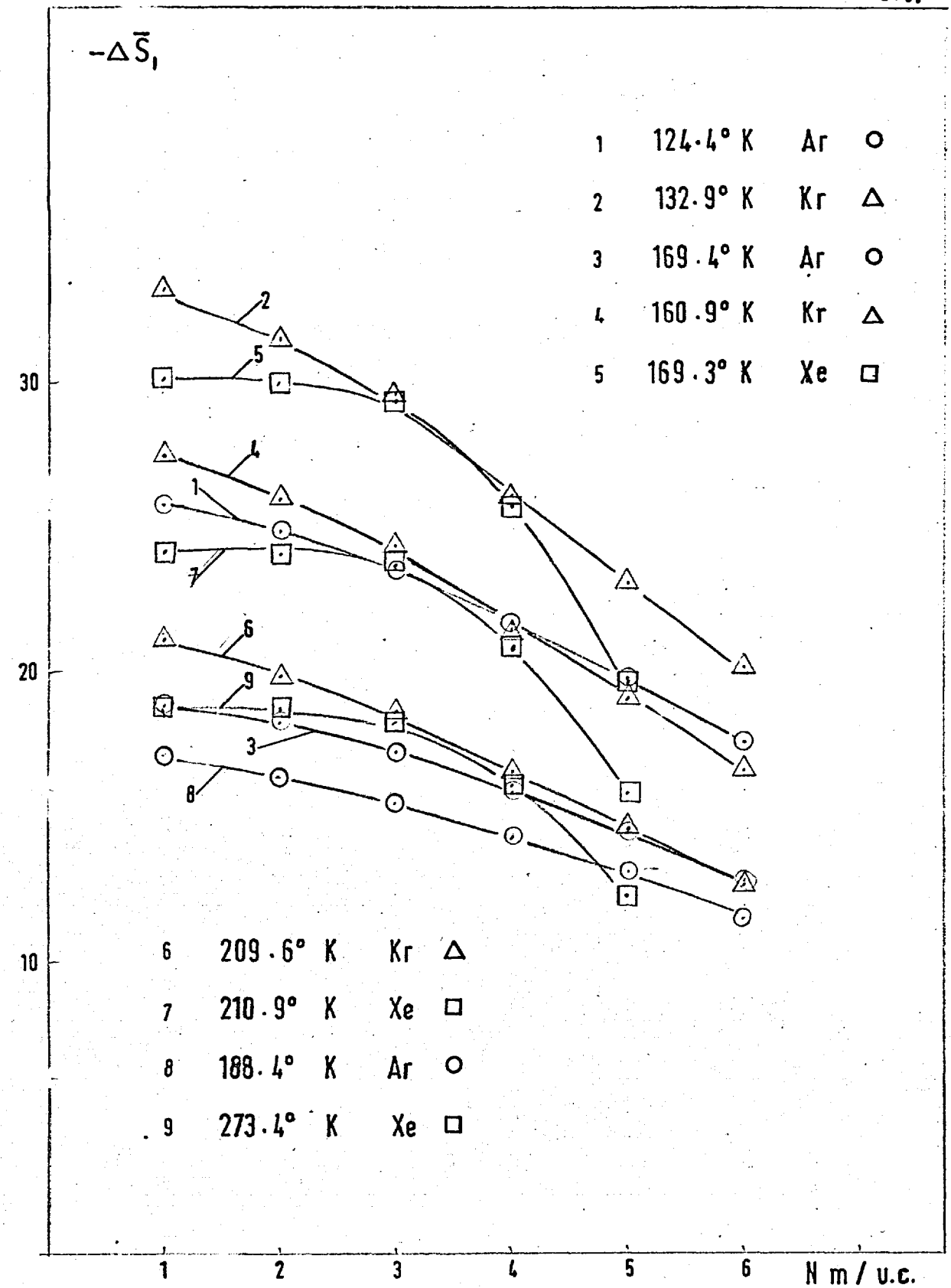

Fig 107 Ar, Kr and Xe on KL

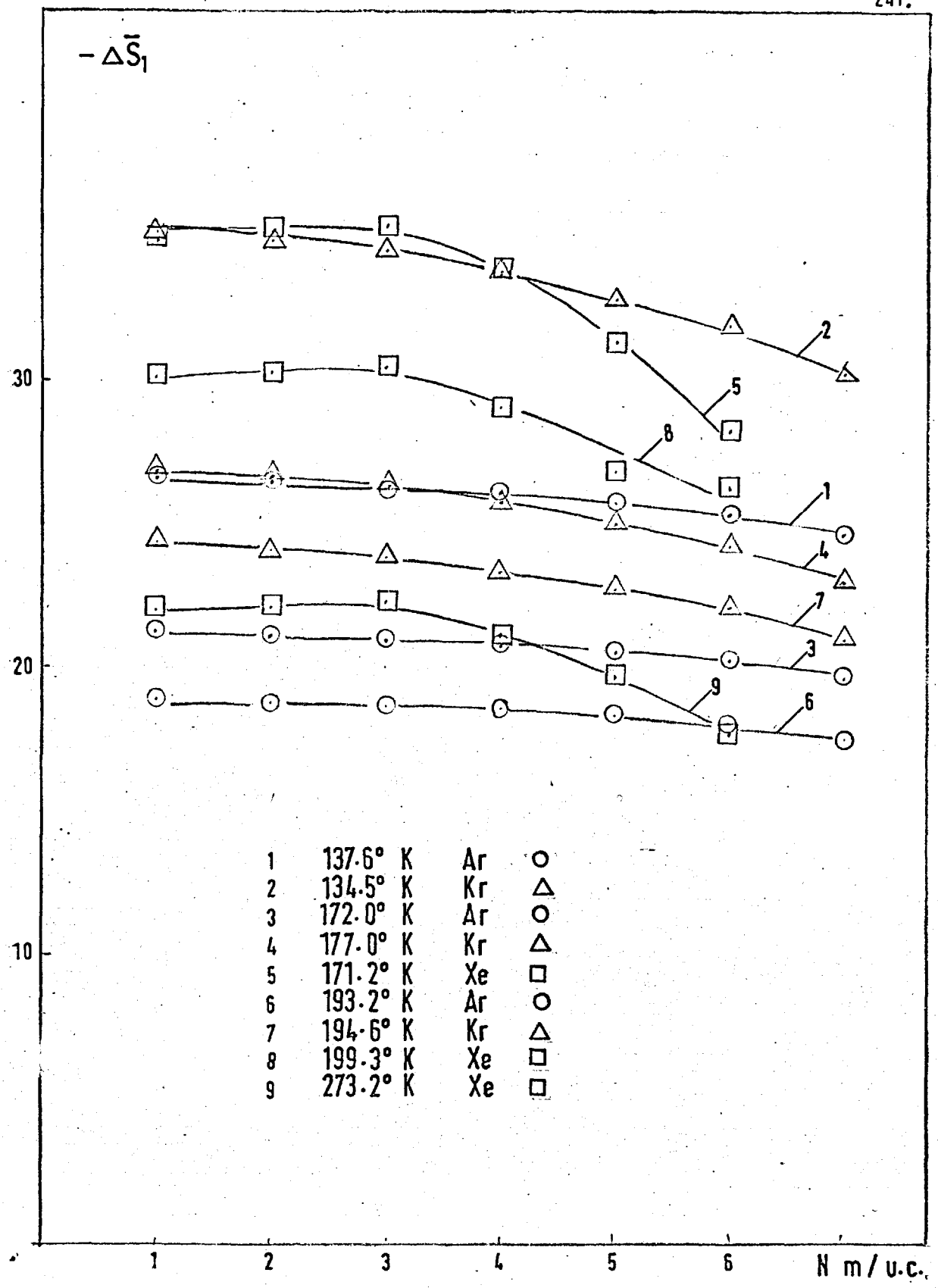

Fig. 108 Ar, Kr and Xe on BaL

the curves of $\Delta\bar{S}_1$ vs N as a measure of the heterogeneity at a given temperature. The heterogeneity so estimated is more strongly in evidence at lower temperatures. Curves of $\Delta\bar{S}_1$ vs N are a convenient basis for comparison of the heterogeneity of different systems at a common temperature.

4.3.4 Empirical isotherm equations for adsorption of Ar, Kr and Xe on BaL.

BaL was chosen as an example for estimation of equilibrium constants and the standard energies of the three gases, Ar, Kr and Xe. Activity coefficients for the sorbed argon were evaluated and were compared with those calculated from isotherm models.

As described before, the equilibrium constant K' can be obtained from the intercept at $N \rightarrow 0$ of the graph of $\ell n \frac{N}{p}$ vs N (p.195). From the equilibrium constant K' the dimensionless equilibrium constant K'' (p.280) was calculated. The values obtained are given in Table 45 (for Kr see Table 36 and 40). The equilibrium constant K'' was used to obtain the standard energies, ΔE^{o} kcal/mole. In Fig. 109 (for Kr see Figs. 82 and 83) the plots of ℓg K" vs 1/T are presented and in Table 45 the values of the energies are tabulated. The values of the equilibrium constants for Xe dominate those at the corresponding temperature for Ar and Kr.

The equilibrium constants for the three gases read at an arbitrary temperature T_a = 166.60 (Table 45a) make this comparison clearer.

The values of the equilibrium constants obtained for Ar were used to calculate the activity coefficients (p.62). The theoretical activity coefficients were also calculated according to both Langmuir(90) and Volmer(90) isotherm models (Table 46) and in Fig. 110 are shown the corresponding

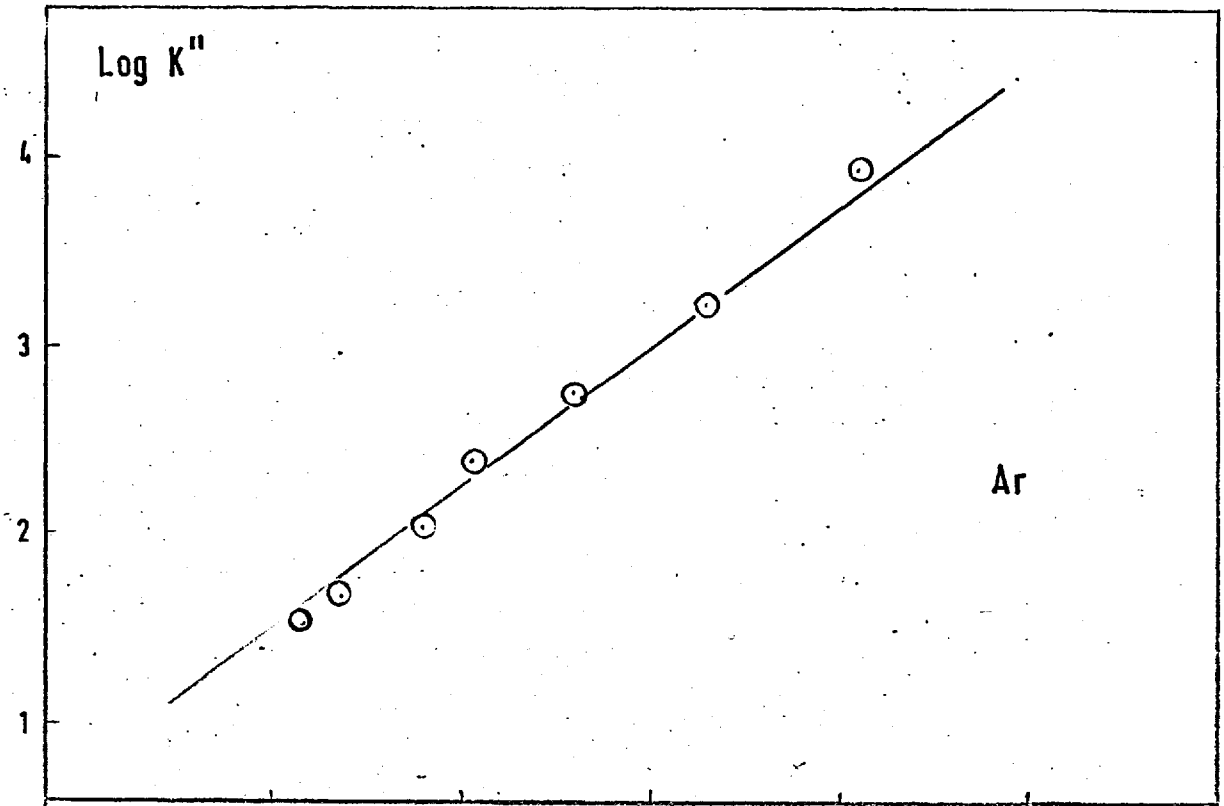

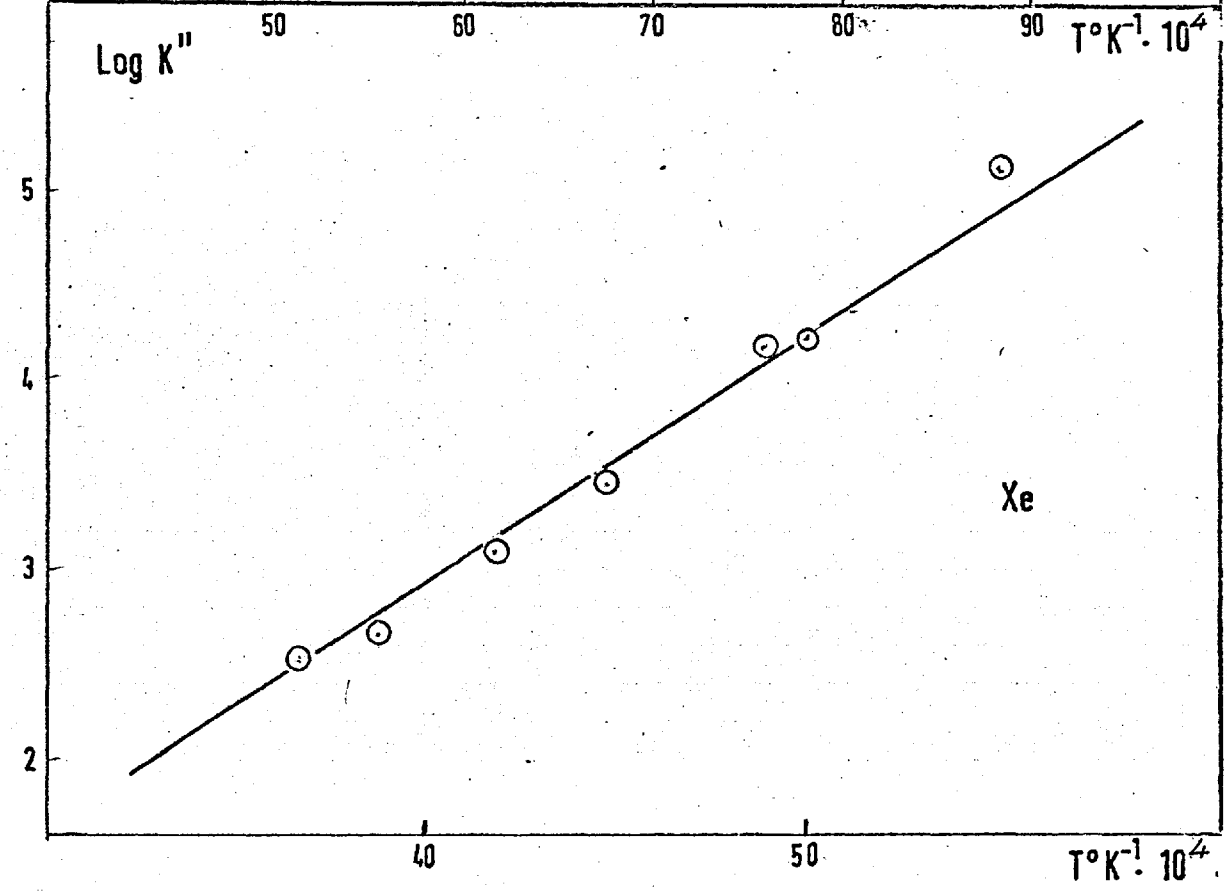

Fig. 109 Ar and Xe on BaL

TABLE 45.

Equilibrium constants, K"*, and energy at standard state ΔE^{o} kcal/mole for adsorption of Ar and Xe on BaL

Ar on BaL $\Delta E^{o} = -2.90 \frac{kcal}{mole}$

$T^{o}K$	123.5	137.5	151.8	164.9	172.0	185.8	193.2
$\ell gK"$	3.93	3.21	2.78	2.40	2.03	1.69	1.58
K"*	$5.61.10^{3}$	$1.45.10^{3}$	$4.57.10^{2}$	$2.00.10^{2}$	$1.26.10^{2}$	57.5	39.8

Xe on BaL $\Delta E^{o} = -5.80 \frac{kcal}{mole}$

$T^{o}K$	181.5	199.3	204.9	223.1	239.2	258.3	273.2
$\ell gK"$	5.12	4.22	4.20	3.45	3.14	2.67	2.33
K"*	$7.95.10^{4}$	$1.66.10^{4}$	$1.26.10^{4}$	$3.52.10^{3}$	$1.51.10^{3}$	$6.30.10^{2}$	$2.14.10$

TABLE 45a.

Equilibrium constants, $K"^{*}_{a}$, at an arbitrary temperature $T_a = 166.6^{o}K$.

Ar	Kr	Xe
$1.66.10^{2}$	$7.90.10^{3}$	$3.40.10^{5}$

TABLE 46.

Activity coefficients of the sorbed phase.

isotherm	equilibrium constant	activity coefficient.
Langmuir.	$K = \frac{\theta}{P(1-\theta)}$	$\gamma_L = \frac{C_{sat}}{C_{sat}-C}$
Volmer.	$K = \frac{\theta}{P(1-\theta)} \exp \frac{\theta}{(1-\theta)}$	$\gamma_V = \frac{C_{sat}}{C_{sat}-C} \exp \frac{C}{C_{sat}-C}$
Empirical	$K = \frac{C}{P} \exp(2A_1C+\frac{3}{2}A_2C^2+..)$	$\gamma_E = \exp(2A_1C+\frac{3}{2}A_2C^2+..)$

curves of γ vs C_s (the concentration C_s is expressed in moles sorbate per litre of free volume of sorbent). Volmer's model gives fairly good agreement with the experimental isotherms at low concentration of the sorbate, but the values at high concentration are quite unrelated to the experimental ones. Calculations on the basis of the Langmuir model give values well below the experimental ones.

To estimate θ (for Langmuir and Volmer equations) the saturation values C_{sat}, were obtained from the limiting slopes of the plots $\frac{P}{C_s}$ vs P (ref. 72) at the experimental temperature. The lower the temperature, the smaller was the deviation from a straight line. Thus the more accurate values for C_{sat}, and θ, are those for the low temperatures, 123.5°K and 137.5°K. The activity coefficients estimated from the empirical isotherm curves, practically coincide with the experimental ones (see p. 62). The poor accuracy of C_{sat} might be one of the reasons for discrepancy between the experimental and theoretical curves. However, it is unlikely that the real thermodynamic state of the sorbate/sorbent systems here discussed can be described satisfactorily

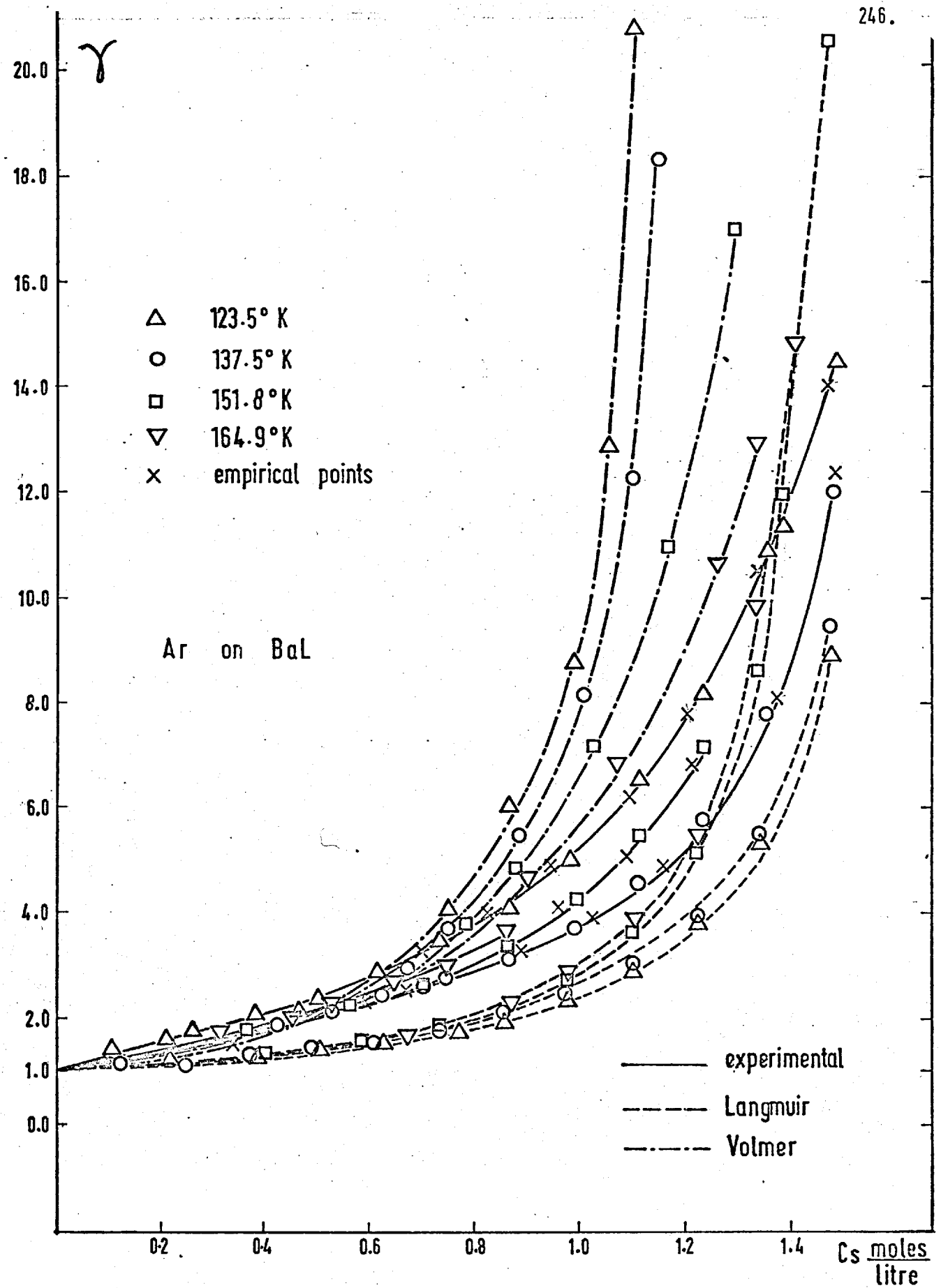

Fig. 110 TEST OF ISOTHERM MODELS

in terms of assumptions needed in deriving either Langmuir's or Volmer's isotherm(90). Numerous additional tests of ideal isotherm models on zeolites(92,19,18) carried out up to now emphasize this point.

SUMMARY

1. Synthesis and crystallographic aspects. Well crystalline zeolite L has been synthesised and it has been shown that this crystallisation from gels occurs best in the presence of K^+ free of Na^+. A repeated co-crystallisation of erionite, offretite and L has been observed and explained in terms of the common structural units which are 11-hedral cancrinite cages and hexagonal prisms. Proof of the epitaxy of L and offretite and the intergrowth of erionite and offretite was obtained by electron diffraction of selected areas.

A clear distinction between erionite and offretite was demonstrated by means of the X-ray powder techniques. As this method is the most common for zeolite identification, the above distinction is of considerable practical importance.

2. Exchange behaviour. Limited exchange was found at room temperature on zeolite L and on erionite (ER), namely 31-34% for L and 45% for ER. Consideration of this in relation to earlier work(11,14) demonstrated differences in exchangeability of distinct cation sites in the structure. On the basis of the ion-exchanged and adsorption results for Ar on K-ER and Na-ER, a suggested distribution per unit cell is: four cations in the four cancrinite cages and five cations near the eight-membered rings in the two large 23-hedral cavities.

The extent of ion-exchange for NH_4^+ was found to be more than twice as great as for the other investigated cations.

3. Thermal stability. DTA investigations distinguished two types of zeolitic water in forms containing small alkali metal cations or polyvalent cations. The TGA curves of HL and LiL showed weight losses (attributed to dehydroxylation) continuing up to temperatures as high as 1000°C. For these samples peculiarities in adsorption properties were found which may be related to the above behaviour on heating.

For ion-exchanged forms of L, the a and c lattice constants showed maximum and minimum values respectively at 200°C. At

550°C the constants were then found to regain their room temperature values, with the exception of HL and LiL. Drastic alteration of the powder line intensities was also observed in the same temperature interval. The migration and loss of the water has been suggested as a main reason for the extreme values of a and c constants at 200°C.

For erionite, heating and outgassing was found to result in contraction in the a and expansion in the c dimension together with an overall contraction of the unit cell volumes. Also at about 200°C drastic alterations of both position and intensity of the powder lines were observed.

The water migration and loss was found to affect in all three zeolites the 100 and 110 reflections.

Structural analysis on BaL has shown Ba^{++} to be positioned, like K^{+} on KL(11), at 0, 0.303, 0 at room temperature in the hydrated state, whereas at high temperature (550°) and after dehydration, the position 0.19, 0.38, 0 was occupied. The importance of rates of cooling after outgassing is a practical implication of the above finding.

4. Sorption Properties. Adsorption of Ar at 77.3°K on all ion-exchanged forms of L showed the following sequence of saturation capacities per unit cell.

$$NaL > KL > LaL > HL > BaL > LiL > CsL$$

The water content per unit cell was found to follow the order

$$LiL > HL > LaL > BaL > NaL > CsL \geqslant KL$$

and the order of the above saturation capacities could not, therefore, be related to the free volume in the structure found on the basis of the water content. Micropore volumes of the sorbents, estimated using Dubinin's method, were in the sequence

$$NaL > LaL > KL > BaL > HL > LiL > CsL$$

and thus relate well to the saturation capacities of Ar observed.

Argon adsorption at 77.3°K on ion-exchanged erionite showed strong dependence on cation size - Na-ER vigorously sorbed Ar whereas K-ER did not sorb this gas at all. Molecular sieving separation of rare and permanent gases on exchanged forms of ER was not achieved as Na-ER included Xe, whereas K-ER rejected even O_2.

The isosteric heats of Kr showed stronger sorbent-sorbate interaction in cases of H-OFF and H-ER, than in HL. This was attributed to the narrower channels in offretite (and cavities in ER) than in L.

The initial isosteric heats, q_{st}, of Kr, for all ion-exchanged forms of L were similar, but differed for HL, H-ER and H-OFF. Different variations of q_{st} with amount sorbed were observed for all the exchanged forms of L towards Kr and for NaL, KL and BaL - towards Ar and Xe. The sorbate/framework interaction was considered to be the determining factor for the initial isosteric heats and the sorbate-cation interaction - for the apparent heterogeneity. Thermodynamic equilibrium constants for the distribution of Kr between the gas phase and the crystals were estimated. Standard energies of sorption of Kr were similar for all L sorbents ($3.7—3.6 \frac{k\ cal}{mole}$) but different for HL, H-ER and H-OFF.

The adsorption isotherms could not be expressed in terms of equations based on idealised models. Empirical equations were, however, found which satisfactorily described the measured isotherms, taking Kr on KL, BaL and LaL as examples. The successful equations had the form

$$K = \frac{C_s}{p} \exp\ (2A_1C_s + \frac{3}{2}A_2C_s^2 + \frac{4}{3}A_3C_s^3 + \ldots .)$$

where the A's depend on temperature and on the gas-sorbent system, but not on concentration.

REFERENCE

1. Deer, W.A. et al, "Rock forming Minerals" Vol.4, J. Wiley & Sons Ltd. 1963.
2. Smith, J.V., Min. Soc. of America, Special paper N:1, 1963.
3. Barrer, R.M., Chem. & Industry, p.1203, 1968.
4. Mercer, B.W., U.S. Atomic Energy Comm. Docum. H-W-6676, 1960.
5. Barrer, R.M., British Chem. Eng., p.1, Issue May 1959.
6. Meier, W.M., Mol. Sieve Conf., S.C.I., London, 1967.
7. Linde Air Prod. Co., Techn. Inform. on Linde Sieves as Desicants and on Drying Gases and Liquids.
8. Venuto, P.B. & Landis, P.S., Adv. in Cat., 18, 259, 1968.
9. Kerr, I.S. & Williams, D.J., Acta Christ. Vol.B, part 6, 1969.
10. Barrer, R.M., Proc. Roy. Soc., A167, 392, 1938.
11. Barrer, R.M. & Villiger, H., Z. Krist; 128, p.352, 1969.
12. Bennet, J.M. & Gard, J.A., Nature, Vol.214, No.3, p.1005, 1967.
13. Staples, L.W. & Gard, J.A., Min. Mag., Vol.32, No.247, p.261, 1969.
14. Gard, J.A. et, Bennet, J.M. & Ingram, L., in preparation.
15. Breck, D.W. & Acara, N., Union Carb. Co., British P.909264; 1960.
16. Barrer, R.M. & Marshal, D.J., J. Chem. Soc., p.2296, 1964.
17. Zdanov, S.P., Isv. Akad. Nauk, Ser. Khim., No.6, p.950, 1965.
18. Barrer, R.M. & Lee, A., Surf. Science, 12, p.354, 1968.
19. Barrer, R.M. & Kanellopoulos, J. Chem. Soc., A, p.765, 1970.
20. Eakle, A.S., Amer. J. Sci. p.66, 1898.
21. Gonnard, M.F., C.R. Acad. Sci (Paris), 111, p.1002, 1890.
22. Deffeyes, K.S. Amer. Miner., 44, p.501, 1959.
23. Durrfield, V., Z. Krist. Miner., 49, p.200, 1911.
24. Hey, M.A. & Fejer, E.E. Miner. Mag., 33, p.66, 1962.
25. Harada, K., Amer. Miner., 52, p.1787, 1967.
26. Sheppard, R.A. & Gude, A.J., Am. Miner., 54, p.875, 1969.
27. Eberly, P.E., Amer. Miner., 49, p.30, 1964.
28. Peterson, D.L. et al, J. Phys. Chem. Sol., 26, p.835, 1965.
29. Barrer, R.M. & Peterson, D.L., J. Phys. Chem., 63, p.3427, 1964.
30. Eberly, P.E., Industry & E.C. Prod. Res. & Dev., 8, 2, p.140, 1969.
31. Ames, L.L., Amer. Miner., 47, p.1317, 1962.
32. Ames, L.L., Amer. Miner., 46, p.1120, 1961.

33.Breck,D.W.&Acara,N.A.,Union Carb.Co.,U.S.P.2950952,1960.
34.Zdanov,S.P.,Izv.Akad.Nauk BSSR,Ser.Khim.,1,p.44,1966.
35.Nikolina,V.&Knysh,L.,Ukr.Khim.Zhurn.,4,p.355,1969.
36.Pigusova,L.I.et al,Izv.Akad.Nauk BSSR,Ser.Khim.,1,p.59,1966.
37.Shirinskaya,L.P.et al,Dokl.Akad.Nauk,BSSR,10,12,1966.
38.Shirinskaya,L.P.et al,Dokl.Akad.Nauk,BSSR,13,4,p.330,1969.
39.Levina,C.A.et al,Dokl.Akad.Nauk,BSSR,12,50,p.908,1968.
40.Zdonov,S.P.et al, Dokl.Akad.Nauk SSSR,166,5,p.1107,1967.
41.Sherry,H.S.,Conf.on Ion-Exchange,S.C.I.,London,1969.
42.Barrer,R.M.& Cole J.F.,Interface Sci.,21,p.415,1966.
43.Bunn,C.W.,"Chem.Cryst",Oxford Univ.Press,1961.
44.Burger,M.J.,"X-ray Cryst.",J.Wiley & Sons,1958.
45.Pinsker,Z.G.,"Electron Diffraction",Chap.5,Butterworth,1953.
46.Gard,A.J.Thesis,Univ.of Aberdeen,1954.
47.Hirsch,P.B.et al,"Elect.Micr.Study of Thin Cryst.,Butterworth, 1965.
48.Burger,M.J."The precession method in X-ray Cryst."Ch.3, J.Wiley & Sons,1964.
49.Kerr,I.S.,Lect.on Electron Diffr.,Private communication.
50.James,R.W.,"X-ray Cryst.",Methuen & Co.,1953.
51.Barrer,R.M.,Endeavour,23,90,p.122,1964.
52.Meier,W.M.,Z.Kristal.,113,430,1960.
53.Fisher,K.,Amer.Miner.,48,p.664,1963.
54.Breck,D.W.,J.Chem.Educ.,41,p.678,1964.
55.Broussard,L.&Shoemaker,D.P.,J.Amer.Chem.Soc.,82,1041,1960.
56.Barrer,R.M.,Berichte Buns, Phys.Chem.,69,p.787,1965.
57.Uytterhoevan,J.B.et al,J.Phys.Chem.,Ithaca,65,2117,1965.
58.Rabo,J.A.et al, U.S.P. 3,130,006,1964.
59.McDaniel,C.V.&Meher,P.K.,Mol.Sieve Conf.,S.C.I.,London,1967.
60.Kerr,T.G.,J.Phys.Chem.,71,p.4155,1967.
61.Barrer,R.M.&Makki,M.B.,Can.J.Chem.,42,p.1481,1964.
62.Zdanov,S.P.&Egorova,E.H.,"Chem.ofZeol."p.103,"Nauka",1968.
63.Barrer,R.M.et al, J.Chem.Soc.,195,1959.
64. Breck,D.W. et al,J. Amer. Chem.Soc. 78,5965,1956

65.Rees,L.V.C.and Berry,T.,Mol.Sieve Conf.,S.C.I.,London,1967.
66.Barrer,R.M.&Langle,D.A.,J.Chem.Soc.,p.3804,1958.
67.Barrer,R.M.& Denny,P.J.,J.Chem.Soc.,p.971,1961.
68.Barrer,R.M.&Stuart,W.I.Proc.Roy.Soc., A,249,p.464,1959.
69.Neimark,E.A.,Izv.Akad.Nauk SSSR,Ser.Khim.,69,p.959,1965.
70.Koffman,L.S.et al,Izv.Akad.Nauk SSSR,Ser.Khim.,6,975,1965.
71.Batushviely,Akad.Nauk GSSR,Izv.Geol.Obz.Georgii,5,p.1,1967.
72.Barrer,R.M.& Sutherland,J.W.,Proc.Roy.Soc.,A,237,p.439,1956.
73.Picuzova,L.E.et al,"Sint.Zeolites",Akad.Nauk SSSR,1962.
74.Flanigen,E.(Union Carb.Co.) Private communication.
75.Barrer,R.M., Chem.in Britain, 3,p.380,1967.
76.Zdonov,S.P.& Ovsepian,M.E.,Dokl.Akad.Nauk SSSR,4,157,p.913, 1964.
77 Zdonov,S.P.,Mol.Sieve,Conf.S.C.I.,London,1967.
78.Breck,D.W.& Flanigen,E.M.,Mol.Sieves,Conf.S.C.I.,London,1967.
79.Alexander,J.,Coll.Chem.,Vol.4,Reinhold Publ.,1946.
80.Kerr,G.T.,J.Phys.Chem.,Ithaca,70,1047,1966.
81.Zdonov,S.P.et al,"Zeolites,syntheses,properties & application", Nauka,1965
82.Coombs,D.S.et al,Geoch.et Cosmoch.Acta,17,53,1959.
83.Barrer,R.M.& Baynham,J.W.,J.Chem.Soc.,562,2882,1956.
84.Coolidge,A.S.,J.Amer.Chem.Soc.,48,1785,1926.
85.Hill,T.L.,Advanc.Catalys.,4,212,1952.
86.Everett,D.H.,Trans.Far.Soc.,46,453,1950.
87.Garden,L.A.et al,Trans.Far.Soc.,51,1558,1955.
88.Hill,T.L.,J.Chem.Phys.,17,520,1949.
89.Brunauer,S.,"Phys.Adsorption of Gases",Princeton Press,1943.
90.Young,D.M.& Crowell.,A.D."Phys.Ads.of Gases",Butterworth,1962.
91.International Crit. Tables, McGraw-Hill Co.,1933.
92.Murphy,V.E.,Thesis,Phys.Chem.,I.C.,London.
93.Langmuir,I.,J.Amer.Chem.Soc.,40,1361,1918.
94.Langmuir,I.,J.Amer.Chem.Soc.,54,p.2798 (Nobel Lec.)1932.
95.Flood,E.A.,"The Solid-Gas Interface",E.Arnold Ltd.,1967.
96.Fowler,R.H.& Guggenhein,E.A.,"Stat.Therm"Univ.Press,1939.
97.Volmer,M.,Z.Phys.Chem.,115,253,1925.
98.Hill,T.L.,J.Chem.Soc.,14,44,1946.

99.Dubinin,M.M.,J.Coll.&Interf.Sci.,23,487,1967.
100.McBain,J.W."The Sorp.of Gases by Solids",Routl.&K.Panl,1932.
101.Barrer,R.M.,10th Colston Symposium,Butterworth,p.6,1958.
102.Polayi,M.,Verh.deut.phys.Ges.,15,55,1916.
103.Gladstone,S.,"Phys.Chem.",McMillan & Co.,1942.
104.London,F.,Z.Phys.Chem.,B11,222,1930.
105.Kirkwood,J.G. & Muller,A.,Proc.Roy.Soc.,A,154,634,1936.
106.London,F. & Polanyi,M.,Naturwisseuch.,18,1099,1930.
107.Boer,J,H.&Custer,J.F.H.,Z.Phys.Chem.,B25,225,1934.
108.Barrer,R.M.& Peterson,D.L.,Proc.Roy.Soc.A,280,466,1964.
109.Barrer,R.M.Gibbons,R.M.Trans.Far.Soc.,59,2569,1963.
110.Barrer,R.M.,Gibbons,R.M.,Trans.Far.Soc.,61,948,1965.
111.Nonius Company Manual for high temperature Guinier.
112.General Electric Co.Manual for powder diffractometry.
113.Duval,C.,"Inorg.Thermogr.Analyses",Elsvier Co.,1963.
114.Vogel,A.I."Quantitative Inorg.Anal.", Longmans,1958.
115.Colder,A.B.,"Photom.Method of Anal",A.Hiller,1969.
116.Bennett,H.& Hamley,W.C.,"Met.of Silic.Anal",B.Chem.Ass.,1958.
117.Sederov,E.E.,Geokimia,9,820,1963.
118.Sand,L.B.,"Mol.Sieves",Conf.S.C.I.,London, 1967.
119.Barrer,R.M.& Denny,P.J.,J.Chem.Soc.,p.983,1961.
120.Koizumi,M.& Roy,R.,J.Geolog.,68,41,1960.
121.Barrer,R.M.& White,E.A.D.,J.Chem.Soc.,1567,1952.
122.Ovsepian,M.E.&Zdanov,S.P.,Izv.Akad.Nauk,SSSR,Ser.Khim.,1, p.11,1965.
123.Langne,G., Handbook in Chem., McGraw & Co.,p.122,10th Edition
124.Conway,B.E."Electrochem.Data",Elsvier, 1952.
125.Kaye,G.W. & Laby,T.H. Tabl.ofPhys.&Chem.Const.,Longmans, p.177,1966.
126.Aiello,R.,Barrer,R.M.& Kerr,I.S., - in preparation.
127.Mainwaring, D.,Comp.Progr.DELKOR,Chem.,I.C.
128.Troughton,P., Comp.Progr.CDLS,Chem.I.C.
129.Cole,J.F.& Villiger,H.,Min.Mag.,37,p.300,1969.
130.ASTM, Powder diffraction file, 1968.
131.Cook,G.A.,"Argon,helium & rare gases",Interscience, 1961.

132."Handbook of Chem.&Physics",48th Edition,Chem.Rub.Co.,1967.
133.Dubinin,M.M. et al, Izv.Akad.Nauk SSSR,535,1958.
134.Brunauer,S.,Deming,L.S.et al,J.Amer.Chem.Soc.,62,1723,1940.
135.Gregg,S.J.&Sing,K.S."Ads.Surf.Area&Por"Acad.Press,1967.
136.Corles,P.E.Comp.Progr.BFPOL,CivilEng.,I.C.
137.Kisselev,A.V.et al,Trans.Far.Soc.,63,2051,1967.
138.Kerr,I.S.,Barrer,R.M.,Gard,A.J.&Galabova,I.M.,Amer.Miner.55,
April 1970.
139.Goldsmith,J.R.,J.Geol.,61,439,1953.
140.Aiello,R. Private communication.
141.Willman,H.,Proc.Phys.Soc.,A64,p.329,1951.
142.Kay,D.,"Tech.of Electr.Micr", Blackwell, 1961.

APPENDIX

ADSORPTION ISOTHERM DATA

Parameters used	Symbols	Accuracy
equilibrium temperature.	$T^{o}K$	$\pm$ 0.1^{o}K
equilibrium pressure in cm Hg.	Pcm Hg	$\pm$ 0.005cm Hg
uptake in cm^3 (S.T.P.) per gram of outgassed zeolite.	a cc/g.	$\pm$ 0.05cc/g.
uptake in number of molecules per unit cell of outgassed zeolite.	Nm/u.c.	$\pm$ 0.005m/n.c

Ar on HL at 77.3°K.

P cmHg	a cc/g	N m/u.c.
0.045	45.21	4.431
0.197	68.92	6.754
0.453	8.15	7.659
0.952	81.14	7.952
2.557	90.07	8.827
4.342	98.75	9.678
6.516	100.08	9.808
8.352	108.75	10.535
11.315	114.01	11.173
13.552	117.62	11.527
15.102	120.75	11.834
18.121	130.10	12.749
15.794	122.10	11.966
12.006	115.01	11.271
9.213	108.32	10.615
7.322	102.26	10.021
1.856	86.10	8.438
0.287	72.15	7.071
Ar on LiL at 77.2_8°K		
0.103	56.16	6.009
0.327	70.23	7.515
1.253	73.94	7.911
2.232	79.13	8.467
4.314	81.92	8.765
7.722	86.40	9.245
11.134	92.04	9.848
14.056	97.37	10.418
17.003	102.24	10.939
15.514	99.15	10.609
10.723	91.84	9.827

contd.

P cmHg	a cc/g	N m/u.c.
6.831	85.23	9.119
3.604	80.78	8.643
0.931	75.20	8.046
Ar on NaL at 77.3_1°K		
0.020	65.63	7.095
0.204	90.32	9.756
0.354	96.64	10.439
0.971	100.25	10.827
2.205	103.04	11.128
2.836	105.76	11.422
5.843	109.21	11.795
7.984	111.28	12.018
12.052	114.72	12.389
13.614	116.81	12.615
15.261	120.80	13.464
18.207	130.23	14.065
15.781	122.04	13.180
10.123	114.02	12.314
6.351	109.63	11.840
4.052	107.21	11.579
1.461	101.68	10.981
Ar on KL at 77.3°K		
0.023	42.37	4.661
0.068	76.42	8.352
0.173	85.22	9.374
0.431	88.41	9.724
1.220	94.02	10.342
3.413	100.03	11.003
8.321	105.60	11.616
11.134	111.21	12.233

contd.

P cmHg	a cc/g	N m/u.c.
13.252	113.36	12.469
16.204	118.10	12.991
18.207	122.81	13.509
13.940	114.04	12.544
9.216	107.63	11.839
5.513	102.24	11.246
2.353	97.20	10.693
0.781	91.28	10.041
Ar on CsL at 77.2$_7^0$K		
0.038	58.26	6.816
0.425	62.15	7.271
0.723	65.28	7.638
2.451	70.10	8.202
7.314	76.40	8.939
9.583	77.76	9.332
14.463	81.05	9.483
18.351	83.67	9.789
16.250	82.43	9.644
11.812	79.31	9.279
8.207	76.98	9.007
6.671	75.44	8.826
3.983	72.02	8.426
1.820	66.86	7.823
0.152	60.96	7.132
Ar on BaL at 77.2$_6^0$K		
0.010	49.34	5.793
0.070	70.31	9.315
0.163	80.45	9.332
0.460	84.48	9.799

contd.

P cmHg	a cc/g	N m/u.c.
0.823	88.40	10.254
1.212	90.34.	10.475
2.551	95.26	11.050
4.724	98.85	11.467
7.682	100.20	11.623
11.670	102.56	11.897
17.231	108.16	12.547
13.923	104.96	12.175
8.423	100.61	11.671
3.671	96.24	11.164
1.576	92.48	10.728
0.625	86.48	10.032
Ar on LaL at 77.3$_2^0$K		
0.065	89.35	10.365
0.263	92.43	10.722
0.914	97.26	11.282
3.422	103.28	11.980
7.264	106.00	12.296
9.843	107.20	12.435
12.860	109.04	12.649
17.811	114.42	13.273
18.434	119.36	13.846
15.412	111.10	12.888
11.863	108.32	12.565
9.220	107.60	12.482
5.061	104.64	12.138
2.074	100.48	11.656
0.532	95.60	11.089

Ar on H-ER at $77.3_3^{\circ}K$ contd.

P cmHg	a cc/g	N m/u.c.
0.023	87.32	8.557
0.152	111.22	10.897
0.713	117.10	11.758
1.620	122.91	12.045
3.124	126.40	12.387
6.262	130.12	12.752
9.251	131.21	12.886
12.314	132.92	13.026
14.662	134.24	13.155
17.414	136.15	13.343
19.703	140.33	13.752
18.614	137.15	13.441
15.631	134.72	13.203
12.822	132.94	13.028
7.113	130.72	12.811
3.814	128.16	12.559
1.182	120.65	11.824
Ar on Na-ER at $77.2_7^{\circ}K$		
0.057	82.13	8.706
0.160	106.10	11.247
0.663	111.12	11.779
2.052	116.73	12.373
4.351	120.11	12.732
7.321	122.50	12.985
9.473	123.76	13.119
14.920	126.22	13.379
17.382	127.15	13.478
19.524	131.32	13.919
18.156	126.91	13.452
12.731	124.85	13.234
8.735	123.20	13.059
5.483	120.75	12.799
2.562	118.31	12.540
1.352	115.15	12.206
Ar on H-OFF at $77.3_2^{\circ}K$		
0.030	68.53	3.426
0.123	111.54	5.577
0.514	121.20	6.060
0.881	127.24	6.362
1.674	134.63	6.731
2.156	137.16	6.705
3.718	141.13	7.056
5.982	143.72	7.186
8.916	146.24	7.312
11.301	148.05	7.403
15.723	150.03	7.501
19.464	156.93	7.846
19.133	152.80	7.640
12.126	148.63	7.431
7.463	145.21	7.261
5.135	143.06	7.153
1.272	131.15	6.558
0.231	115.24	5.762

Ar on K-ER at 77.3_4 °K.

P cmHg	a cc/g	N m/u.c.
0.612	3.20	0.342
1.863	5.56	0.594
2.581	7.13	0.763
5.914	9.53	1.020
9.631	10.98	1.175
14.623	11.06	1.183
18.547	11.63	1.244
19.630	12.12	1.497
20.153	23.60	2.525
19.063	11.08	1.186
15.257	11.00	1.177
11.753	10.99	1.176
7.718	10.56	1.130
3.894	8.51	0.911
1.103	4.62	0.494

Ar on NaL at 127.9°K contd.

P cmHg	N m/u.c.
0.231	1.045
0.456	1.837
0.682	2.372
1.925	3.489
3.012	4.172
4.869	5.021
9.348	5.846
17.399	6.783
27.620	7.513
43.353	8.194
48.971	8.249
38.970	8.001
21.216	7.099
13.062	6.308
7.892	5.634
4.694	4.816
1.664	3.023
Ar on NaL at 145.5°K	
0.380	0.456
0.947	0.915
2.047	1.823
2.613	2.187
3.734	2.785
6.562	3.825
7.282	4.047
14.380	5.205
23.016	6.007
37.968	6.954
49.158	7.381
33.716	6.701

contd.

P cmHg	N m/u.c.
19.759	5.736
10.266	4.641
4.642	3.163
1.367	1.312
Ar on NaL at 162.0°K	
0.302	0.153
0.487	0.248
3.006	1.201
5.941	1.797
12.420	2.846
20.518	3.804
30.416	4.759
43.730	5.697
50.031	6.052
40.615	5.499
27.860	4.501
14.956	3.241
8.164	2.212
1.783	0.681
Ar on NaL at 176.9°K	
0. 526	0.122
0.889	0.207
2.433	0.335
4.386	0.586
6.884	0.866
10.701	1.301
16.130	1.803
27.264	2.806
42.399	3.980
33.265	3.251

contd.

P cmHg	N m/u.c.
19.963	2.163
13.262	1.509
5.484	0.711
3.408	0.417
Ar on NaL at 189.7°K	
0.386	0.032
1.480	0.118
6.289	0.487
13.837	0.963
19.937	1.271
28.316	1.764
44.083	2.503
38.308	2.261
24.993	1.578
9.867	0.701
3.386	0.287
Ar on NaL at 195.0°K	
0.938	0.041
2.011	0.087
7.487	0.249
18.003	0.579
22.468	0.711
34.103	0.993
45.780	1.205
40.583	1.092
29.497	0.871
11.751	0.356
4.385	0.172

Kr on NaL at 130°K

P cmHg	N m/u.c.
0.011	4.551
0.312	6.150
1.140	6.807
5.162	7.786
7.345	8.043
13.334	8.513
19.448	8.799
29.780	9.149
41.612	9.487
52.496	9.708
39.009	9.372
21.392	8.871
15.050	8.610
10.554	8.311
4.268	7.534

Kr on NaL at 144.8°K

0.050	2.352
0.357	3.994
0.866	5.332
3.302	6.573
7.885	7.266
10.093	7.430
19.963	7.921
28.990	8.203
45.162	8.625
52.230	8.832
40.855	8.527
22.162	7.996
14.702	7.762
6.024	7.031
1.705	5.903

Kr on NaL at 153.6°K

P cmHg	N m/u.c.
0.015	1.352
0.341	2.771
1.205	4.619
4.155	6.148
10.136	6.989
18.416	7.409
26.035	7.683
40.322	7.993
51.329	8.303
32.381	7.811
19.327	7.416
12.943	7.129
7.480	6.678
1.586	5.085

Kr on NaL at 163.7°K

0.342	1.943
0.825	2.963
1.713	3.802
3.825	4.902
11.703	6.301
19.008	6.812
31.938	7.287
44.512	7.609
40.512	7.501
25.003	7.008
13.337	6.411
6.296	5.597
2.382	4.354
1.052	3.387

Kr on NaL at 175.2°

P cmHg	N m/u.c.
0.397	0.738
0.867	1.505
2.487	3.064
5.508	4.175
7.050	4.645
12.700	5.410
18.823	5.973
25.832	6.289
42.585	6.720
33.310	6.502
20.398	6.130
15.061	5.730
9,351	4.989
3.656	3.629
1.322	2.165

Kr on NaL at 186.2°K

0.497	0.454
1.192	1.030
3.015	2.094
6.776	3.473
11.416	4.336
16.995	5.007
27.845	5.683
42.530	6.299
34.170	5.949
24.517	5.452
13.339	4.654
8.853	3.843
4.556	2.772
1.607	1.315

Kr on NaL at 195.3°K contd.

P cmHg	N m/u.c.
1.018	0.572
4.545	1.823
7.266	2.546
12.700	3,403
17.020	3.991
24.524	4.485
42.275	5.355
37.497	5.132
29.312	4.709
14.988	3.738
9.685	2.894
5.061	1.982
2.990	1.358

Kr on NaL at 209.7°K

P cmHg	N m/u.c.
0.430	0.150
1.391	0.392
3.100	0.704
8.067	1.652
14.546	2.428
26.865	3.647
41.644	4.622
51.101	4.948
33.742	4.105
19.902	3.074
10.188	1.967
5.503	1.183

Xe on NaL at 169.4°K

P cmHg	N m/u.c.
0.092	1.475
0.158	3.136
0.783	4.256
3.822	5.291
5.410	5.498
10.717	6.065
14.141	6.313
26.300	6.784
44.103	7.256
47.539	7.463
31.711	6.963
18.006	6,498
7.595	5.785
1.769	4.708

Xe on NaL at 181.0°K

P cmHg	N m/u.c.
0.236	1.962
0.551	2.901
0.892	3.551
1.867	4.160
4.238	4.763
8.943	5.208
12.620	5.457
20.075	5.747
32.513	6.034
44.142	6.377
50.840	6.566
36.314	6.118
24.810	5.881
16.864	5.671
6.095	4.932
2.783	4.396

Xe on NaL at 207.5°K

P cmHg	N m/u.c.
0.391	1.573
0.907	2.759
1.961	3.604
4.668	4.280
10.559	4.695
13.371	4.829
22.972	5.087
44.521	5.448
42.619	5.398
29.088	5.236
17.736	4.948
8.559	4.598
3.527	4.064

Xe on NaL at 223.2°K

P cmHg	N m/u.c.
0.431	0.810
0.818	1.346
1.012	2.067
1.894	2.437
2.315	2.962
6.474	3.887
7.800	4.018
15.791	4.505
26.100	4.770
37.919	4.930
47.133	5.069
44.496	5.031
33.298	4.878
20.647	4.624
10.972	4.257
3.720	3.308

Xe on NaL at 239.2°K

P cmHg	N m/u.c.
1.015	0.751
2.697	1.701
6.909	2.953
9.166	3.387
14.022	3.808
17.556	3.998
29.681	4.307
43.615	4.624
36.758	4.470
26.215	4.243
11.330	3.578
4.432	2.390
2.135	1.378

Xe on NaL at 258.1°K

P cmHg	N m/u.c.
1.510	0.464
3.015	0.826
5.253	1.437
6.908	1.756
11.115	2.433
13.447	2.698
16.868	2.974
27.953	3.508
45.112	3.985
33.154	3.706
21.178	3.269
16.278	2.914
9.142	2.171
4.656	1.301

Xe on NaL at 273.6°K

P cmHg	N m/u.c.
1.226	0.233
5.117	0.862
8.025	1.295
18.002	2.235
25.528	2.758
35.862	3.127
46.146	3.453
43.035	3.361
32.110	2.988
12.263	1.770
6.717	1.086
2.699	0.479

Ar on KL at 124.4°K

P cmHg	N m/u.c.
0.283	1.381
0.451	2.104
0.937	2.924
1.135	3.271
2.838	4.520
3.399	5.081
5.610	5.658
10.641	6.503
21.323	7.435
37.750	8.126
46.589	8.383
41.128	8.214
29.295	7.798
14.472	6.983
6.290	5.768
4.511	5.322
2.368	4.098
0.623	2.452

Ar on KL at 145.2°K

P cmHg	N m/u.c.
0.692	0.457
1.524	0.864
2.514	1.508
4.492	2.557
5.518	2.883
10.431	4.194
14.078	4.856
23.714	5.919
37.126	6.827
46.308	7.115
42.163	6.989
32.586	6.521
16.523	5.109
7.331	3.429
3.416	2.053
0.879	0.654

Ar on KL at 158.4°

P cmHg	N m/u.c.
0.634	0.251
1.513	0.478
2.035	0.719
3.374	0.915
6.318	1.792
8.924	2.393
11.887	2.907
14.718	3.407
19.049	4.012
25.011	4.649
34.253	5.410
44.004	5.907
40.723	5.751
31.921	5.198

contd.

P cmHg	N m/u.c.
22.732	4.347
10.979	2.796
4.513	1.358
Ar on KL at 169.4°K	
1.853	0.304
3.314	0.551
5.013	0.816
6.924	1.102
8.518	1.368
11.217	1.652
16.313	2.261
22.918	2.958
32.813	3.882
44.409	4.643
39.382	4.372
28.516	3.487
21.269	2.752
13.342	1.879
9.138	1.416
4.326	0.708
Ar on KL at 188.4°K	
1.387	0.124
3.291	0.197
6.207	0.384
8.213	0.468
11.264	0.659
17.892	1.012
29.412	1.684
39.579	2.139
45.612	2.412

contd.

P cmHg	N m/u.c.
43.264	2.268
34.627	1.873
25.534	1.402
14.121	0.798
9.621	0.507
4.692	0.279
Ar on KL at 176.9°K	
0.795	0.063
1.623	0.185
2.908	0.338
4.491	0.465
10.825	1.031
19.685	1.685
32.863	2.638
43.915	3.189
48.418	3.411
38.641	2.973
28.046	2.315
13.703	1.277
7.315	0.739
2.248	0.263
Kr on KL at 132.9°K	
0.112	2.453
0.205	3.385
0.815	5.003
1.860	5.891
7.191	6.809
10.488	7.081
14.878	7.498
19.489	7.686

contd.

P cmHg	N m/u.c.
29.218	8.005
42.639	8.364
49.125	8.667
38.846	8.314
27.830	7.971
19.160	7.623
12.625	7.358
4.870	6.599
Kr on KL at 160.9°K	
0.118	0.488
0.224	1.108
0.520	1.596
0.613	2.317
1.328	3.433
4.127	5.128
5.612	5.552
10.672	6.209
17.450	6.688
28.235	7.202
46.240	7.739
40.053	7.508
25.441	7.081
13.307	6.456
7.789	5.889
1.921	4.082
0.838	2.869
Kr on KL at 177.3°K	
0.338	0.385
0.674	0.758
2.471	2.196

contd.

P cmHg	N m/u.c.
3.869	2.978
8.306	4.253
11.119	4.879
16.609	5.325
25.893	5. 98
43.151	6.429
34.371	6.281
24.370	5.802
16.165	5.301
6.188	3.831
1.382	1.153
Kr on KL at 192.3°K	
0.924	0.678
1.638	0.849
2.641	1.249
3.713	1.622
6.122	2.412
8.197	2.783
13.386	3.685
17.987	4.203
26.627	4.938
41.526	5.759
34.819	5.407
24.624	4.783
16.868	4.063
11.321	3.387
5.316	2.066
Kr on KL at 209.6°K	
0.628	0.287
1.623	0.537
3.128	0.859

contd.

P cmHg	N m/u.c.
5.521	1.367
6.673	1.613
10.718	2.276
13.821	2.681
19.986	3.278
26.612	3.806
33.768	4.261
46.119	4.913
42.561	4.723
34.896	4.288
24.619	3.652
16.937	3.006
8.322	1.863
4.113	1.062
Kr on KL at 221.7°K	
1.300	0.263
5.016	0.859
9.050	1.488
11.962	1.832
15.931	2.178
22.583	2.716
32.200	3.436
45.325	4.038
51.279	4.444
40.827	3.865
29.538	3.198
20.686	2.513
13.970	1.985
6.744	1.175
3.408	0.666

Xe on KL at 169.3°K

P cmHg	N m/u.c.
0.109	2.273
0.260	3.366
2.504	4.478
7.205	5.053
11.070	5.352
24.964	5.938
45.857	6.599
35.280	6.335
19.015	5.789
9.423	5.254
5.107	4.849
0.858	3.716
Xe on KL at 180.5°K	
0.120	1.561
0.295	2.527
2.568	3.687
8.282	4.664
18.019	5.189
21.795	5.482
27.246	5.625
45.126	6.095
49.970	6.212
38.900	5.898
24.258	5.454
12.281	4.915
5.534	4.297
1.008	3.041
Xe on KL at 199.2°K	
0.059	0.407
0.133	0.879
0.312	2.005

contd. -

P cmHg	N m/u.c.	P cmHg	N m/u.c.	P cmHg	N m/u.c.
0.830	2.780	Xe on KL at 226.6°K		Xe on KL at 273.4°K	
3.280	3.578	0.735	0.487	1.177	0.133
4.579	3.803	1.470	0.879	2.292	0.226
7.291	4.197	2.006	1.343	4.995	0.506
9.330	4.375	4.495	2.296	10.759	1.138
18.025	4.583	7.701	2.798	15.345	1.555
29.681	4.818	11.019	3.095	23.000	2.045
46.665	4.978	15.421	3.367	30.297	2.351
37.596	5.946	23.485	3.588	44.024	2.713
23.315	4.721	31.790	3.748	33.725	2.451
12.211	4.431	42.613	3.901	20.112	1.962
5.705	3.968	48.742	3.938	13.227	1.374
2.058	3.217	39.240	3.863	7.472	0.813
0.632	2.372	24.225	3.636	Ar on BaL at 123.5°K	
Xe on KL at 210.9°K		14.109	3.301	0.221	1.294
0.412	1.018	5.680	2.498	0.485	3.051
0.561	1.289	2.735	1.658	0.623	3.614
1.036	1.705	Xe on KL at 258.3°K		1.674	5.153
2.516	2.501	1.160	0.247	1.803	5.614
4.017	3.021	3.008	0.635	2.312	6.005
6.372	3.442	4.572	0.925	5.247	6.861
10.215	3.798	5.575	1.066	7.473	7.382
15.418	4.052	11.344	1.878	13.105	7.955
23.841	4.236	14.429	2.124	20.350	8.352
30.692	4.397	22.821	2.634	29.968	8.573
46.401	4.572	40.755	3.198	45.895	8.789
39.723	4.521	32.308	2.971	36.626	8.695
34.214	4.446	18.175	2.343	25.559	8.497
22.342	4.203	8.118	1.431	18.926	8.321
13.226	3.946	2.290	0.491	9.851	7.693
5.467	3.283			4.367	6.650
1.623	2.145			0.805	4.562

Ar on BaL at 137.6°K contd.

P cmHg	N m/u.c.
0.142	0.302
0.315	0.657
0.867	1.458
1.232	1.845
1.712	2.411
2.341	2.956
3.608	3.862
5.211	4.492
7.403	5.158
9.526	5.592
12.410	5.961
18.233	6.591
31.187	7.115
44.512	7.487
37.794	7.283
26.789	6.976
14.526	6.212
10.918	5.812
5.896	4.743
2.671	3.228
Ar on BaL at 151.8°K	
0.393	0.328
1.214	0.774
1.803	1.090
2.987	1.549
3.801	2.087
6.612	2.864
10.589	3.678
12.018	3.942
13.426	4.109
18.392	4.610
24.610	5.066
29.609	5.382
44.748	6.042
41.583	5.848
35.096	5.587
27.248	5.229
19.396	4.698
14.728	4.262
8.811	3.418
5.419	2.591
Ar on BaL at 164.9°K	
0.965	0.239
1.870	0.451
3.477	0.919
4.758	1.205
8.979	2.018
11.758	2.467
14.607	2.701
19.163	3.098
23.928	3.394
35.326	3.864
46.785	4.372
38.240	4.022
31.008	3.712
20.798	3.190
10.545	2.271
6.222	1.593
2.310	0.643
Ar on BaL at 172.0°K	
0.772	0.195
2.381	0.438
3.326	0.568
5.607	0.891
6.610	1.036
9.615	1.357
18.967	2.195
30.984	2.907
44.515	3.585
40.003	3.386
33.448	3.125
24.283	2.503
13.844	1.696
8.623	1.232
4.364	0.730
Ar on BaL at 185.8°K	
0.941	0.079
2.954	0.210
4.281	0.321
8.325	0.604
12.629	0.863
19.783	1.250
28.321	1.681
43.172	2.384
50.000	2.724
40.518	2.235
26.273	1.574
18.662	1.184
10.104	0.731
6.057	0.451

Ar on BaL at 193.2°K

P cmHg	N m/u.c.
0.922	0.071
3.062	0.155
6.496	0.358
11.515	0.665
15.872	0.828
24.010	1.216
35.314	1.586
47.503	2.045
44.938	1.838
27.915	1.350
19.548	1.025
9.209	0.503
4.463	0.256

Kr on BaL at 134.5°K

P cmHg	N m/u.c.
0.108	2.510
0.245	4.244
0.316	4.861
0.506	5.714
0.892	6.420
1.626	6.789
4.154	7.410
4.897	7.506
12.859	7.943
23.321	8.235
37.521	8.402
45.643	8.466
42.934	8.418
33.033	8.397
18.422	8.125
8.725	7.778
2.170	6.889

Kr on BaL at 140.3°K

P cmHg	N m/u.c.
0.168	1.864
0.333	3.750
0.512	5.321
1.328	6.163
4.780	6.899
6.658	7.127
12.744	7.497
19.836	7.718
36.968	8.093
50.738	8.231
40.326	8.056
32.127	7.923
16.266	7.642
9.232	7.330
2.089	6.391

Kr on BaL at 162.3°K

P cmHg	N m/u.c.
0.318	1.341
0.754	2.833
1.920	4.277
2.368	4.736
3.614	5.462
6.750	6.037
10.600	6.496
13.923	6.693
22.618	6.976
28.348	7.119
44.088	7.333
35.565	7.292
20.043	6.903
8.750	6.360
5.163	5.843
0.986	3.659

Kr on BaL at 177.0°K

P cmHg	N m/u.c.
0.635	1.045
1.578	1.943
2.615	2.684
4.834	3.765
5.421	4.036
11.425	5.097
18.233	5.642
32.284	6.193
39.315	6.350
43.726	6.419
48.437	6.589
42.103	6.398
30.580	6.121
15.042	5.433
7.928	4.638
3.284	3.082
1.347	1.507

Kr on BaL at 182.7°K

P cmHg	N m/u.c.
0.280	0.274
0.659	0.683
0.927	0.926
1.155	1.188
2.309	1.931
3.246	2.442
6.781	3.687
8.006	3.915
14.160	4.813
20.053	5.281
30.013	5.632
44.523	5.916
47.120	6.020
41.612	5.903

contd.

P cmHg	N m/u.c.
27.340	5.551
17.826	5.092
11.279	4.496
4.066	2.829
1.978	1.584
Kr on BaL at 190.4°K	
0.624	0.531
1.707	1.087
3.784	1.856
4.863	2.265
7.795	2.885
11.520	3.464
15.823	3.917
25.587	4.712
29.256	4.916
44.500	5.459
40.830	5.371
26.293	4.772
21.485	4.402
8.970	3.076
5.896	2.485
2.520	1.384
Kr on BaL at 194.6°K	
0.598	0.292
1.628	0.787
2.549	1.109
3.760	1.507
5.777	2.144
9.418	2.838
10.869	3.115

contd.

P cmHg	N m/u.c.
15.136	3.527
19.527	3.974
24.760	4.327
36.450	4.908
44.370	5.113
38.753	4.987
29.819	4.640
18.082	3.758
13.015	3.312
7.530	2.452
4.067	1.632
Kr on BaL at 209.3°K	
1.327	0.309
2.781	0.696
4.892	1.123
6.810	1.472
8.929	1.743
11.821	2.126
13.806	2.359
18.017	2.706
24.811	3.172
33.221	3.723
49.597	4.530
43.278	4.163
36.812	3.862
26.614	3.327
21.138	2.943
15.816	2.548
10.372	1.958
3.077	0.773

P cmHg	N m/u.c.
Xe on BaL at 171.2°K	
0.054	2.437
0.126	3.999
0.292	4.234
0.783	4.672
1.637	5.058
3.716	5.462
9.432	5.799
19.560	6.141
27.729	6.332
41.635	6.605
48.981	6.712
38.780	6.527
25.416	6.317
13.643	5.983
6.360	5.645
2.265	5.217
0.348	4.486
Xe on BaL at 181.5°K	
0.186	2.364
0.318	3.725
1.682	4.672
2.997	4.993
7.635	5.507
9.850	5.632
21.765	5.962
32.007	6.094
43.915	6.234
47.805	6.286
40.724	6.197

contd.

P cmHg	N m/u.c.
31.308	6.083
14.281	2.786
5.613	5.348
0.503	4.048
Xe on BaL at 199.3°K	
0.163	1.736
0.399	2.787
0.963	3.963
2.856	4.478
6.130	4.904
12.253	5.211
25.462	5.399
46.862	5.492
44.356	5.468
32.067	5.403
19.874	5.324
7.664	5.008
4.392	4.761
1.640	4.236
Xe on BaL at 204.9°K	
0.335	1.739
0.604	3.038
0.935	3.562
2.219	4.141
3.810	4.486
7.780	4.836
11.130	4.997
18.135	5.139
23.126	5.206
33.495	5.309
50.840	5.416

contd.

P cmHg	N m/u.c.
44.524	5.327
41.658	5.272
26.277	5.236
14.305	5.075
4.438	4.575
1.213	3.821
Xe on BaL at 223.1°K	
0.342	0.924
1.031	1.431
1.836	2.294
2.298	2.642
4.579	3.594
7.880	4.045
12.293	4.301
21.215	4.531
34.190	4.640
43.513	4.723
39.858	4.691
27.161	4.614
15.525	4.394
9.845	4.186
5.744	3.812
3.430	3.217
1.405	1.888
Xe on BaL at 239.2°K	
0.965	0.463
1.180	0.847
1.738	1.389
3.423	2.197
5.114	2.782
9.077	3.352

contd.

P cmHg	N m/u.c.
16.980	3.976
27.091	4.298
42.564	4.423
33.975	4.374
21.316	4.154
14.037	3.782
6.782	3.031
3.702	2.303
2.360	1.720
1.523	1.059
Xe on BaL at 258.3°K	
0.975	0.315
3.158	0.913
6.212	1.552
7.465	1.778
14.550	2.659
22.919	3.095
35.236	3.430
43.311	3.495
40.928	3.468
28.229	3.296
17.715	2.833
12.112	2.398
4.770	1.264
1.772	0.532
Xe on BaL at 273.2°K	
1.153	0.165
2.655	0.429
4.596	0.695
6.425	0.973
11.520	1.587

contd.

P mHg	N m/u.c.
14.158	1.862
21.327	2.387
26.175	2.608
42.515	3.075
36.410	2.976
18.544	2.187
8.701	1.298
3.133	0.510
Kr on HL at 142.5°K	
0.065	1.748
0.213	2.380
0.441	2.883
0.910	3.411
1.823	3.794
2.075	3.902
3.685	4.470
7.765	4.956
15.550	5.399
21.030	5.587
31.110	5.863
44.517	6.019
48.472	6.181
35.134	5.904
24.213	5.687
11.458	5.190
4.974	4.526
3.567	4.167
Kr on HL at 161.7°K	
0.374	0.712
0.662	1.306
1.099	1.694

contd.

P cmHg	N m/u.c.
1.354	2.182
2.110	2.684
4.064	3.305
6.027	3.628
9.910	4.124
15.064	4.415
22.319	4.779
29.231	4.907
43.680	5.203
41.185	5.175
32.486	4.948
20.703	4.682
14.980	4.408
8.214	3.912
1.203	1.874
Kr on HL at 189.9°K	
0.518	0.179
1.096	0.324
3.260	0.817
4.112	1.002
6.771	1.502
9.511	1.907
11.909	2.221
14.950	2.497
18.845	2.876
23.963	3.157
34.743	3.627
43.926	4.058
40.819	3.896
27.322	3.321
15.838	2.597

contd.

P cmHg	N m/u.c.
7.876	1.708
1.656	0.428
Kr on HL at 210.1°K	
1.390	0.101
4.615	0.358
6.246	0.507
10.955	0.816
16.982	1.243
22.532	1.558
33.361	2.030
46.076	2.628
44.427	2.529
35.106	2.163
29.616	1.906
15.990	1.179
7.834	0.624
3.026	0.202
Kr on HL at 230.6°K	
2.314	0.069
3.867	0.124
5.928	0.254
9.546	0.367
16.184	0.612
21.328	0.793
27.165	0.974
44.719	1.496
38.627	1.312
32.135	1.143
24.213	0.858
18.345	0.687
13.073	0.493
7.982	0.315

Kr on LiL at 143.5°K contd.

P cmHg	N m/u.c.
0.133	1.655
0.327	2.731
0.538	3.462
1.015	4.196
1.909	4.755
3.614	5.281
5.798	5.579
9.656	5.923
11.600	5.958
16.430	6.204
22.340	6.350
30.005	6.477
45.112	6.568
41.753	6.534
27.915	6.413
18.103	6.273
7.864	5.721
2.130	4.796
0.316	2.502
Kr on LiL at 162.1°K	
0.738	1.316
1.060	2.203
2.015	2.719
2.957	3.495
3.968	4.002
7.906	4.851
12.460	5.279
14.823	5.387
19.500	5.528
28.480	5.795
45.002	5.986

contd.

P cmHg	N m/u.c.
52.690	6.069
31.921	5.801
22.853	5.632
16.072	5.394
6.518	4.573
2.834	3.312
1.013	1.807
Kr on LiL at 176.6°K	
0.632	0.586
1.295	1.164
2.451	1.705
2.932	1.900
4.010	2.412
6.944	3.154
9.480	3.716
12.070	3.954
19.038	4.491
25.335	4.705
31.898	4.923
45.231	5.237
35.624	5.004
29.923	4.824
20.200	4.492
15.206	4.196
5.583	2.821
1.017	0.872
Kr on LiL at 195.3°K	
1.012	0.362
1.538	0.746
2.376	1.032
4.186	1.607

contd.

P cmHg	N m/u.c.
8.592	2.392
13.314	2.956
18.987	3.322
23.804	3.582
32.724	3.978
46.312	4.352
44.809	4.283
37.321	4.058
29.213	3.862
20.079	3.376
11.613	2.725
5.207	1.833
Kr on LiL at 221.0°K	
1.551	0.150
2.519	0.206
4.110	0.340
7.650	0.705
12.420	1.091
17.715	1.481
25.794	1.990
32.839	2.379
45.136	2.854
50.385	3.018
35.095	2.426
27.023	2.012
21.632	1.698
10.318	0.897
6.816	0.596

Kr on CsL at 143.2°K

P cmHg	N m/u.c.
0.194	1.538
0.305	2.184
0.613	2.661
0.915	3.654
1.243	3.906
3.312	4.577
6.503	5.065
14.381	5.387
27.384	5.535
44.513	5.593
50.382	5.614
36.485	5.522
25.138	5.505
9.757	5.191
1.857	4.287
0.103	3.220

Kr on CsL at 176.7°K

P cmHg	N m/u.c.
0.847	0.796
1.093	0.895
2.023	1.584
2.959	1.978
5.501	2.749
8.831	3.288
15.500	3.809
19.366	3.992
28.447	4.264
44.613	4.563
40.198	4.519
24.329	4.198
12.375	3.596
4.973	2.589
1.916	1.449

Kr on CsL at 193.4°K contd.

P cmHg	N m/u.c.
0.928	0.312
2.107	0.494
3.321	0.769
4.164	0.897
6.322	1.308
7.116	1.434
11.723	2.079
13.018	2.313
21.145	2.869
28.231	3.218
45.614	3.728
44.102	3.697
35.007	3.476
23.624	3.002
17.118	2.553
9.625	1.842
5.133	1.124
2.726	0.616

Kr on CsL at 211.7°K

P cmHg	N m/u.c.
0.777	0.139
1.903	0.286
3.798	0.537
6.476	0.818
7.679	0.995
12.185	1.312
15.012	1.503
17.285	1.659
25.519	2.117
34.418	2.408
45.410	2.698
43.412	2.638
33.015	2.388

P cmHg	N m/u.c.
21.690	1.929
9.700	1.107
5.215	0.687
2.687	0.339

Kr on CsL at 223.8°K

P cmHg	N m/u.c.
0.215	0.023
1.903	0.069
3.321	0.122
5.474	0.192
10.770	0.388
15.925	0.522
20.422	0.669
25.626	0.838
32.080	1.011
45.487	1.354
43.817	1.294
34.212	1.215
23.278	0.735
7.107	0.253

Kr on LaL at 141.9°K

P cmHg	N m/u.c.
0.180	2.924
0.346	3.902
0.887	5.573
1.875	6.294
3.791	6.924
4.390	7.077
8.980	7.594
12.380	7.734
18.887	7.939
27.908	8.057
45.121	8.293
51.187	8.318

contd.

P cmHg	N m/u.c.
41.987	8.178
32.418	8.098
21.231	7.953
14.015	7.725
3.211	6.752
0.520	4.763
Kr on LaL at 159.6°K	
0.453	2.096
1.104	3.592
1.676	4.125
2.815	4.989
5.004	5.719
6.280	6.044
9.250	6.289
13.305	6.569
19.180	6.760
28.958	7.043
42.513	7.162
53.780	7.405
41.017	7.138
33.672	7.008
19.195	6.789
11.186	6.432
3.948	5.452
0.631	2.584
Kr on LaL at 166.3°K	
0.315	0.658
0.673	1.011
1.435	1.879
1.782	2.254

contd.

P cmHg	N m/u.c.
2.843	2.932
4.915	3.693
6.634	4.362
7.913	4.518
12.631	5.163
15.710	5.358
21.696	5.617
31.364	5.898
45.324	6.234
41.397	6.168
33.012	5.970
26.843	5.768
18.104	5.487
10.664	4.973
5.723	4.065
3.928	3.438
1.122	1.462
Kr on LaL at 175.9°K	
0.432	0.310
1.256	0.931
3.312	1.745
4.739	2.421
6.625	2.792
9.642	3.396
13.921	3.932
19.875	4.306
28.013	4.635
36.338	4.860
46.380	5.066
41.012	4.897

contd.

P cmHg	N m/u.c.
25.614	4.508
16.158	4.039
8.716	3.232
2.017	1.213
Kr on LaL at 196.4°K	
1.212	0.459
2.919	0.916
3.748	1.206
6.686	1.950
10.535	2.597
12.660	2.856
16.960	3.356
21.905	3.667
25.075	3.749
35.875	4.179
44.518	4.292
49.980	4.372
37.126	4.173
29.516	3.953
15.627	3.147
8.311	2.198
Kr on LaL at 218.2°K	
1.894	0.324
3.625	0.496
6.217	0.849
9.423	1.320
14.617	1.849
18.824	2.197
24.586	2.516
43.018	3.162

contd.

P cmHg	N m/u.c.
40.485	3.078
30.978	2.828
21.527	2.384
17.620	2.003
12.132	1.564
8.318	1.076
4.625	0.729
Kr on LaL at 223.8°K.	
1.115	0.182
2.312	0.224
5.134	0.458
9.847	0.795
12.470	0.991
15.815	1.155
21.259	1.443
27.008	1.669
41.956	2.105
37.012	1.911
22.618	1.481
17.868	1.293
7.106	0.614
4.011	0.356
Kr on HER at 141.9°K.	
0.002	1.044
0.029	3.629
0.248	4.492
0.433	5.598
1.382	6.215
2.768	6.579
4.983	7.038
8.580	7.409
13.680	7.717

contd.

P cmHg	N m/u.c.
21.294	7.912
31.627	8.048
45.325	8.187
39.768	8.173
26.138	7.991
15.614	7.768
7.139	7.310
3.896	6.842
0.018	3.016
Kr on H-ER at 171.3°K.	
0.245	0.943
0.897	2.530
2.271	3.564
3.590	4.042
6.380	4.709
7.321	4.893
11.455	5.306
16.310	5.697
20.777	5.955
26.121	6.194
33.240	6.415
40.590	6.579
44.848	6.704
39.019	6.510
23.568	6.071
8.914	5.068
4.583	4.371
1.318	2.842
Kr on HER at 187.4°K	
0.703	1.023
1.328	1.524
2.693	2.387

contd.

P cmHg	N m/u.c.
4.247	2.963
7.976	3.686
9.398	3.917
12.960	4.291
18.763	4.667
24.064	4.879
30.105	5.158
37.995	5.396
46.700	5.599
43.321	5.498
32.013	5.183
21.639	4.743
14.619	4.382
5.887	3.382
1.968	1.963
Kr on HER at 211.5°K	
0.874	0.448
2.813	0.984
6.792	1.674
8.219	1.983
11.343	2.428
16.026	2.296
21.813	3.128
28.145	3.397
37.097	3.642
46.321	3.786
42.230	3.679
34.626	3.582
25.431	3.321
17.157	3.024

contd.

P cmHg	N m/u.c.
11.816	2.448
9.321	2.156
5.128	1.468
Kr on HER at 229.3°K	
0.720	0.062
2.132	0.231
3.823	0.384
8.016	0.781
9.438	0.872
15.873	1.263
21.739	1.624
25.132	1.843
35.078	2.189
44.739	2.456
40.006	2.372
29.756	2.007
20.283	1.513
13.002	1.132
5.624	0.564
Kr on H-OFF at 144.4°K	
0.091	0.644
0.109	1.429
0.396	2.185
0.789	2.476
3.812	3.077
5.112	3.261
7.100	3.388
12.004	3.613
14.214	3.689
20.442	3.867
28.301	4.039

contd.

P cmHg	N m/u.c.
36.429	4.153
46.445	4.255
42.834	4.193
30.012	4.008
15.384	3.720
9.612	3.495
2.351	2.836
0.238	1.845
Kr on H-OFF at 163.8°K	
0.014	0.275
0.462	1.356
0.618	1.554
2.173	2.081
2.928	2.197
4.630	2.409
5.588	2.487
8.730	2.881
12.992	2.911
18.791	2.971
26.745	3.111
37.887	3.336
43.103	3.412
39.896	3.383
31.254	3.186
20.511	2.987
15.493	2.896
6.621	2.518
1.016	1.827
Kr on H-OFF at 178.2°K	
0.279	0.723
0.865	1.248

contd.

P cmHg	N m/u.c.
2.187	1.587
4.319	1.932
5.828	2.089
10.812	2.342
18.146	2.578
21.068	2.675
28.654	2.792
36.715	2.867
45.230	2.986
38.615	2.892
32.132	2.826
25.014	2.713
14.421	2.496
8.754	2.273
3.296	1.784
1.625	1.432
0.458	1.034
Kr on H-OFF at 190.7°	
0.002	0.228
0.537	0.705
0.823	0.941
1.345	1.075
2.518	1.308
4.257	1.550
7.989	1.805
10.952	1.922
15.810	2.060
20.348	2.123
25.635	2.223

contd.

P amHg	N m/u.c.
32.478	2.315
34.927	2.388
45.732	2.493
40.968	2.414
29.629	2.292
22.003	2.182
12.589	1.987
5.517	1.656
0.783	0.853
Kr on H-OFF at 213.8°K	
0.586	0.432
1.012	0.597
1.978	0.872
2.693	1.013
5.986	1.389
10.012	1.668
12.321	1.720
17.938	1.864
23.652	1.958
29.005	2.066
39.286	2.137
44.927	2.175
43.321	2.162

contd.

P cmHg	N m/u.c.
34.385	2.076
24.757	1.973
14.458	1.784
7.569	1.506
3.862	1.174
Kr on H-OFF at 231.3°K	
0.623	0.073
1.346	0.178
3.321	0.385
7.543	0.726
12.738	1.003
16.015	1.126
24.232	1.382
33.160	1.548
44.372	1.694
49.463	1.816
39.315	1.647
25.973	1.403
18.014	1.187
10.521	0.898
6.034	0.597
2.126	0.253

Auxiliary terms used for calculation of the equilibrium constant K" and the thermodynamic properties in the corresponding standard state (a_s' $m'/\ell = 1$).

$C_s = k_1 N$, hence $a_s' = k_1 a_s$, where $k_1 = \frac{10^3}{M.W.}$

$C_g = k_2 P$, where $k_2 = \frac{1}{76RT}$

M - weight of the unit cell (Table 15).

W - water content, cc/g (Table 15).

T - temperature ^oK.

R - gas constant.

The relation between the equilibrium constants K' and K" is, consequently, $K'' = \frac{k_1}{k_2} K'$ and the activity coefficients are independent of the units of concentration used.

In the standard state associated with K" ($a_s' = 1$) the concentration of the sorbed phase c_s^o can be obtained. Graphs of a_s as a function of N, Fig. 85,86 and 87, give, for each temperature, the N which corresponds to $a_s = \frac{1}{k_1}$ ($a_s' = k_1 a_s$, when $a_s' = 1$, $a_s = \frac{1}{k_1}$). The γ's corresponding to these values of N can be obtained from Fig. 88, 89 and 90 and c_s^o calculated, as $c_s^o = \frac{1}{\gamma}$ when $a_s' = \gamma c_s^o = 1$.

Structure analyses on BaL based on Fourier syntheses.

The analyses were carried out in collaboration with Dr. H. Villiger. The computer programs used were those given in reference 11. Both hydrated and dehydrated forms of BaL were investigated. For the intensity measurement in the former case a powder diffractometer pattern, obtained at room temperature was used and in the latter - Lenné powder pattern at 550°C, measured by means of Joyce double-beam microdensitometer.

The structure of the hydrated form was refined with final reliability factor $R_I = 0.18$. Ba^{++} was found to be positioned like K^+ in KL(11). The present stage of refinement of the dehydrated structure at high temperature (R_I as given on p. 150) corresponds to the following parameters:

Atom	Fractional occupancy.	x	y	z	B
Ba1	0.0350	0.1885	0.3770	0.0000	4.0
Ba2	0.0480	0.1262	0.2524	0.1000	6.0
Ba3	0.067	0.3620	0.7240	0.1476	6.0
Ba4	0.063	0.0000	0.1380	0.3524	6.0
Ba5	0.018	0.0500	0.1000	0.5000	6.0
K1	0.070	0.3333	0.6666	0.5000	4.0
K2	0.090	0.0000	0.5000	0.5000	4.0
K	0.032	0.3333	0.6666	0.0000	4.0
06	0.50	0.1262	0.4640	0.0000	2.8
05	0.50	0.4267	0.8534	0.2388	2.5
04	1.00	0.1010	0.4078	0.3560	3.0
03	0.50	0.2675	0.5350	0.2760	4.5
02	0.25	0.1654	0.3308	0.5000	2.0
01	0.25	0.0000	0.2687	0.5000	2.0
Si2	1.00	0.1662	0.4965	0.2087	2.0
Si1	0.50	0.0916	0.3595	0.5000	2.5